NASA
Technical
Paper
2749

September 1987

Evolution, Calibration, and Operational Characteristics of the Two-Dimensional Test Section of the Langley 0.3-Meter Transonic Cryogenic Tunnel

Charles L. Ladson
and Edward J. Ray

NASA

NASA Technical Paper 2749

1987

Evolution, Calibration, and Operational Characteristics of the Two-Dimensional Test Section of the Langley 0.3-Meter Transonic Cryogenic Tunnel

Charles L. Ladson
and Edward J. Ray

Langley Research Center
Hampton, Virginia

National Aeronautics
and Space Administration

Scientific and Technical Information Office

CONTENTS

SUMMARY

This paper presents a review of the development of the world's first cryogenic pressure tunnel, the Langley 0.3-Meter Transonic Cryogenic Tunnel (0.3-m TCT). Descriptions of the instrumentation, data acquisition systems, and physical features of the two-dimensional 8- by 24-in. (20.32- by 60.96-cm) and advanced 13- by 13-in. (33.02- by 33.02-cm) adaptive-wall test-section inserts of the 0.3-m TCT are included. In addition, several of the major auxiliary systems of the tunnel are reviewed, and they include the drive, nitrogen, thermal insulation, and boundary-layer control systems. Future plans for the facility are briefly addressed.

Extensive calibration results and other operational characteristics are presented for the 0.3-m TCT with the two-dimensional 8- by 24-in. (20.32- by 60.96-cm) test section. In addition to the test-section Mach number distributions, results include tunnel circuit Mach number distributions, stagnation temperature distributions, power requirements, operational envelopes, flow quality characteristics, and sidewall boundary-layer characteristics.

The tunnel-empty calibration results obtained for the 0.3-m TCT with the 8- by 24-in. (20.32- by 60.96-cm) test section indicated acceptable Mach number distributions throughout the range of Mach number and Reynolds number of the facility. At Mach numbers below about 0.80, the standard deviation was generally about 0.002. The temperature distributions in the settling chamber were shown to be extremely good, with an average standard deviation of about 0.20 K. At ambient temperature, drive-system speed restraints limited the test Mach number to about 0.7. At lower temperatures, the drive-system speed and power boundaries were broadened and the maximum Mach number was limited to transonic speeds by choking at the entrance to the diffuser. Operational envelopes are presented that indicate fan speed, saturation temperature, and drive-motor power boundaries.

The 0.3-m TCT with the 8- by 24-in. (20.32- by 60.96-cm) test section has provided a unique research capability enabling the simulation of flight-equivalent airfoil results. The automatic controls of the facility have demonstrated the ability to hold Mach number and Reynolds number conditions to acceptable tolerances at subsonic Mach numbers for airfoil testing. At transonic speeds, where control of Mach number becomes more critical, Mach control was acceptable but not as exact as at the lower speeds. This reduction in Mach control was related to a degradation in diffuser performance associated with higher tunnel speeds. Flow-quality studies have substantiated that the primary source of tunnel noise with the 8- by 24-in. test-section insert was in the diffuser.

INTRODUCTION

The application of the cryogenic concept to high Reynolds number transonic tunnels has been under study at the Langley Research Center since late 1971. Results from early theoretical studies and tests in a small, low-speed, ambient pressure tunnel were presented in reference 1. Based on the promising results of these early studies, the design and construction of a pilot transonic cryogenic tunnel was begun in early 1973. This facility, now designated as the Langley 0.3-Meter Transonic

Cryogenic Tunnel (0.3-m TCT), is a continuous-flow fan-driven pressure tunnel that uses nitrogen as the test gas. This tunnel first operated in late 1973 with a three-dimensional slotted-wall octagonal test section. A description of its design features and operational characteristics is contained in reference 2. Considerable operational experience was obtained that included not only tests of models and instruments but also the development of test techniques. A summary of much of this operational experience is contained in reference 3.

The original three-dimensional test section of the facility was replaced by an 8- by 24-in. (20.32- by 60.96-cm) two-dimensional insert in mid-1976. The purpose of this extensive modification, as discussed in reference 3, was to explore the capabilities of two-dimensional testing at cryogenic temperatures and to develop the necessary test techniques, apparatus, and data reduction procedures to demonstrate this capability. In addition, the two-dimensional approach allowed the testing of relatively large chord airfoils, thus taking advantage of the high unit Reynolds number capability of this relatively small wind tunnel. The two-dimensional test section was in operation until late 1984 and has been extensively used to produce airfoil data at flight-equivalent Reynolds numbers, develop cryogenic test techniques, and provide instrument checkout and calibration for the National Transonic Facility (NTF) at the Langley Research Center. A description of the Advanced Technology Airfoil Test (ATAT) program, the largest airfoil test program undertaken in this test section, is contained in reference 4.

In mid-1976 a preliminary design was undertaken for the construction of an adaptive-wall test section to replace the existing two-dimensional section. This test section, as described in reference 5, would have computer-controlled, solid, flexible top and bottom walls to reduce or eliminate wall interference effects. Construction of this 13- by 13-in. (33.02- by 33.02-cm) test section was completed in 1981 and was followed by an extensive bench checkout to develop and integrate the computer and software. Installation into the tunnel circuit was begun in late 1984 and operation was begun in late 1985.

The purpose of this paper is to present a brief history of the 0.3-m TCT, to describe both the 8- by 24-in. (20.32- by 60.96-cm) two-dimensional test section (hereinafter referred to as the "8 × 24 test section") and the 13- by 13-in. (33.02- by 33.02-cm) two-dimensional adaptive-wall test section (hereinafter referred to as the "13 × 13 test section"), and to present detailed calibration results for the 8 × 24 test section throughout the operational envelope. Included in the calibration results are Mach number distributions, stagnation temperature distributions, tunnel power requirements, and curves of the facility operational envelope. Also included in the paper are descriptions of the instrumentation, data acquisition systems, and auxiliary systems, some of which have been upgraded, modified, or added since previous publications. For completeness, boundary-layer parameters are included that are based on the results of boundary-layer pressure distributions from the test-section sidewall obtained from other investigations.

SYMBOLS

Values are given in both SI and U.S. Customary Units. The measurements and calculations were made in U.S. Customary Units.

b	axis intercept
h	dimension shown in figures 5 and 11
i	number of terms
j	dimension shown in figure 5
M	average stream Mach number, $\frac{M_{l,1} + M_{l,2} + \ldots + M_{l,i}}{i}$
M_l	local stream Mach number
M_{TC}	reference test-chamber Mach number
ΔM	deviation of average stream Mach number from reference test-chamber Mach number, $M_{TC} - M$
ΔM_{AV}	standard deviation of local Mach number from average Mach number, $\left[\frac{(M - M_{l,1})^2 + (M - M_{l,2})^2 + \ldots + (M - M_{l,i})^2}{i}\right]^{1/2}$
m	slope
n	fan speed, rpm
p_{TC}	reference test-chamber static pressure
p_t	stream stagnation pressure, atm
δp_{TC}	variation from mean test-chamber static pressure
δp_t	variation from mean stagnation pressure
q	free-stream dynamic pressure
δq	variation from mean free-stream dynamic pressure
R	free-stream Reynolds number
δR	variation from mean free-stream Reynolds number
r	fan pressure ratio (see fig. 54)
T_t	free-stream stagnation temperature, K
$\bar{T}_t$	average stagnation temperature, K
$T_1, T_2, \ldots T_{25}$	local stagnation temperature on survey rake ahead of screen section (see fig. 52)
x,y,z	distance along longitudinal, lateral, and vertical axis, respectively, in. (cm)

δ variation from mean

δ^* boundary-layer displacement thickness

Subscript:

max maximum

Abbreviations:

BL boundary layer

BLC boundary-layer control

CRT cathode ray tube

GN,N_2 gaseous nitrogen

LED light-emitting diode

APPARATUS

History

The 0.3-m TCT has undergone almost continual evolution from the original pilot facility concept to the present airfoil research capability. This section of the paper is intended to provide a brief summary of these changes and to give some of the rationale for the changes.

A sketch of the Langley 0.3-m TCT with the original octagonal three-dimensional test section is shown in figure 1, and a photograph taken during initial assembly is shown in figure 2. This tunnel was first operated in late 1973 as a pilot facility to demonstrate the validity of the cryogenic wind-tunnel concept at transonic speeds. Because of the pilot facility status and the requirement to keep construction costs at a minimum, the facility was designed for a limited lifetime of about 60 hr of operation. As a result of this austere pilot facility approach, the tunnel (1) was located in a small readily available building, (2) made use of an existing drive motor with variable-frequency power supply, and (3) incorporated only the most basic instrumentation and control systems. However, after about 1 year of successful operation, the designation of the facility was changed from a pilot status to a research facility status.

At about the same time, the construction of a two-dimensional test section with an associated contraction section and diffuser was begun to demonstrate the airfoil test capability at high Reynolds numbers and to evaluate airfoil test techniques at cryogenic temperatures. In late 1975, installation of the two-dimensional test section was begun, a workshop and model preparation area were constructed adjacent to the tunnel, a new control and instrumentation room was added, and the data acquisition system was upgraded by connecting it to a remote central data acquisition system. These modifications to the facility were completed in early 1977. From that time until early 1978, evaluation of the two-dimensional test section was conducted and airfoil test techniques were developed.

During 1978 the tunnel was taken out of operation for extensive recertification. Two objectives were to be accomplished during this process. First, because the tunnel had been designed for only a very short lifetime and the weld joints had not been X-rayed at the time of construction, all welds in the pressure shell were subjected to X-ray inspection and rewelded if necessary to bring them up to current-day pressure vessel codes. Upon completion of this task, the facility could be certified for a more reasonable lifetime. Second, the maximum permissible operating pressure was increased from 5 to 6 atm absolute. Although no fatigue failure in the welds was noted during this inspection, considerable rewelding was necessary to meet current codes for a minimum lifetime of 10 years. The facility was placed back in an operational mode in early 1979.

During late 1980 and early 1981, a two-story-building addition was constructed adjacent to the facility complex. The first floor of this addition was used to relocate the tunnel controls and provide space for a new on-site data acquisition system, and the second floor was used to provide space for a shop and model preparation area that could be used while the facility was running. This two-story addition was enlarged in late 1985 to provide additional model preparation area and on-site office space for the operators and test engineers of the data acquisition system.

8 × 24 Test Section

When the two-dimensional test section was installed, the contraction section of the original three-dimensional test section (ref. 2) was modified and a new diffuser-transition section was installed. A sketch of the 0.3-m TCT with the 8 × 24 two-dimensional test section is presented in figure 3 and a photograph is presented in figure 4.

Contraction section.- The original contraction section was 81.00 in. (2.057 m) long and provided a transition from the circular upstream end to the octagonal test section. To provide for the rectangular two-dimensional test section, the existing contraction was cut and flanged at a point 38.63 in. (98.1 cm) upstream of the test-section entrance. A new transition-contraction section replaced the removed section as shown in figure 3. The two-dimensional test section had a larger cross-section area than the original test section, and as a result the contraction ratio for this test section was 9.42 compared with the original value of 11.97. A sketch of this new part of the contraction section is shown in figure 5, and the area distribution is given in table I.

Test section.- A side view cross-section sketch and top view photograph of the two-dimensional test section are presented in figures 6(a) and 7, respectively. The rectangular cross-section test area, which was 8.00 in. (20.32 cm) wide and 24.00 in. (60.96 cm) high, began at station -28.50 in. (-72.39 cm) and ended at station 31.00 in. (78.74 cm). Circular turntables, which had a diameter of 9.00 in. (22.86 cm) and were located in the sidewalls, provided for the model support and were part of the angle-of-attack drive mechanism. The center of rotation of the turntables was located at station 0.0. Two longitudinal slots were located in both of the 8.00-in-wide top and bottom walls and were symmetric about the longitudinal centerline with a slot spacing of 4.00 in. (10.16 cm). Details of the slotted-wall design are shown in figure 6(b). The slotted walls were removable so that changes in slot design could be made if desired. The slot design was based on the work presented in reference 6 and provided an open area ratio of 0.05. The slotted walls

were also adjustable so that their slope could be changed with respect to the tunnel axis. For the calibration data presented herein, both the slotted walls and the solid sidewalls were fixed parallel to the tunnel axis.

The test gas that passed through the slotted walls into the plenum chamber was returned to the main stream over reentrance flow fairings that began at tunnel station 20.50 in. (52.07 cm). The minimum cross-section area in this mixing region was located at the end of the test section and was 6.3 percent larger than the test-section area to provide space for the low-energy reentrant flow to return to the main flow stream.

As shown in the sketch in figure 6(a), the test-section sidewalls had removable plates located just upstream of the turntables to enable the incorporation of a sidewall boundary-layer removal system. This boundary-layer system allowed for the removal of tunnel sidewall boundary-layer flow through smooth porous plates in a manner described in a latter section of this paper. When the boundary-layer removal system was not being used, solid inserts could be mounted in these locations, as was the case for the tunnel calibration tests reported herein.

The angle-of-attack and survey-probe drive mechanisms are also shown in the sketch in figure 6(a). The angle-of-attack drive system was computer controlled and was capable of rotating the turntables through an angle-of-attack range from -20° to 20°. The survey-probe system is discussed in the instrumentation section of this paper. A typical airfoil section mounted in the test section with a wake survey rake located downstream of the trailing edge is also shown in the test-section photograph in figure 7.

Diffuser.- As shown in figure 3, a transition section-diffuser combination extended from the end of the test section at station 31.00 in. (78.74 cm) to station 168.00 in. (426.7 cm). This diffuser is rectangular at the entrance and changes to a circular section with a diameter of 30.00 in. (76.2 cm) at the downstream end. The variation of the ratio of diffuser local cross-section area to test-section area and the equivalent conical half-angle of the diffuser as a function of length are presented in figure 8. As seen in the table in figure 8, the conical half-angle at the upstream end of the diffuser is larger than the desirable value of about 3.0°, a compromise which had to be made to install a two-dimensional test-section insert into the existing tunnel configuration.

13 × 13 Test Section

The 13.00- by 13.00-in. (33.02- by 33.02-cm) two-dimensional adaptive-wall test section was installed into the tunnel circuit in late 1985. The design and operational features of this test section were based on work carried out at the University of Southampton in Southampton, England, under NASA Grant 7172. (See refs. 7 and 8.) At the same time that this test section was being installed into the tunnel circuit, the basic length of the circuit was increased by 94.63 in. (2.404 m). This increase in length was intended to provide space for a longer and more efficient diffuser entrance section and, at some future date, an enlarged diameter contraction section. These modifications were directed toward improvements in the flow quality of the facility. A sketch of the lengthened tunnel circuit with this test section installed is presented in figure 9 and a photograph is shown in figure 10.

Contraction section.- As was the case for the 8 × 24 test section, the contraction section for the 13 × 13 test section mates with the existing tunnel structure at a point 38.63 in. (98.12 cm) upstream of the entrance of the test section. Because the entrance area of this test section is smaller than the 8 × 24 test section that it replaced, the area distribution of the contraction section had to be modified accordingly. This modification was accomplished by decreasing the local cross-section area linearly over the length of the contraction section such that the exit area matched the test-section entrance area. The contraction ratio is 10.71. A sketch of this section is shown in figure 11, and coordinates are presented in table II.

Test section.- The test section is 13.00 in. (33.02 cm) square at the entrance, 73.20 in. (185.9 cm) long, and 13.00 in. (33.02 cm) wide by 15.36 in. (39.01 cm) high at the exit. Circular turntables, 15.00 in. (38.10 cm) in diameter, are located on both sidewalls with the center of rotation located 31.75 in. (80.65 cm) downstream of the entrance. These turntables are used to support two-dimensional-airfoil models and are connected to the computer-controlled angle-of-attack drive system. This drive system is the same as that on the 8 × 24 test section and has a range from -20° to 20°. As seen in figure 12 (which has the nearside turntable and drive rod removed), "D"-shaped quartz windows can be incorporated into the turntables for limited flow-visualization capability. Also visible just below the viewing port is a rectangular, removable, model mounting plate that is utilized in mounting various models to the turntable. Portions of the upper and lower flexible walls and their drive rods are also visible. Although not shown, the wake survey drive mechanism is mounted to the near wall downstream of the opening. The center of rotation of the windows is arbitrarily defined as tunnel station 0.00, with positive values indicating locations downstream of this position.

The width of the test section is constant throughout the entire length but the height is variable from station -29.75 in. (-75.57 cm) to station 40.95 in. (104.0 cm). This variation in height is accomplished by having the tunnel floor and ceiling flexible. These flexible walls are fixed at the upstream end and are supported by 21 jacks along their length. The downstream end is fixed in the vertical direction but is free to translate longitudinally in slots provided for this purpose. The portion of these flexible walls downstream of station 25.05 in. (63.63 cm) is used to provide a smooth transition from the end of the effective test section to the fixed diffuser.

The jacks that support the flexible walls are driven by computer-controlled electric stepping motors and are designed to be capable of a 3.00-in. (7.62-cm) movement in the positive z-direction and a 1.00-in. (2.54-cm) movement in the negative z-direction. All components of the drive system except the push rods that connect to the wall are located outside of the pressure vessel and thus are not subjected to the actual cryogenic test conditions. A position transducer is attached to the drive linkage at each jack location to provide position data to the control computer. The computer programs that control the wall-positioning system are also based on those developed at the University of Southampton.

Diffuser.- As seen in figure 9, a diffuser transition section with a 24.00-in-(60.96-cm-) long rectangular-to-circular cross section is located downstream of the test-section exit. This section provides the transition between the test section and the two-piece diffuser that follows. The first of the two sections of the diffuser has a length of 60.00 in. (152.4 cm) and a conical half-angle of 1.2°. The second

section has a length of 110.5 in. (287.7 cm) and a half-angle of 3.00°. This second section of the diffuser is the same as that used with the original octagonal test section of the facility. (See fig. 1.)

Auxiliary Systems

Some of the auxiliary systems associated with the 0.3-m TCT have been described in detail in references 2 and 9. Many of these systems, however, have been modified or upgraded since the publication of these references, and thus other subsystems have been incorporated. For this reason, details of these changes and additions are incorporated herein.

Drive control, motor, and fan.- The 0.3-m TCT is powered by a water-cooled, two-pole, alternating-current induction motor rated at 2240 kW at 7200 rpm which drives a 12-blade fan. The tunnel Mach number is controlled by varying the motor speed from a minimum of about 600 rpm to a maximum of 5600 rpm. This maximum motor speed is a restriction caused by excessive resonance-induced vibrations of the fan drive shaft that occur at these higher speeds. Originally, the motor speed was manually controlled, but in 1980 a closed-loop microprocessor-based control system was installed. This system provides for control of either speed or Mach number and is also capable of manual override if necessary. Some of the design considerations and specifications of this control system are presented in appendixes A and B of reference 10.

Nitrogen system.- A schematic drawing of the liquid nitrogen injection and the gaseous nitrogen exhaust system is shown in figure 13. The liquid nitrogen (LN_2) is stored in two double-walled, vacuum-insulated tanks having a total volume of 56 000 gal (212 000 L). Two pumps are available to circulate the liquid nitrogen in a closed circulation loop past the injection control valves located at the tunnel. The closed loop was found to be required so that liquid (as opposed to gas) was always available at the control valve inlet to provide optimum temperature control. The liquid nitrogen pumps have a capacity of 150 g/min (570 L/min) at a pressure of about 10 atm. An additional pump with a flow rate about 20 percent higher can be substituted for either of the other two if higher flow rates are needed. Past experience has shown that the combinations of pumps available are sufficient to provide the maximum liquid nitrogen flow rates required, even when special models or test apparatus that require their own nitrogen supply are used. Immediately prior to tunnel operation, the liquid nitrogen supply tanks must be pressurized to a pressure of about 2 atm to provide adequate inlet pressure (net positive suction head) at the pump inlet to prevent cavitation. The pressure control valve located in the return portion of the closed-loop system is used to maintain constant pressure at the injection valve inlets for varying flow rates.

Stagnation temperature is controlled by the amount of liquid nitrogen injected into the tunnel circuit. The amount of liquid nitrogen injected is controlled by a closed-loop, microprocessor-based, digital control system. This system in turn operates four parallel 10-bit digital control valves, each connected to a single injection nozzle. The 1023:1 turndown ratio provided by these valves is sufficient to provide accurate temperature control over the entire range of Mach number and Reynolds number of the facility. A thermocouple located in the settling chamber is used to provide the temperature input signal to the microprocessor.

To maintain stagnation pressure, it is necessary to vent gaseous nitrogen from the tunnel circuit in an amount equivalent to the liquid nitrogen injection required

to compensate for the heat of compression generated by the fan. As seen in figure 13, three exhaust valves are located in the tunnel return passage to accomplish this task. These valves are controlled by a second control loop in the previously mentioned microprocessor-based digital controller. A total pressure probe located in the settling chamber is connected to a pressure transducer that provides the input signal to the pressure controller. This system is capable of setting and maintaining stagnation pressure at values from about 1.2 to about 6.1 atm abs.

Details of the modeling and control algorithms incorporated in the temperature and pressure control system microprocessor have been published in several progress reports. A summary of this development is presented in reference 11.

Thermal insulation system.- The external thermal insulation system used on the 0.3-m TCT was significantly modified in 1979 from the original system installed in 1973. Details of this revised system are presented in reference 12. Basically, the current system consists of wrapping each section of the tunnel with four layers of spun glass fiber insulation. These layers are held in place by metal bands and wires and are covered by a layer of woven glass fiber cloth. This glass fiber cloth serves as a foundation for the vapor barrier coating which consists of three coats of painted-on compounds. The first coat is a tough, impact-resistant compound that bonds well to the fiber cloth; the second coat is a butyl rubber compound that serves as the primary vapor barrier; the third, or outer, coat is a polyethylene paint that serves as a protective coating for the butyl rubber layer.

Between the third and fourth layers of glass fiber mat, 0.38-in. (0.95-cm) copper tubes are installed to provide a flow of dry nitrogen gas into and out of the insulation region. This gas flow is automatically controlled to maintain a pressure slightly above atmospheric in the insulation under all tunnel operating conditions. By maintaining this positive pressure, problems associated with condensation of either moisture or oxygen from atmospheric air in this region are eliminated. As noted in reference 12, compared with the original system, this revised system is much lower in cost of materials and labor to repair or modify when necessary.

Boundary-layer control system.- In 1980 a passive sidewall boundary-layer removal system was installed in the facility. The purpose of this system is to reduce the thickness of the boundary layer in the region of the test section occupied by the model, thus reducing the possibility of sidewall boundary-layer separation at high lift coefficients or high Mach numbers. Experience has shown that this type of separation can be detrimental to the validity of the data obtained during tests of two-dimensional airfoils.

Porous plates are located on both sides of the test section (slightly upstream of the model mounting turntables) and extend the full height of the test section. For the 8 × 24 test section, these plates are about 6.00 in. (15.24 cm) long and the downstream edge is located about the same distance upstream of the center of rotation of the turntable. For the 13 × 13 test section, the plates are 6.99 in. (17.75 cm) long and the downstream edge is about 10.75 in. (27.31 cm) upstream of the center of the turntable. These plates are manufactured with a sandwich-type construction. The airstream side consists of a thin plate with small electron-beam drilled holes, the interior contains a honeycomb structure, and the backside consists of a relatively thick perforated plate. Photographs of a typical plate are shown in figure 14.

A duct system, shown in figure 15, is connected to the back of the porous plate assembly to provide for the removal of the boundary-layer flow. Two control valves

are located in the removal lines to control the mass flow removal rate, one valve for each side of the test section. As originally installed, the flow was exhausted to the atmosphere. As a result, the test envelope was restricted since the maximum mass flow removal rate is limited by the liquid nitrogen injection rate required to maintain the test conditions in equilibrium, and the test-section pressure must be above the atmospheric exhaust pressure.

Provisions were made in the original design of the boundary-layer removal system for the incorporation of a compressor into the circuit so that the exhausted mass flow could be reinjected into the tunnel circuit downstream of the test section. This compressor and the necessary auxiliary equipment, which were installed into the circuit in late 1984, significantly increased the system capability. A drawing of the boundary-layer removal system is shown in figure 16, and a photograph of the compressor and drive motor is shown in figure 17. Further details of this system are contained in reference 13.

The mass flow removal rate is controlled by a closed-loop, microprocessor-based control system. Mass flow rates for each of the sidewalls of the tunnel can be input to the controller. With the compressor operating, flow removal rates up to 4 percent of the tunnel mass flow are possible at Mach numbers up to about 0.60. At the maximum Mach number, the removal rate is limited to about 2 percent of tunnel mass flow rate. Some details of the design of the control system are contained in reference 14.

Plans

Plans and final designs for upgrades to the facility are currently being implemented. These upgrades include replacing the contraction section with a larger one to increase the contraction ratio to about 15:1, incorporation of a honeycomb section and new screens in the settling chamber to reduce turbulence, providing a three-dimensional-model angle-of-attack system with vertical translation as well as pitch capability, and automation of the existing liquid nitrogen supply system for increased operator safety. Several approaches to providing a variable second minimum for reduction of test-section noise are also being investigated.

INSTRUMENTATION

Pressure Instrumentation

For two-dimensional-airfoil tests, the 0.3-m TCT is equipped to measure static pressures on the airfoil surface, total pressures in the airfoil wake, and static pressures on the tunnel sidewall, floor, and ceiling. Static pressure taps are also located throughout the tunnel circuit to provide measurements of contraction and diffuser section performance, fan pressure rise, and pressure loss across various elements of the tunnel circuit.

Because of the large changes in dynamic pressure of the facility over its operational range (a factor of about 75), the range of static pressures to be measured is large and conventional strain gauge transducers are not used. Instead, commercially available high-precision capacitive-type transducers are used. A more complete description of this type of pressure instrumentation is presented in reference 15.

The transducers are mounted in instrument racks located adjacent to the test section. A typical cabinet containing 25 of the pressure transducers is shown on the right in figure 18. To provide increased accuracy, the transducers are mounted on thermostatically controlled heater bases to maintain a constant temperature and are shock mounted to reduce possible vibration effects. The electrical outputs from the transducers are connected to individual signal conditioners located in the control room. (See fig. 19.)

These signal conditioners are autoranging and have seven ranges available. By means of the autoranging capability, the analog electrical output to the data acquisition system is kept at a high level even though the transducer may be operating at the low end of its range. Transducers with a maximum range from -100 to 100 lb/in^2 (-690 to 690 kN/m^2) are available for measurement of model and tunnel wall pressures. Transducers with a maximum range from -20 to 20 lb/in^2 (-138 to 138 kN/m^2) are available for measuring pressures in the model wake. These transducers have an accuracy of ±0.25 percent of reading from 25 percent of negative full scale to 100 percent of positive full scale.

Because of the limited number of analog input channels on the original data acquisition system (see the following section), a scanivalve system capable of operating ten 48-port scanivalves was used in the data acquisition process to acquire the large number of readings desired. As a result of the delay times incorporated into the system to account for pressure lag in the tubing and transducers, the time on each data point was much higher than desired. The current data acquisition system was designed to accommodate 125 channels of pressure instrumentation, thus allowing individual transducers to be used for most measurements. The scanivalve system is retained, however, for those cases where larger numbers of measurements are necessary.

To determine free-stream Mach number to an accuracy of ±0.001, it is necessary to use a much more accurate type of instrumentation than the capacitive potentiometer type. As a result, commercially available quartz Bourdon tube pressure gauges are used for the measurement of stagnation pressure, reference static pressure, and the reference pressure on other differential pressure transducers. This system has an accuracy of about ±0.01 percent full scale at low pressures to about ±0.02 percent full scale at the high end of its range.

Traversing Survey-Probe System

For both of the two-dimensional test sections, a vertical traversing survey-probe system is located on the left sidewall of the test section downstream of the turntable. The probe is driven over a traversing range of about 10.0 in. (25.4 cm) by an electric stepper motor system and can operate at speeds from about 0.1 in/sec (0.25 cm/sec) to about 6.0 in/sec (15.2 cm/sec). The stroke and speed can be remotely controlled from the operator's panel in the control room. The vertical position of the probe is recorded on the data acquisition system by using a digital shaft encoder. Although the primary purpose of this traversing system is to survey the total pressures in airfoil wakes by the use of a pitot tube survey rake, the system can be equipped with other types of instruments such as thermocouple or hot wire probes if desired.

8 × 24 test section.- In the 8 × 24 test section, the centerline of the probe support can be located at either tunnel station 10.25 in. (26.04 cm) or 12.25 in.

(31.12 cm). Figure 7 presents a photograph showing a survey rake that contains both static and total pressure probes located in the most forward of these two positions. For this forward configuration, the openings of the pitot tubes are located 0.88 chord downstream of a typical airfoil trailing edge. Details of this multitube pitot probe are shown in figure 20. This type of multitube probe allows an assessment of the spanwise variations in pressures to be made, thus aiding in the evaluation of two-dimensionality of the flow field. Three disk-type static probes as well as six pitot probes are mounted on the assembly. Individual transducers are used for each tube on the probe assembly to keep pressure response time low. Two vertical rows of test-section-sidewall static pressure taps are provided on the opposite test-section wall in the plane of the pitot tubes. Experience has indicated that the sidewall static pressure measurements are more reliable than those from the disks on the probe for use in determination of the airfoil drag coefficient.

13 × 13 test section.- For the 13 × 13 test section, the survey-probe drive system is the same as that used for the 8 × 24 test section. The survey probe can be located in any of three positions downstream of the test-section turntables. These locations are 12.5 in. (31.8 cm), 17.5 in. (44.5 cm), and 22.5 in. (57.2 cm) downstream of the center of rotation of the turntable.

DATA ACQUISITION SYSTEM

Original Capability

Data from the 0.3-m TCT were recorded on magnetic tape by use of a central data recording system from mid-1976 until early 1982. This centralized system at the Langley Research Center, located in a remote data acquisition complex, was installed in the late 1950's and serves various facilities on a time share basis. A photograph of this central system is presented in figure 21. A total of 99 analog channels of recording capability were available to the facility with a maximum range of 100 mV and a resolution of 1 part in 10 000. In a continuous mode all data channels could be scanned at a rate of about 20 scans per second, whereas in a single scan mode a rate of about 4 scans per second was maximum. All analog data were filtered with a 4-Hz low-pass filter.

A small computer at the 0.3-m TCT (shown on the left side of fig. 19(a)) was used to sequence the data acquisition system, provide timing input signals for the scanivalve drive system, provide real-time visual displays and plots, and control the angle-of-attack and wake survey drive systems. The computer was programmed to allow the recording of from one to nine single frames of data for each port on the scanivalves. Both the time between each frame of data and the dwell time on port before the first frame of data was taken were variables and could be input by the system operator at any time.

All inputs to the on-site computer were made through the teletype keyboard, which is shown on the right in figure 22. Shown on the left of this figure is the XY plotter that was used to produce real-time plots of pressure distribution over the airfoil and total head loss in the airfoil wake. Other real-time displays included digital readouts of Mach number and Reynolds number. Commands for the angle-of-attack and wake survey drive systems were entered through the teletype also. The commands were then transmitted through the computer to the respective drive systems.

The wake survey drive could operate in either of two modes. In the first, or manual, mode the initial and final locations of the probe in the tunnel as well as the number of steps between were the input parameters. In the second, or automatic, mode the computer determined the upper and lower boundaries of the airfoil wake automatically by first making a continuous sweep of the survey probe through the tunnel before the data recording sequence began. Because of limitations in the speed and memory capability of the computer used, this automatic mode was not fully successful on this early data acquisition system.

The wake survey drive system was also synchronized with the scanivalves so that the probe was moved to a different vertical location each time that the scanivalves were advanced to a new port. If more survey probe points were desired than scanivalve ports, the probe continued on its traverse after the scanivalves had reached their last port at the speed and dwell time that were previously set.

Current Capability

As previously mentioned, in 1981 an enlarged on-site data acquisition and control room was constructed. The tunnel controls were moved to this new location and installation of a new on-site data acquisition system was begun. This system became operational in early 1982. The purpose of this new system was to increase the number of digital and analog channels available, provide more real-time data reduction capability, provide a capability for future on-site post-run data reduction, and, in general, increase the accuracy and reliability of the data acquisition system.

This current data acquisition system consists of a high-speed microcomputer with 1 megabyte of random access memory, a 256-megabyte hard disk unit, a tape drive unit, a high-speed line printer, an analog-to-digital front end, and CRT displays for alpha numerics and graphics. Two software programs are used to operate the system: (1) An operating and acquisition program (OAP) acquires data from the analog-to-digital front end and records these raw data on magnetic tape as well as on the line printer. (2) A real-time program (RTP) computes tunnel parameters, model data, and wake survey data; controls the angle-of-attack and survey drive systems; and provides visual output on CRT and LED displays for tunnel operators and test engineers. Photographs of various parts of this system are presented in figure 23.

The analog front end of the system is configured to acquire data from 192 analog channels with five programmable ranges from 8.191 mV full scale to 131.06 mV full scale. The resolution of the raw data is 1 part in 8191 for a sensitivity of 1 data count per microvolt on the lowest range. Each channel has a 10-Hz low-pass filter installed to reduce dynamic effects. If a future need arises, the number of channels installed can be increased and the filter cutoff frequency can be changed easily.

The control of the survey probe system with this data acquisition system is essentially the same as with the original system. One important advantage, however, is that the automatic mode is now fully operational and has been very successful in routine operations.

Tunnel-Drive Monitoring System

During the operation of the tunnel it is necessary to monitor and record various temperatures, pressures, accelerations, and power-consumption readings for the main

drive motor, fan bearing assembly, and auxiliary drive units. This is accomplished by the use of a stand-alone datalogger unit, which has the capability to monitor 50 channels, give a visual display of engineering units for any selected channel, and provide a printed record of all channels automatically at preselected time intervals. In addition, dual alarm levels can be set for critical measurements. The first alarm gives both a visual and audible signal that some parameter is near a critical value. If corrective action is not taken, the second alarm level can automatically shut the tunnel down in a fail-safe mode. Use of this system has considerably reduced the manpower necessary to operate the facility. An oscilloscope for monitoring proximity pickups on the main drive shaft and television monitors for viewing critical areas while running are also incorporated in this monitoring system for safety purposes. A photograph of the tunnel control consoles is presented in figure 24.

CALIBRATION TESTS OF 8 × 24 TEST SECTION

Range of Tests

The calibration tests of the 8 × 24 test section were conducted at stagnation pressures of about 1.2, 3.1, 5.1, and 6.0 atm and at stagnation temperatures of about 300 K, 200 K, and 100 K. The Mach number was varied from a minimum of 0.20 to a maximum of about 0.92 in increments of 0.10 at the lower Mach numbers and of 0.05 at Mach numbers above 0.70. These test conditions covered most of the operational envelope of the facility. During this investigation, the test section was empty and the wake survey probe was installed at the downstream location in a fixed position on the tunnel vertical centerline. All four tunnel walls were set parallel to the tunnel centerline.

Results from two sets of calibration data are presented in this paper. The original calibration runs were conducted in July 1980 on the original data acquisition system, and check calibration runs were made in February 1984 on the current data system. The data recorded during these investigations consisted of measurements of the static pressure distributions at various locations throughout the tunnel circuit (along the test-section sidewalls, floor, and ceiling) and of detailed distributions along five rows of orifices on the turntables. A sketch of this instrumented turntable showing orifice locations is presented in figure 25. An array of thermocouple probes was located in the settling chamber upstream of the screens to determine the total temperature distribution in this area. Measurements of the power delivered to the drive motor were also recorded.

Corrections to Data

Because of the pressure and temperature levels at which this facility operates, all data measurements must be corrected for real-gas effects. All data presented in this paper have been corrected using the procedure presented in reference 16. In general, these corrections amounted to less than 1 percent of the uncorrected values in the most extreme cases.

PRESENTATION OF RESULTS

The results of sidewall static pressure measurements are presented as plots of local Mach number distribution as a function of longitudinal distance. Detailed

plots for the various areas of the test section are presented for all the combinations of stagnation pressure and temperature achieved during this test program. An index to these figures is presented in the following table:

Result	p_t, atm	Figure
Longitudinal distribution of Mach number along test-section floor	1.2	26
	3.1	27
	5.1	28
	6.0	29
Longitudinal distribution of Mach number along test-section ceiling	1.2	30
	3.1	31
	5.1	32
	6.0	33
Mach number distribution along test-section left turntable	1.2	34
	3.1	35
	5.1	36
	6.0	37
Mach number distribution along test-section right turntable	1.2	38
	3.1	39
	5.1	40
	6.0	41
Mach number distribution along contraction-section sidewall	1.2	42
	3.1	43
	5.1	44
	6.0	45
Mach number distribution along diffuser sidewall	1.2	46
	3.1	47
	5.1	48
	6.0	49
Calibration factor as function of R		50
Calibration factor curve fit		51
Typical temperature distribution		52
Drive motor power versus fan speed		53
Fan pressure ratio correlation		54
Operational envelope curves		55
Time variation of parameters		56, 57
Sidewall boundary-layer parameters		58

DISCUSSION

During this investigation, the test section was empty and the wake survey probe was installed at the downstream location in a fixed position on the tunnel vertical centerline. All four tunnel walls were set parallel to the tunnel centerline.

Local Mach Number Distributions

Floor and ceiling distributions.- The longitudinal local Mach number distributions along the centerline of the test-section floor are presented in figures 26 through 29 and along the test-section ceiling in figures 30 through 33. For Mach numbers up to about 0.80, the distribution is relatively flat for all values of stagnation pressure and temperature. At the higher Mach numbers, the test section has a slight negative Mach number gradient followed by an increase at about 10 in. downstream of station 0.0. This is the result of blockage caused by the wake survey probe that was located longitudinally at station 10.25 in. (26 cm) and was centered between the tunnel floor and ceiling. Thus, the similarity of the signature on the floor and ceiling is to be expected.

Turntable distributions.- The distributions of local Mach number along five orifice rows on the left turntable are presented in figures 34 through 37 and along the right turntable in figures 38 through 41. A sketch showing the orientation of these five orifice rows is presented in figure 25. At the top of each of these figures on Mach number distribution, a key is presented giving values of M_{TC}, M, and ΔM_{AV}.

The test-chamber reference Mach number M_{TC} is the Mach number based on the measured static pressure from the reference orifices located on the test-section sidewall as far upstream as physically possible. For this measurement, four orifices, two on each sidewall, are interconnected to give an averaged reading. The average test-section Mach number M is defined as the average of the local Mach numbers measured at the 36 orifices on each turntable. The parameter labeled ΔM_{AV} is the standard deviation of M_l (the measured local stream Mach number) from M (the average test-section Mach number).

In general, these figures do not indicate the presence of any significant Mach number gradients in either the vertical or horizontal planes in the test-section region at Mach numbers below 0.80 for all test conditions. At Mach numbers below about 0.80, where the majority of two-dimensional airfoil testing occurs, the standard deviation of Mach number in the model test region is generally about 0.002 or less. This value is considered to be reasonable for this type of facility. At the higher values of Mach number, however, a longitudinal gradient does exist because of the presence of the survey probe, as was mentioned previously.

Contraction distributions.- The longitudinal local Mach number distributions along the wall of the contraction section were measured during the February 1984 calibration and are presented in figures 42 through 45 for the various stagnation pressures and temperatures. In general, these data indicate a smooth, gradual increase in velocity with length as desired. However, two local areas of discontinuity are observed and are located between stations -39.37 in. (-100 cm) and -45.28 in. (-115 cm) and at the final orifice, station -32.28 in. (-82 cm). Upon examination of the contraction section when it was later removed from the tunnel

circuit, it was found that measurable differences in the "design" and "as built" ordinates exist in these two areas and account for the observed variations in Mach number distribution.

Diffuser distributions.- The longitudinal local Mach number distributions along the wall of the diffuser section were also measured during the February 1984 calibration and are presented in figures 46 through 49 for the various stagnation pressures and temperatures. Again, the data indicate a smooth and gradual deceleration of local Mach number with length as desired. It should be noted, however, that the Mach number at the final measurement station is only about one-half the value at the first station for all test conditions. The area ratio between these two stations, as listed in figure 8, is about 3. This difference between the ratios of cross-section area and Mach number indicates that some separation is occurring in the diffuser, probably associated with the large local wall angles on the upstream sidewalls. The equivalent conical half-angle in this upstream area is on the order of 5° as indicated in the table in figure 8. This is well above 3°, which is generally accepted as the value at which separation can occur for this type of diffuser. Although some separation is possible with this diffuser design, it is the best design that could be employed at the time of construction because of the constraints of length and diameter imposed by adapting an existing tunnel configuration.

Determination of Calibration Factor

A calibration factor has been developed that enables the determination of the test-section Mach number from an upstream reference Mach number with a model installed. This calibration factor, defined as ΔM in this paper, is the difference between the reference test-chamber Mach number M_{TC} and the average test-section Mach number M. Plots of this parameter as a function of Reynolds number for various reference Mach numbers are presented in figure 50. Two sets of calibration data are presented; the first was obtained in July 1980 on the original data acquisition system and the second was obtained in February 1984 on the current data acquisition system. From these data it is apparent that the calibration factor for this facility is a function of the test Reynolds number. The repeatability of the data from the 1980 calibration to the 1984 calibration is good for most cases. The exception is for the left turntable (flagged symbols) at the higher Mach numbers. This exception is attributed to the warping of the tunnel sidewall in this region with time. As a result of this warping, the left turntable was no longer parallel to the tunnel centerline but was inclined a small fraction of a degree.

A linear curve fit program was applied to the 1980 data to obtain slope and intercept constants that could be used in automatic data reduction programs. The values of the slope m and the axis intercept b of this curve fit were plotted as a function of the reference Mach number, and the results are presented in figure 51. These values were then curve fitted using a fifth-power polynomial, and the resulting constants were programmed into the airfoil data reduction program. This curve fit is also plotted in figure 51. Because the results of the 1984 check calibration were generally within acceptable limits of the 1980 results, no changes to the data reduction procedures were made.

Stagnation Temperature Distribution

An array of 25 copper constantan thermocouple probes was located upstream of the screens in the settling chamber of the facility during the tunnel calibration

runs. The purpose of this array was primarily to determine the stagnation temperature distribution in this region. A sketch of this thermocouple array is shown in figure 52 along with a table listing the individual temperatures for a Mach number of 0.70, a Reynolds number of 50.1×10^6, and an average stagnation temperature of 105.9 K. For this case, the standard deviation of the local temperatures from the average is 0.20 K. This distribution of temperature is considered to be very good, especially when considering the problems that could have been introduced with the injection of liquid nitrogen into the tunnel circuit. A listing of the average temperature and the standard deviation in stagnation temperature for all data points in the calibration is presented as table III. An examination of these results indicates a maximum deviation on the order of 0.5 K with no evidence of any systematic variation with either stagnation pressure, stagnation temperature, or Mach number.

Power Requirements

During the tunnel calibration tests, a type of transducer was attached to the drive motor controls that provided an analog output proportional to the electrical power delivered to the drive motor. The results of these measurements are presented in figure 53 as a function of fan speed for several values of stagnation pressure. Also plotted in this figure is the drive motor power limit which increases linearly with fan speed. Several points are to be noted from this figure. First, at a stagnation temperature of 300 K, the maximum Mach number obtainable before reaching the fan speed limit of 5600 rpm is about 0.7. As the temperature is decreased, the fan speed restraints are alleviated and the maximum obtainable Mach number is then limited by choking in the entrance to the diffuser. This choking condition and the consequent requirement for large amounts of drive power limit the operation to a Mach number of about 0.9. For the minimum stagnation temperature of 105 K, the maximum Mach number at the maximum stagnation pressure is also limited to about 0.85 by the available drive power. All these limits are for tunnel-empty conditions and will vary because of additional blockage when models are installed.

To provide information on the required fan drive power, the pressure rise across the fan was also recorded. Details of these measurements have been presented in reference 17 and the required fan pressure ratio was correlated as a function of Mach number and Reynolds number. Figure 54, taken from reference 17, presents this fan pressure correlation.

Operational Envelope

As seen in the drive power curves, there are several constraints on the tunnel operational envelope. To provide a guide for planning tests in this facility, operational curves of the required stagnation pressures and temperatures for constant Reynolds numbers were developed using the computer program outlined in reference 18. Superimposed on these plots are lines defining boundaries such as maximum fan speed, saturation temperature limits, and drive-motor power limits. Again, these curves are approximate and are for tunnel-empty conditions. Samples of these operational curves for several Mach numbers are shown in figure 55.

Time Variations of Tunnel Parameters

Variations of measured and calculated tunnel parameters with time were obtained during a recent test of a 12-percent-thick symmetrical supercritical airfoil at zero

lift coefficient, and the results are presented in figures 56 and 57 for Mach numbers of 0.60 and 0.80, respectively. These data are presented to give an indication of the controllability of the facility during a typical airfoil test program. All values are plotted as ratios of the incremental variations from the mean to the mean except for stagnation temperature, fan speed, and Mach number where only the incremental values are shown. These data were obtained at a scan rate of 20 scans per second and an averaging time of either 0.5 or 1.0 sec. Thus, each point shown is actually the average of 10 or 20 individual scans. The data points with the longer averaging time are evident by the longer time scale on the plotted results. The results show that at a Mach number of 0.60, the test conditions were held well within acceptable limits for all Reynolds numbers with the variations in dynamic pressure being generally less than 1/2 percent and in Mach number less than 0.002. At a Mach number of 0.80 (fig. 57), short-duration spikes in the fan speed are noted for all Reynolds numbers tested. These variations in fan speed result in the observed spikes in the other related parameters. For example, at a Reynolds number of 6×10^6, variations in dynamic pressure of about 1.5 percent and in Mach number of about 0.01 are observed. Although the causes of these short-duration spikes are not understood at present, they do indicate that improvements to the drive control system at the highest Mach numbers are required for optimal performance of the facility.

Flow Quality

Limited tests have been made at various times to determine the flow quality of the facility and to develop techniques for making these measurements at transonic and cryogenic conditions. One of these tests, described in reference 19, used a three-wire hot-wire probe to determine the temperature, velocity, and density fluctuations in the 8×24 test section at Mach numbers up to 0.70. The conclusions of reference 19 indicate the temperature fluctuations to be from about 0.05 to 0.3 percent and the velocity and density fluctuations to be between 0.3 and 4.5 percent. The major disturbances at the higher Mach numbers were determined to be caused by sound from the diffuser moving upstream. With the installation of the adaptive-wall test section, improvements in the diffuser were made and these levels of disturbance should be reduced.

It should be mentioned that with this type of hot-wire probe, the variations in velocity, density, and total temperature can be measured directly; whereas with a single-wire probe, as has been widely used in the past, only mass flow variations could be measured. These mass flow variations have been referred to as velocity variations in the literature. If the data from the three-wire probe are reduced to give mass flow variations, the results are about an order of magnitude lower than the values mentioned previously. Reference 20 contains a discussion of these variations in more detail and presents a comparison of the data from reference 19 in several forms.

Another test, described in reference 21, was made to determine if step changes or "temperature fronts" could be detected in the flow for several tunnel circuit times after an abrupt change in liquid nitrogen injection rate had been made. Although some theoretical and experimental evidence had shown that this condition could exist, reference 21 concluded that there were no indications of temperature fronts in the 0.3-m TCT resulting from significant changes in the rate of liquid nitrogen injection.

Sidewall Boundary-Layer Distributions

During the course of the initial tunnel calibrations and subsequent calibrations of the sidewall boundary-layer removal system, measurements of the stagnation pressure distribution through the sidewall boundary layer were made at locations 6.12 in. (15.54 cm) and 15.25 in. (38.74 cm) upstream of the turntables. Measurements were made with the porous boundary-layer removal plates installed and also with the solid plates installed in the test-section sidewalls between these two probe locations. Details of some of these measurements in terms of displacement thickness, momentum thickness, and shape parameter have been presented in references 13 and 22 for the case with the porous plates installed.

In recent years it has been recognized that the interference from the tunnel sidewall boundary layer can affect the data obtained in two-dimensional-airfoil tests. Reference 23 presents a method to correct for these effects, but information on the displacement thickness and shape parameter of the tunnel-empty sidewall boundary layer at the center of the model location is required. Using some of the data obtained during the tests reported in reference 13 for the solid plates installed, the values of displacement thickness and shape parameter at the model centerline location were determined using the integral boundary-layer calculation method of reference 24. Results of these calculations at Mach numbers from 0.30 to 0.76 are presented in figure 58 for Reynolds numbers from 3×10^6 to 30×10^6. These data are presented to provide information for the correction of airfoil data with the solid sidewall plates installed.

CONCLUDING REMARKS

The Langley 0.3-Meter Transonic Cryogenic Tunnel is the world's first transonic cryogenic pressure tunnel and has been extensively used for testing two-dimensional-airfoil sections. With the 8- by 24-in. (20.32- by 60.96-cm) test section installed, the facility is capable of operation from Mach numbers of about 0.20 to about 0.90. The stagnation pressure can be varied from 1.2 to 6.1 atm and the stagnation temperature can be varied from 80 K to 327 K. For a 6.0-in. (15.2-cm) model chord, a maximum Reynolds number of about 45×10^6 can be obtained.

Results of tunnel-empty calibration tests indicate acceptable Mach number distributions in the test region with a standard deviation generally of about 0.002 for Mach numbers up to about 0.80. Stagnation temperature distributions in the settling chamber were extremely good with an average standard deviation of about 0.2 K. At ambient stagnation temperatures, drive-system speed restraints limited the maximum Mach number to about 0.7. At lower temperatures, the Mach number is limited to about 0.90 by choking of the flow at the diffuser entrance.

Data obtained with an airfoil installed in the test section demonstrate that the automatic control systems can maintain tunnel conditions within acceptable tolerances at the lower speeds. At Mach numbers near 0.8, however, some improvements in the speed control system are seen to be desirable.

NASA Langley Research Center
Hampton, VA 23665-5225
July 9, 1987

REFERENCES

1. Kilgore, Robert A.; Goodyer, Michael J.; Adcock, Jerry B.; and Davenport, Edwin E.: The Cryogenic Wind-Tunnel Concept for High Reynolds Number Testing. NASA TN D-7762, 1974.

2. Kilgore, Robert A.: Design Features and Operational Characteristics of the Langley 0.3-Meter Transonic Cryogenic Tunnel. NASA TN D-8304, 1976.

3. Ray, Edward J.; Ladson, Charles L.; Adcock, Jerry B.; Lawing, Pierce L.; and Hall, Robert M.: Review of Design and Operational Characteristics of the 0.3-Meter Transonic Cryogenic Tunnel. NASA TM-80123, 1979.

4. Ladson, Charles L.; and Ray, Edward J.: Status of Advanced Airfoil Tests in the Langley 0.3-Meter Transonic Cryogenic Tunnel. Advanced Aerodynamics - Selected NASA Research, NASA CP-2208, 1981, pp. 37-53.

5. Ladson, Charles L.: A New Airfoil Research Capability. Advanced Technology Airfoil Research, Volume I, NASA CP-2045, Part 1, 1979, pp. 425-432.

6. Barnwell, Richard W.: Design and Performance Evaluation of Slotted Walls for Two-Dimensional Wind Tunnels. NASA TM-78648, 1978.

7. Wolf, S. W. D.; and Goodyer, M. J.: Self Streamlining Wind Tunnel - Low Speed Testing and Transonic Test Section Design. NASA CR-145257, 1977.

8. Wolf, S. W. D.: Self Streamlining Wind Tunnel - Further Low Speed Testing and Final Design Studies for the Transonic Facility. NASA CR-158900, 1978.

9. Kilgore, Robert A.: The NASA Langley 0.3-m Transonic Cryogenic Tunnel. Special Course on Cryogenic Technology for Wind Tunnel Testing, AGARD-R-722, July 1985, pp. 13-1 - 13-15.

10. Balakrishna, S.: Modeling and Control of Transonic Cryogenic Wind Tunnels: A Summary Report. NASA CR-159376, 1980.

11. Balakrishna, S.: Automatic Control of a Liquid Nitrogen Cooled, Closed-Circuit, Cryogenic Pressure Tunnel. Research Grant NSG 1503, Old Dominion University Research Foundation, Mar. 1980. (Available as NASA CR-162636.)

12. Lawing, Pierce L.; Dress, David A.; and Kilgore, Robert A.: Description of the Insulation System for the Langley 0.3-Meter Transonic Cryogenic Tunnel. NASA TM-86274, 1985.

13. Murthy, A. V.; Johnson, Charles B.; Ray, Edward J.; Lawing, Pierce L.; and Thibodeaux, Jerry J.: Studies of Sidewall Boundary Layer in the Langley 0.3-Meter Transonic Cryogenic Tunnel With and Without Suction. NASA TP-2096, 1983.

14. Balakrishna, S.: Effects of Boundary-Layer Treatment on Cryogenic Wind-Tunnel Controls. NASA CR-159372, 1980.

15. Bynum, D. S.; Ledford, R. L.; and Smotherman, W. E.: Wind Tunnel Pressure Measuring Techniques. AGARD-AG-145-70, Dec. 1970.

16. Adcock, Jerry B.: Real-Gas Effects Associated With One-Dimensional Transonic Flow of Cryogenic Nitrogen. NASA TN D-8274, 1976.

17. Lawing, Pierce L.; Adcock, Jerry B.; and Ladson, Charles L.: A Fan Pressure Ratio Correlation in Terms of Mach Number and Reynolds Number for the Langley 0.3-Meter Transonic Cryogenic Tunnel. NASA TP-1752, 1980.

18. Dress, David A.: Computer Program for Calculating Flow Parameters and Power Requirements for Cryogenic Wind Tunnels. NASA TM-87609, 1985.

19. Stainback, P. Calvin; Johnson, Charles B.; and Basnett, Constance B.: Preliminary Measurements of Velocity, Density and Total Temperature Fluctuations in Compressible Subsonic Flow. AIAA-83-0384, Jan. 1983.

20. Johnson, C. B.; Johnson, W. G., Jr.; and Stainback, P. C.: A Summary of Reynolds Number Effects on Some Recent Tests in the Langley 0.3-Meter Transonic Cryogenic Tunnel. SAE Tech. Paper Ser. 861765, Oct. 1986.

21. Johnson, Charles B.; and Stainback, P. Calvin: Dynamic Measurement of Total Temperature, Pressure, and Velocity in the Langley 0.3-Meter Transonic Cryogenic Tunnel. NASA TP-2584, 1986.

22. Murthy, A. V.; Johnson, C. B.; Ray, E. J.; Lawing, P. L.; and Thibodeaux, J. J.: Investigation of the Effects of Upstream Sidewall Boundary-Layer Removal on a Supercritical Airfoil. AIAA-83-0386, Jan. 1983.

23. Barnwell, Richard W.; and Sewall, William G.: Similarity Rules for Effects of Sidewall Boundary Layer in Two-Dimensional Wind Tunnels. Wall Interference in Wind Tunnels, AGARD-CP-335, Sept. 1982, pp. 3-1 - 3-10.

24. Towne, Charles E.: Evaluation of Analytical Procedures for Prediction of Turbulent Boundary Layers on a Porous Wall. NASA TM X-3063, 1974.

TABLE I.- CONTRACTION-SECTION COORDINATES FOR 8 × 24 TEST SECTION[a]

Station, x		y dimension		z dimension		j dimension		h dimension		Area	
in.	cm	in.	cm	in.	cm	in.	cm	in.	cm	in^2	cm^2
0	0	13.440	34.138	13.440	34.138	5.567	14.140	5.567	14.140	598.58	3861.80
3.000	7.620	12.115	30.772	12.328	31.313	5.130	13.030	5.130	13.030	496.87	3205.61
6.000	15.240	10.705	27.191	11.900	30.226	5.000	12.700	5.015	12.738	431.02	2780.77
9.000	22.860	9.290	23.597	11.812	30.002	4.865	12.357	5.000	12.700	378.66	2442.96
12.000	30.480	7.860	19.964	11.820	30.023	4.730	12.014	5.000	12.700	328.92	2122.06
15.000	38.100	6.440	16.358	11.840	30.074	4.595	11.671	5.000	12.700	279.78	1805.03
16.000	40.640	5.967	15.156	11.848	30.094	4.550	11.557	5.000	12.700	263.39	1699.29
16.891	42.903	5.600	14.224	11.855	30.112	4.510	11.455	5.000	12.700	250.60	1616.77
18.062	45.877	5.209	13.231	11.864	30.135	4.457	11.321	5.000	12.700	236.88	1528.26
19.238	48.865	4.897	12.438	11.873	30.157	4.404	11.186	5.000	12.700	225.81	1456.84
20.423	51.874	4.651	11.814	11.882	30.180	4.351	11.052	5.000	12.700	216.92	1399.48
21.613	54.897	4.460	11.328	11.891	30.203	4.297	10.914	5.000	12.700	209.89	1354.13
22.807	57.930	4.316	10.963	11.900	30.226	4.244	10.780	5.000	12.700	204.45	1319.03
24.004	60.970	4.210	10.693	11.909	30.249	4.190	10.643	5.000	12.700	200.27	1292.06
25.202	64.013	4.136	10.505	11.918	30.272	4.136	10.505	5.000	12.700	197.16	1272.00
26.401	67.059	4.086	10.378	11.927	30.295					194.95	1257.74
27.600	70.104	4.052	10.292	11.936	30.317					193.45	1248.06
28.800	73.152	4.028	10.231	11.945	30.340					192.48	1241.80
30.000	76.200	4.014	10.196	11.954	30.363					191.94	1238.32
31.200	79.248	4.006	10.175	11.964	30.389					191.71	1236.84
32.400	82.296	4.002	10.165	11.973	30.411					191.66	1236.51
33.600	85.344	4.001	10.163	11.982	30.434					191.72	1236.90
34.800	88.392	4.000	10.160	11.991	30.457					191.87	1237.87
36.000	91.440	4.000	10.160	12.000	30.480					192.00	1238.71
38.630	98.120	4.000	10.160	12.000	30.480					192.00	1238.71

[a]See sketch in figure 5.

TABLE II.- CONTRACTION-SECTION COORDINATES FOR 13 × 13 TEST SECTION[a]

Station, x		y dimension		h dimension		Area	
in.	cm	in.	cm	in.	cm	in^2	cm^2
0	0	13.44	34.14	5.57	14.15	598.58	3861.8
.63	1.60	12.68	32.21	5.44	13.82	538.29	3472.8
3.27	8.31	12.43	31.57	5.40	13.72	519.18	3349.5
5.95	15.11	11.47	29.13	5.23	13.28	448.37	2892.7
8.60	21.84	10.58	26.87	5.07	12.88	387.03	2497.0
11.30	28.70	9.76	24.79	4.93	12.52	334.37	2157.2
13.94	35.41	9.01	22.89	4.80	12.19	289.27	1866.3
16.64	42.27	8.36	21.23	4.71	11.96	252.91	1631.7
19.40	49.28	7.83	19.89	4.67	11.86	225.26	1453.3
22.20	56.39	7.41	18.82	4.70	11.94	204.94	1322.2
25.03	63.58	7.07	17.96	4.78	12.14	189.45	1222.3
27.86	70.76	6.83	17.35	4.95	12.57	179.53	1158.3
30.75	78.11	6.64	16.87	5.17	13.13	172.04	1109.9
33.67	85.52	6.55	16.64	5.51	14.00	169.45	1093.2
36.63	93.04	6.50	16.51	5.95	15.11	168.40	1086.4
38.63	98.12	6.50	16.51	6.50	16.51	169.00	1090.3

[a]See sketch in figure 11.

TABLE III.- AVERAGE AND STANDARD DEVIATION IN STAGNATION TEMPERATURE MEASURED ON SURVEY RING IN SETTLING CHAMBER

(a) 300 K

Mach number	Stagnation pressure, atm	Reynolds number	$\bar{T}_t$, K	Standard deviation in T_t, K
0.20	1.4	0.9×10^6	298.4	0.12
.30	↓	1.4	298.5	.13
.40		1.8	298.3	.11
.50		2.2	300.6	.24
.60		2.4	301.8	.19
.71		2.7	303.9	.50
0.20	3.1	2.1×10^6	300.9	0.12
.30	↓	3.0	303.2	.12
.41		4.0	300.1	.45
.50		4.6	303.1	.36
.60		5.3	302.3	.18
.71		5.7	300.9	.07
0.20	5.1	3.5×10^6	303.4	0.10
.30	↓	5.0	302.5	.09
.40		6.5	299.3	.23
.50		7.8	299.4	.09
.60		9.0	300.5	.25
.70		10.1	298.3	.16
.75		10.2	303.1	.26
0.20	5.9	4.1×10^6	299.4	0.05
.30	↓	5.7	303.1	.09
.40		7.6	296.8	.12
.50		9.3	297.0	.24
.60		10.0	304.0	.31
.70		11.2	304.6	.30

TABLE III.- Continued

(b) 200 K

Mach number	Stagnation pressure, atm	Reynolds number	$\bar{T}_t$, K	Standard deviation in T_t, K
0.20	1.4	1.6×10^6	198.3	0.49
.30	↓	2.4	199.9	.50
.40		3.0	198.8	.41
.50		3.7	201.2	.50
.61		4.2	200.9	.41
.71		4.7	200.3	.35
.75		4.8	200.6	.22
.80		4.8	200.4	.27
.85		5.0	200.4	.25
.90		5.3	200.3	.37
.92		5.3	200.5	.38
0.20	3.1	3.6×10^6	200.6	0.10
.30	↓	5.2	198.4	.08
.41		6.7	198.9	.18
.50		8.0	200.6	.09
.60		8.9	201.9	.28
.70		10.1	200.4	.25
.75		10.7	200.3	.30
.80		11.0	201.1	.23
.85		11.3	202.0	.30
.90		11.8	199.9	.21
.94		11.8	200.2	.28
0.20	5.1	6.0×10^6	198.3	0.19
.30	↓	8.5	199.5	.16
.40		11.2	200.1	.16
.50		13.4	200.7	.21
.60		15.2	201.3	.22
.70		17.1	199.8	.17
.75		18.0	198.9	.19
.80		18.2	200.9	.18
.85		18.9	201.4	.19
.90		19.3	201.0	.22
0.20	5.9	7.1×10^6	197.1	0.23
.30	↓	9.7	201.5	.15
.40		12.9	201.2	.12
.50		15.1	203.4	.13
.60		17.9	201.6	.16
.70		19.6	201.2	.21
.75		19.9	203.9	.23
.80		21.1	201.3	.19
.85		21.2	204.1	.17

TABLE III.- Concluded

(c) 105 K

Mach number	Stagnation pressure, atm	Reynolds number	$\bar{T}_t$, K	Standard deviation in T_t, K
0.20	1.4	4.5×10^6	97.9	0.51
.30		6.7	98.5	.43
.40		8.3	100.3	.38
.50		9.5	100.6	.31
.60		11.9	100.4	.27
.70		13.0	97.4	.21
.75		13.3	98.8	.18
.80		13.4	100.8	.18
.90		14.4	100.4	.17
.94		14.2	103.0	.24
0.20	3.1	10.3×10^6	99.8	0.46
.30		14.6	100.1	.32
.40		17.4	103.3	.27
.50		22.6	99.8	.19
.60		23.9	102.7	.16
.70		27.2	103.0	.20
.75		28.4	102.2	.23
.80		31.2	98.8	.23
.85		32.8	97.5	.25
.90		33.7	98.4	.22
0.20	5.1	14.3×10^6	107.3	0.23
.30		22.3	105.4	.16
.40		26.8	108.8	.15
.50		35.8	103.1	.16
.60		38.8	106.1	.15
.70		43.9	105.8	.19
.75		45.0	106.4	.22
.80		44.5	109.3	.22
.85		48.1	106.6	.17
.94		49.2	106.9	.17
0.20	5.9	16.3×10^6	103.7	0.16
.30		26.8	102.5	.16
.40		33.6	102.8	.14
.50		39.7	104.1	.19
.60		46.4	102.8	.21
.70		50.1	105.9	.20
.75		51.2	106.5	.17
.80		56.5	102.8	.18
.87		54.7	107.4	.17

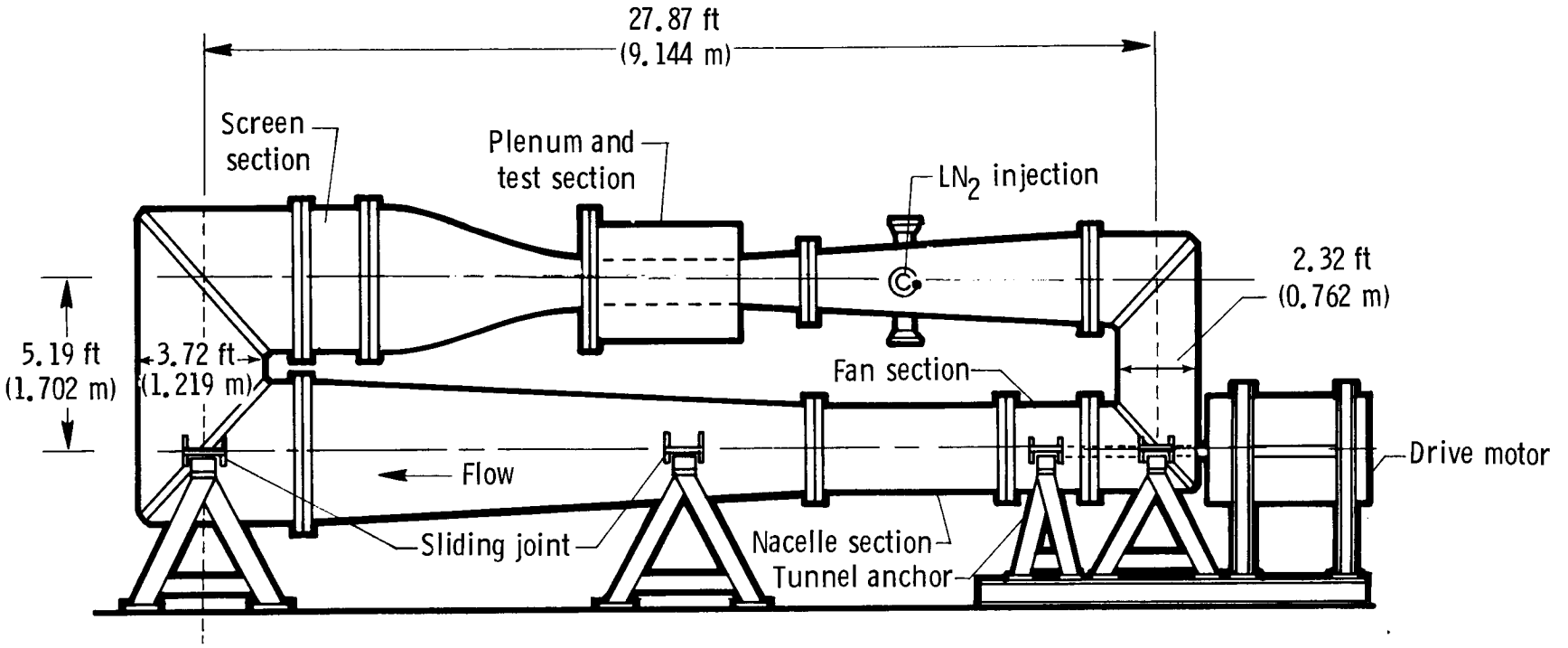

Figure 1.- Sketch of the Langley 0.3-m TCT with three-dimensional test section installed.

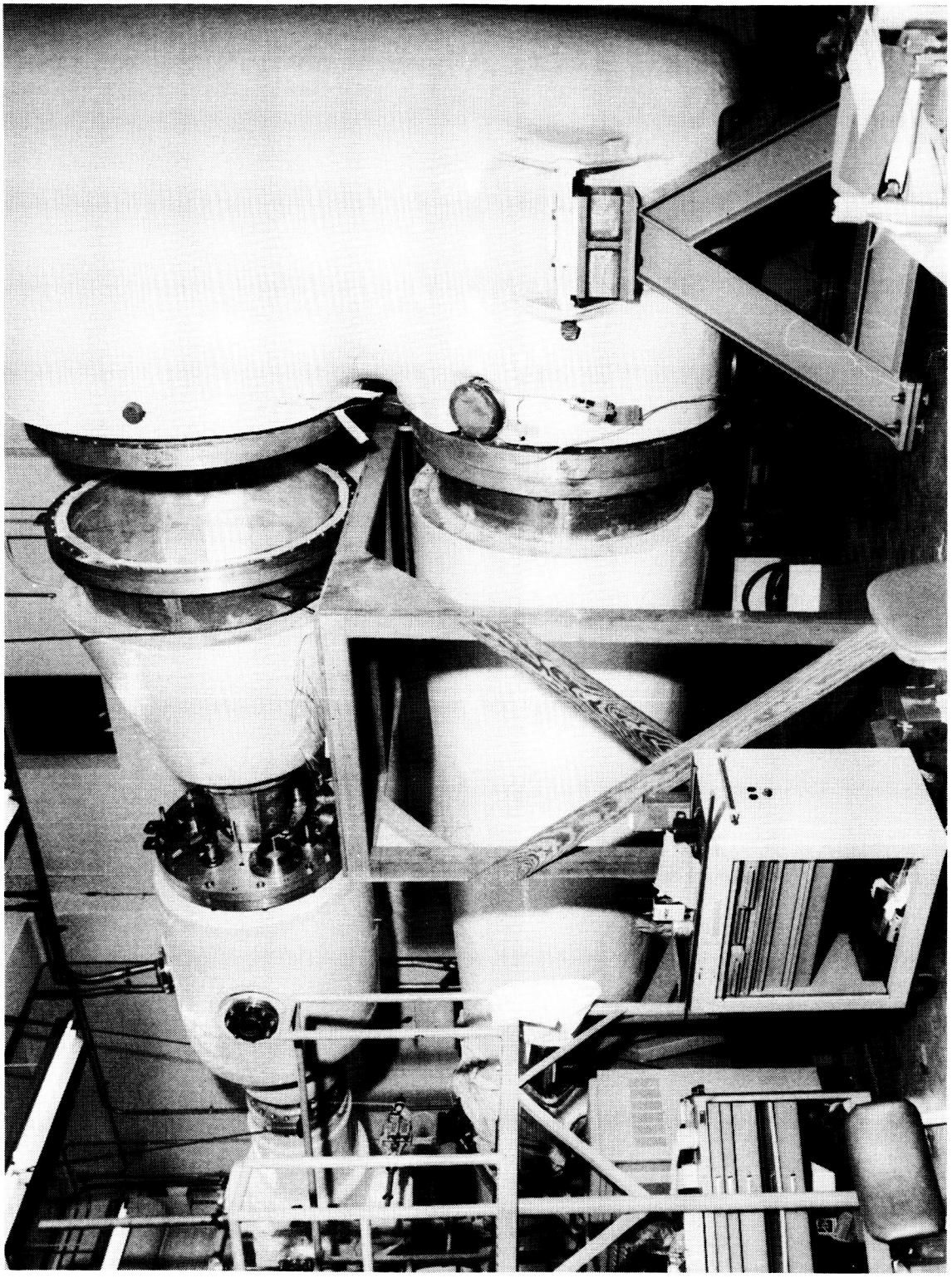

L-73-6155

Figure 2.- The Langley 0.3-m TCT with three-dimensional test section during initial assembly.

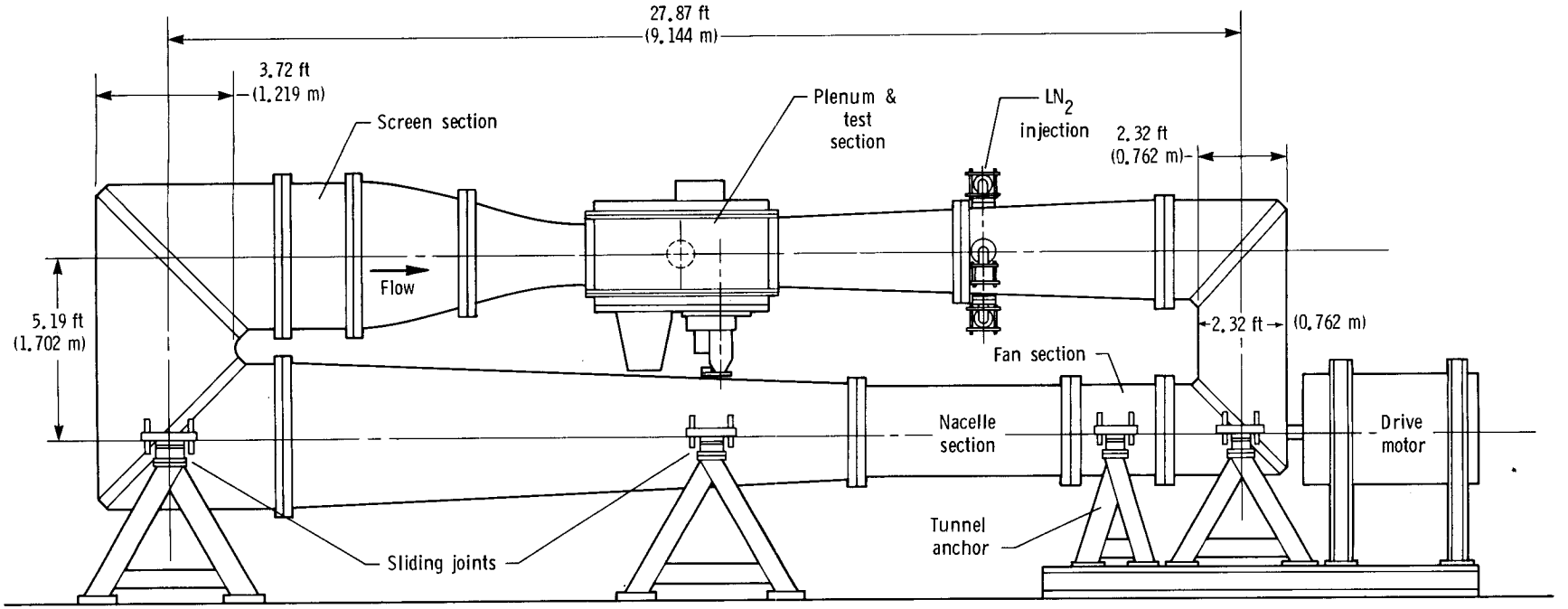

Figure 3.- Sketch of the Langley 0.3-m TCT with 8 × 24 two-dimensional test section installed.

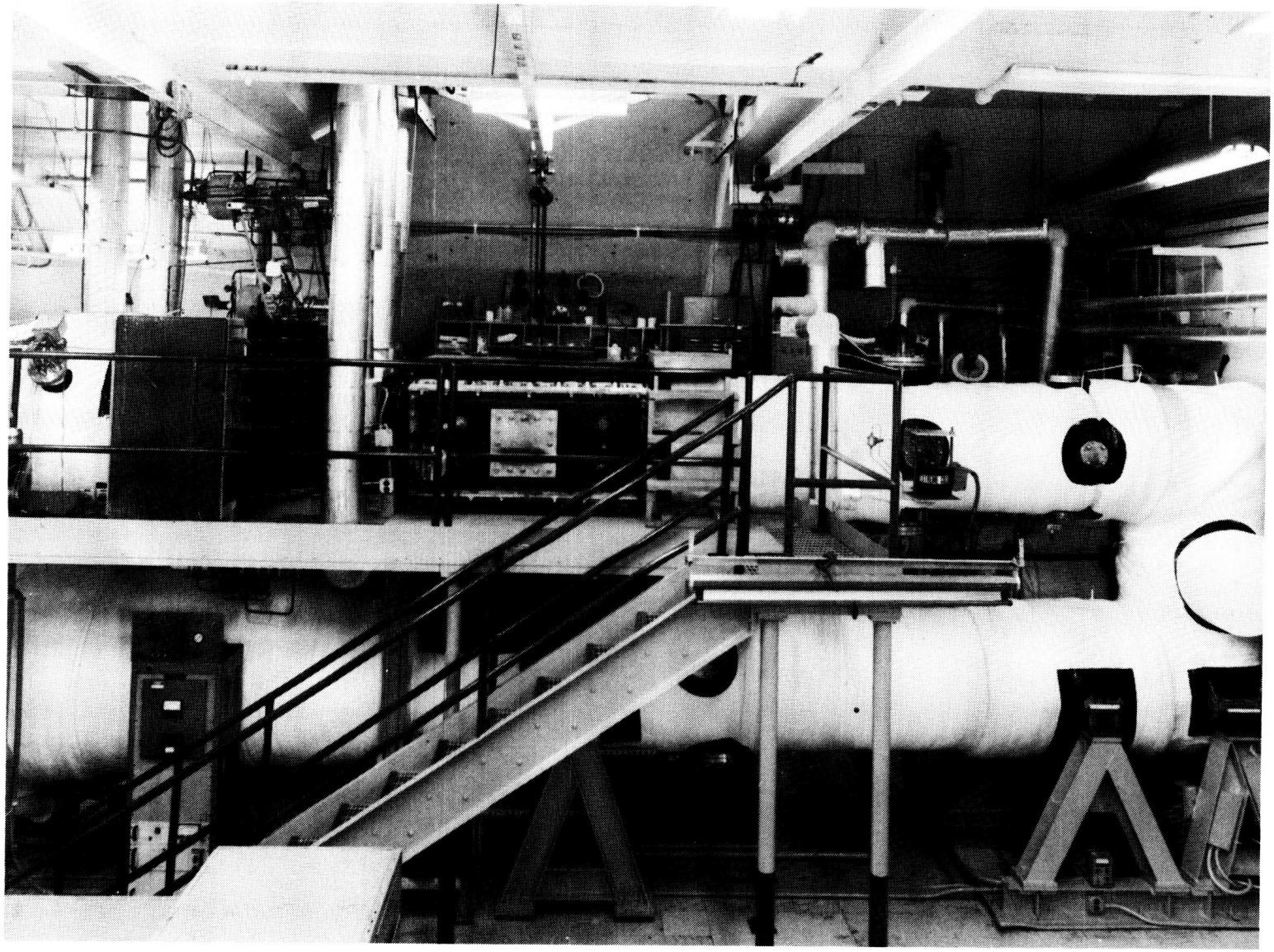

L-79-2147

Figure 4.- Elevation photograph of the Langley 0.3-m TCT with two-dimensional test section installed.

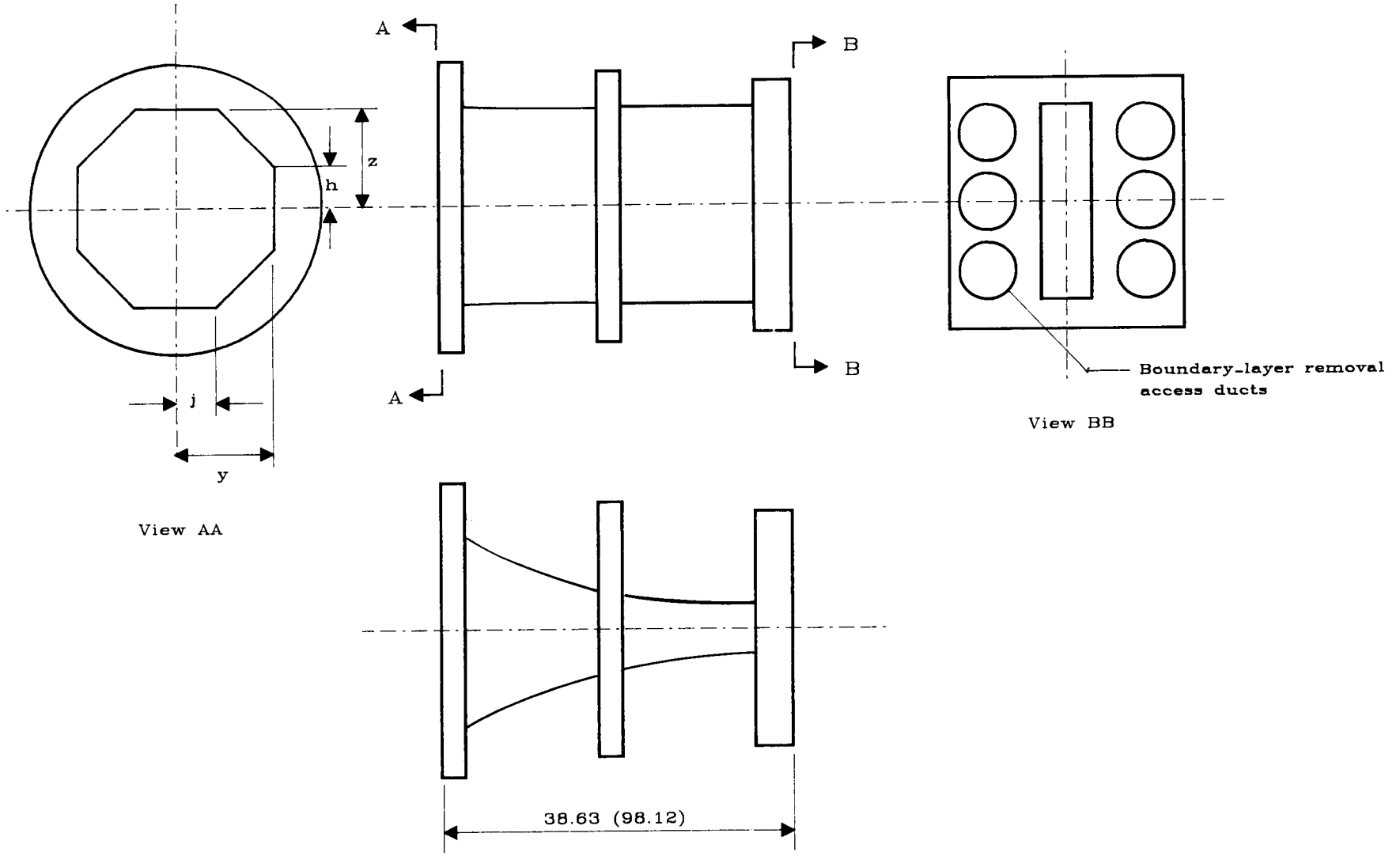

Figure 5.- Details of contraction section for 8 × 24 test section. See table I for ordinates. Linear dimensions are given in inches (centimeters).

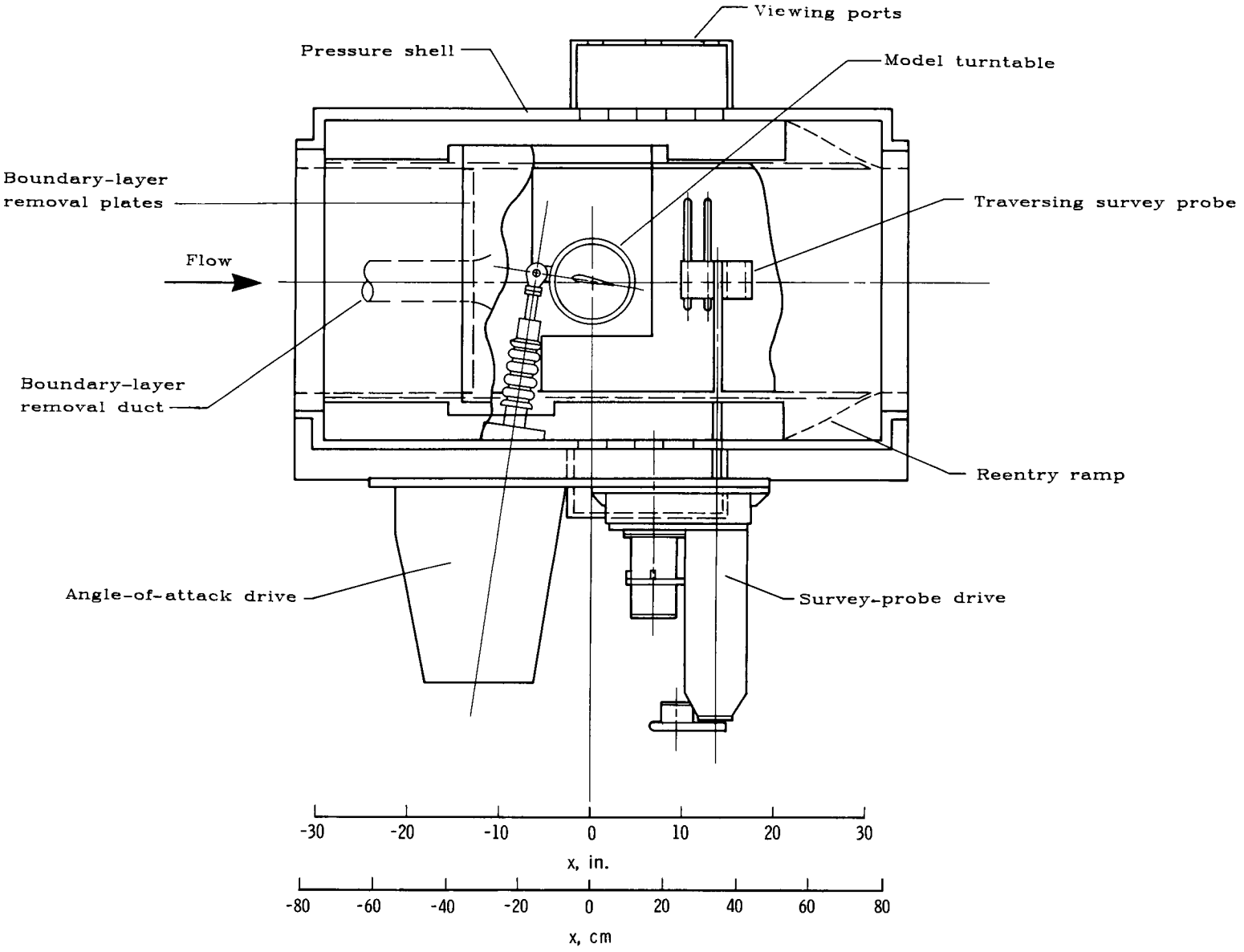

(a) Sideview of test section.

Figure 6.- Details of 8 × 24 test section.

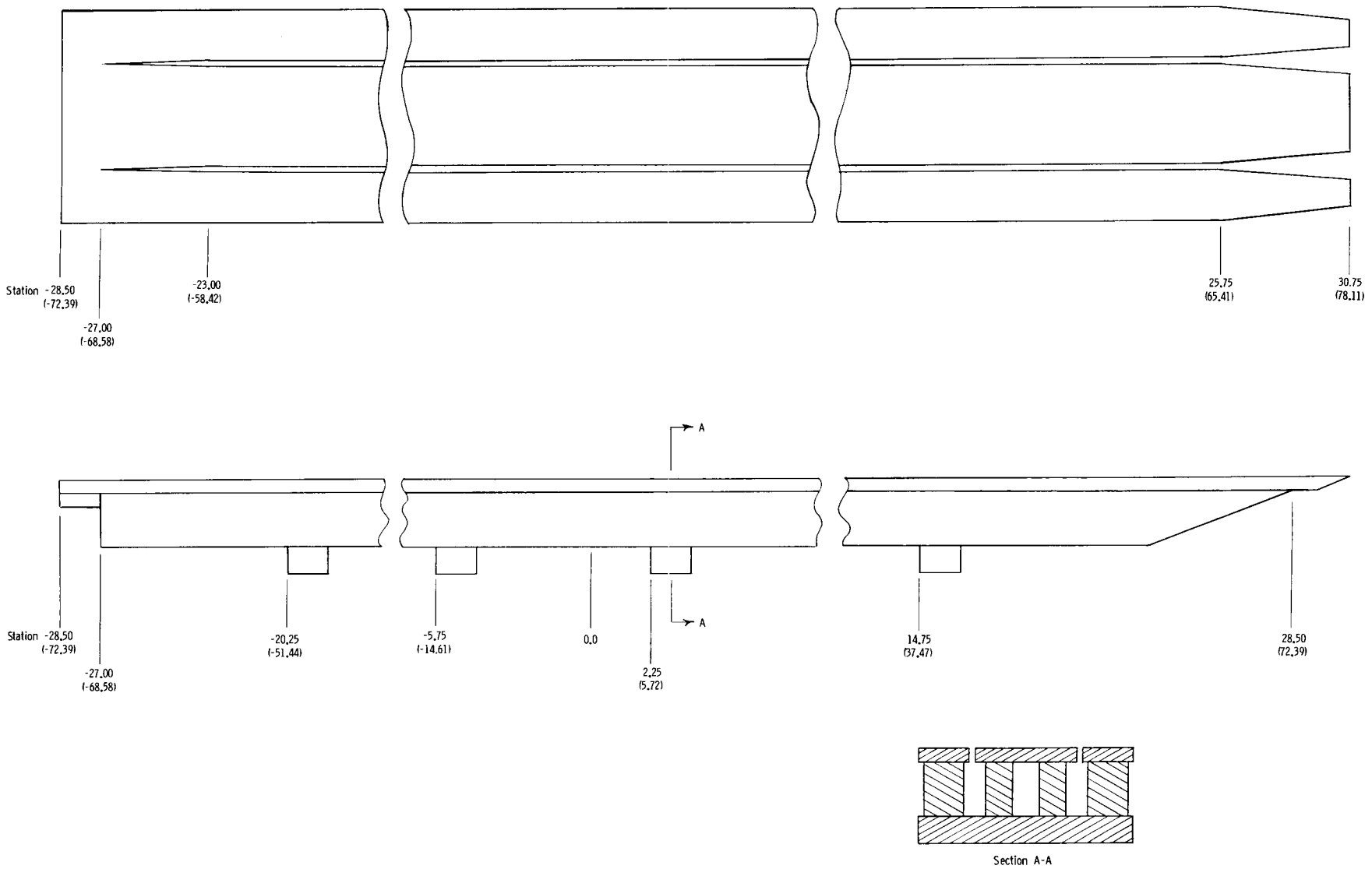

(b) Slotted top and bottom walls. Linear dimensions are given in inches (centimeters).

Figure 6.- Concluded.

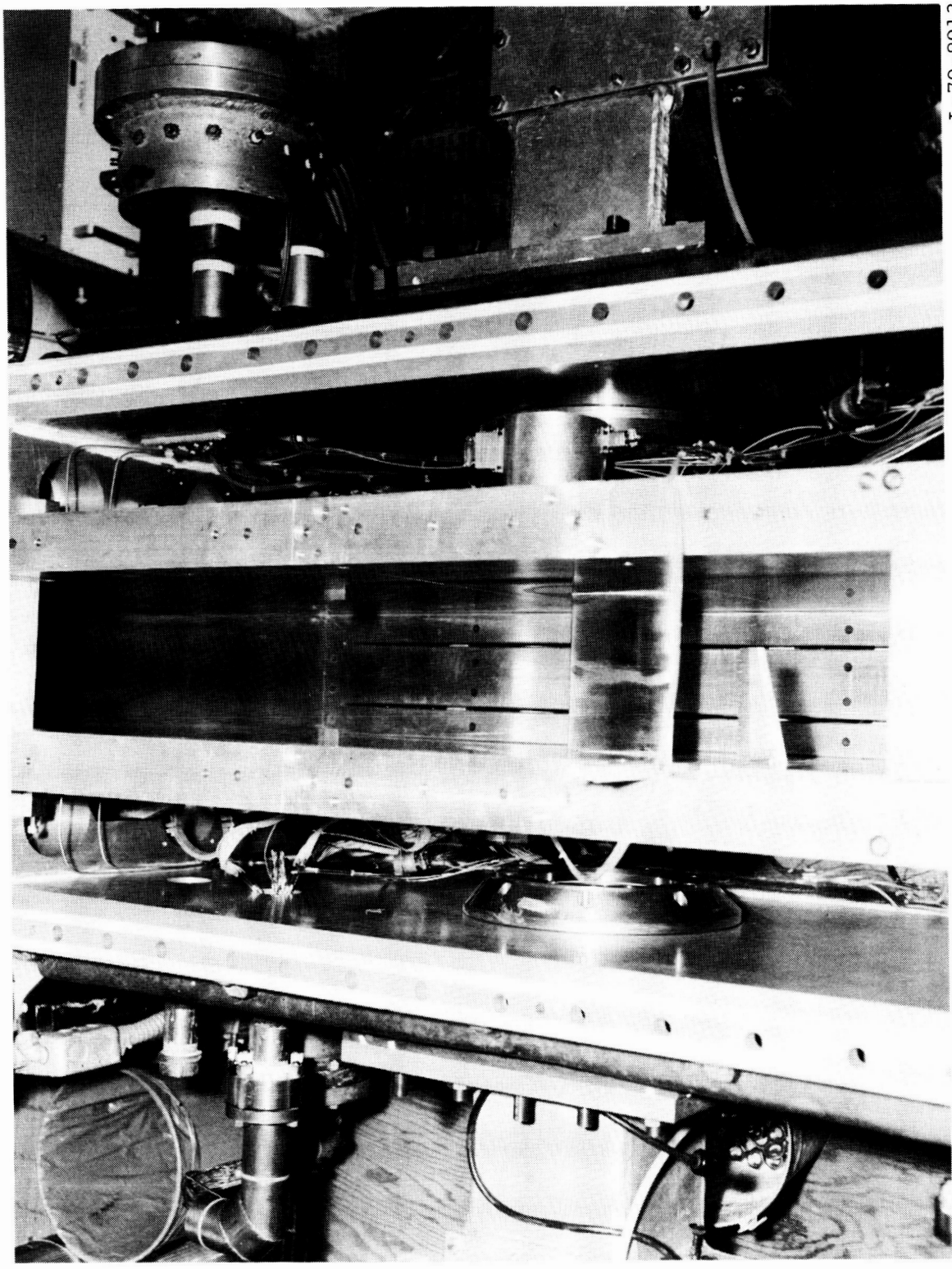

L-79-8913

Figure 7.- Photograph of top view of two-dimensional test section with airfoil model and wake survey probe installed.

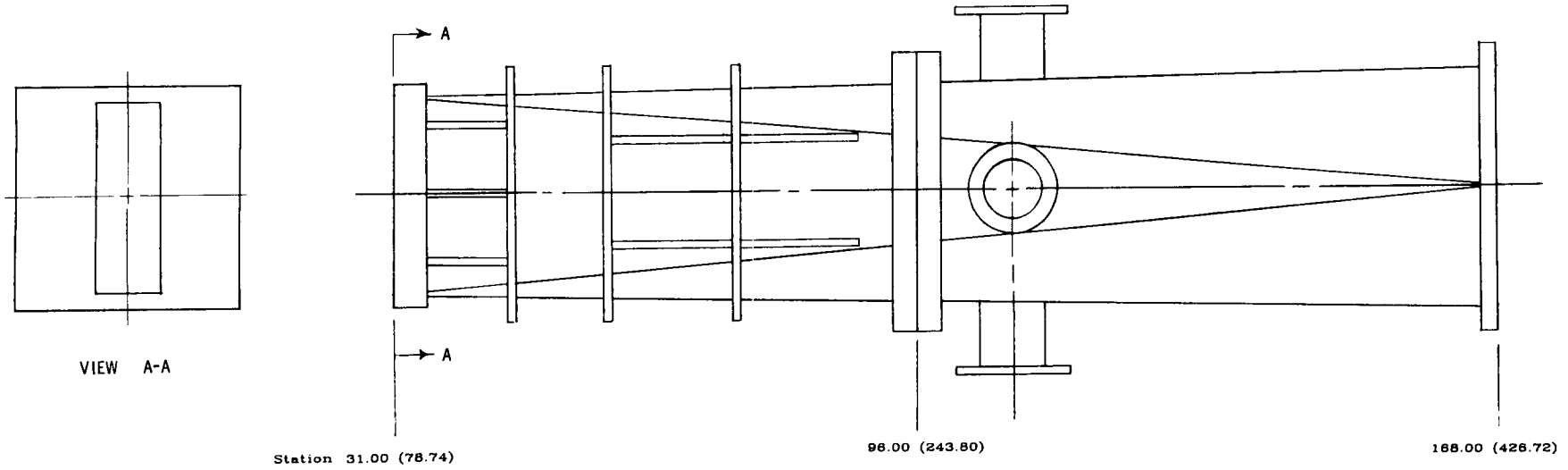

Longitudinal station		Area ratio	Conical half-angle
x, in.	x, cm		deg
31.00	78.74	1.020	
31.10	78.99	1.023	4.90
35.00	88.90	1.109	4.72
41.00	104.14	1.241	4.41
51.00	129.54	1.456	4.03
61.00	154.94	1.668	3.71
71.00	180.34	1.875	3.42
81.00	205.74	2.079	3.18
91.00	231.14	2.279	3.03
101.00	256.54	2.474	2.84
111.00	281.94	2.666	2.68
121.00	307.34	2.853	2.53
131.00	332.74	3.037	2.39
141.00	358.14	3.217	2.27
151.00	383.54	3.392	2.16
161.00	408.94	3.564	2.06
168.00	426.72	3.682	1.98

Figure 8.- Details of high-speed diffuser-transition section for two-dimensional test section. Linear dimensions are given in inches (centimeters).

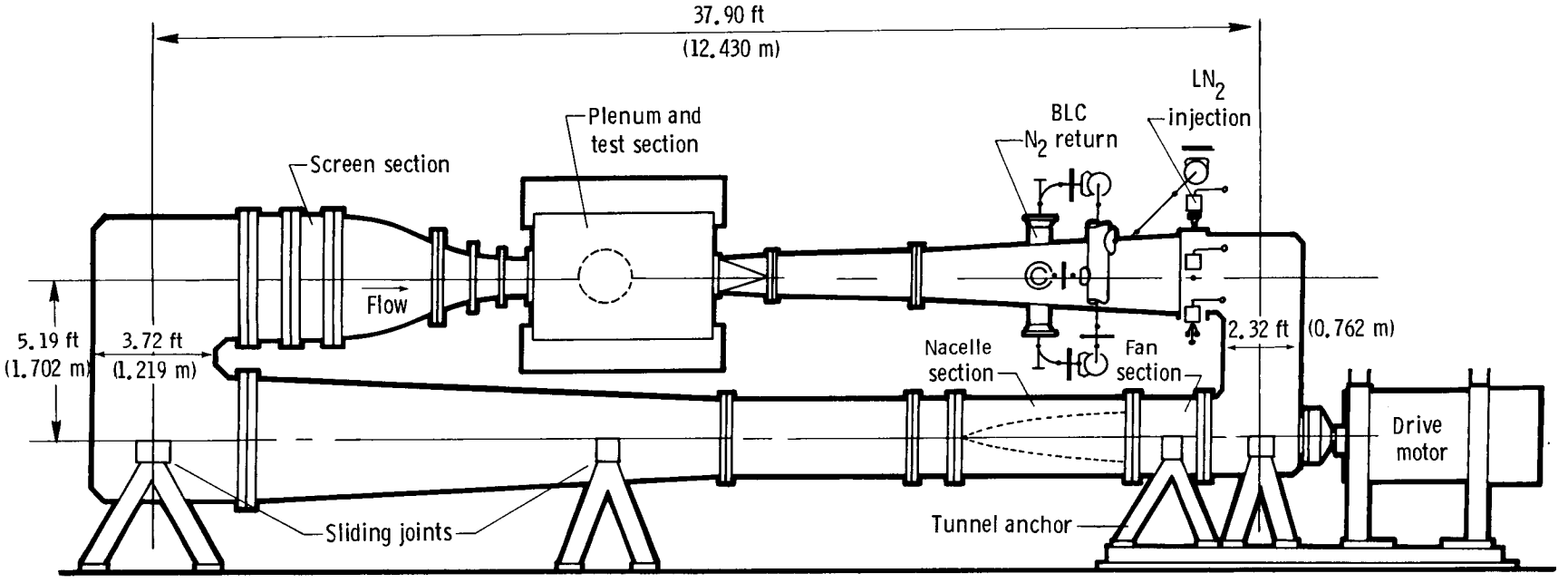

Figure 9.- Sketch of the Langley 0.3-m TCT with 13 × 13 two-dimensional test section installed.

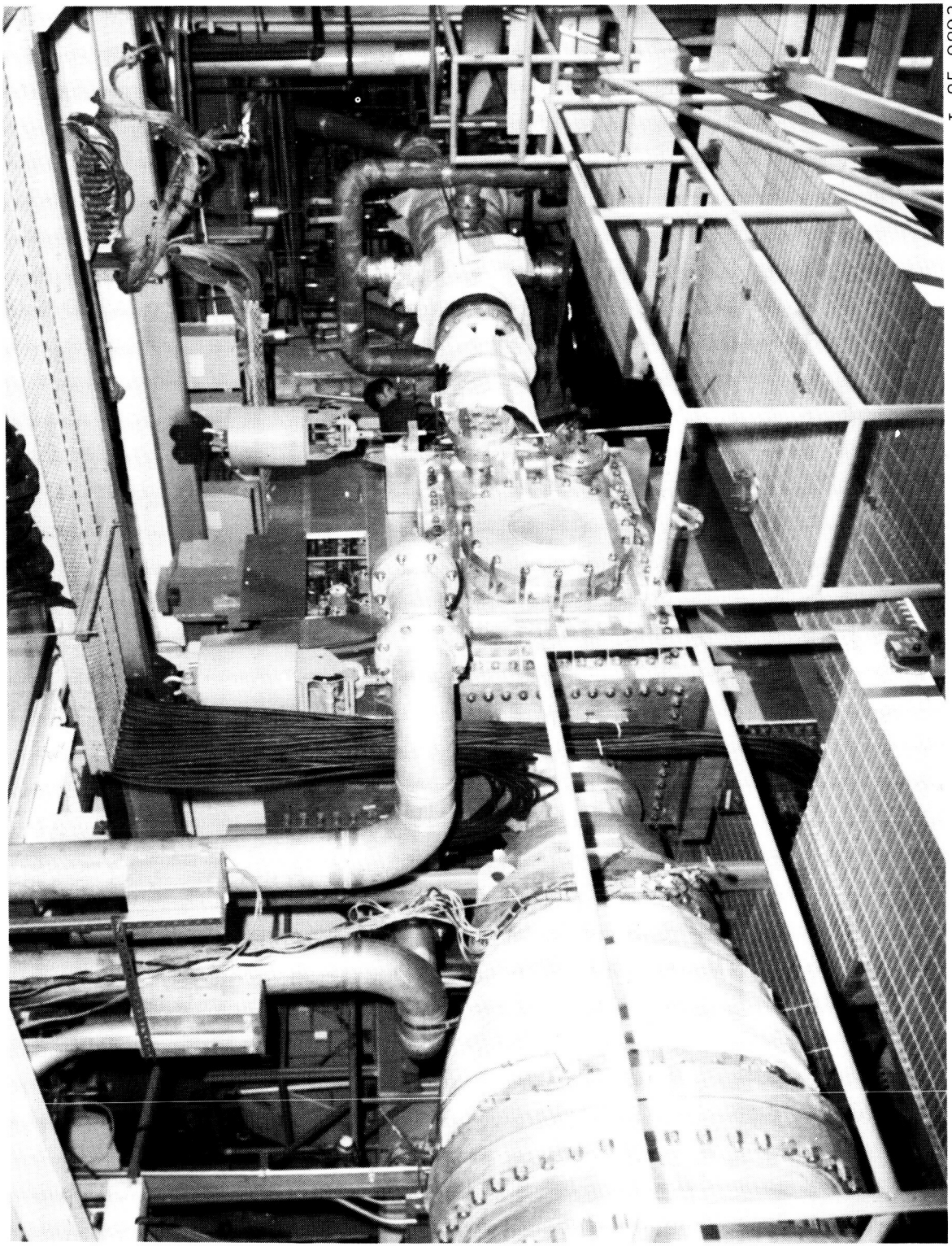

L-85-9893

Figure 10.- Photograph of the Langley 0.3-m TCT with 13 × 13 two-dimensional test section installed.

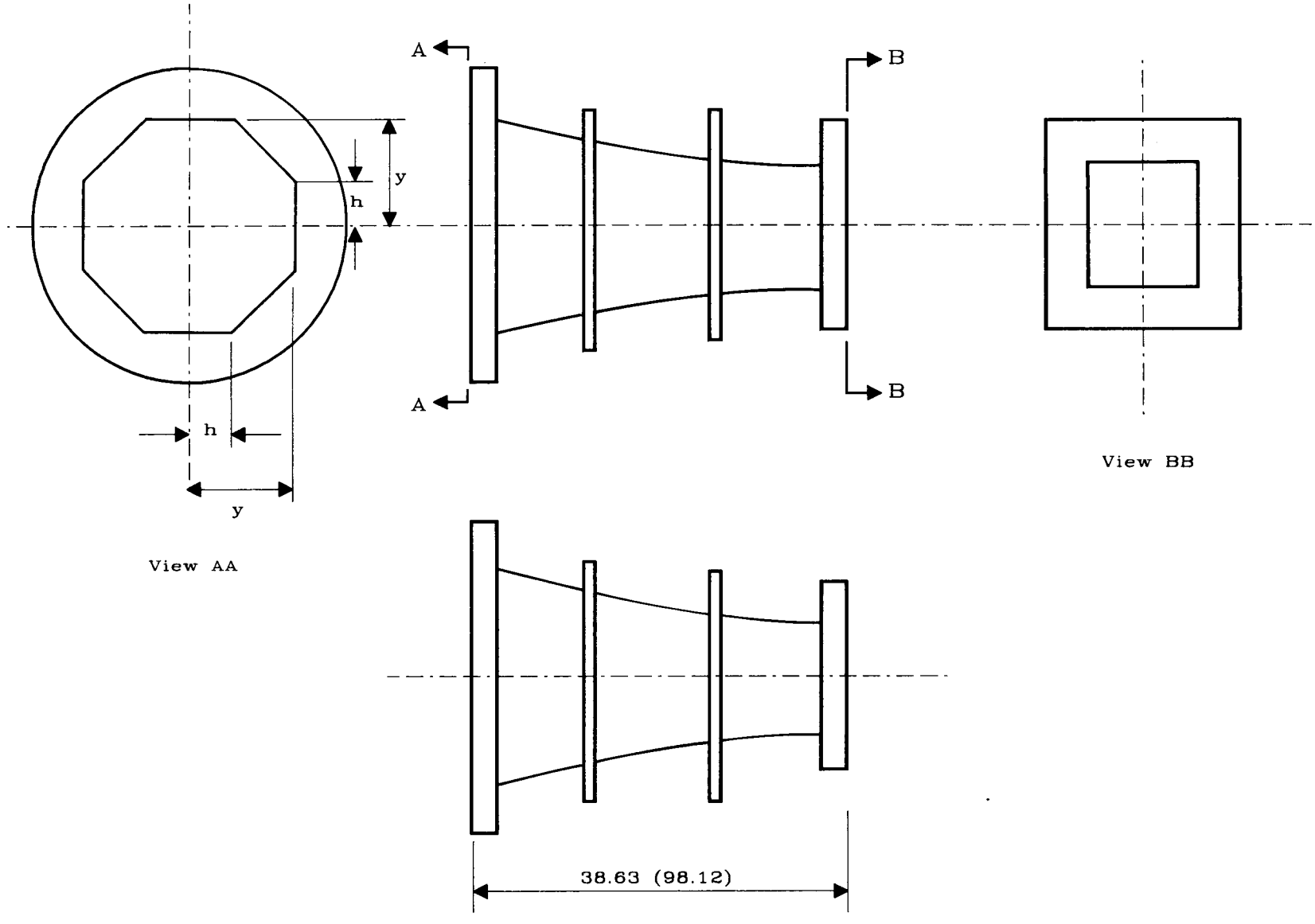

Figure 11.- Details of contraction section for 13 × 13 test section. See table II for ordinates. Linear dimensions are given in inches (centimeters).

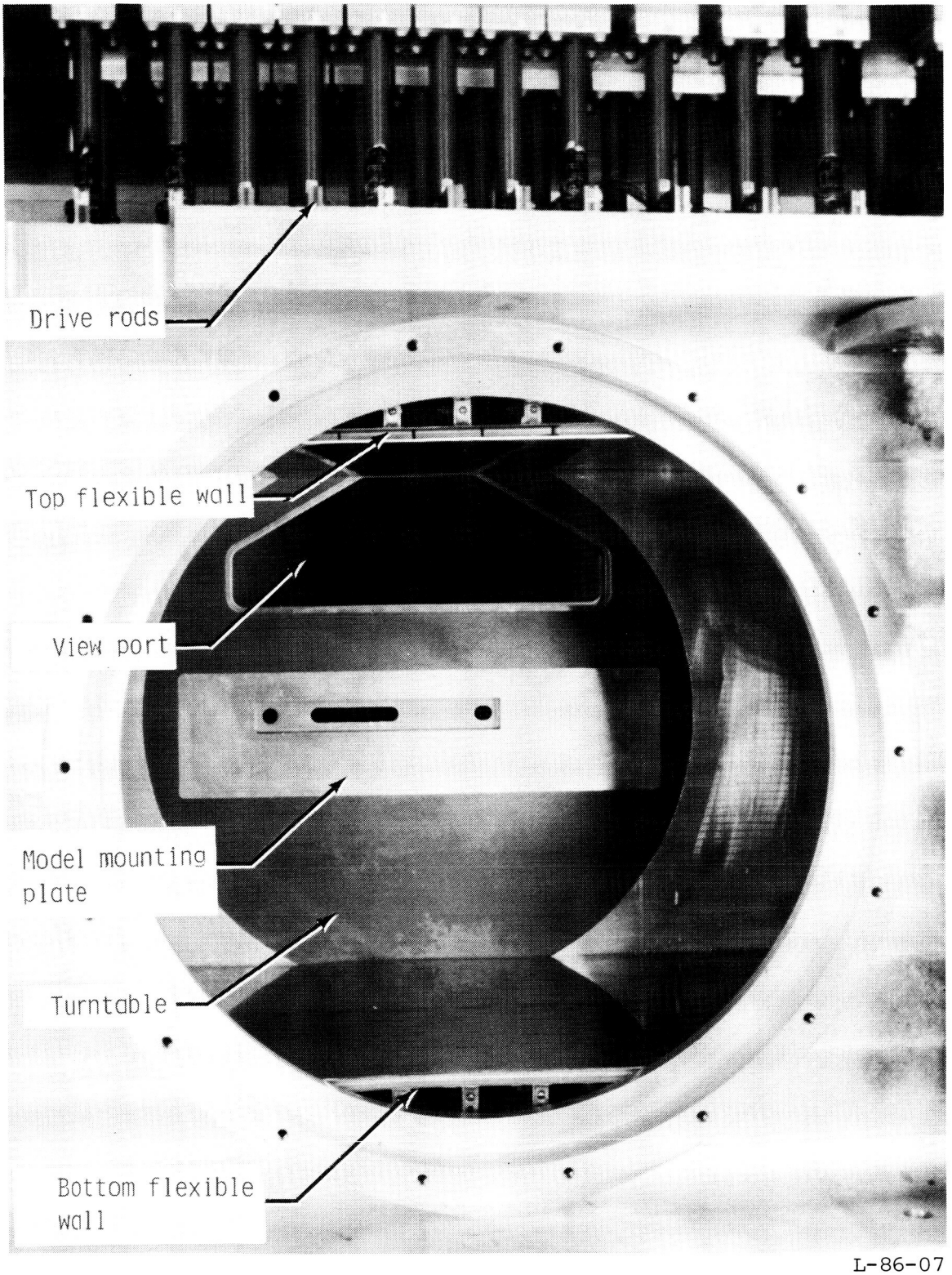

L-86-07

Figure 12.- Photograph of interior of test section showing details of model mounting plate and flexible walls.

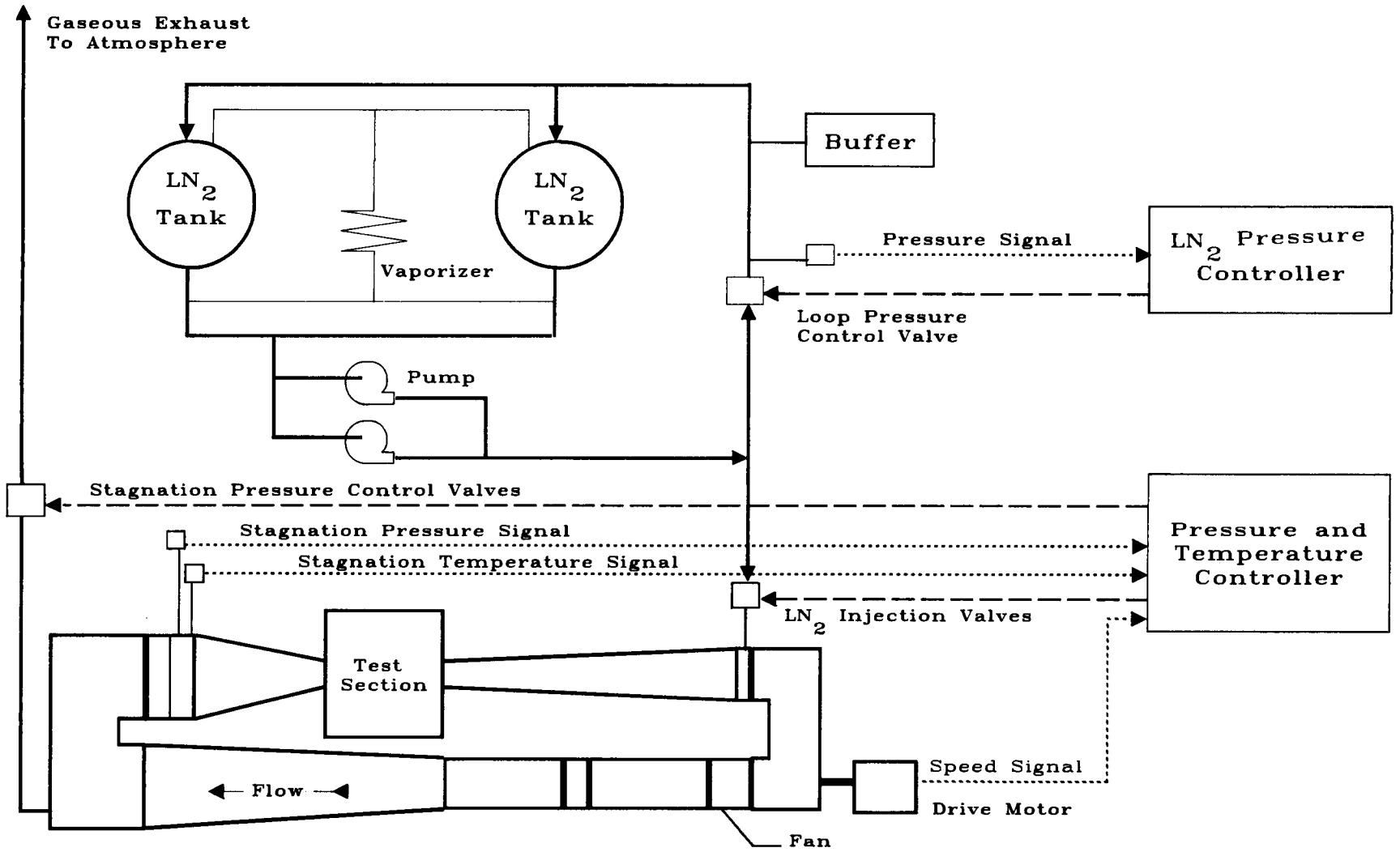

Figure 13.- Schematic drawing of liquid nitrogen injection and gaseous nitrogen exhaust system.

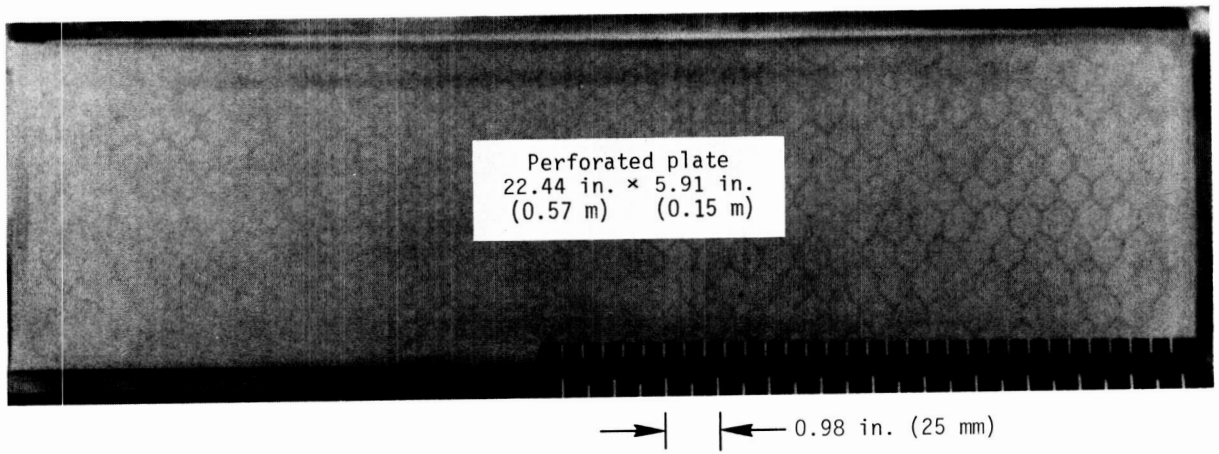

(a) Full plate.

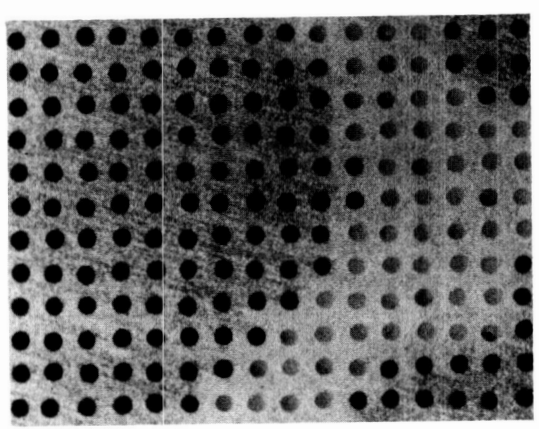

(b) Approximate magnification, × 11.

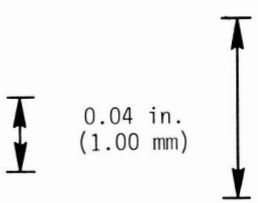

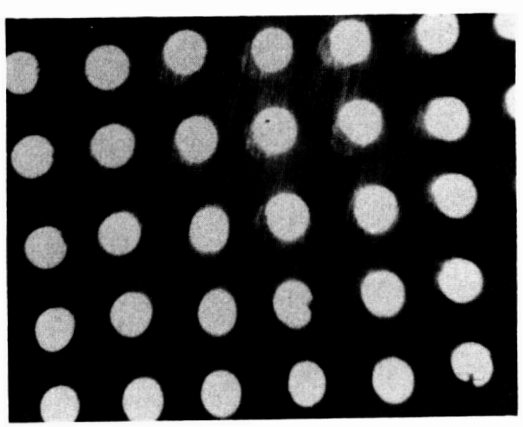

(c) Approximate magnification, × 30.

L-82-211

Figure 14.- Photographs of porous plate used in boundary-layer removal system.

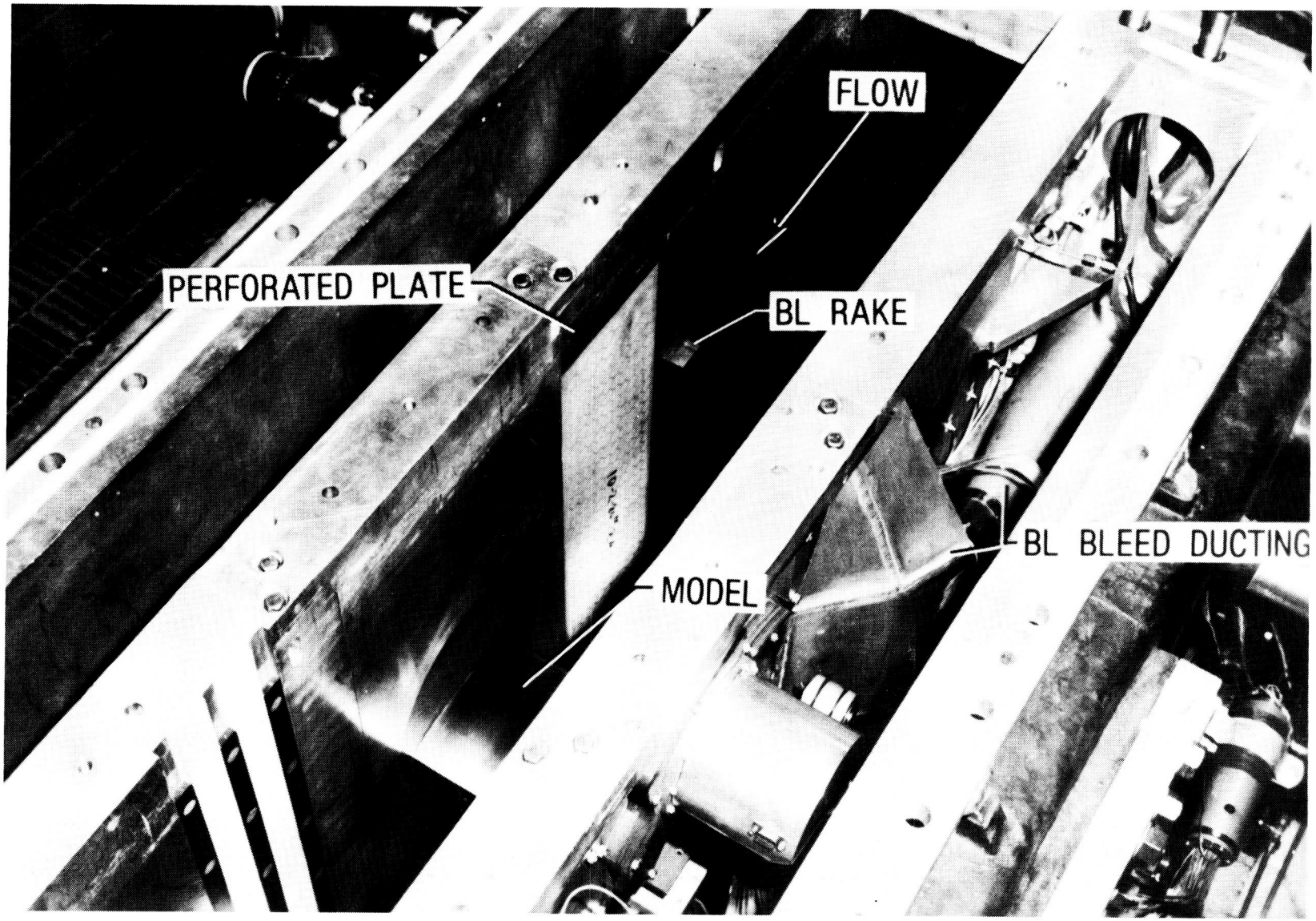

L-82-210

Figure 15.- Photograph of 8 × 24 two-dimensional test section showing details of boundary-layer removal plates.

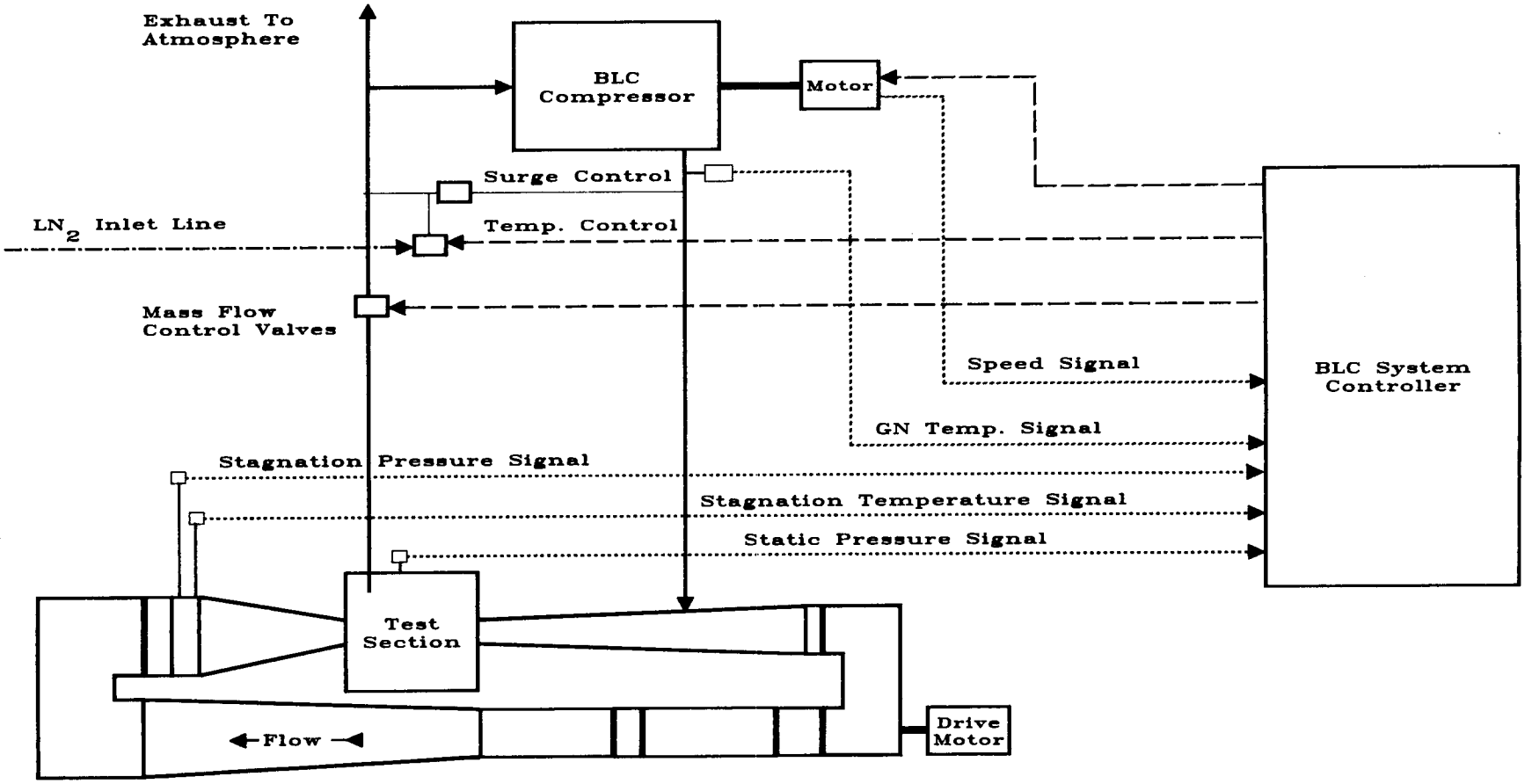

Figure 16.- Schematic diagram of boundary-layer removal system.

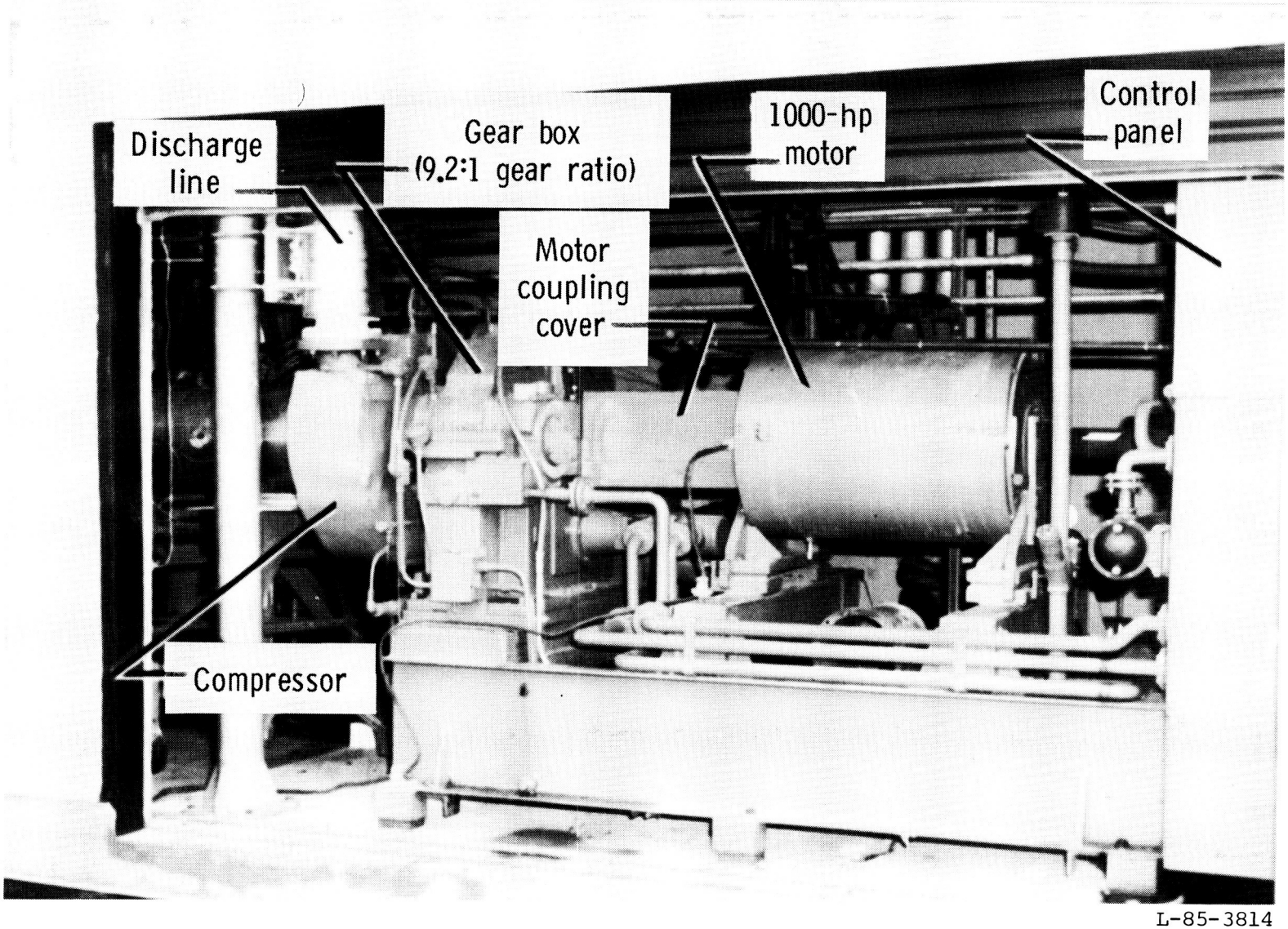

L-85-3814

Figure 17.- Photograph of compressor and drive motor for boundary-layer removal system.

L-86-08

Figure 18.- Photograph of rack of pressure transducers showing proximity to test section.

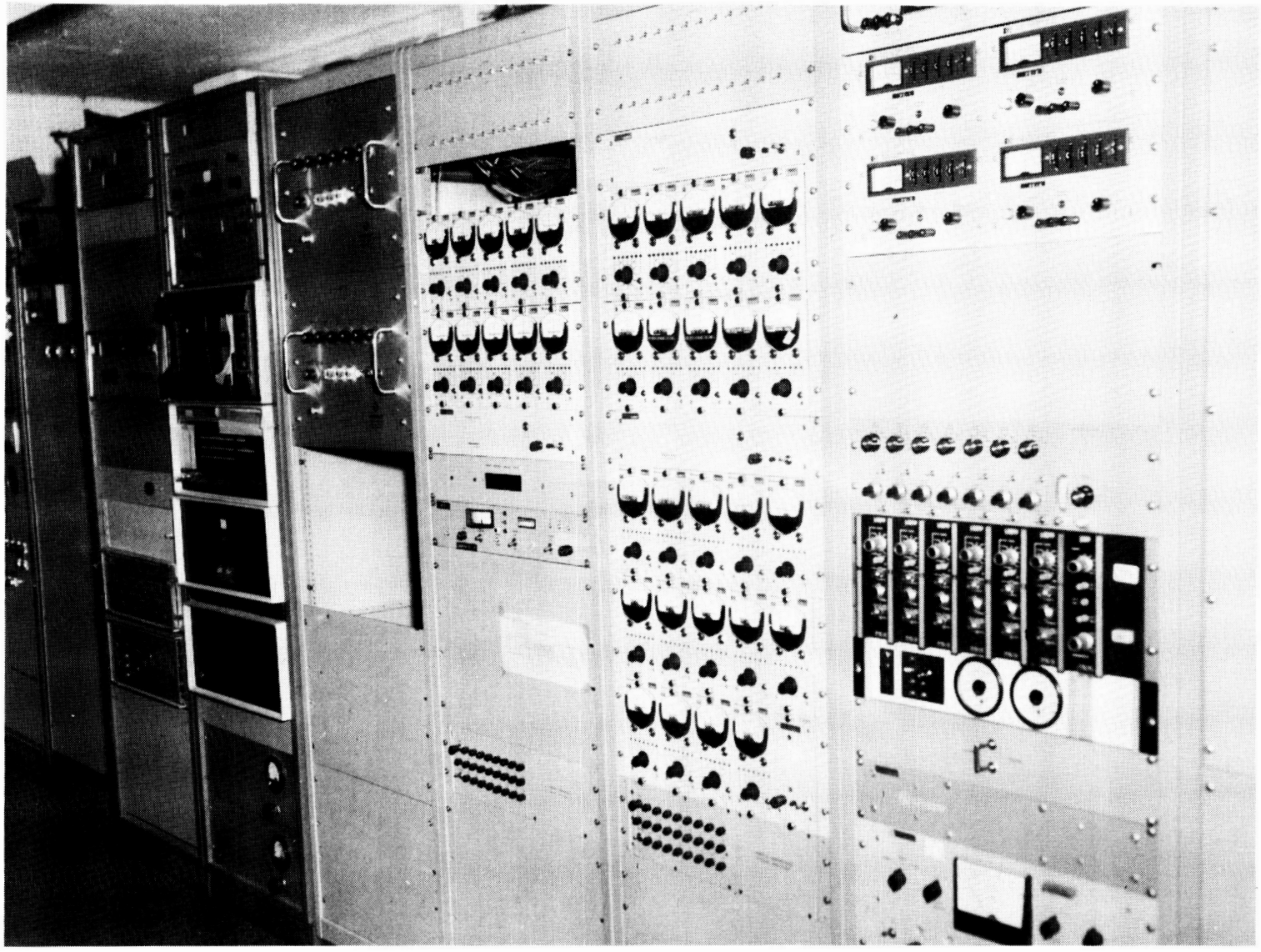

L-77-7395

(a) Original control room arrangement of power supplies, control computer, and autoranging signal conditioners.

Figure 19.- Photograph of instrumentation racks.

L-86-2090

(b) Current control room arrangement of autoranging signal conditioners.

Figure 19.- Concluded.

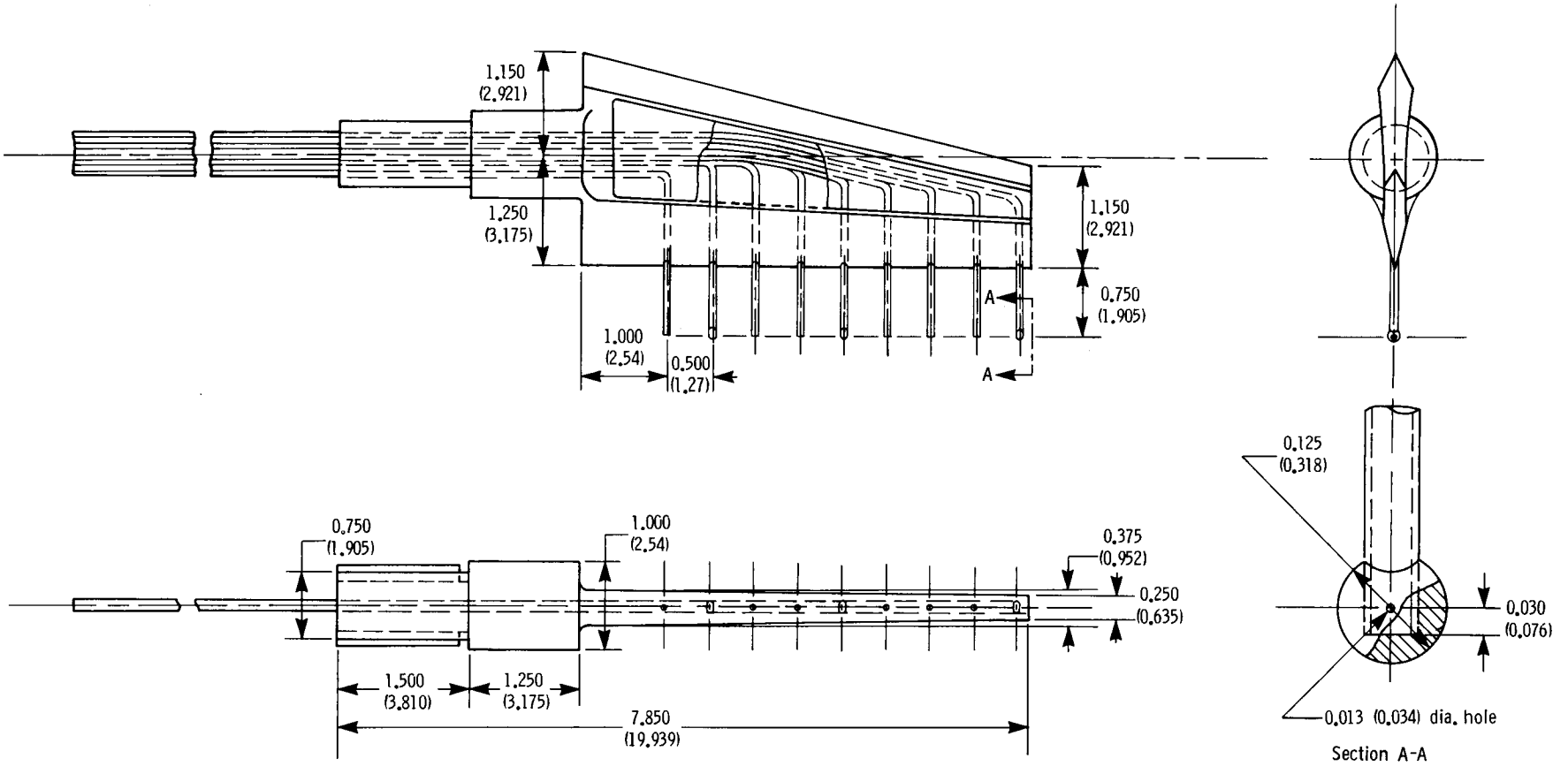

Figure 20.- Details of wake survey probe. All dimensions are given in inches (centimeters).

L-65-7816

Figure 21.- Photograph of central data acquisition system.

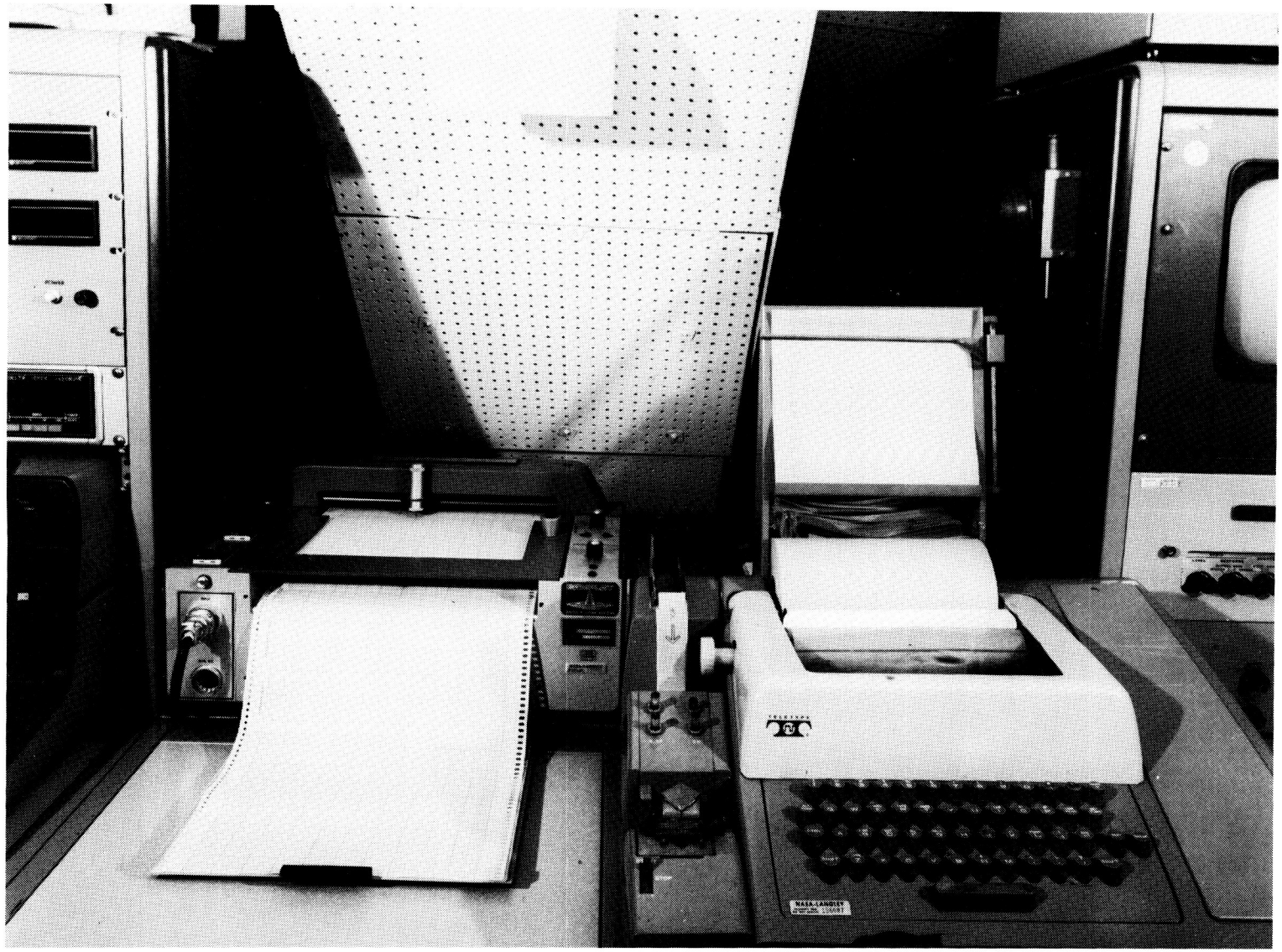

L-77-7685

Figure 22.- Photograph of XY plotter and teletype used with original data acquisition system.

L-86-2086

Figure 23.- Photograph of arrangement of data acquisition system in current control room.

L-86-6423

Figure 24.- Photograph of data acquisition system and tunnel control consoles.

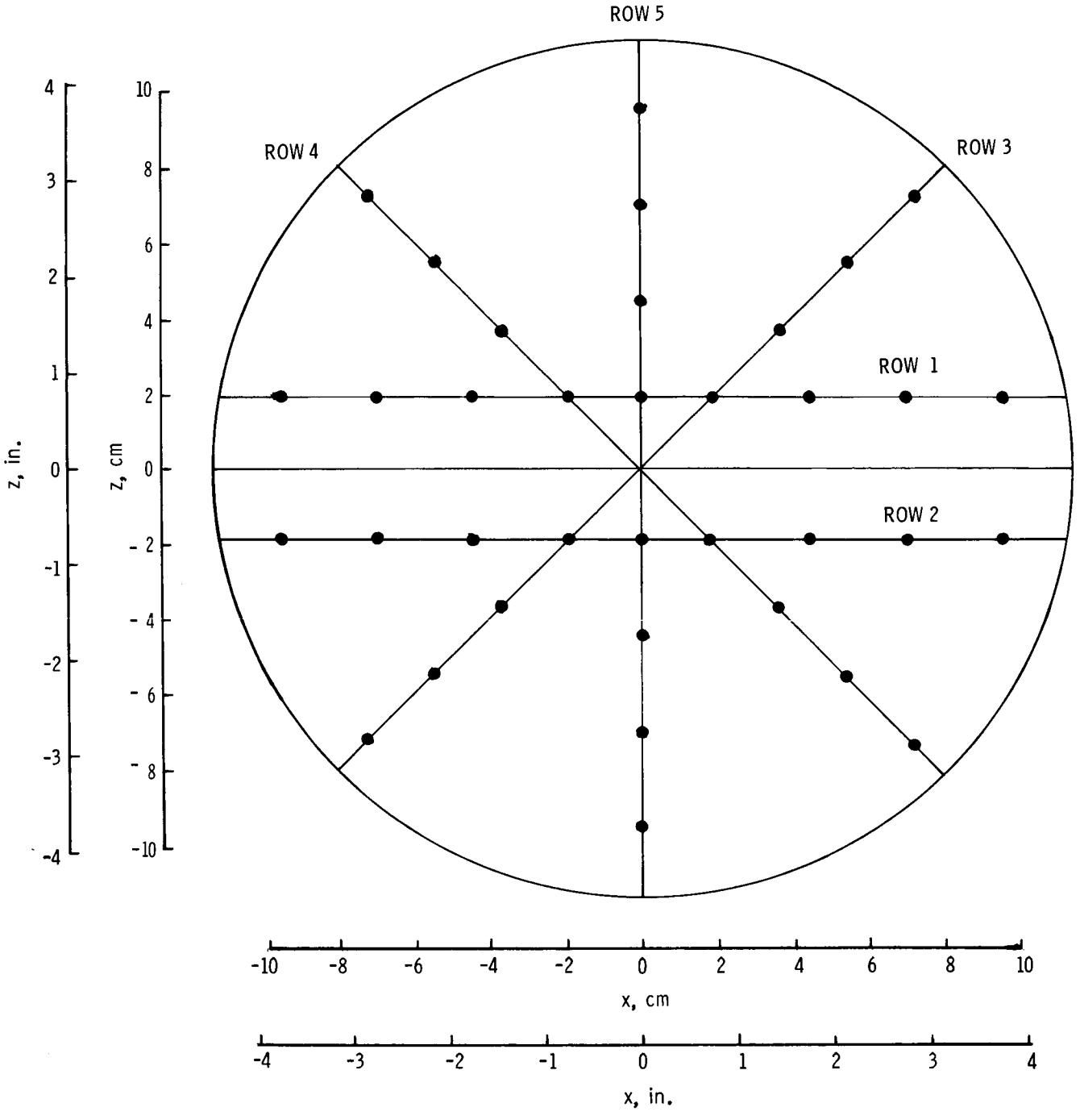

Figure 25.- Orifice location for turntable.

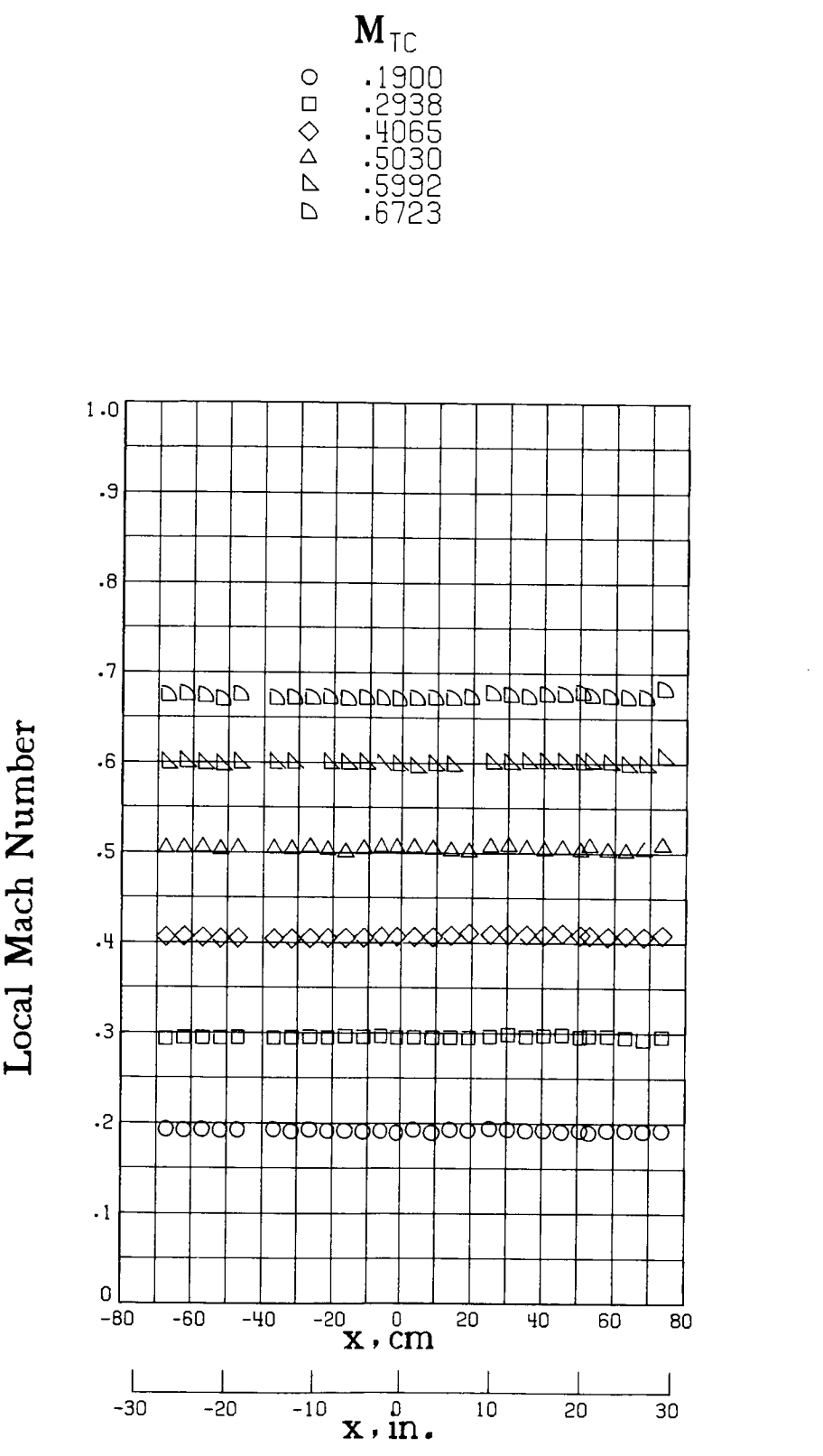

(a) T_t = 300 K.

Figure 26.- Longitudinal distribution of local Mach number along test-section floor for stagnation pressure of 1.2 atm.

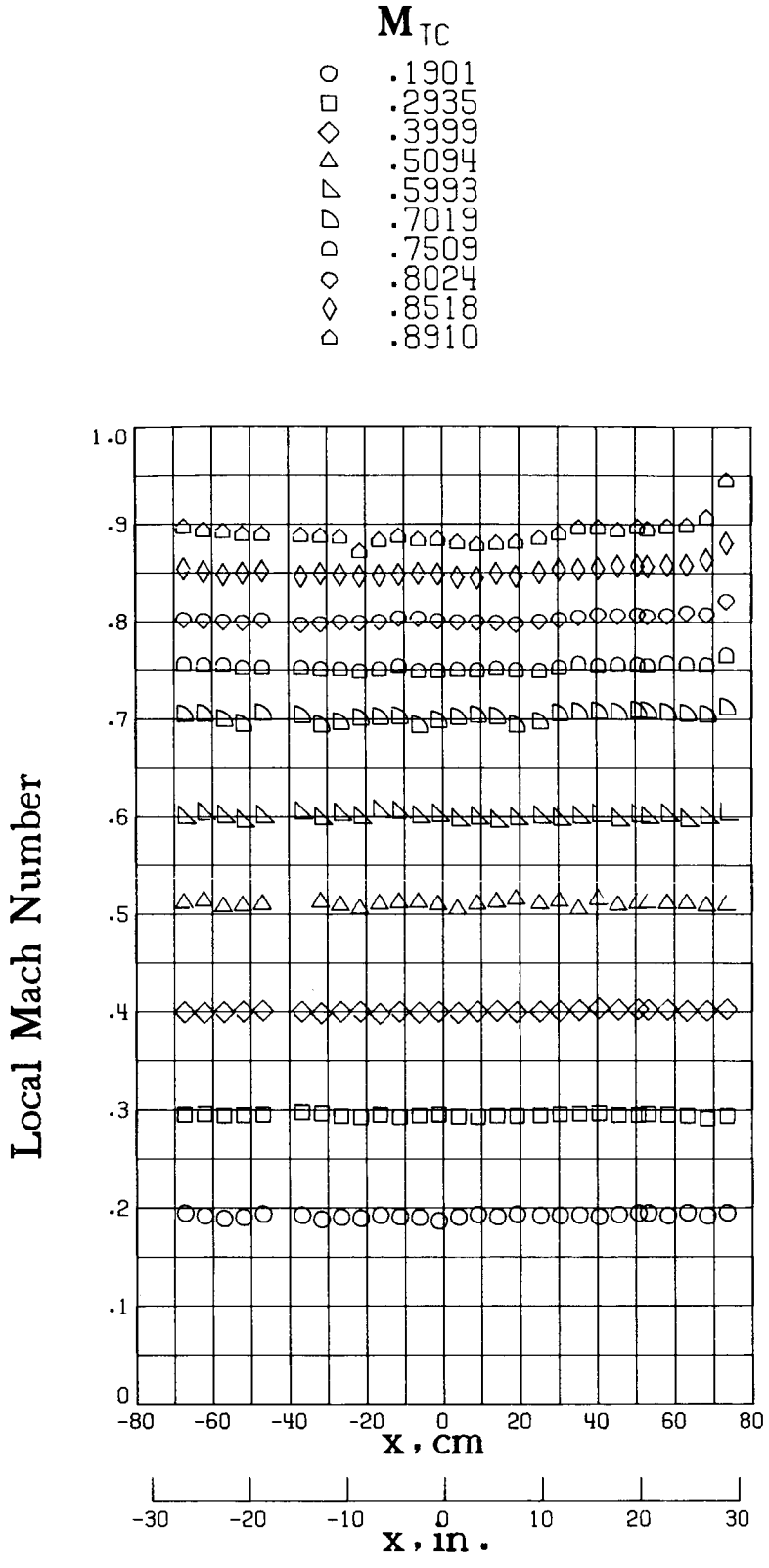

(b) T_t = 200 K.

Figure 26.- Continued.

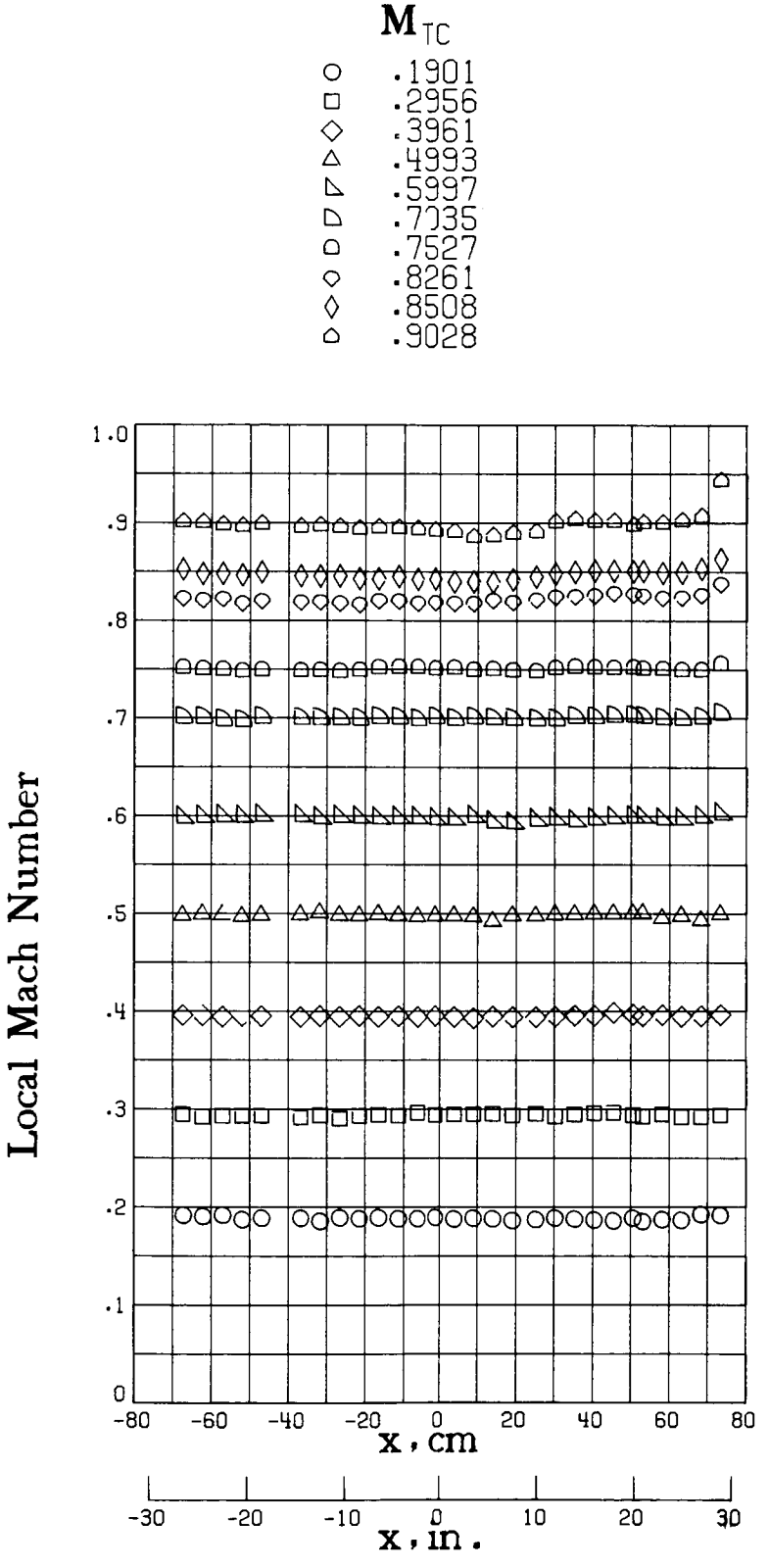

(c) T_t = 105 K.

Figure 26.- Concluded.

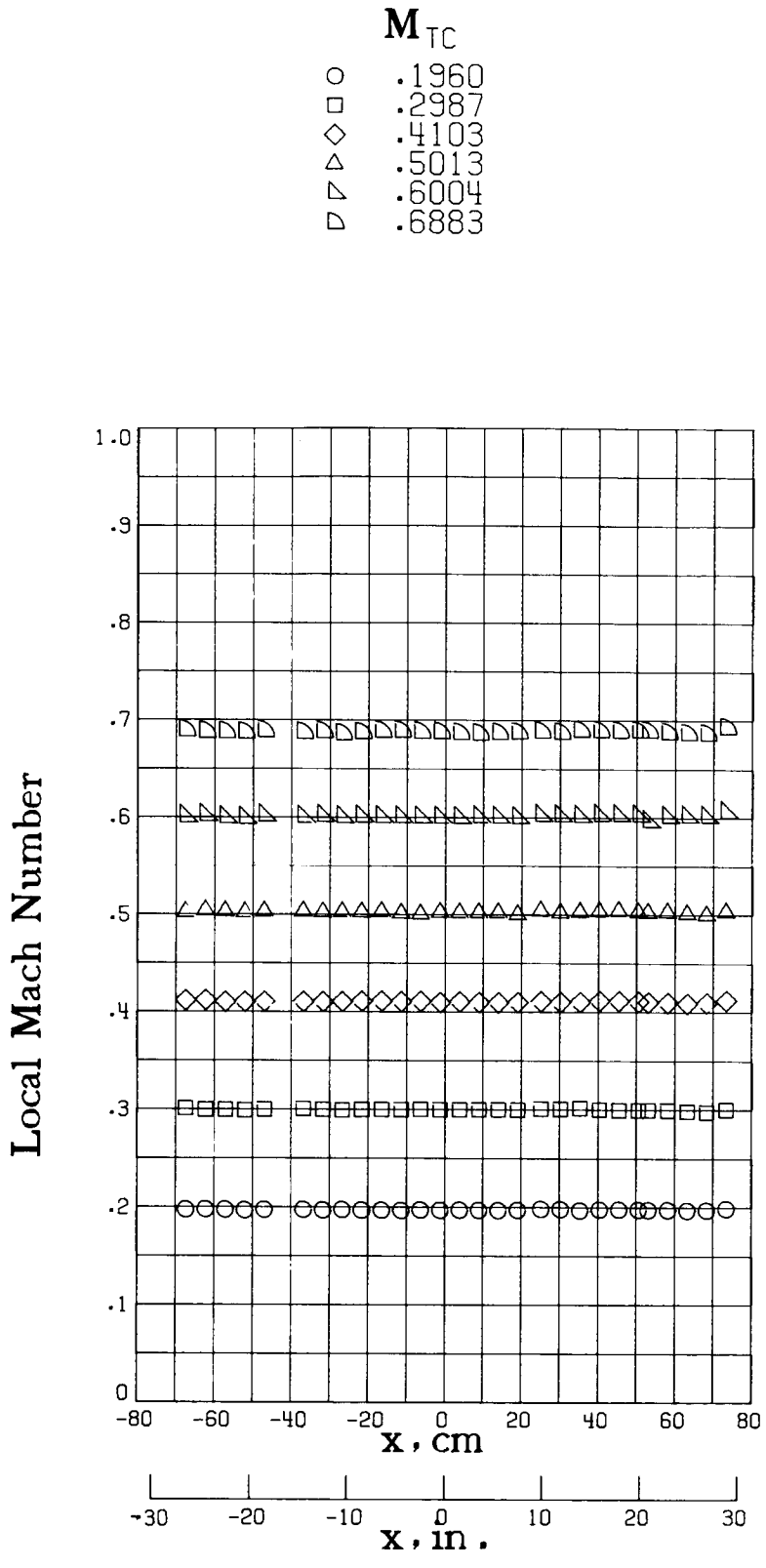

(a) T_t = 300 K.

Figure 27.- Longitudinal distribution of local Mach number along test-section floor for stagnation pressure of 3.1 atm.

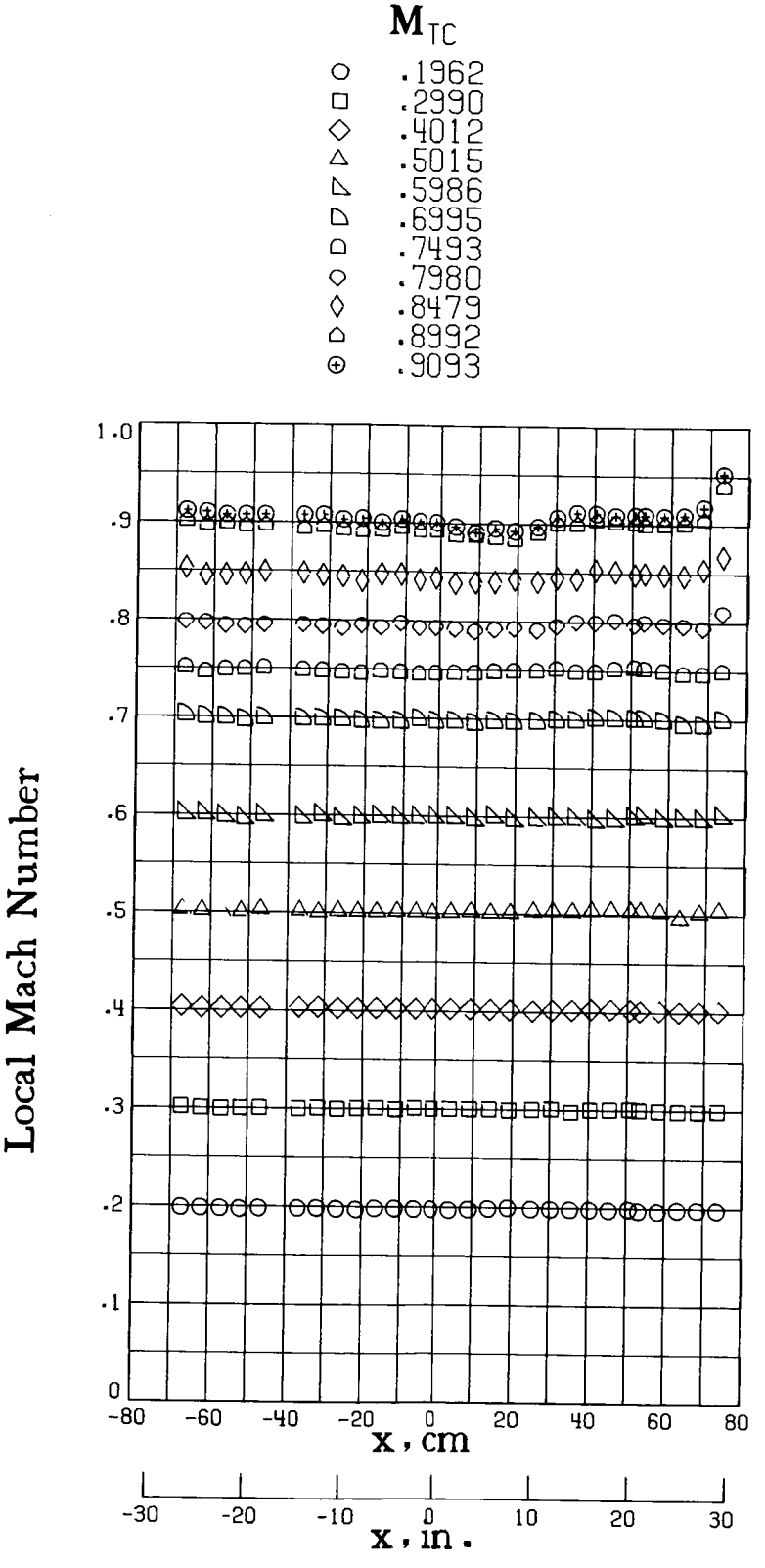

(b) T_t = 200 K.

Figure 27.- Continued.

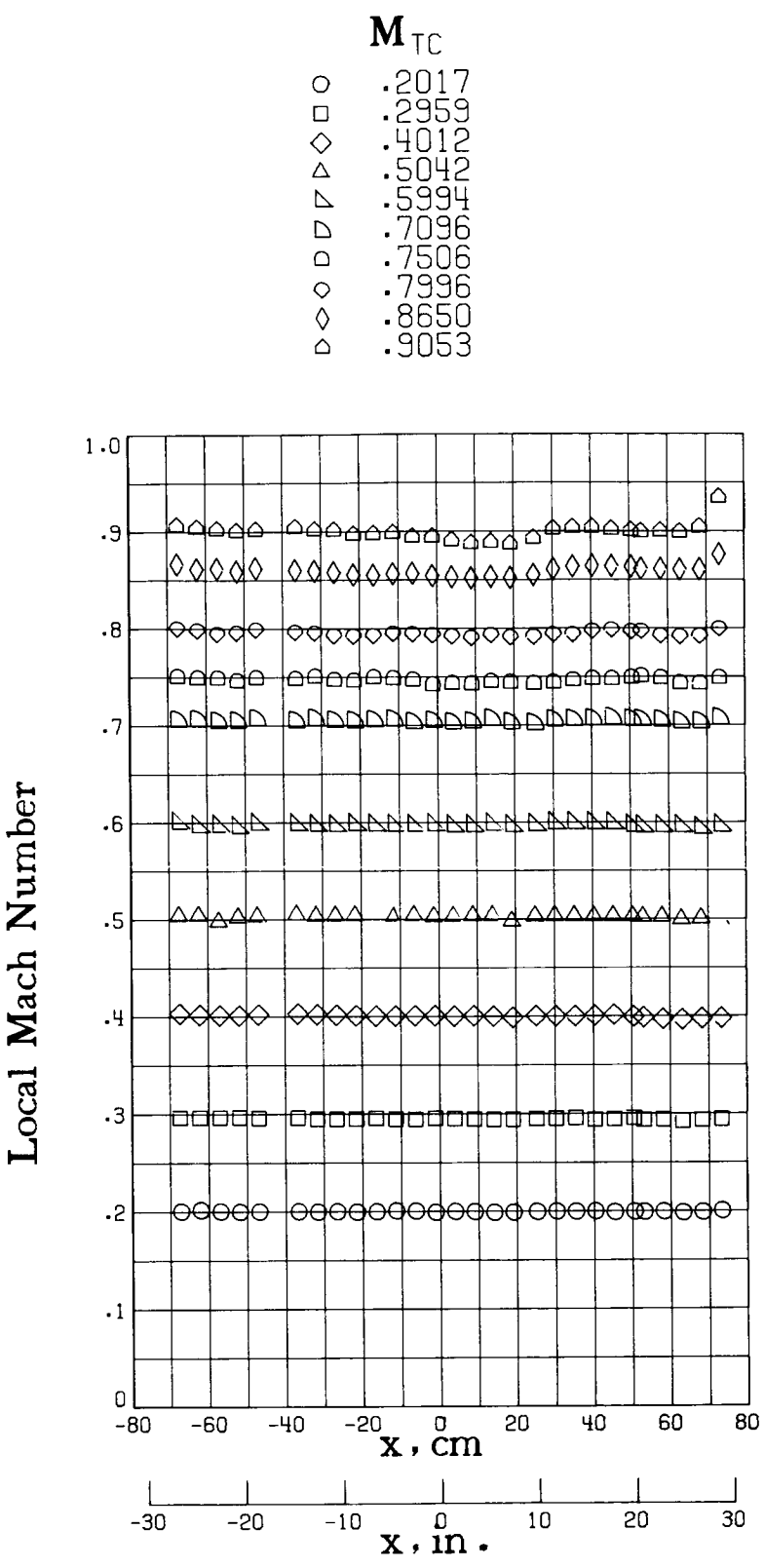

(c) T_t = 105 K.

Figure 27.- Concluded.

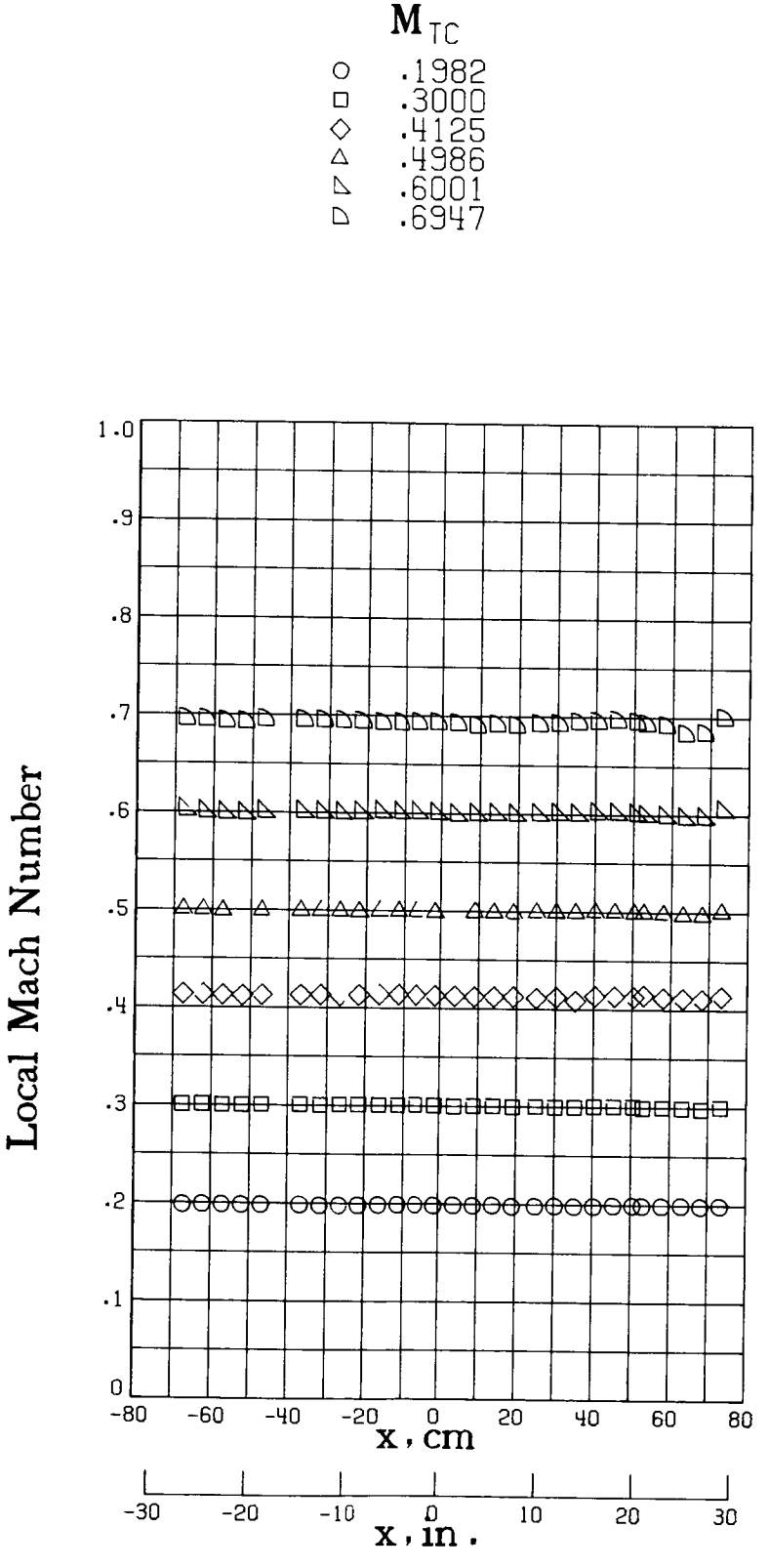

(a) T_t = 300 K.

Figure 28.- Longitudinal distribution of local Mach number along test-section floor for stagnation pressure of 5.1 atm.

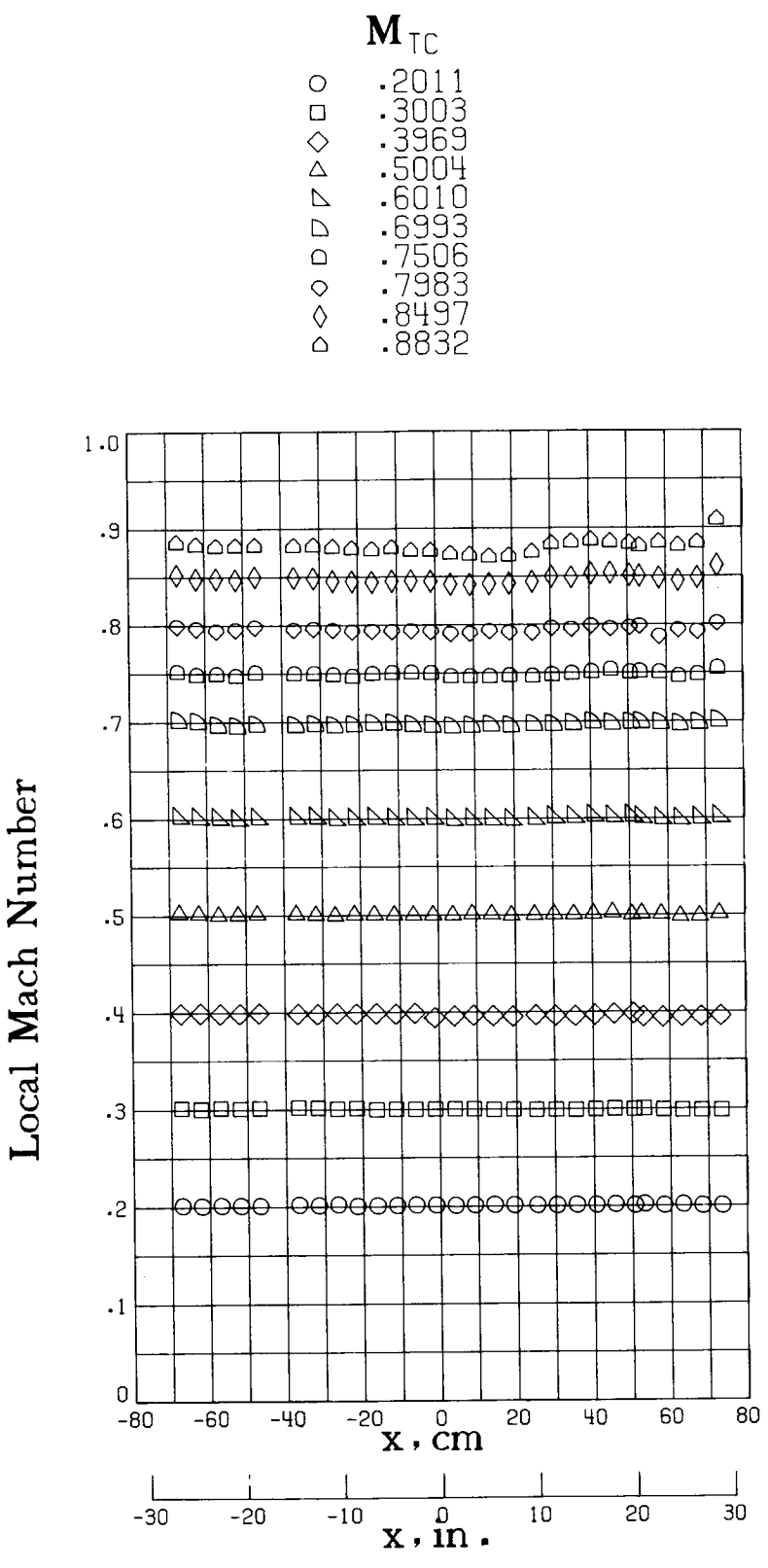

(b) T_t = 200 K.

Figure 28.- Continued.

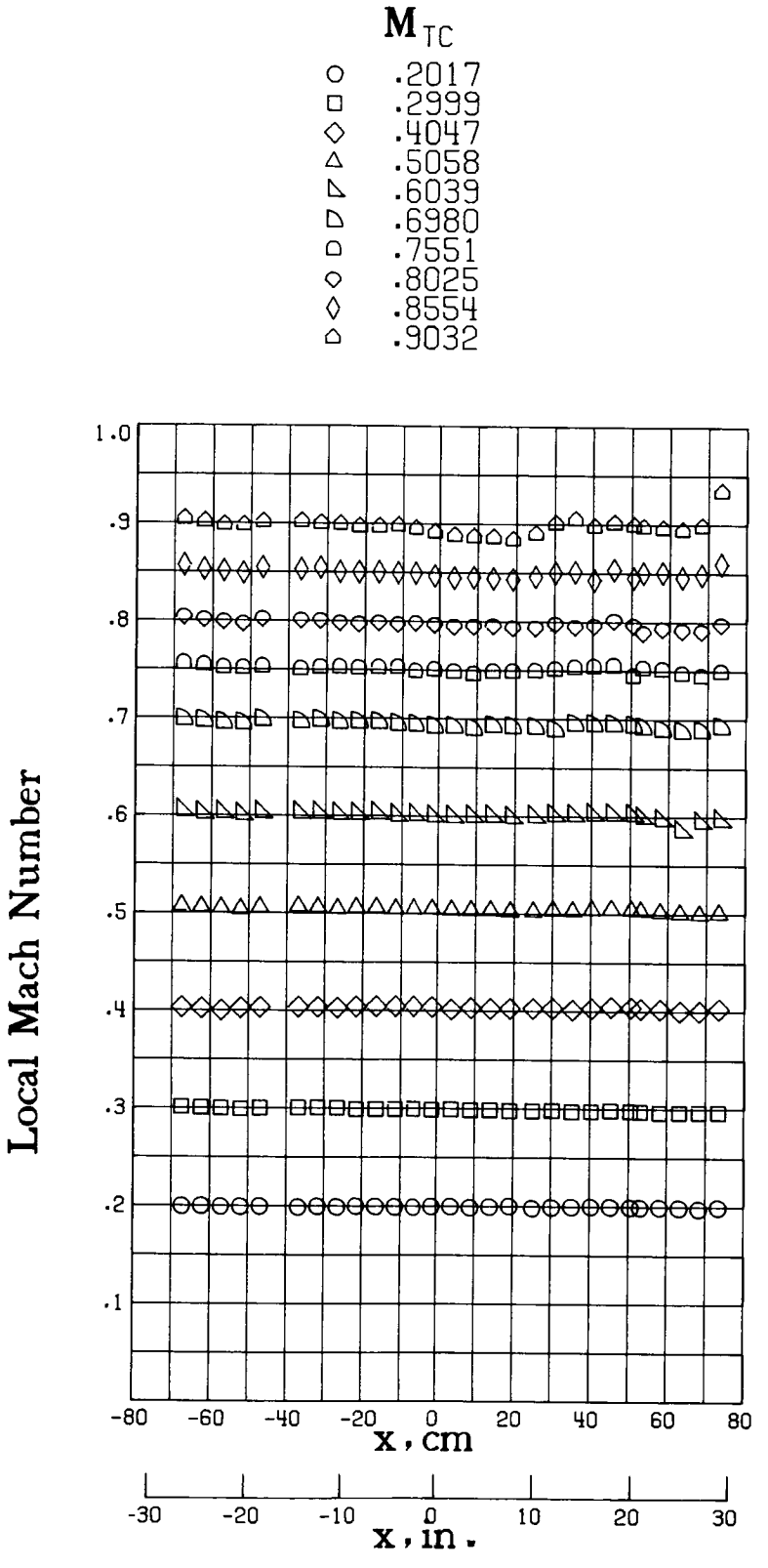

(c) T_t = 105 K.

Figure 28.- Concluded.

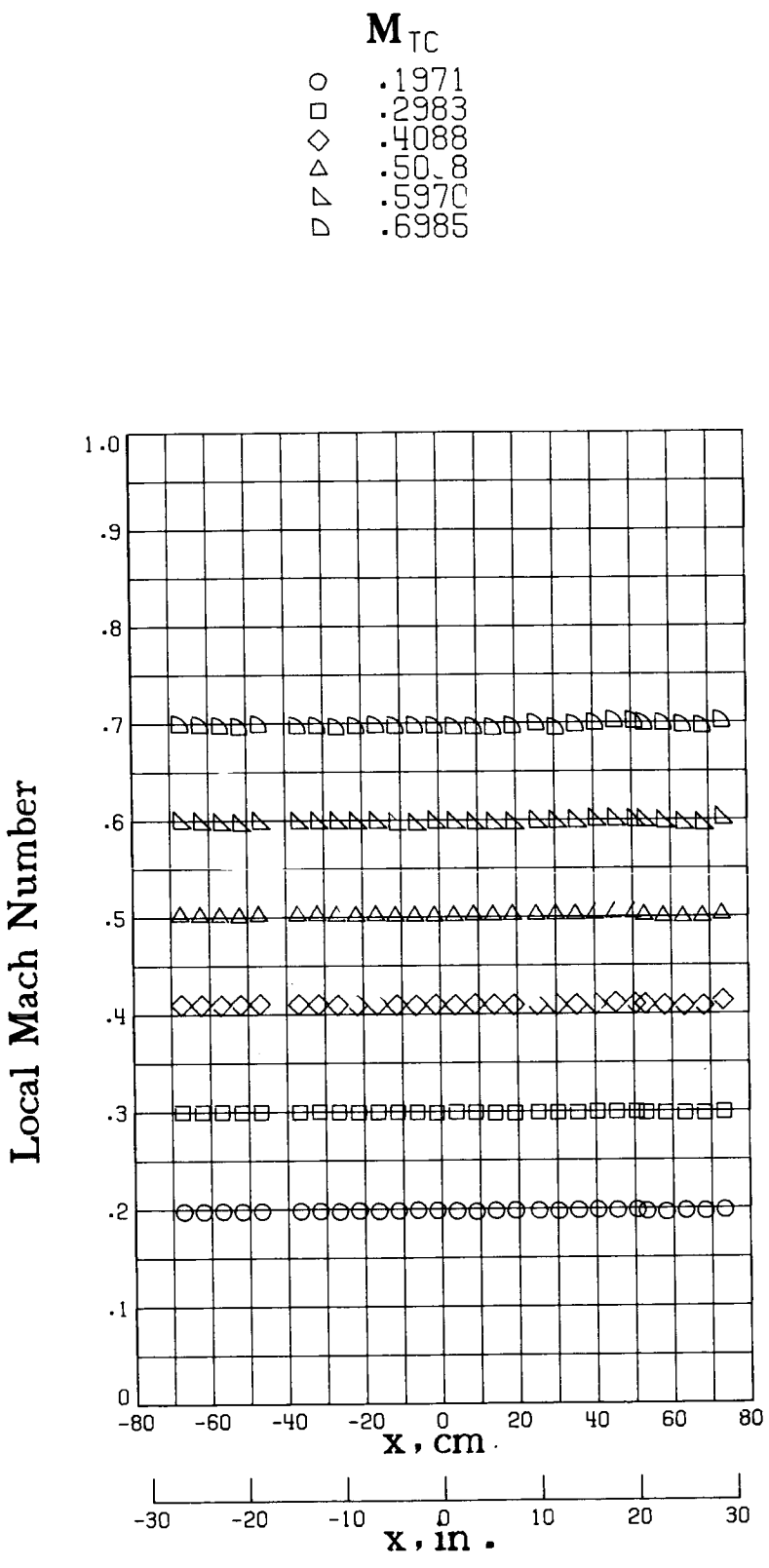

(a) T_t = 300 K.

Figure 29.- Longitudinal distribution of local Mach number along test-section floor for stagnation pressure of 6.0 atm.

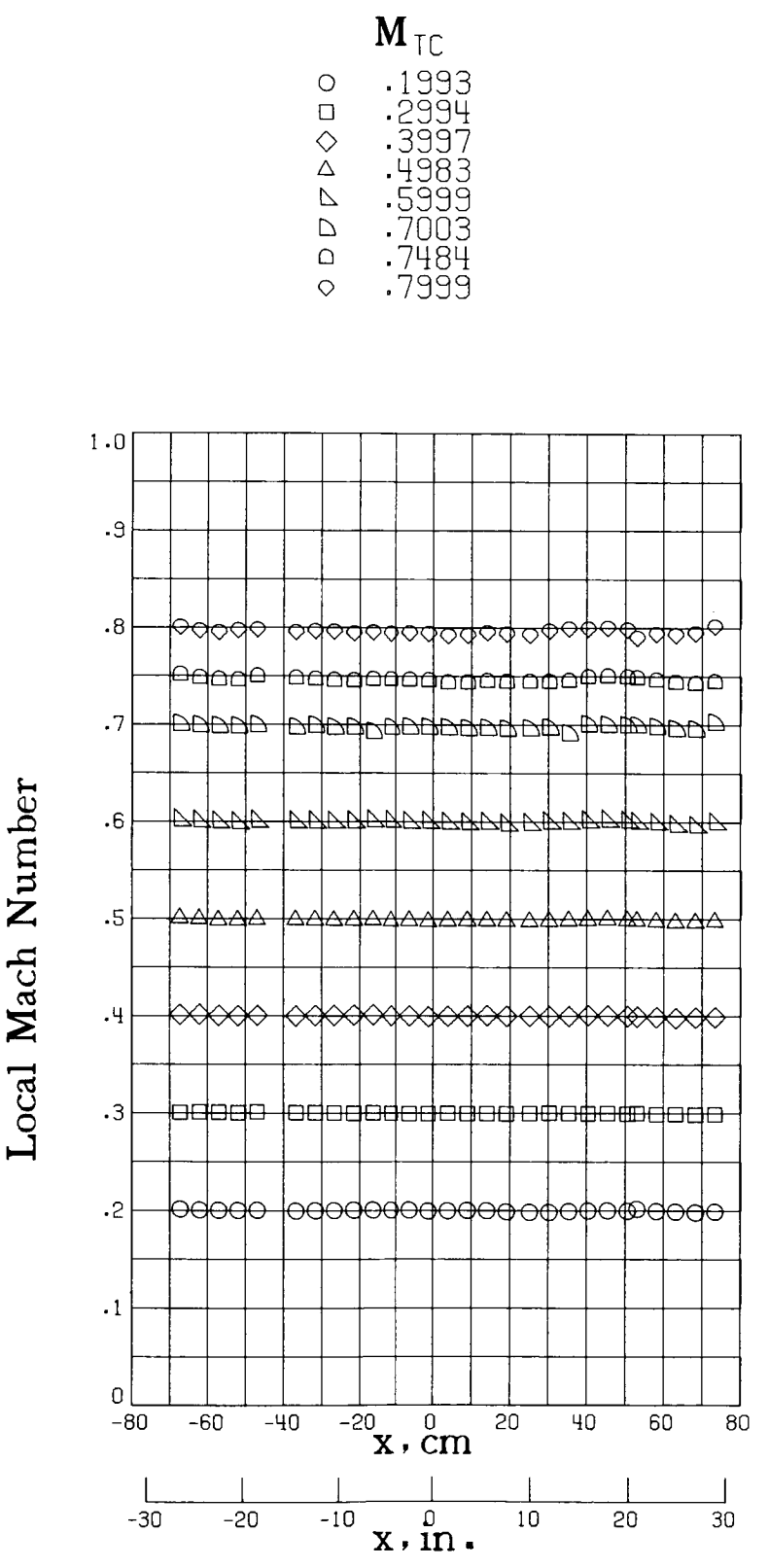

(b) T_t = 200 K.

Figure 29.- Continued.

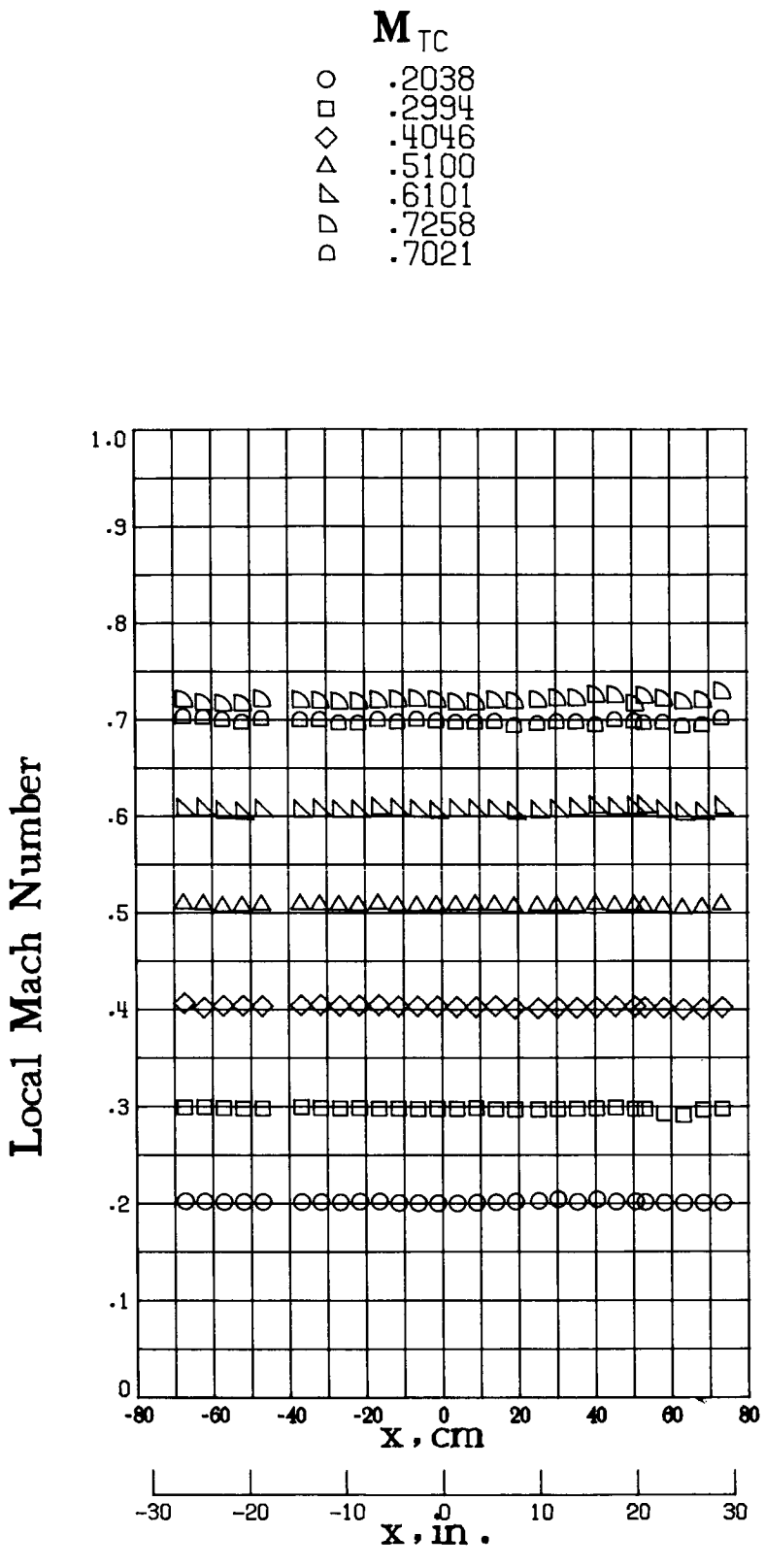

(c) T_t = 105 K.

Figure 29.- Concluded.

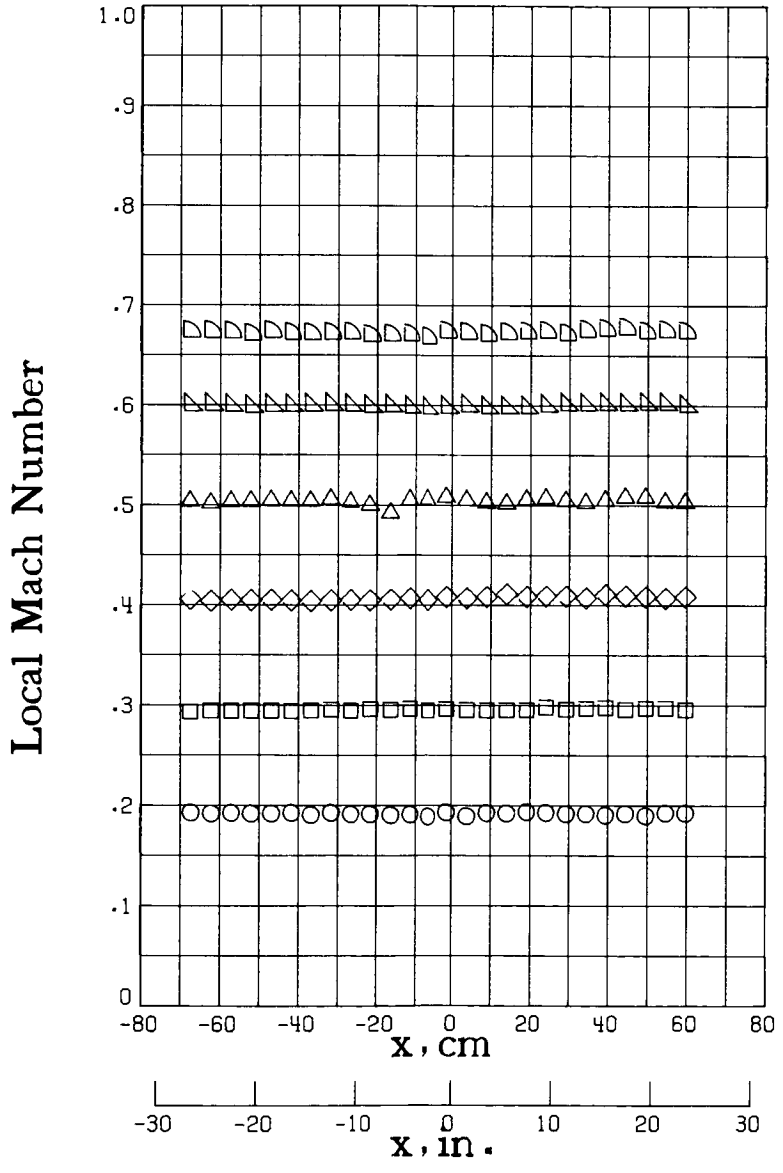

(a) T_t = 300 K.

Figure 30.- Longitudinal distribution of local Mach number along test-section ceiling for stagnation pressure of 1.2 atm.

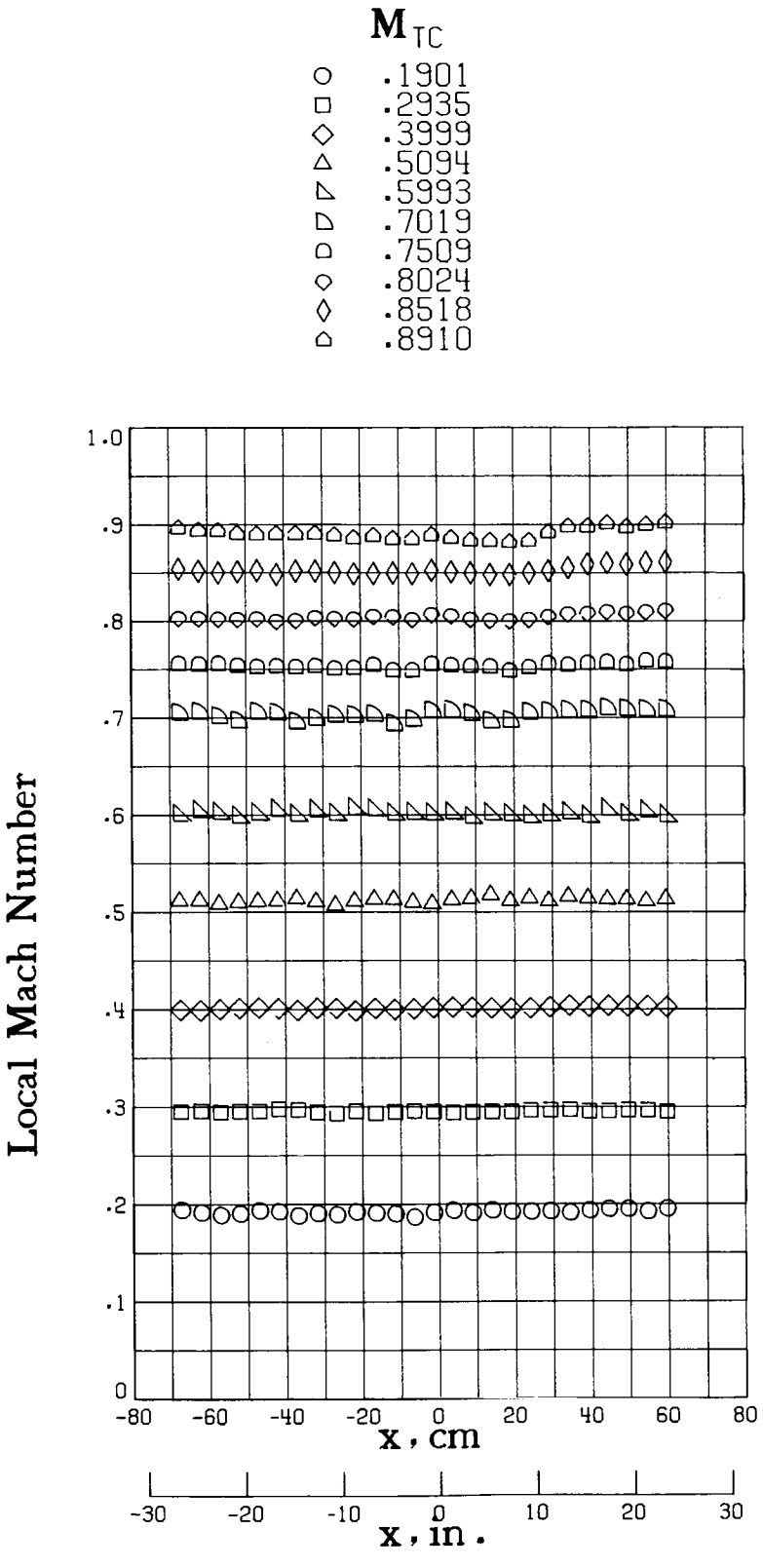

(b) T_t = 200 K.

Figure 30.- Continued.

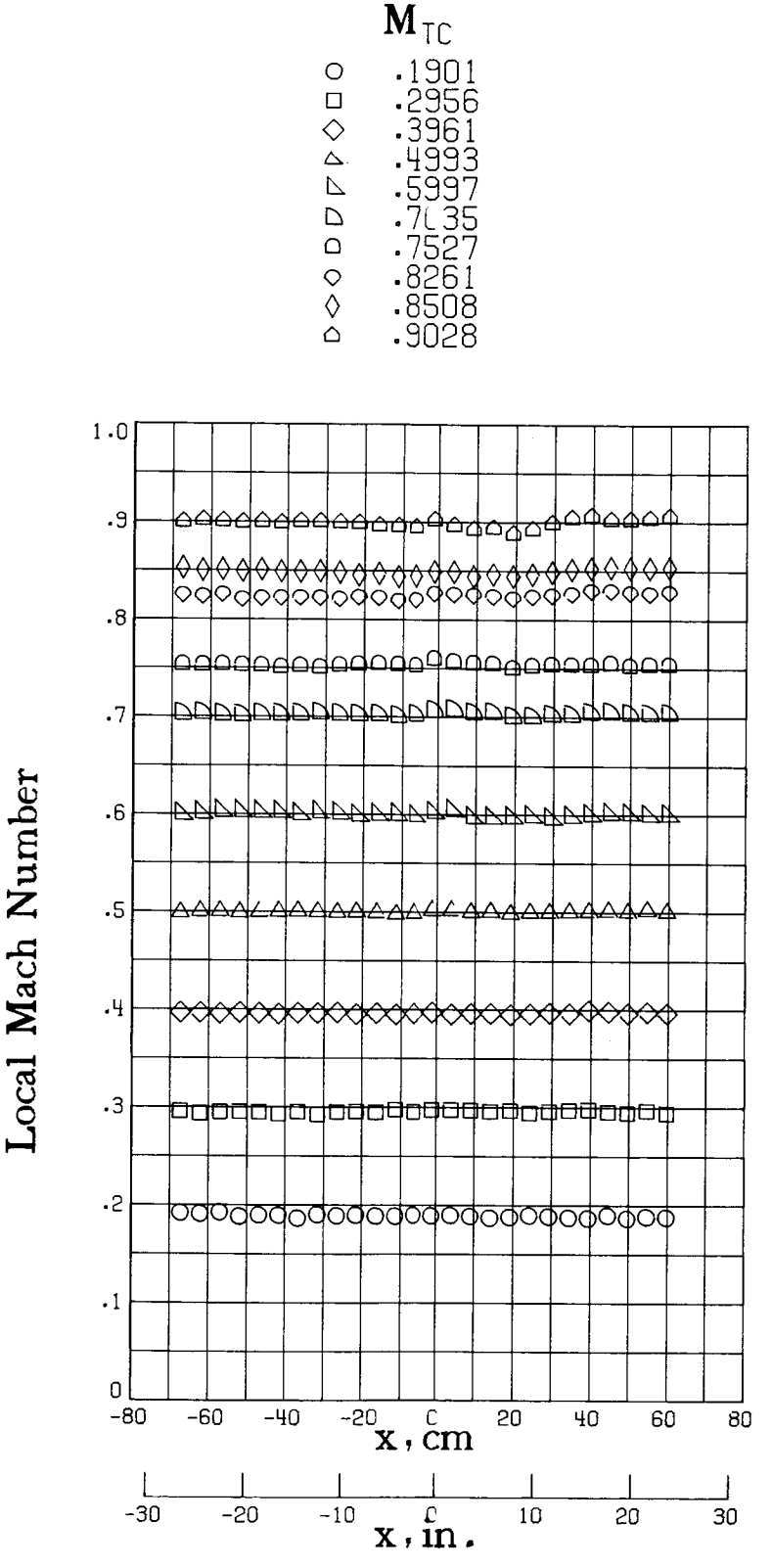

(c) T_t = 105 K.

Figure 30.- Concluded.

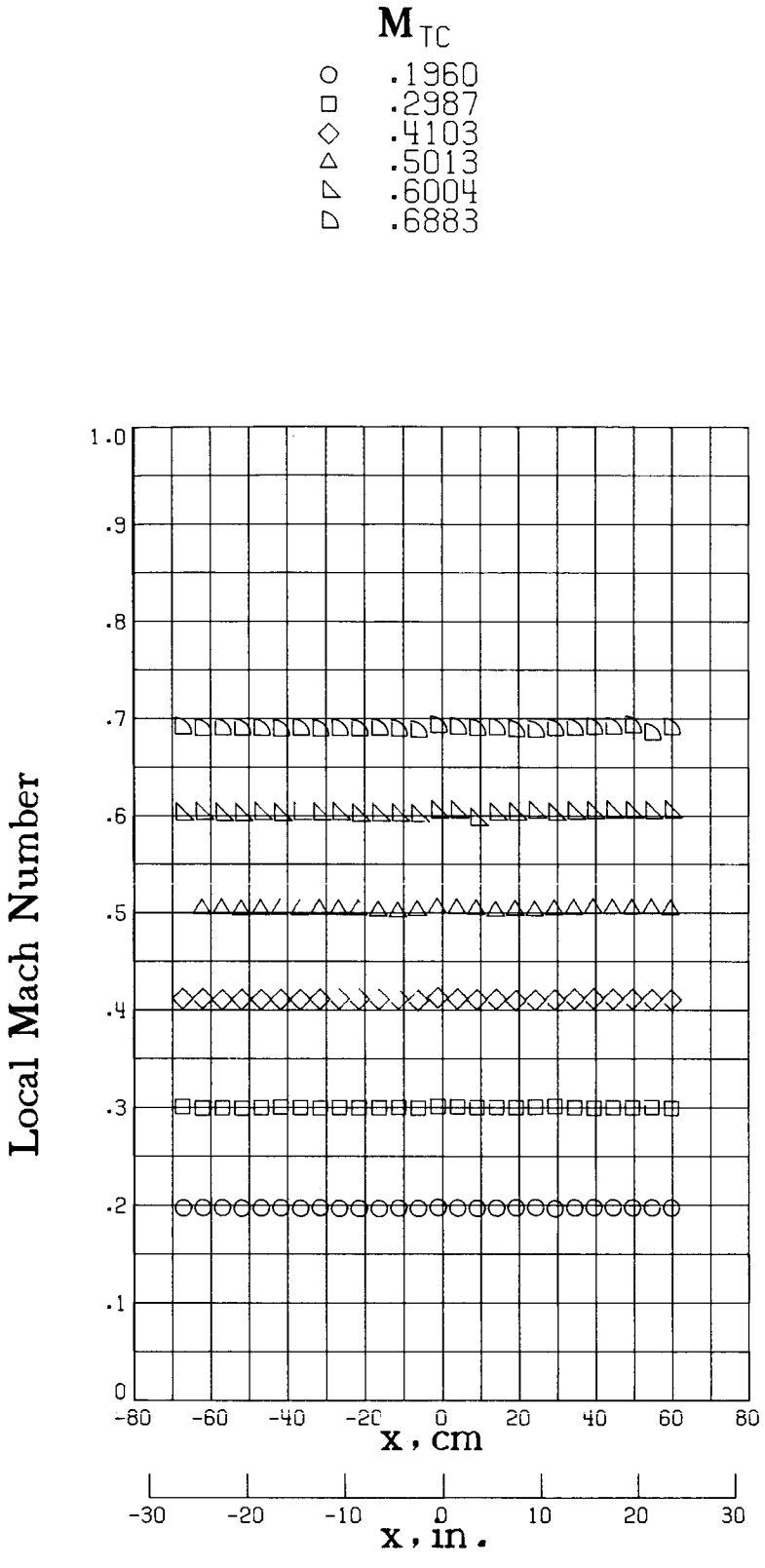

(a) T_t = 300 K.

Figure 31.- Longitudinal distribution of local Mach number along test-section ceiling for stagnation pressure of 3.1 atm.

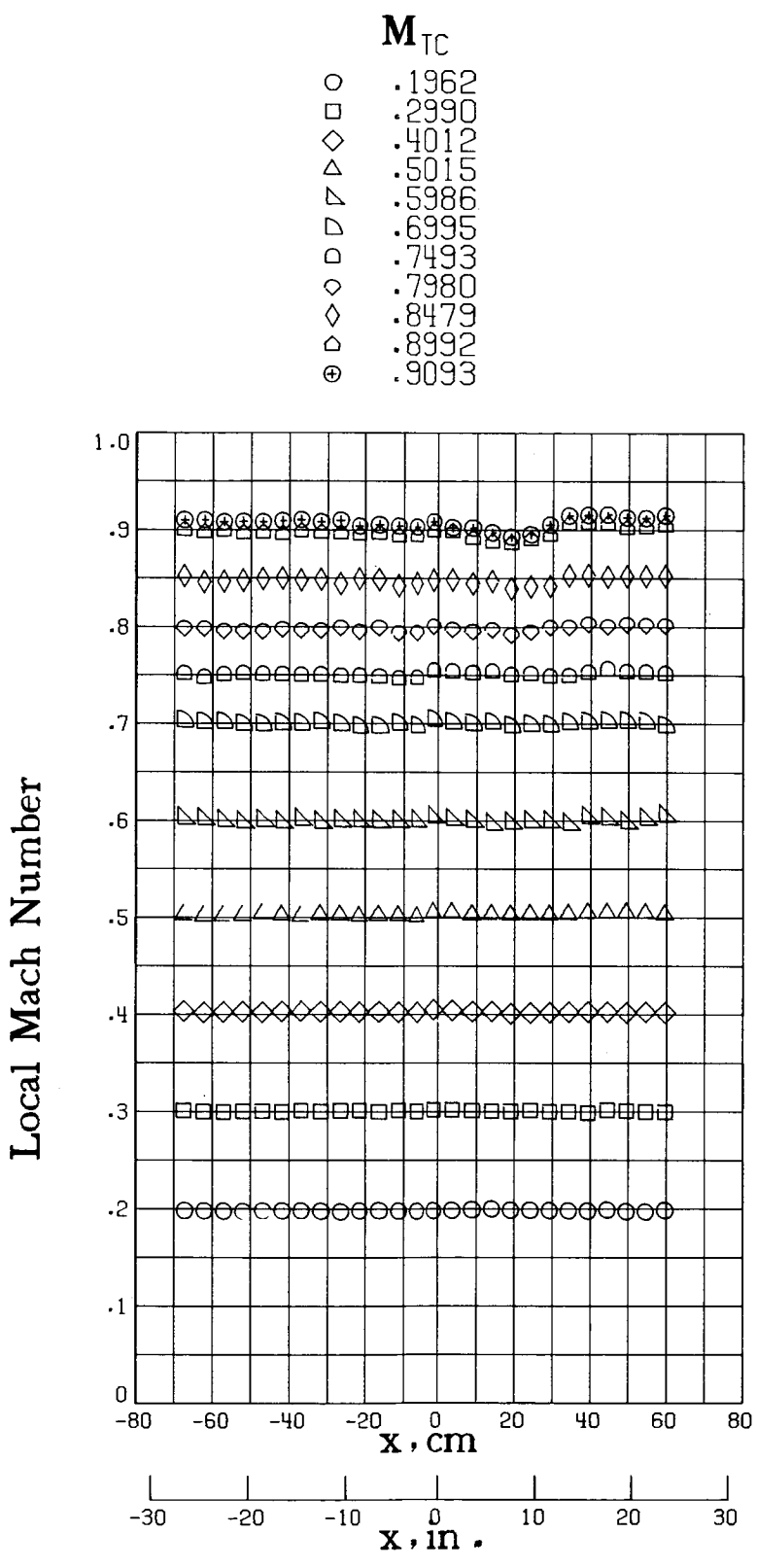

(b) T_t = 200 K.

Figure 31.- Continued.

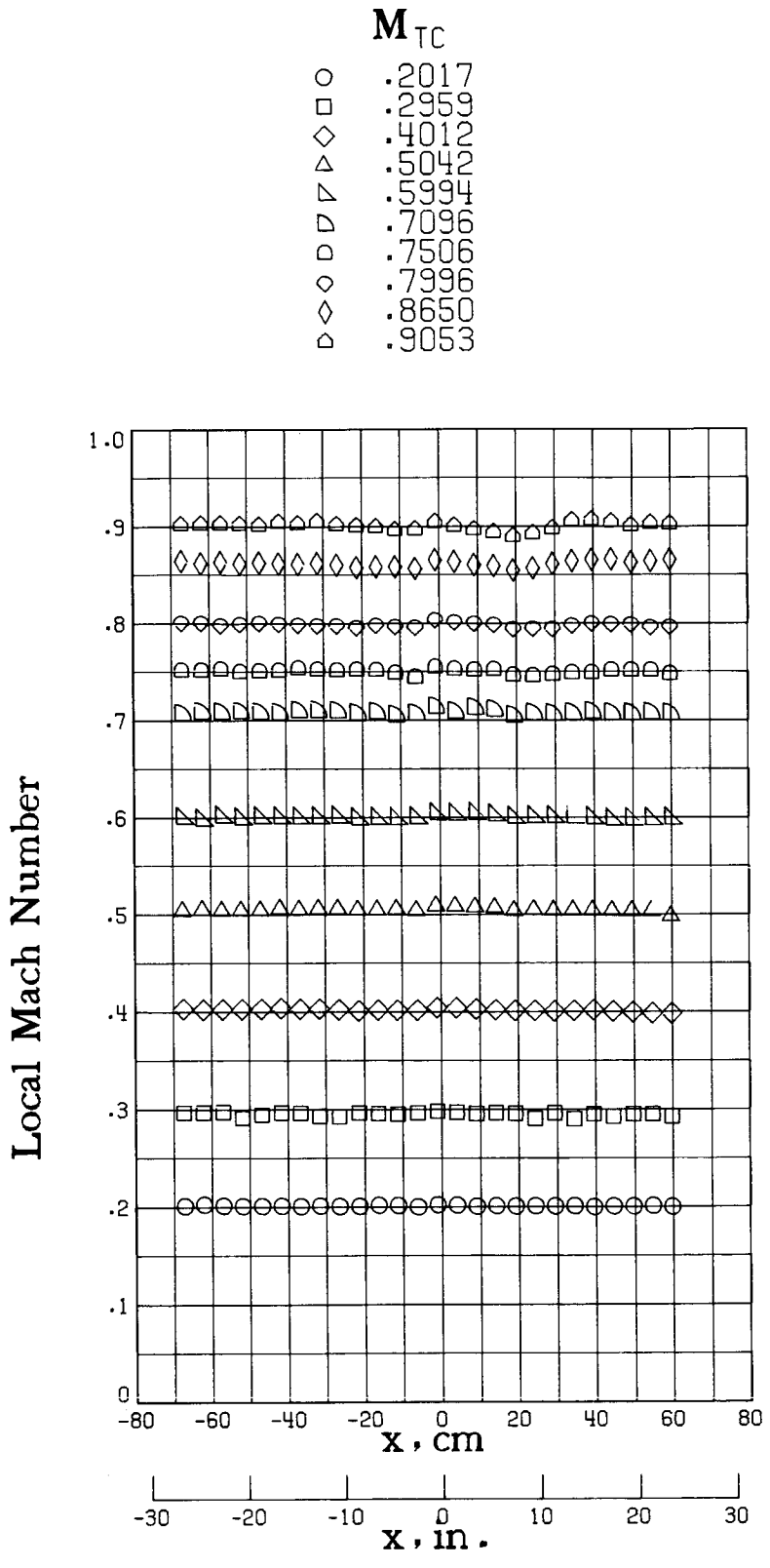

(c) T_t = 105 K.

Figure 31.- Concluded.

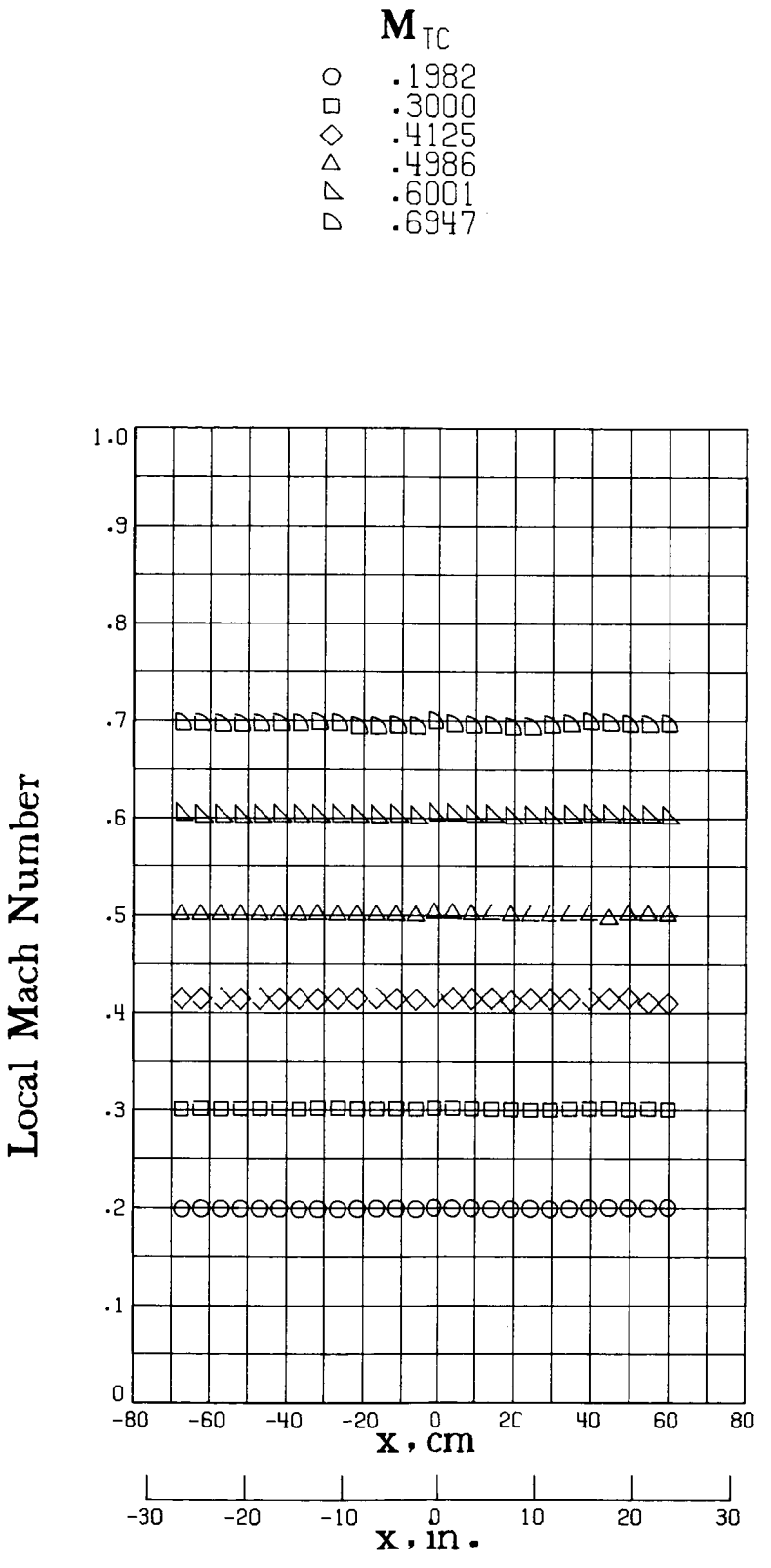

(a) T_t = 300 K.

Figure 32.- Longitudinal distribution of local Mach number along test-section ceiling for stagnation pressure of 5.1 atm.

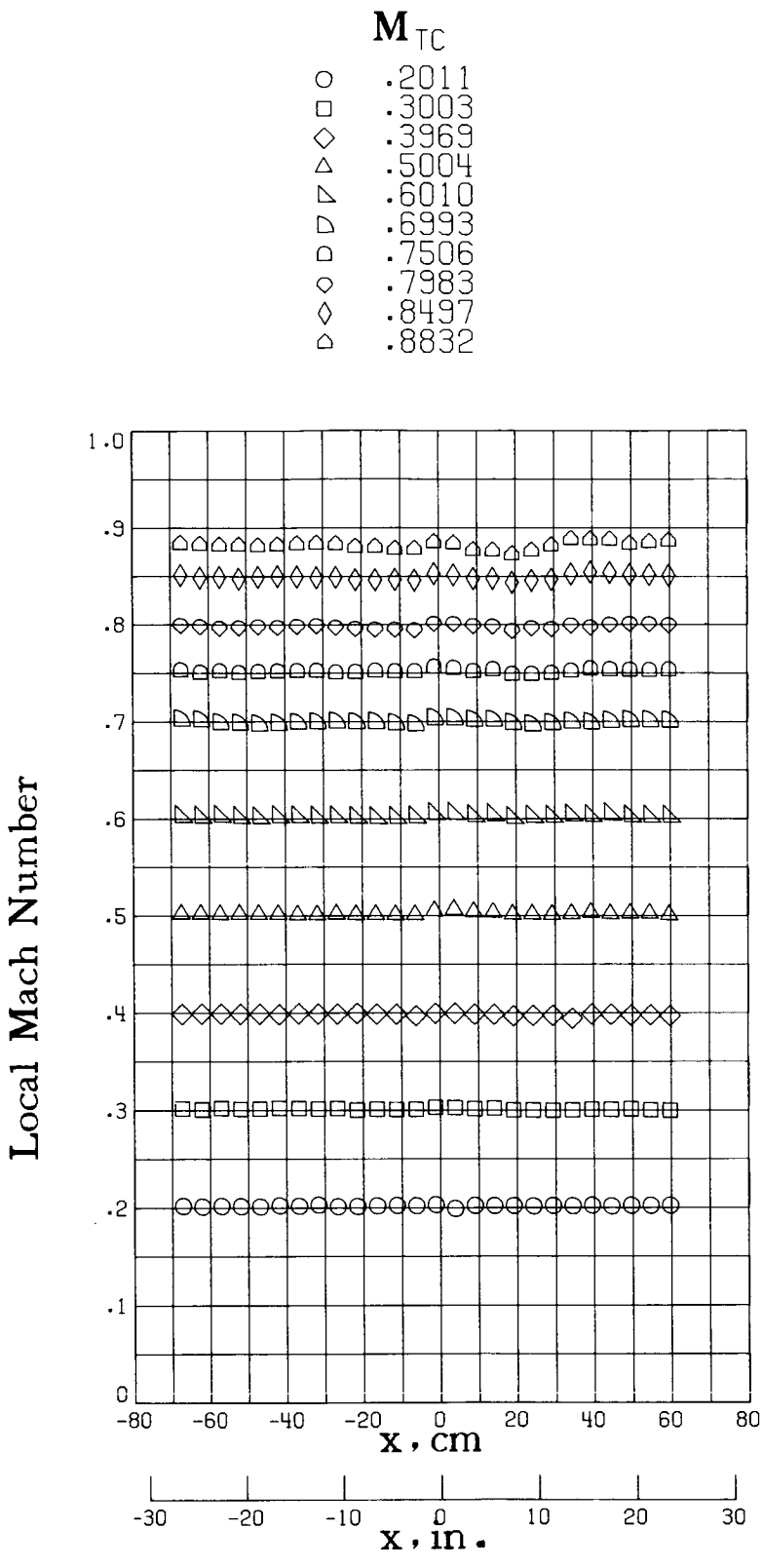

(b) T_t = 200 K.

Figure 32.- Continued.

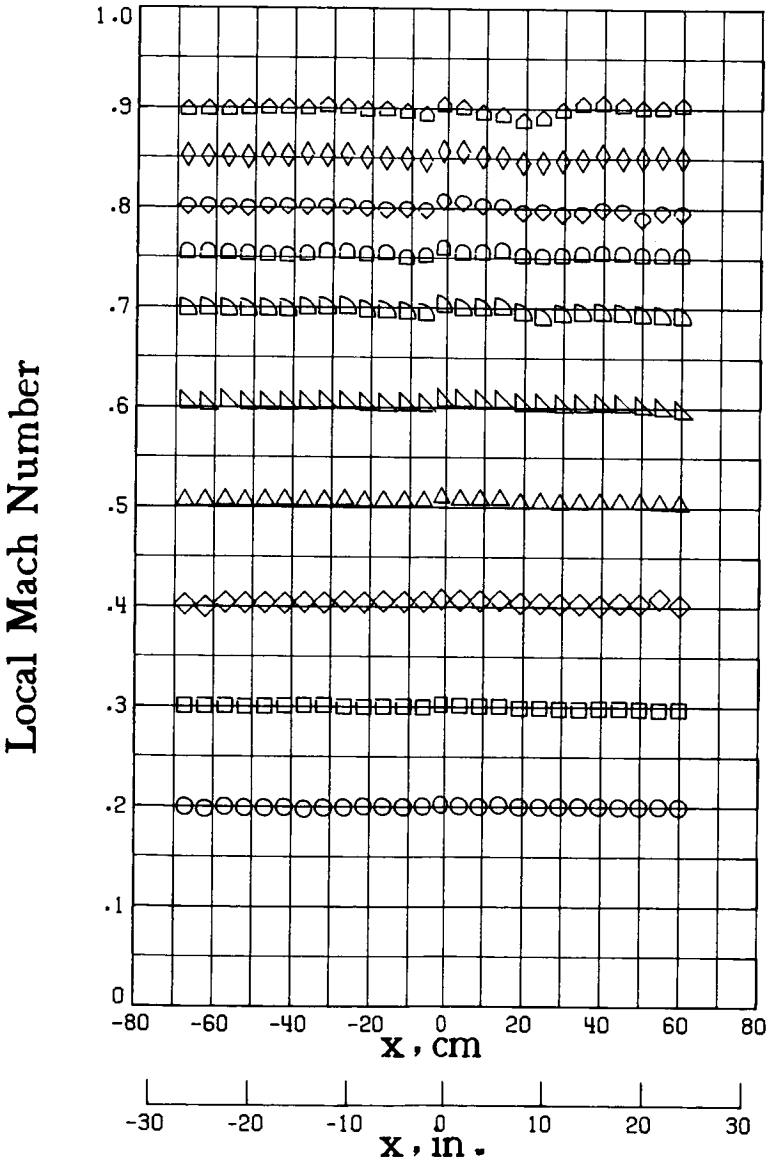

(c) T_t = 105 K.

Figure 32.- Concluded.

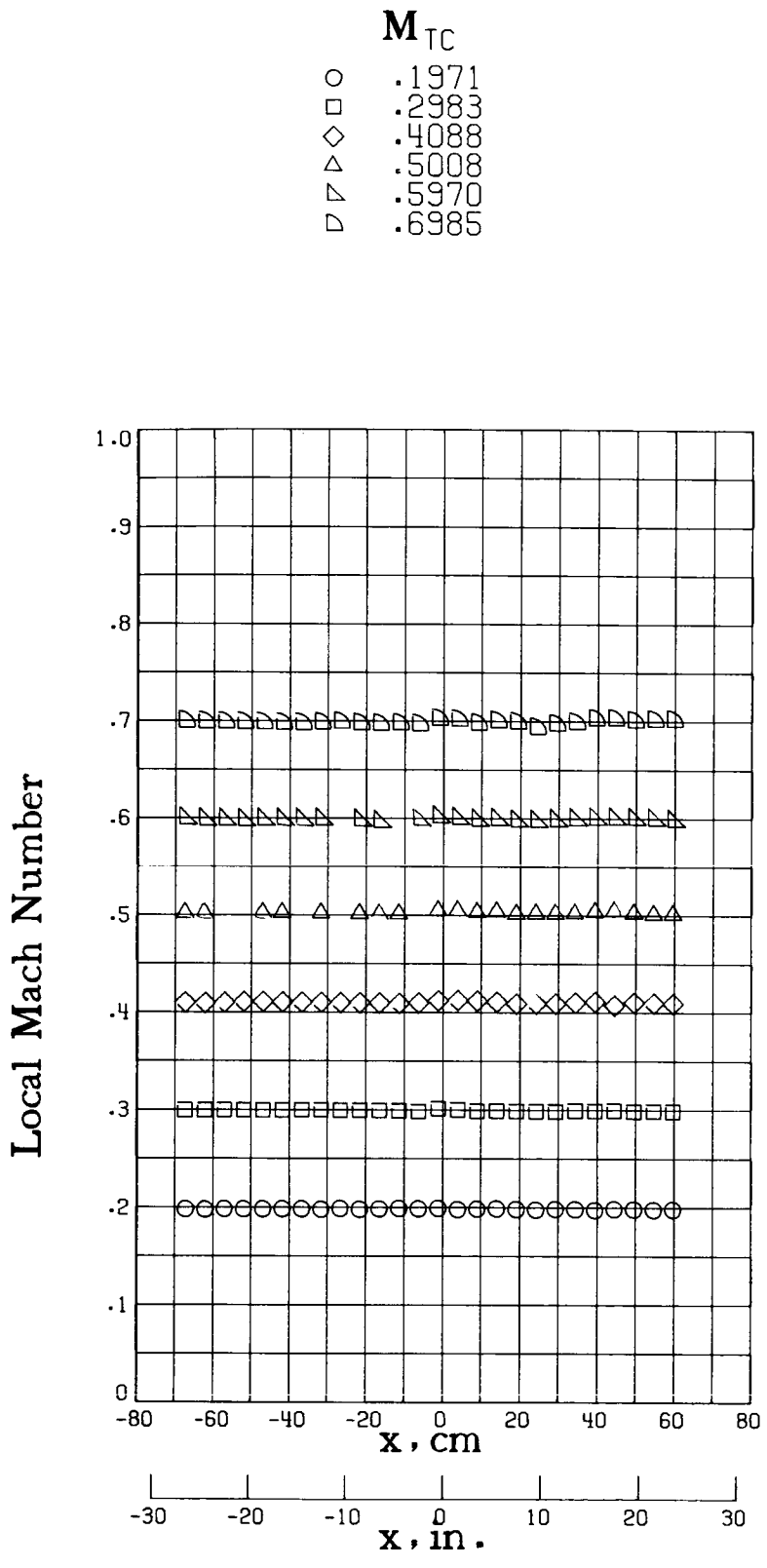

(a) T_t = 300 K.

Figure 33.- Longitudinal distribution of local Mach number along test-section ceiling for stagnation pressure of 6.0 atm.

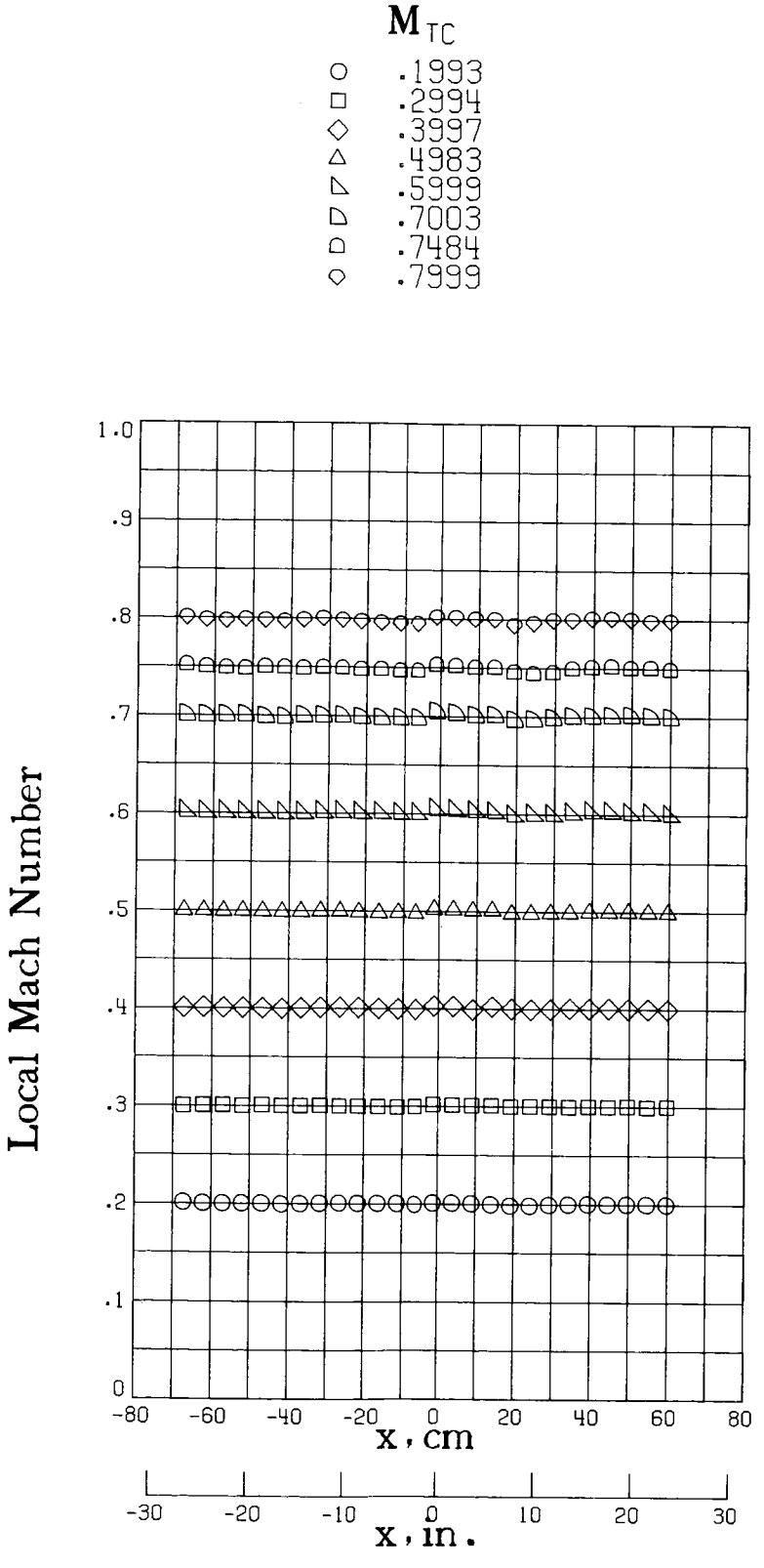

(b) T_t = 200 K.

Figure 33.- Continued.

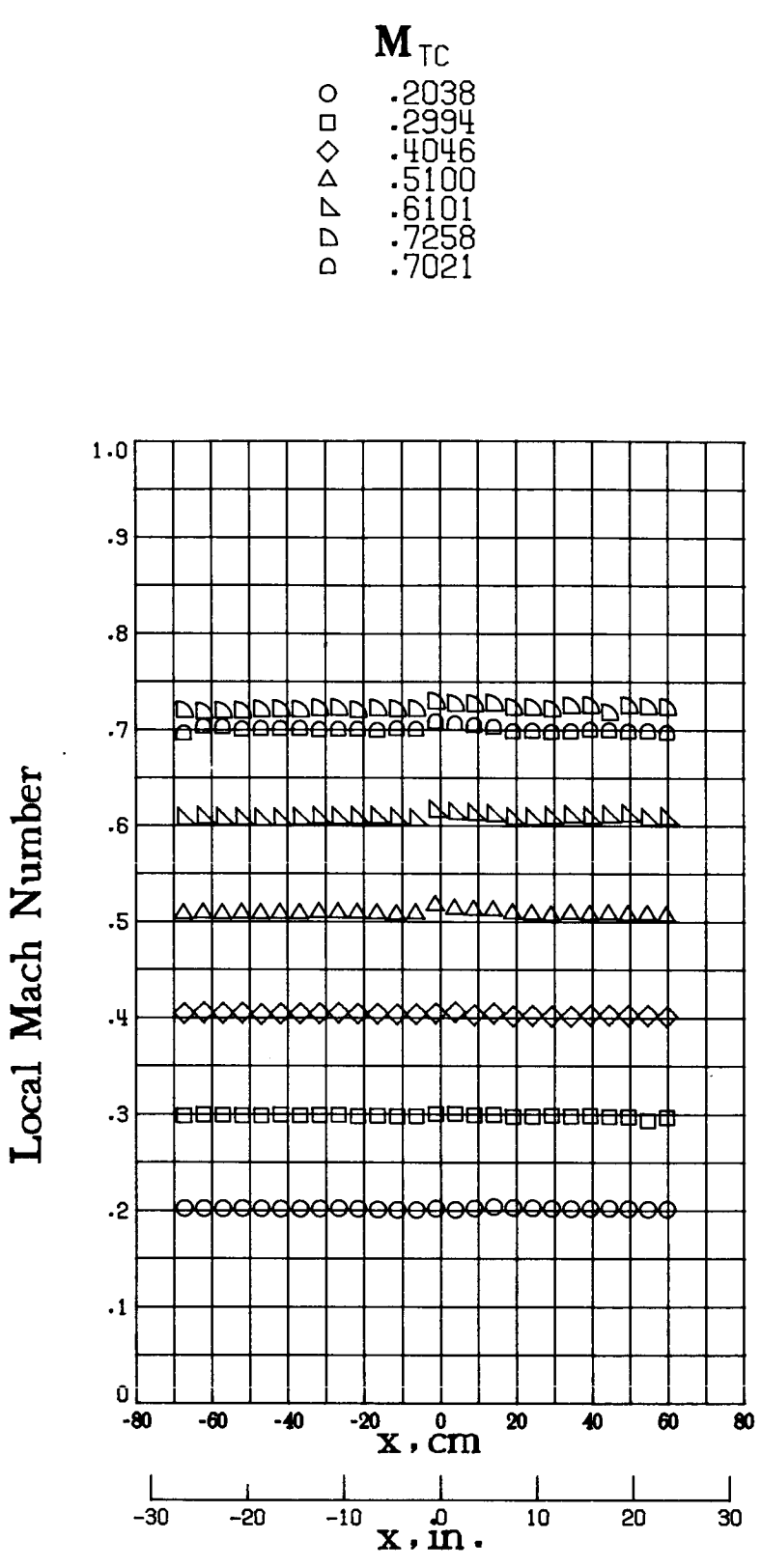

(c) T_t = 105 K.

Figure 33.- Concluded.

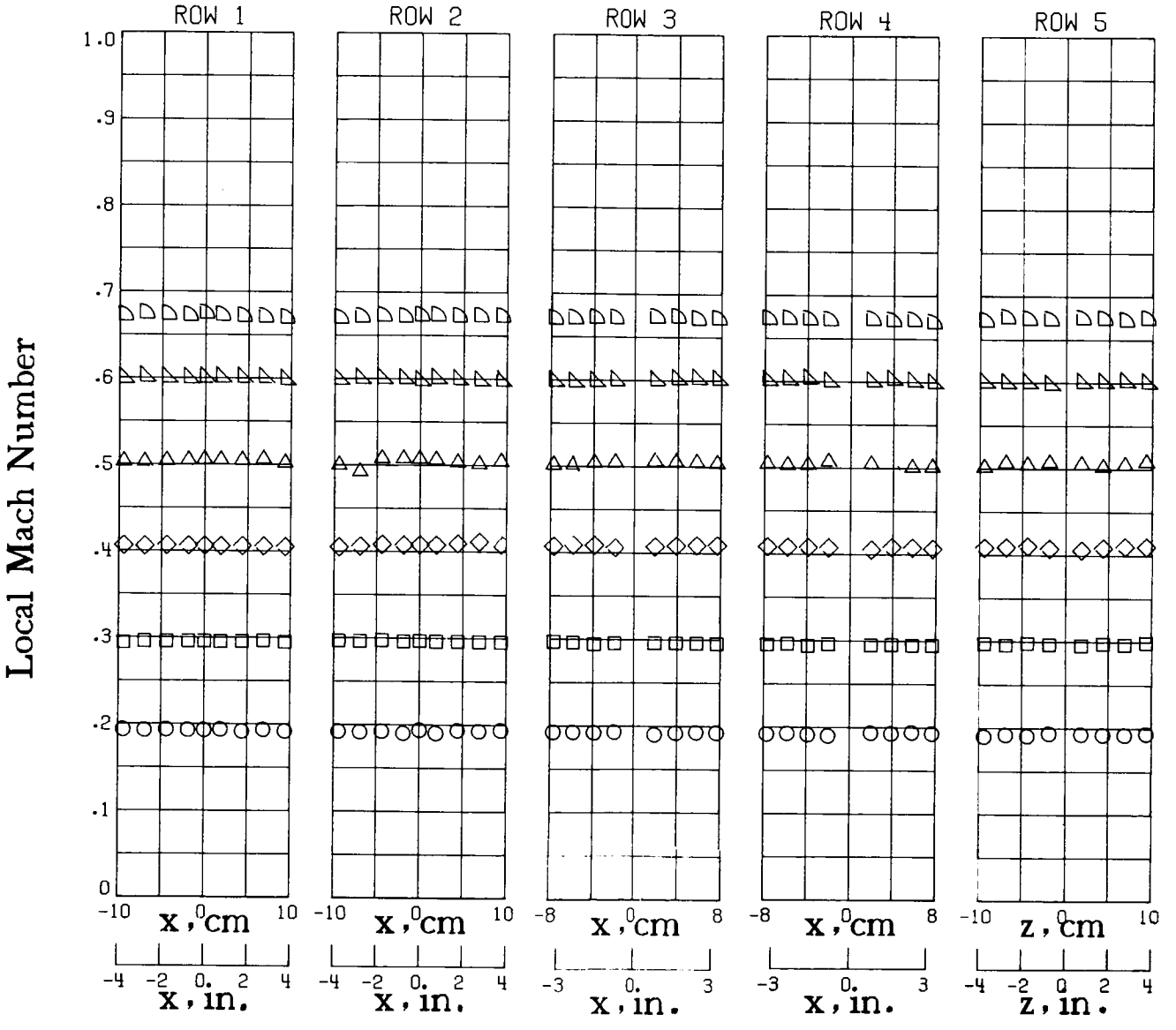

(a) T_t = 300 K.

Figure 34.- Local Mach number distribution along test-section left turntable at stagnation pressure of 1.2 atm.

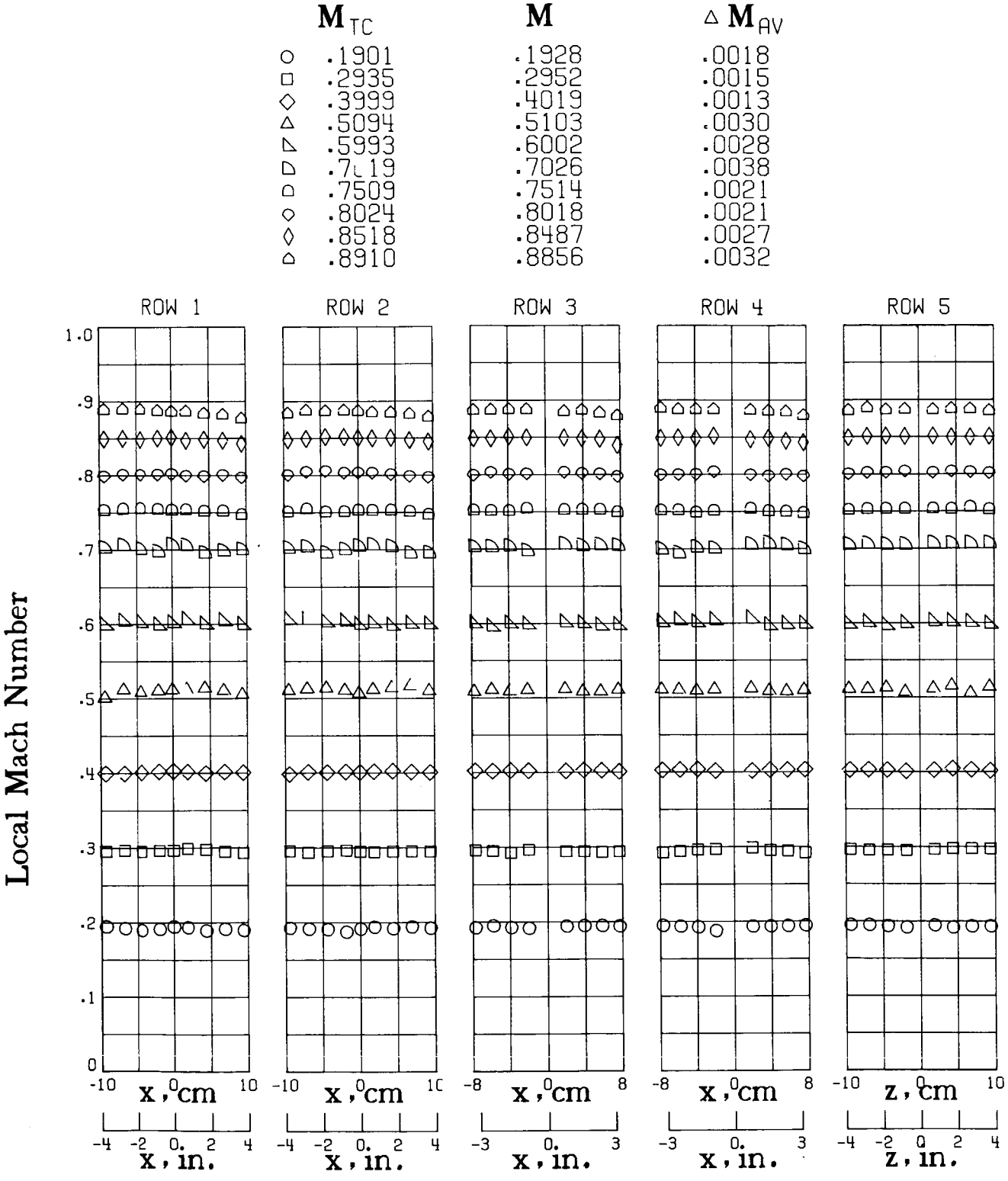

(b) T_t = 200 K.

Figure 34.- Continued.

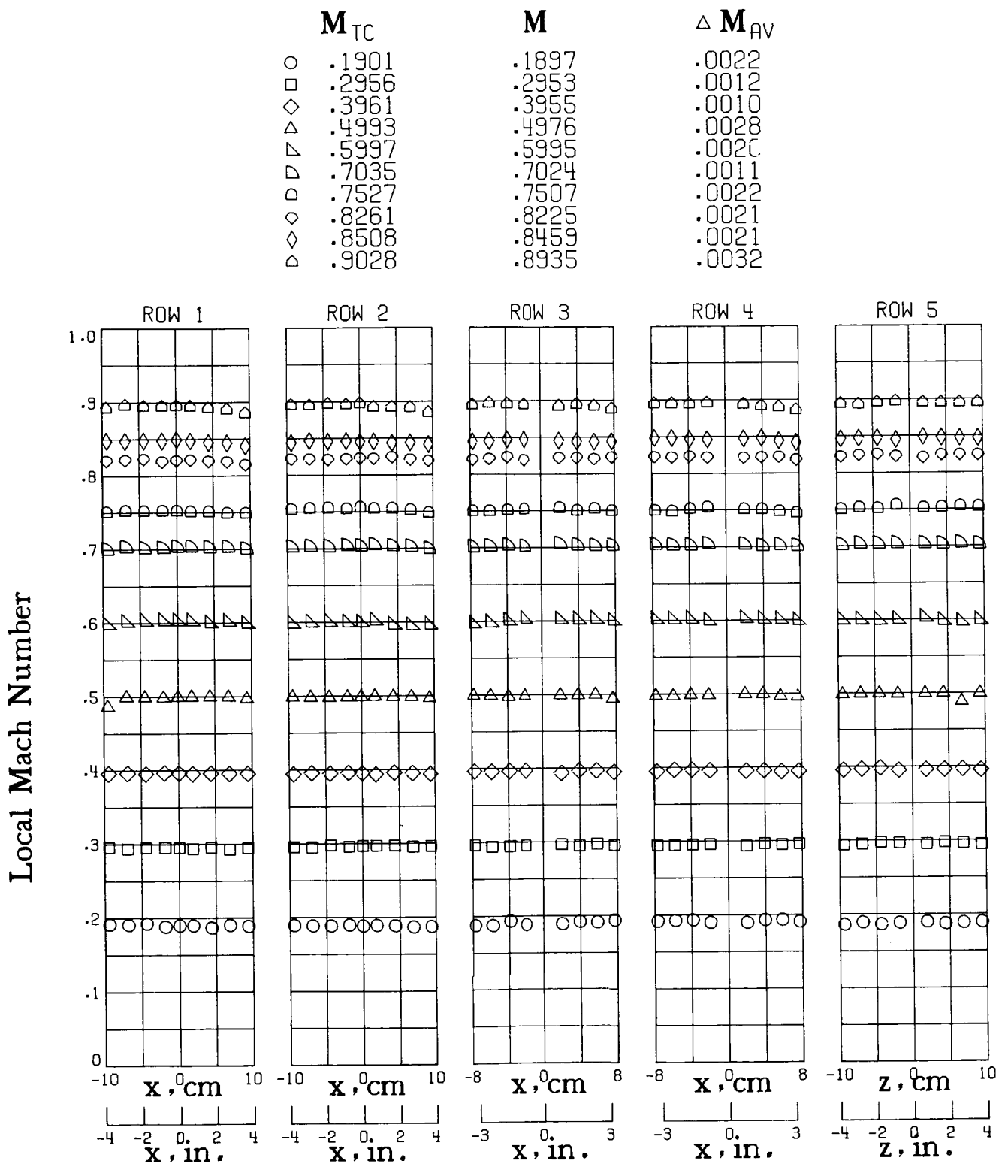

(c) T_t = 105 K.

Figure 34.- Concluded.

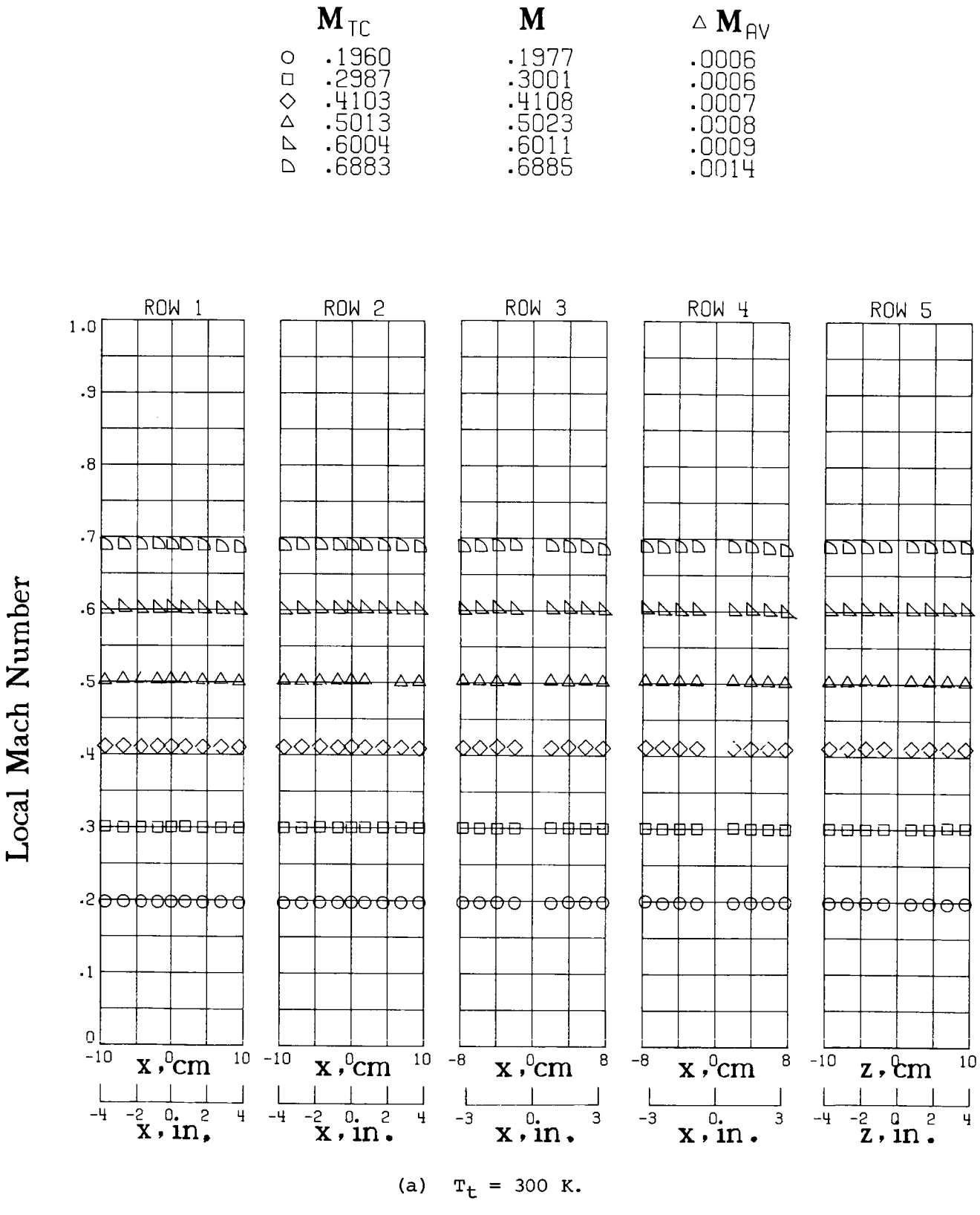

(a) T_t = 300 K.

Figure 35.- Local Mach number distribution along test-section left turntable at stagnation pressure of 3.1 atm.

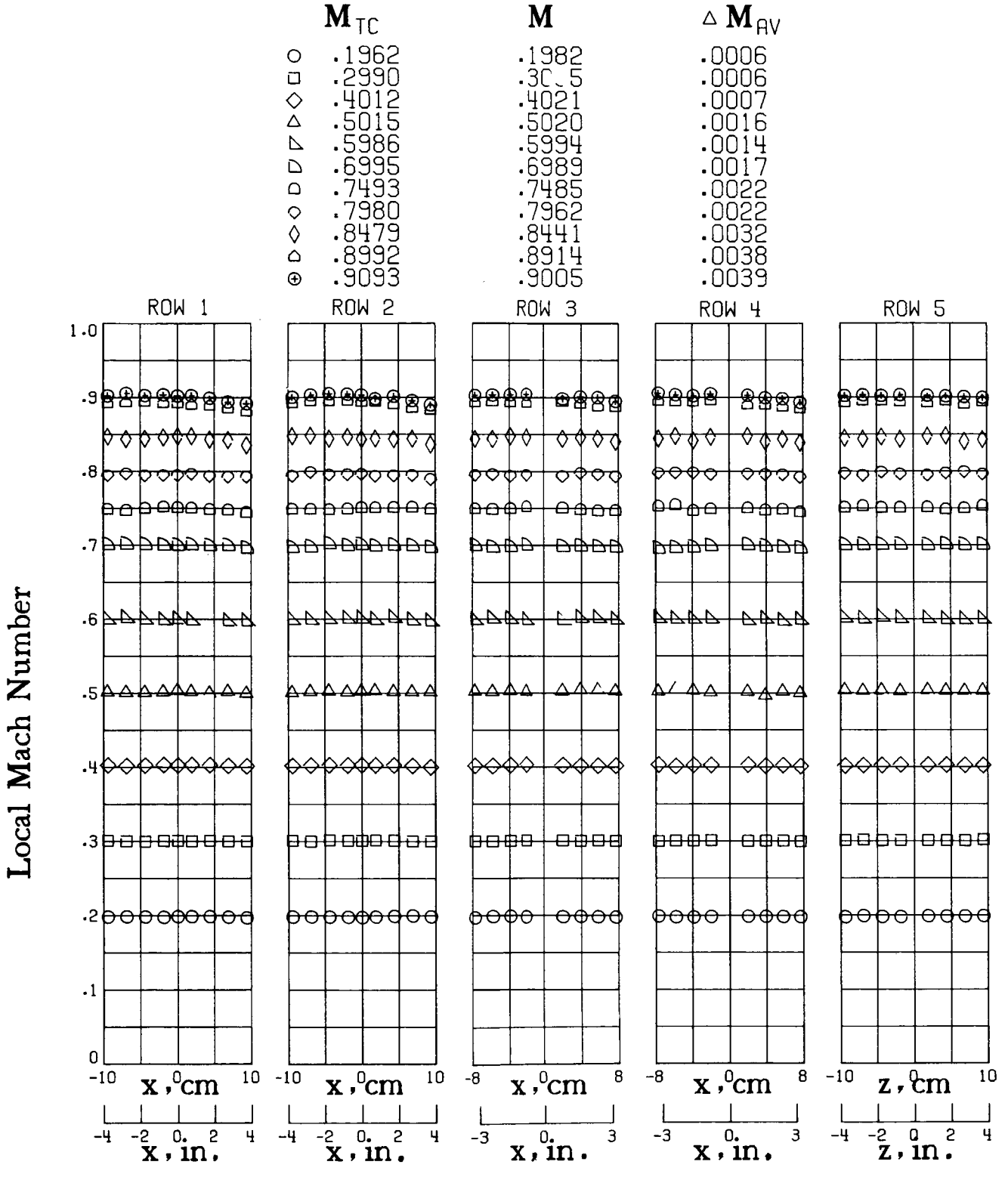

(b) T_t = 200 K.

Figure 35.- Continued.

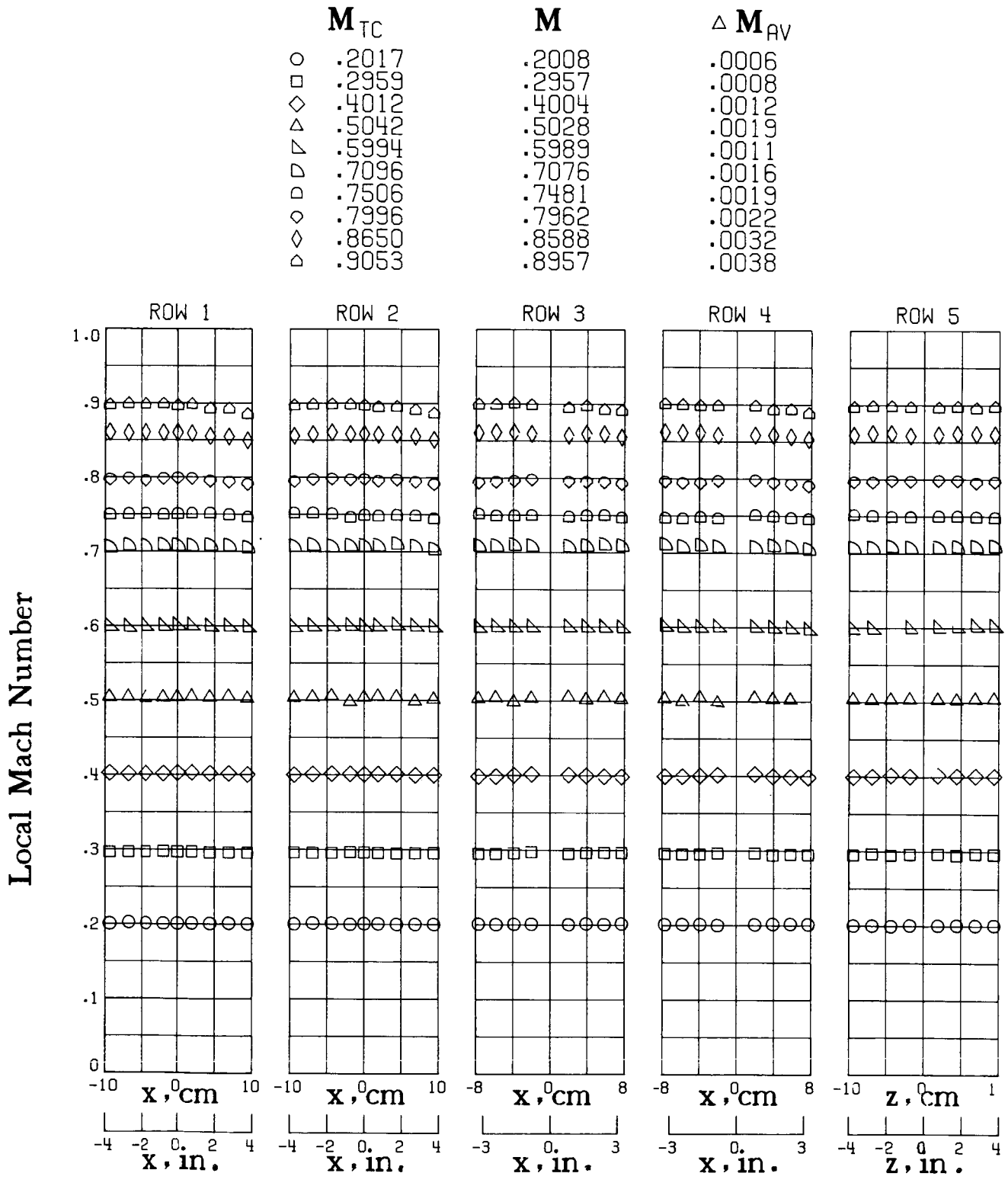

(c) T_t = 105 K.

Figure 35.- Concluded.

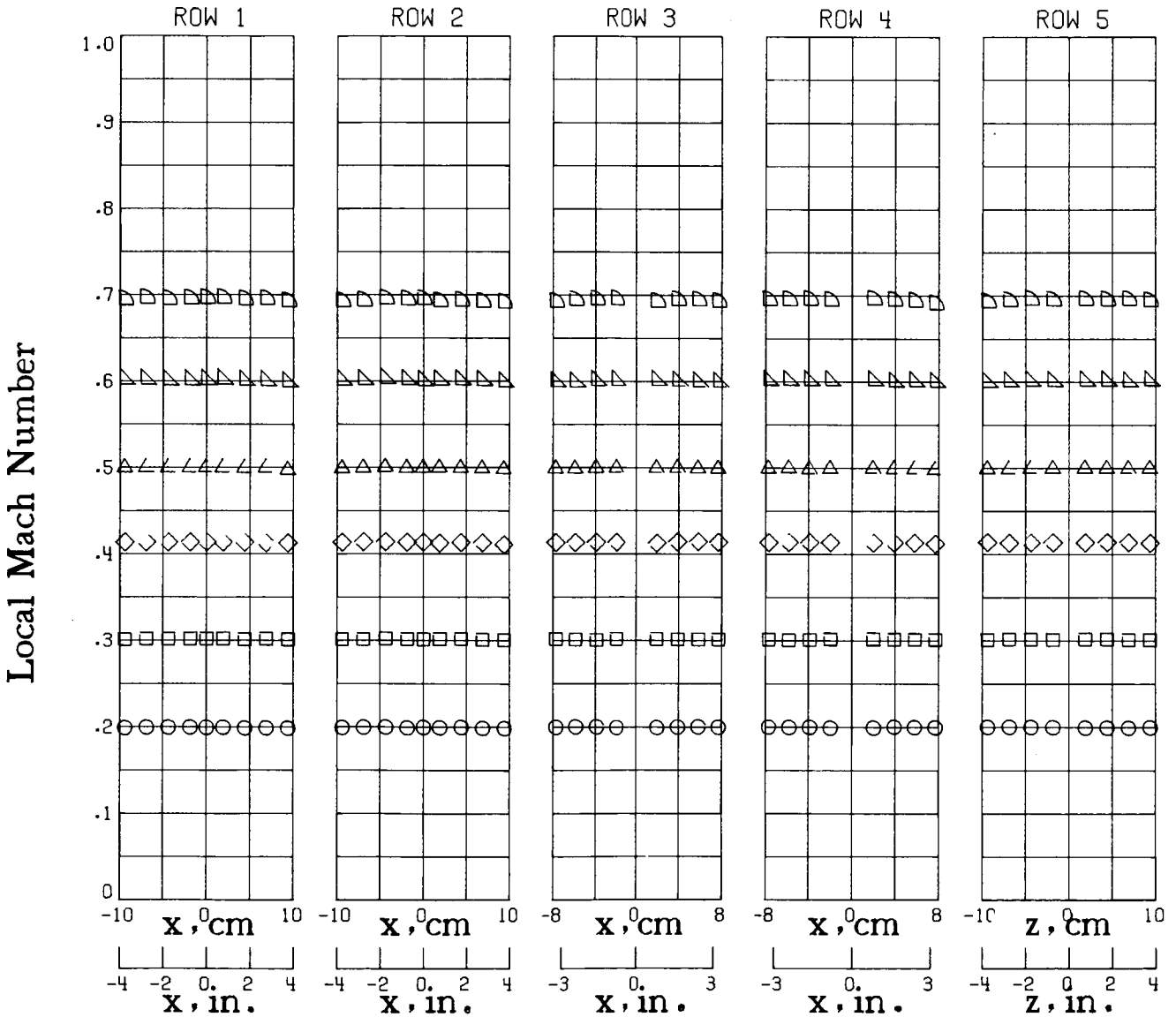

(a) T_t = 300 K.

Figure 36.- Local Mach number distribution along test-section left turntable at stagnation pressure of 5.1 atm.

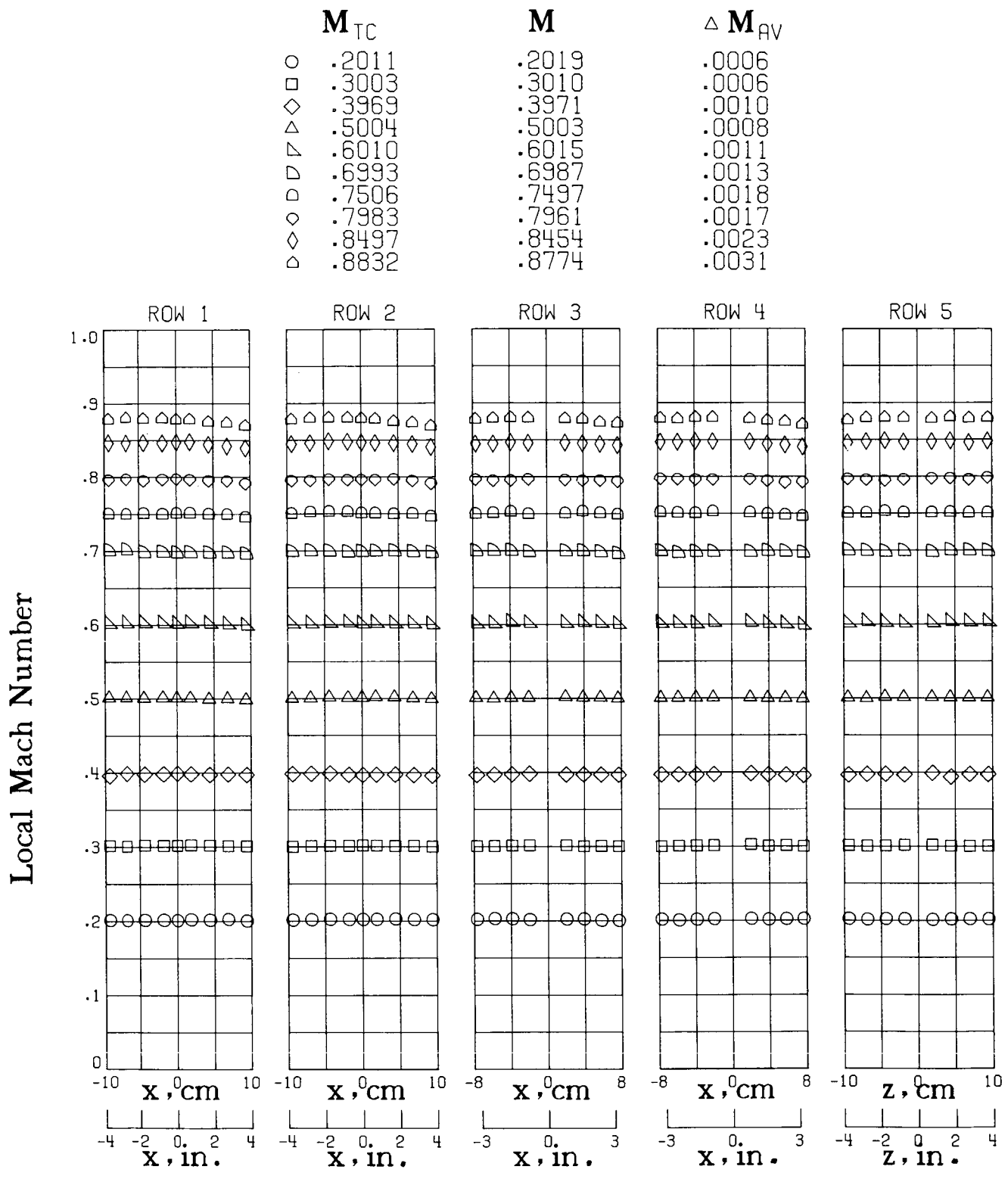

(b) T_t = 200 K.

Figure 36.- Continued.

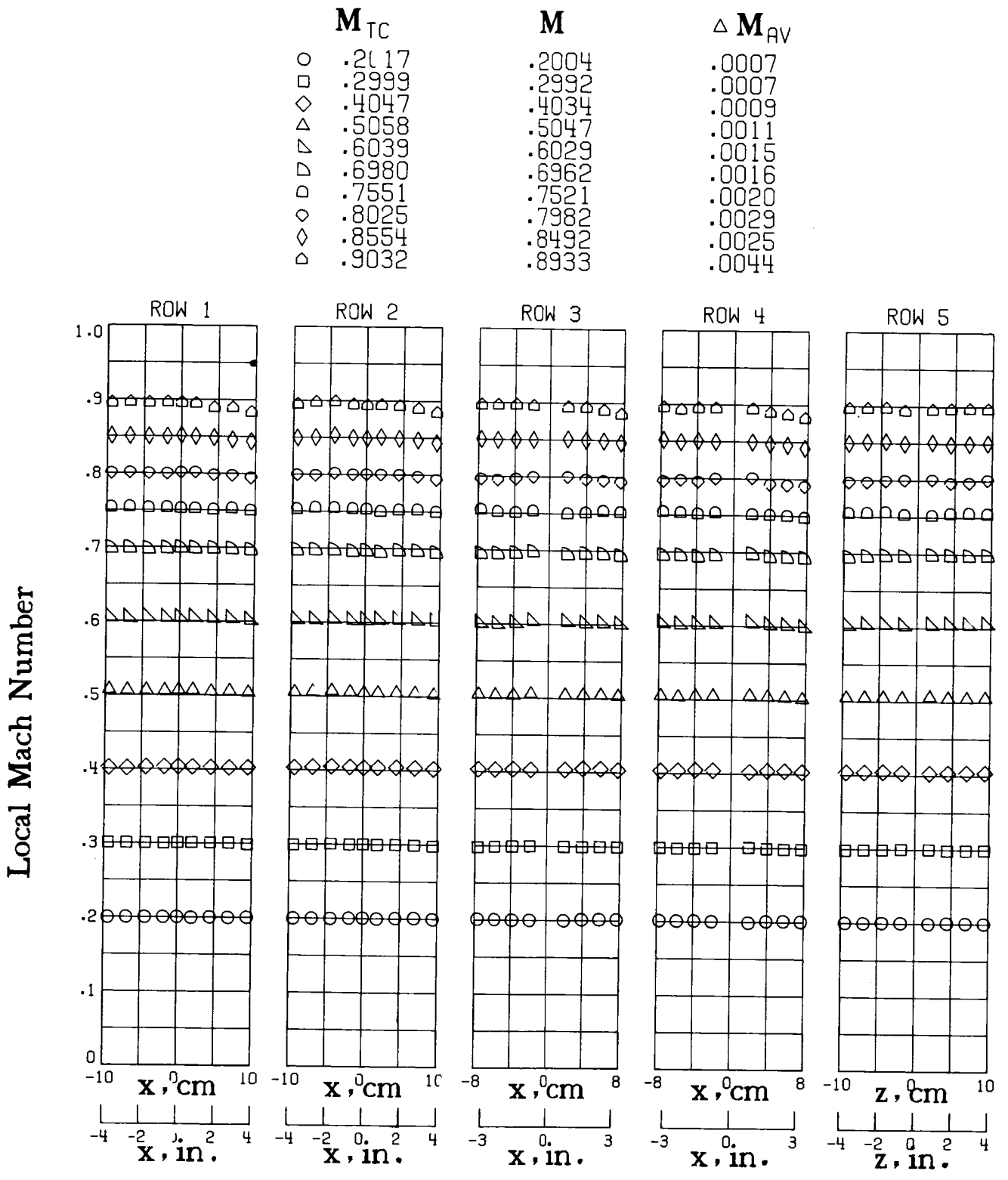

(c) T_t = 105 K.

Figure 36.- Concluded.

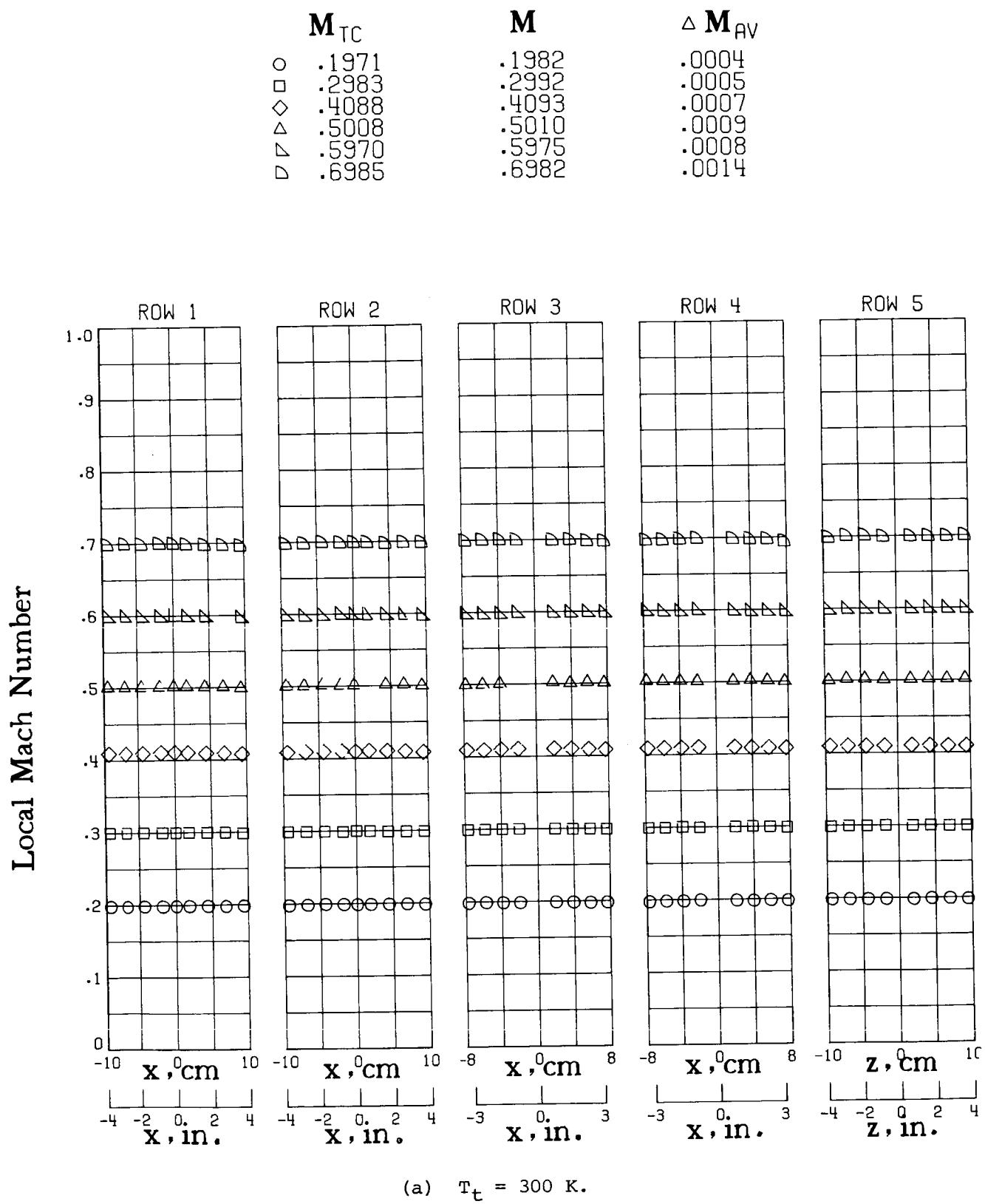

(a) T_t = 300 K.

Figure 37.- Local Mach number distribution along test-section left turntable at stagnation pressure of 6.0 atm.

	M_{TC}	M	ΔM_{AV}
○	.1993	.2003	.0007
□	.2994	.3003	.0005
◇	.3997	.3999	.0006
△	.4983	.4981	.0008
◺	.5999	.6004	.0011
◻	.7003	.6995	.0014
◻	.7484	.7472	.0015
◇	.7999	.7974	.0021

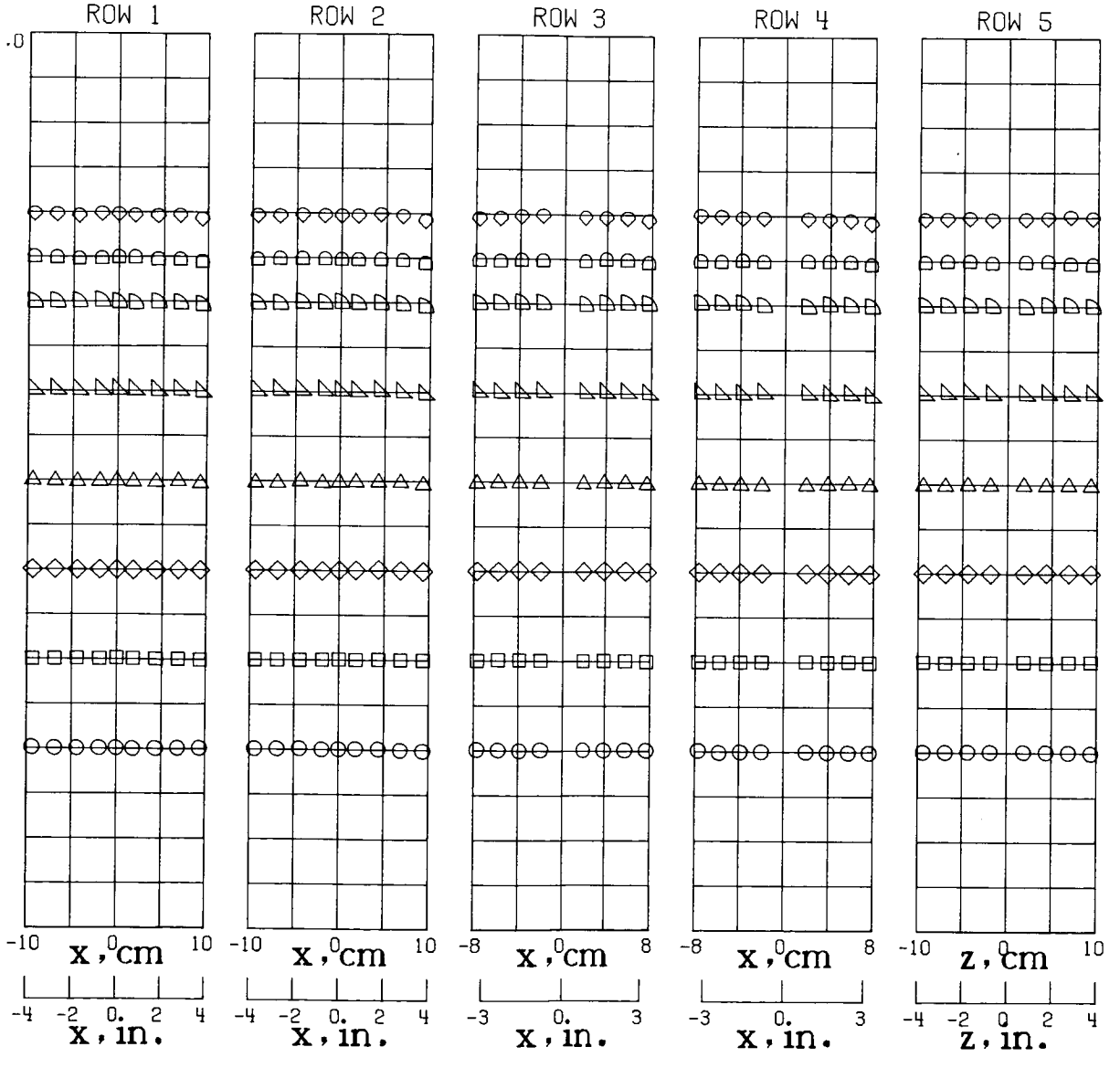

(b) T_t = 200 K.

Figure 37.- Continued.

	M_{TC}	M	ΔM_{AV}
○	.2038	.2022	.0006
□	.2994	.2986	.0010
◇	.4046	.4032	.0009
△	.5100	.5087	.0010
◺	.6101	.6089	.0015
◺	.7258	.7236	.0029
◺	.7021	.7002	.0017

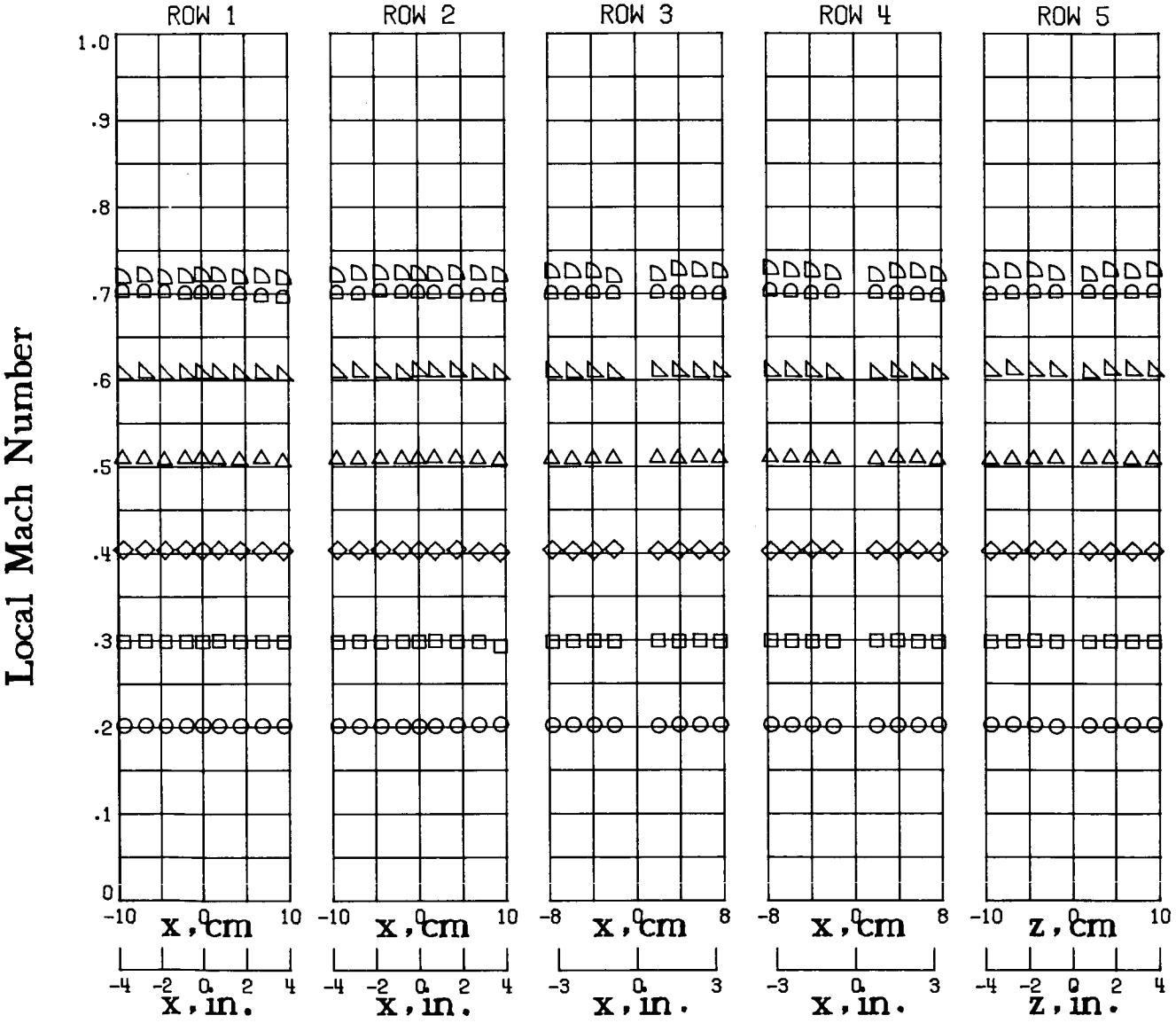

(c) T_t = 105 K.

Figure 37.- Concluded.

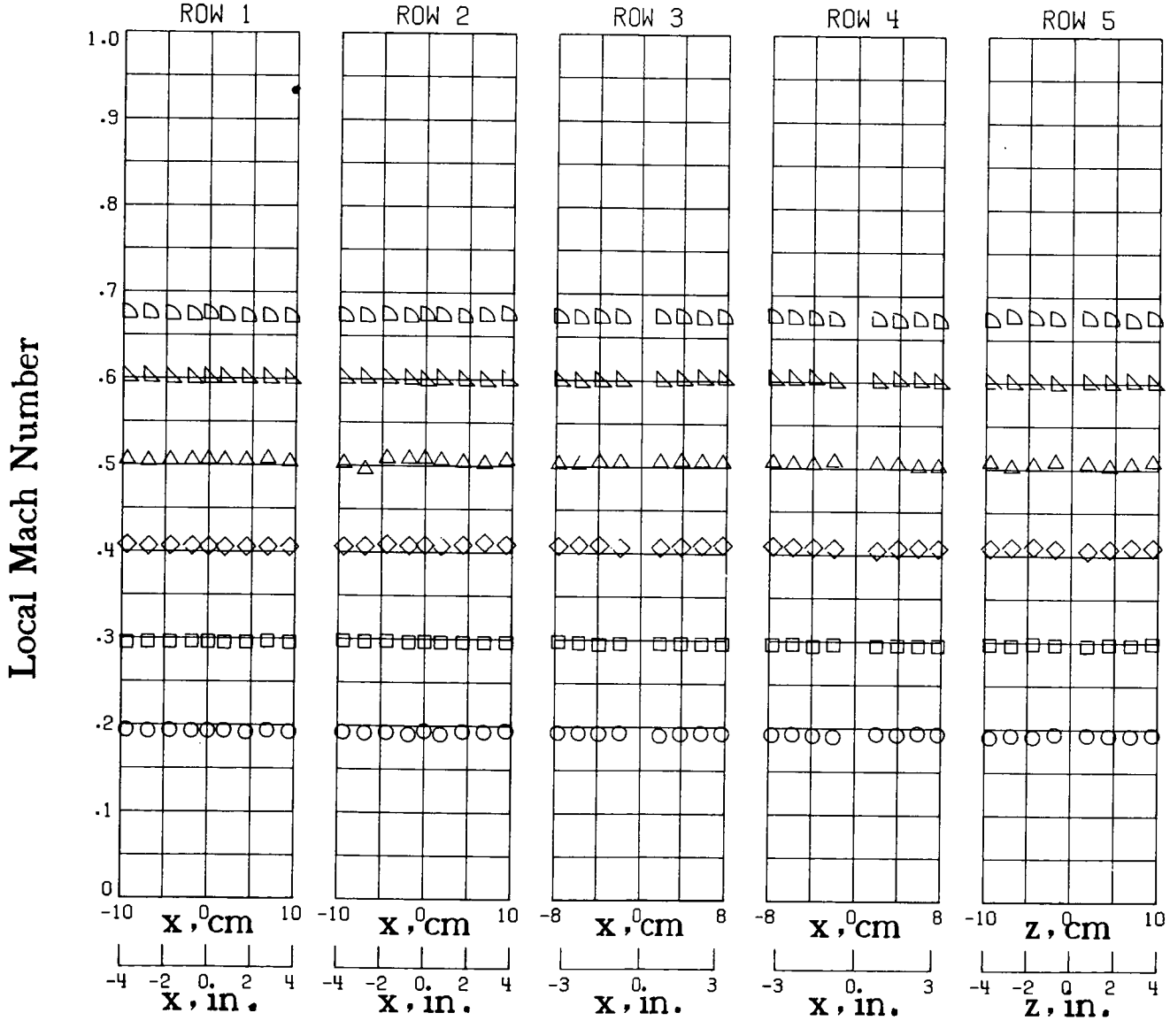

(a) T_t = 300 K.

Figure 38.- Local Mach number distribution along test-section right turntable at stagnation pressure of 1.2 atm.

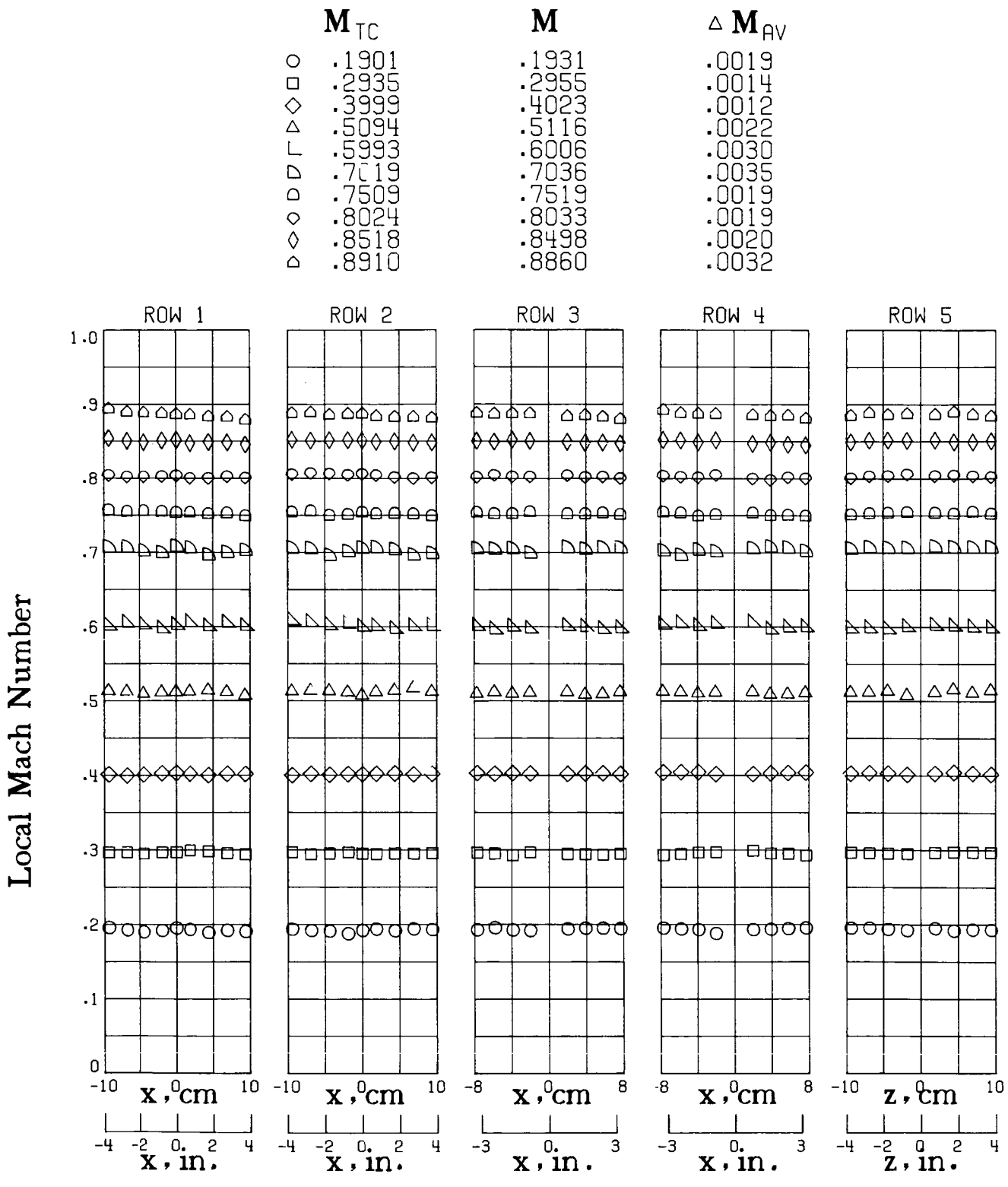

(b) T_t = 200 K.

Figure 38.- Continued.

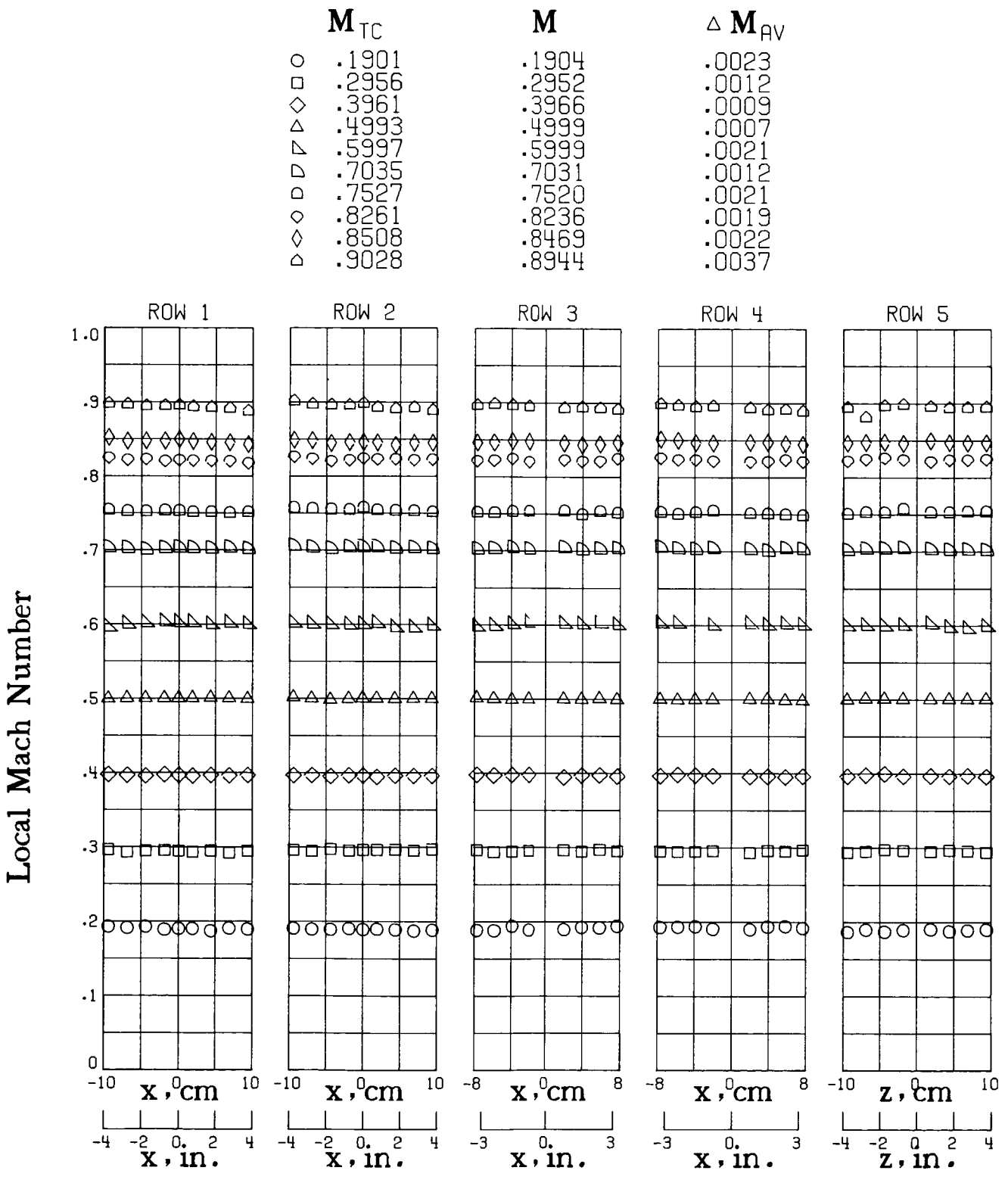

(c) T_t = 105 K.

Figure 38.- Concluded.

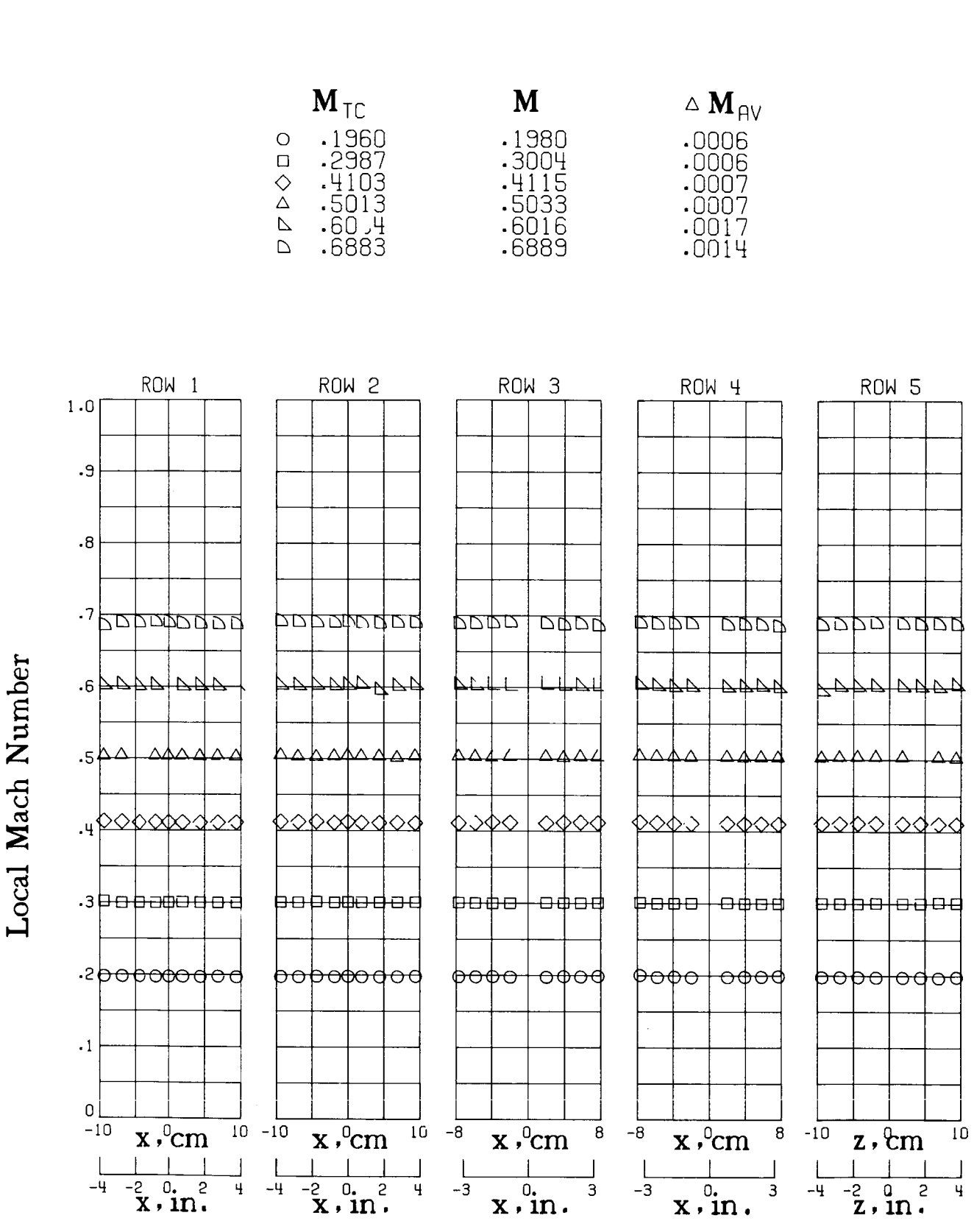

(a) T_t = 300 K.

Figure 39.- Local Mach number distribution along test-section right turntable at stagnation pressure of 3.1 atm.

C-2

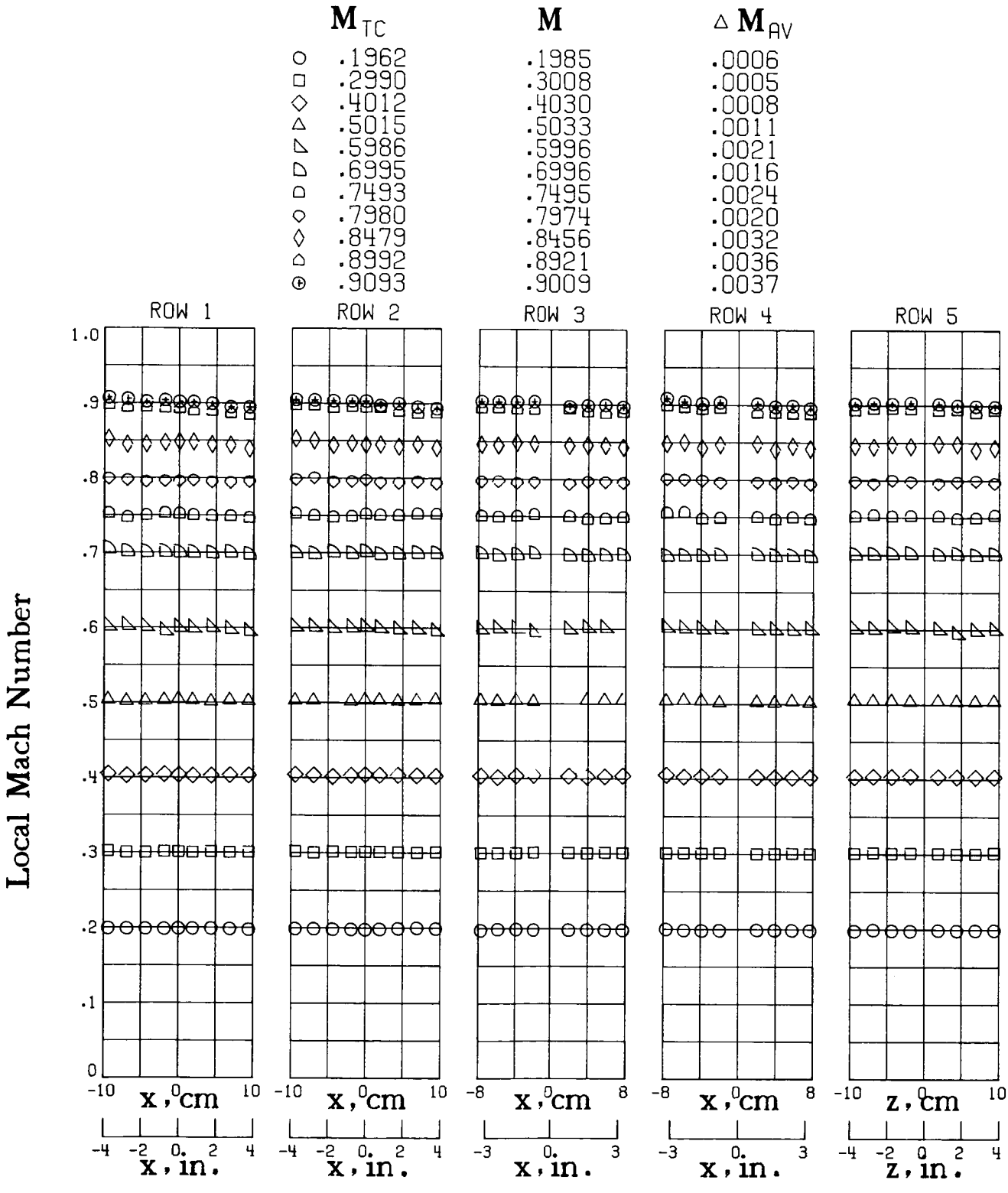

(b) T_t = 200 K.

Figure 39.- Continued.

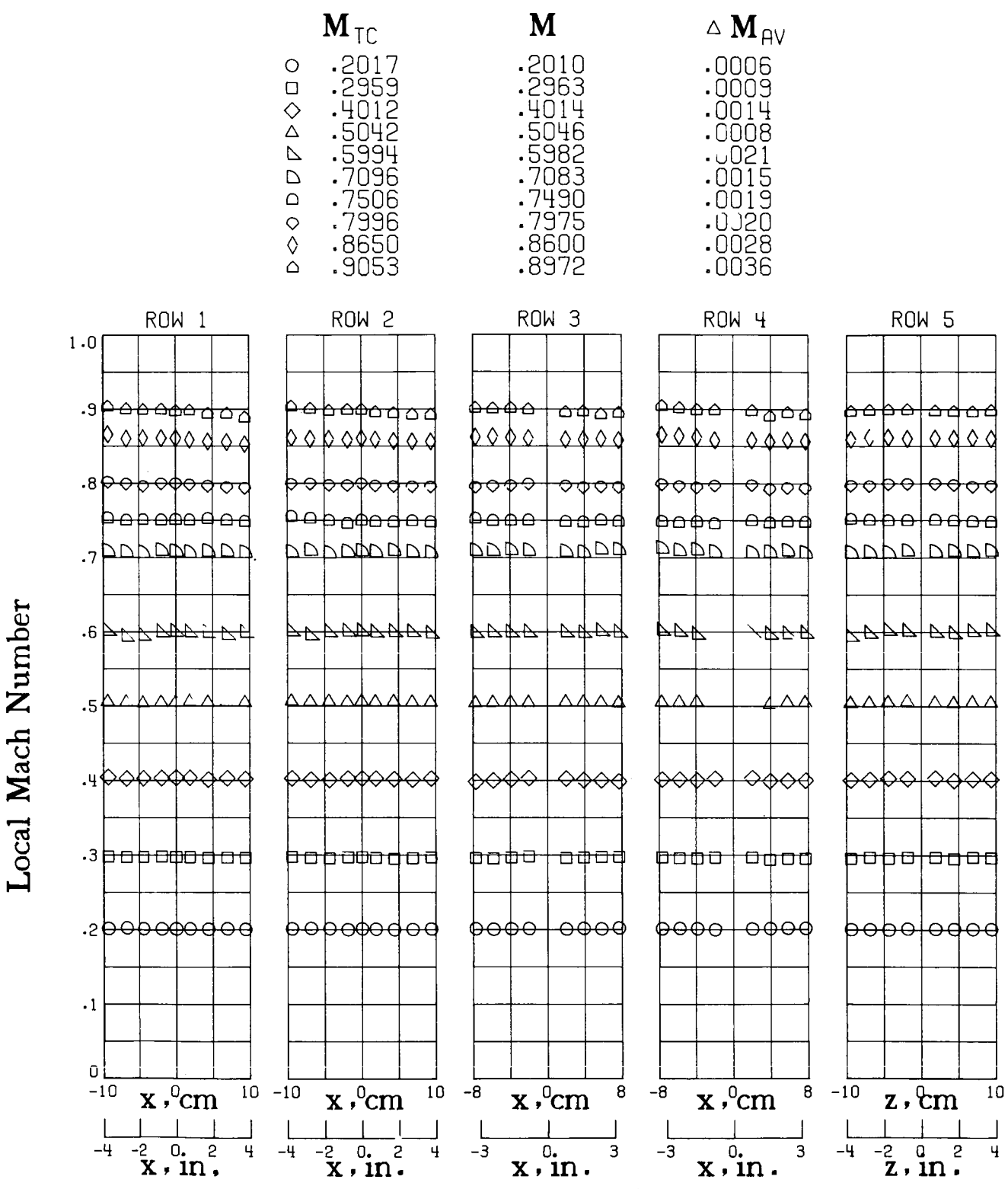

(c) T_t = 105 K.

Figure 39.- Concluded.

	M_{TC}	M	ΔM_{AV}
○	.1982	.1996	.0005
□	.3000	.3014	.0004
◇	.4125	.4142	.0006
△	.4986	.4998	.0006
◺	.6001	.6011	.0011
◺	.6947	.6953	.0013

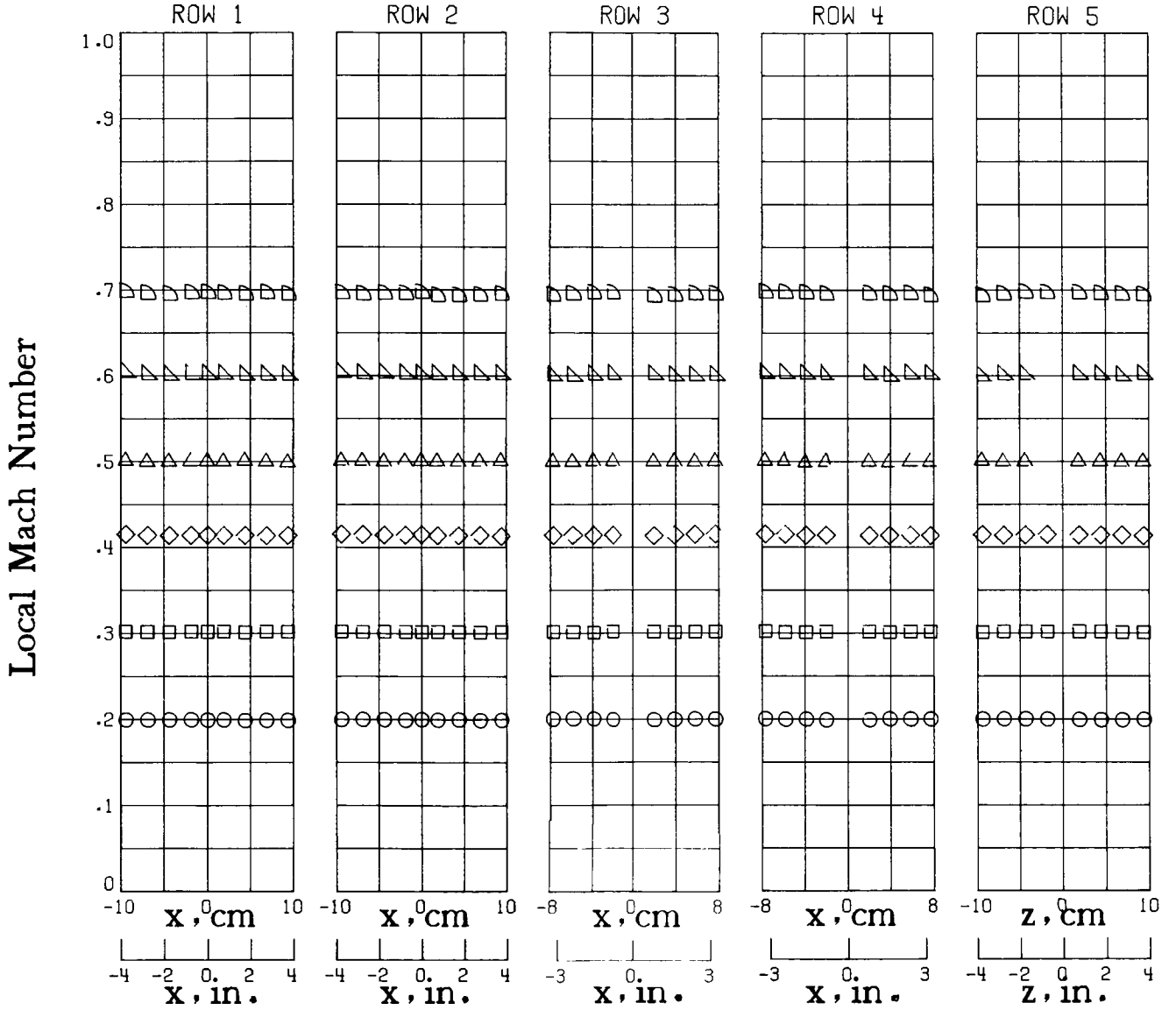

(a) T_t = 300 K.

Figure 40.- Local Mach number distribution along test-section right turntable at stagnation pressure of 5.1 atm.

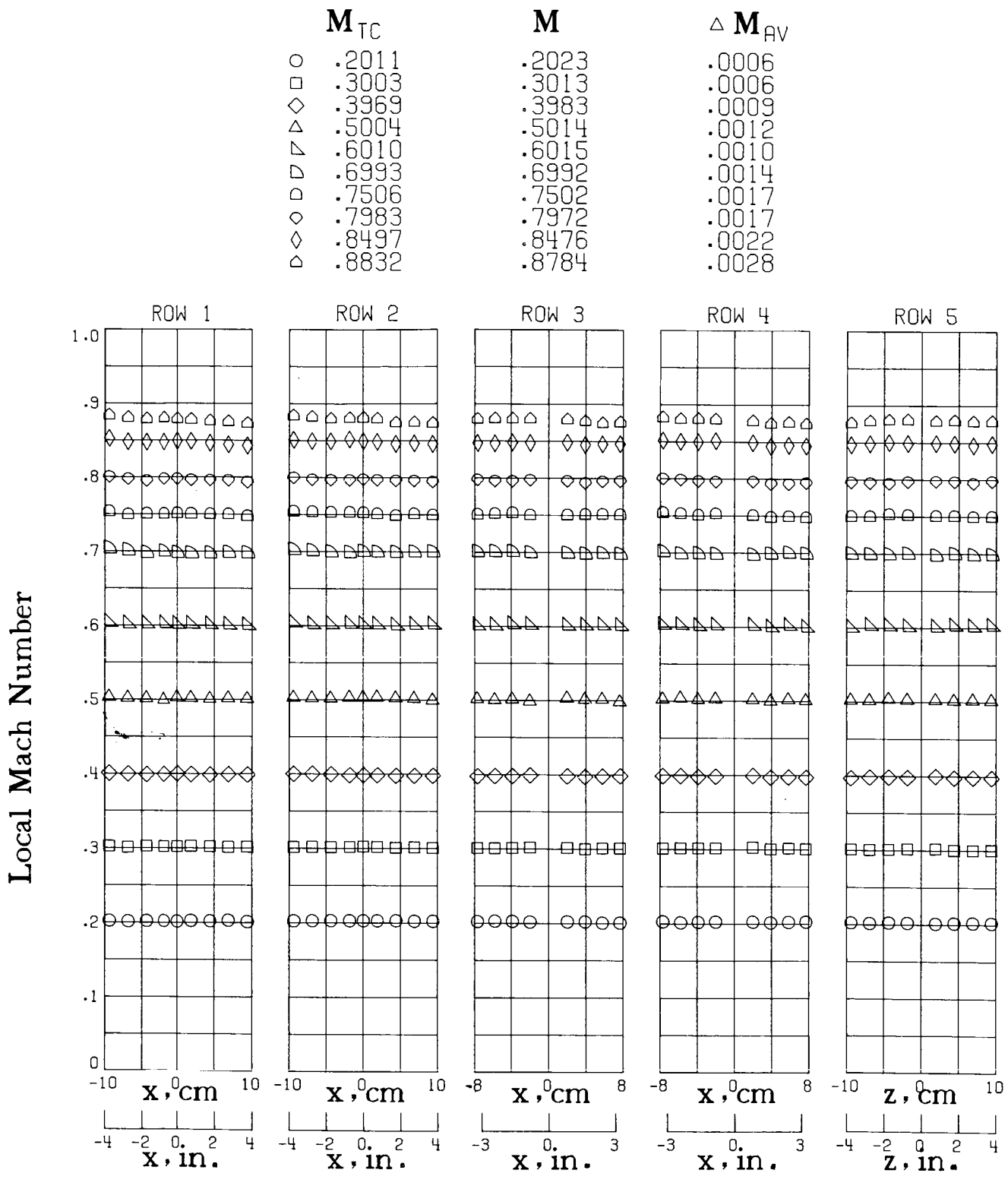

(b) T_t = 200 K.

Figure 40.- Continued.

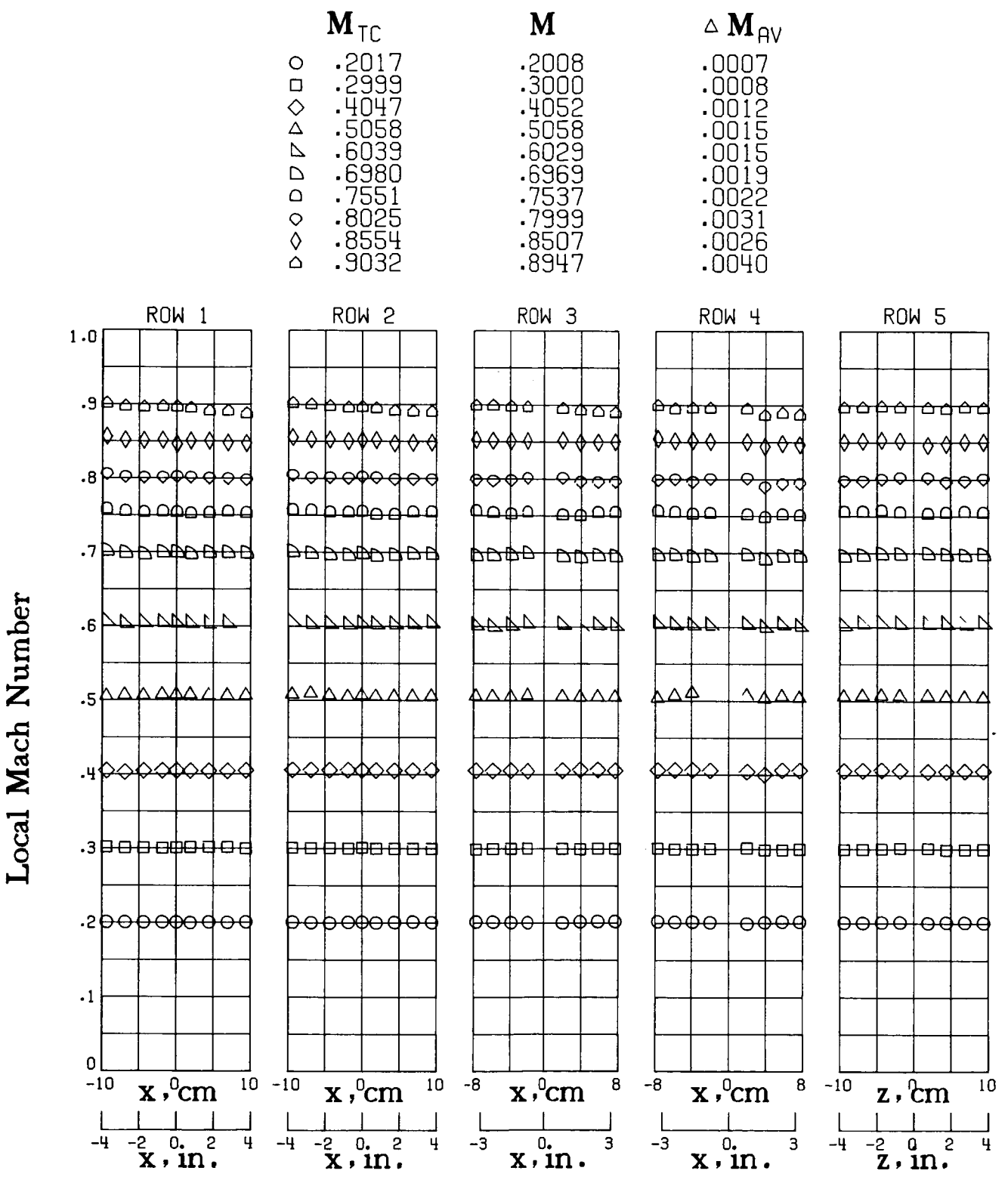

(c) T_t = 105 K.

Figure 40.- Concluded.

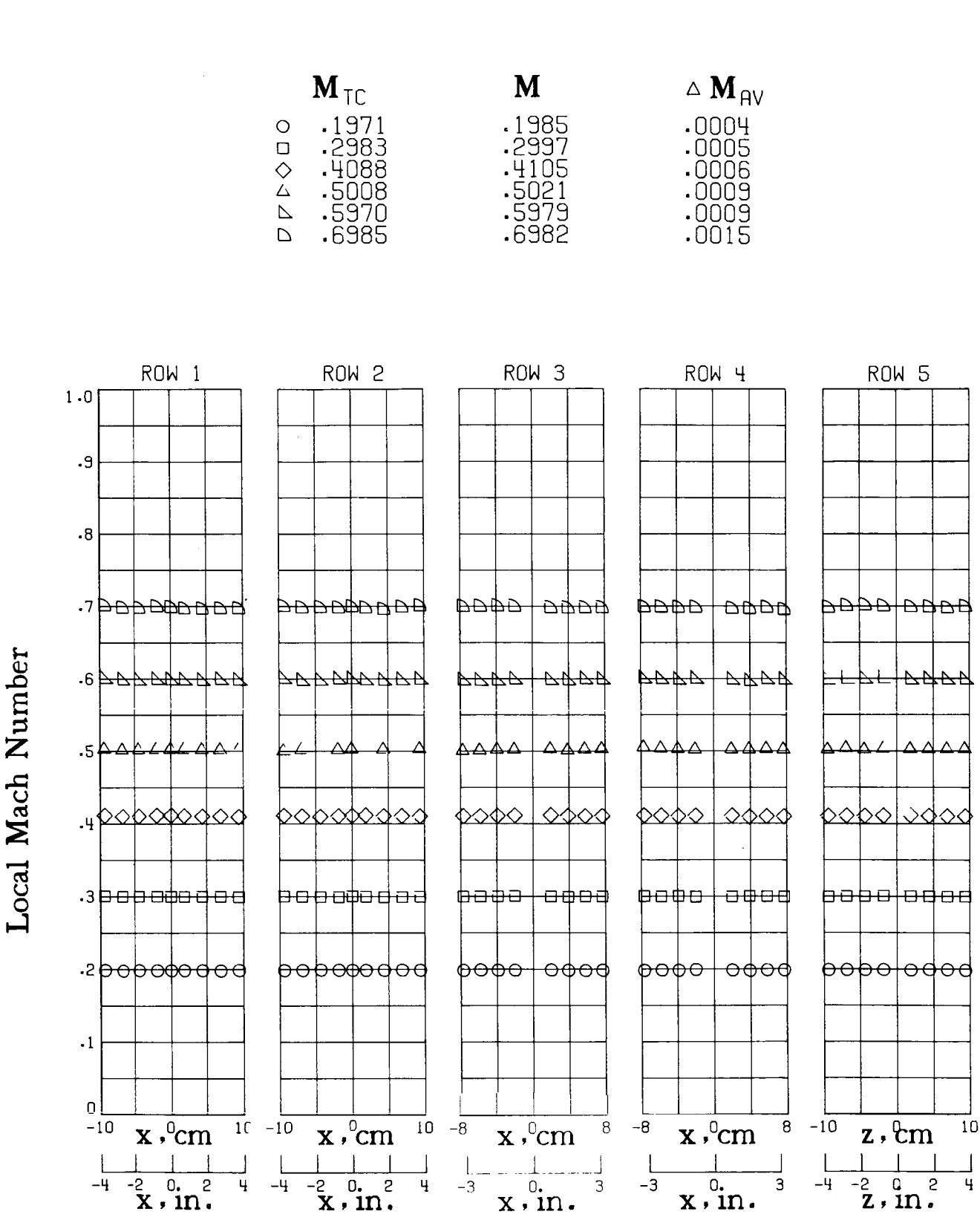

(a) T_t = 300 K.

Figure 41.- Local Mach number distribution along test-section right turntable at stagnation pressure of 6.0 atm.

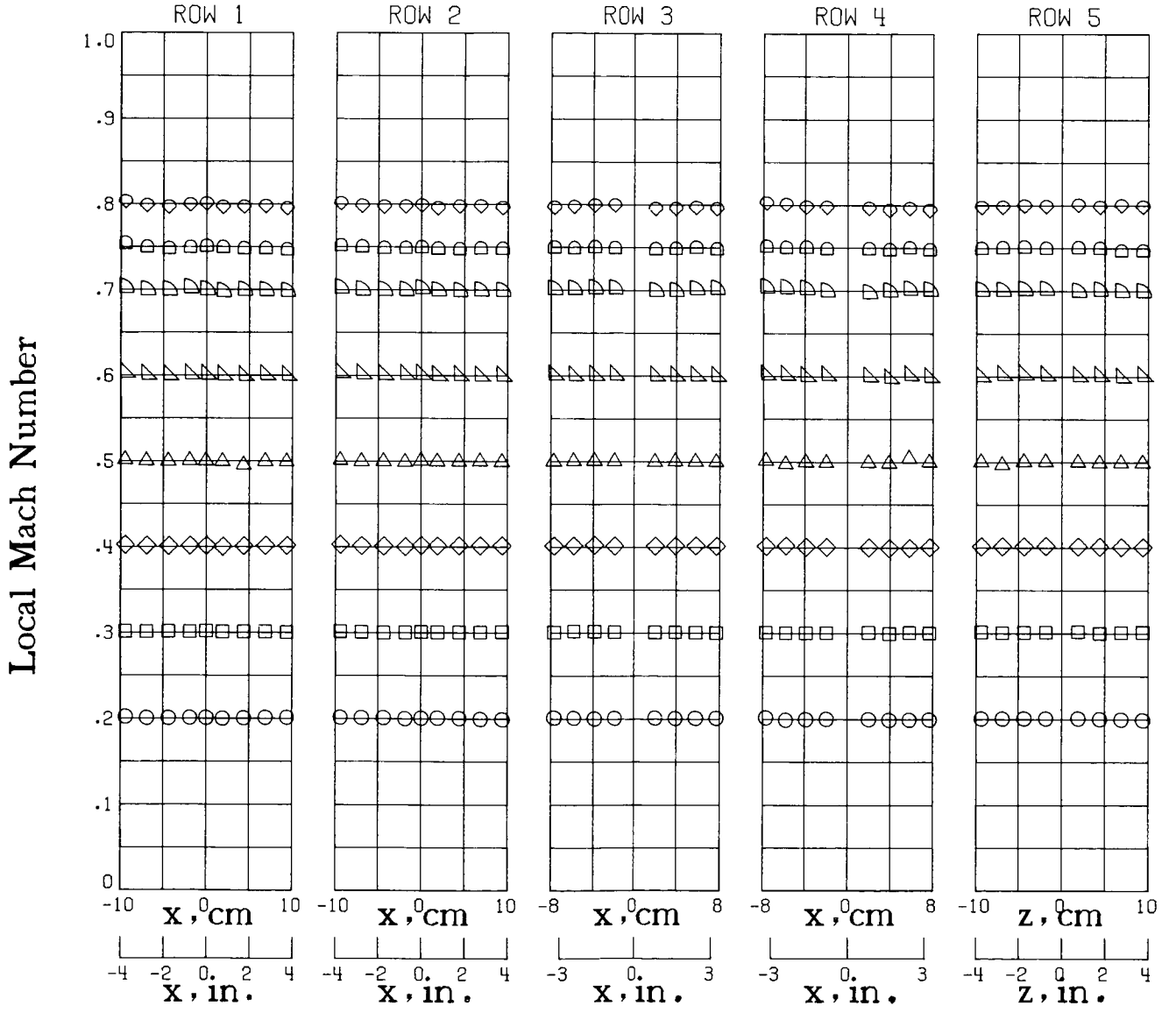

(b) T_t = 200 K.

Figure 41.- Continued.

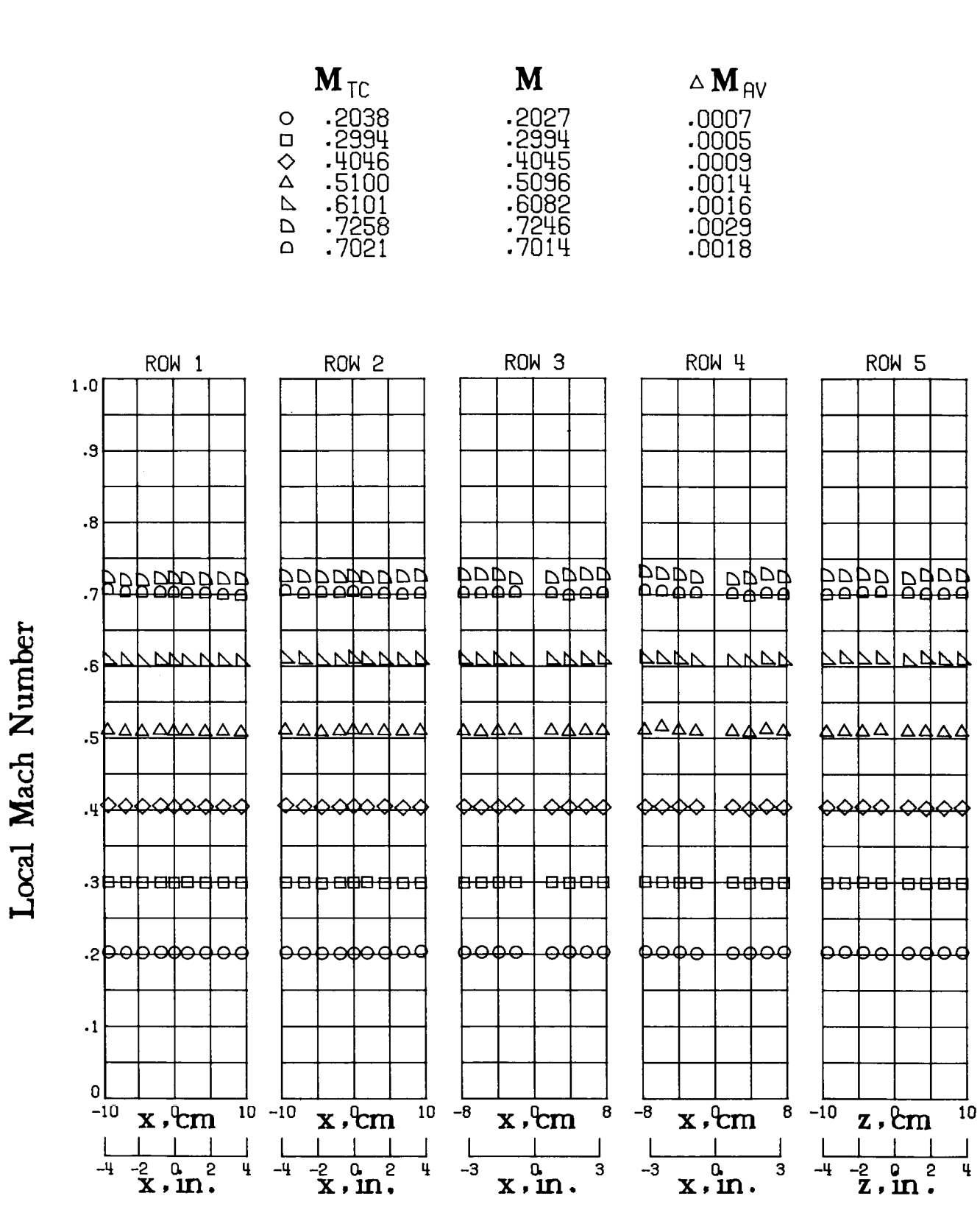

(c) T_t = 105 K.

Figure 41.- Concluded.

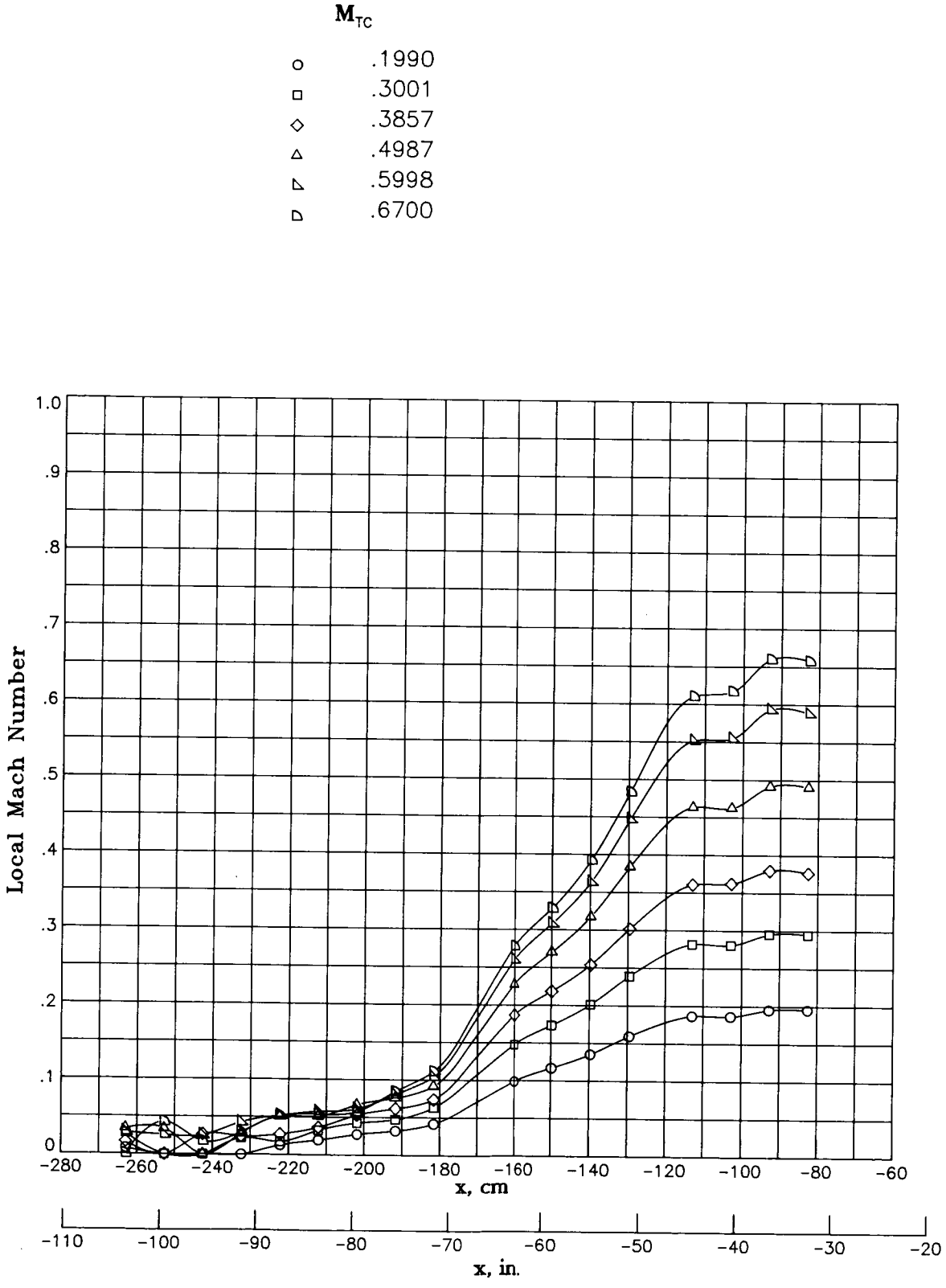

(a) T_t = 300 K.

Figure 42.- Local Mach number distribution along contraction-section sidewall at stagnation pressure of 1.2 atm.

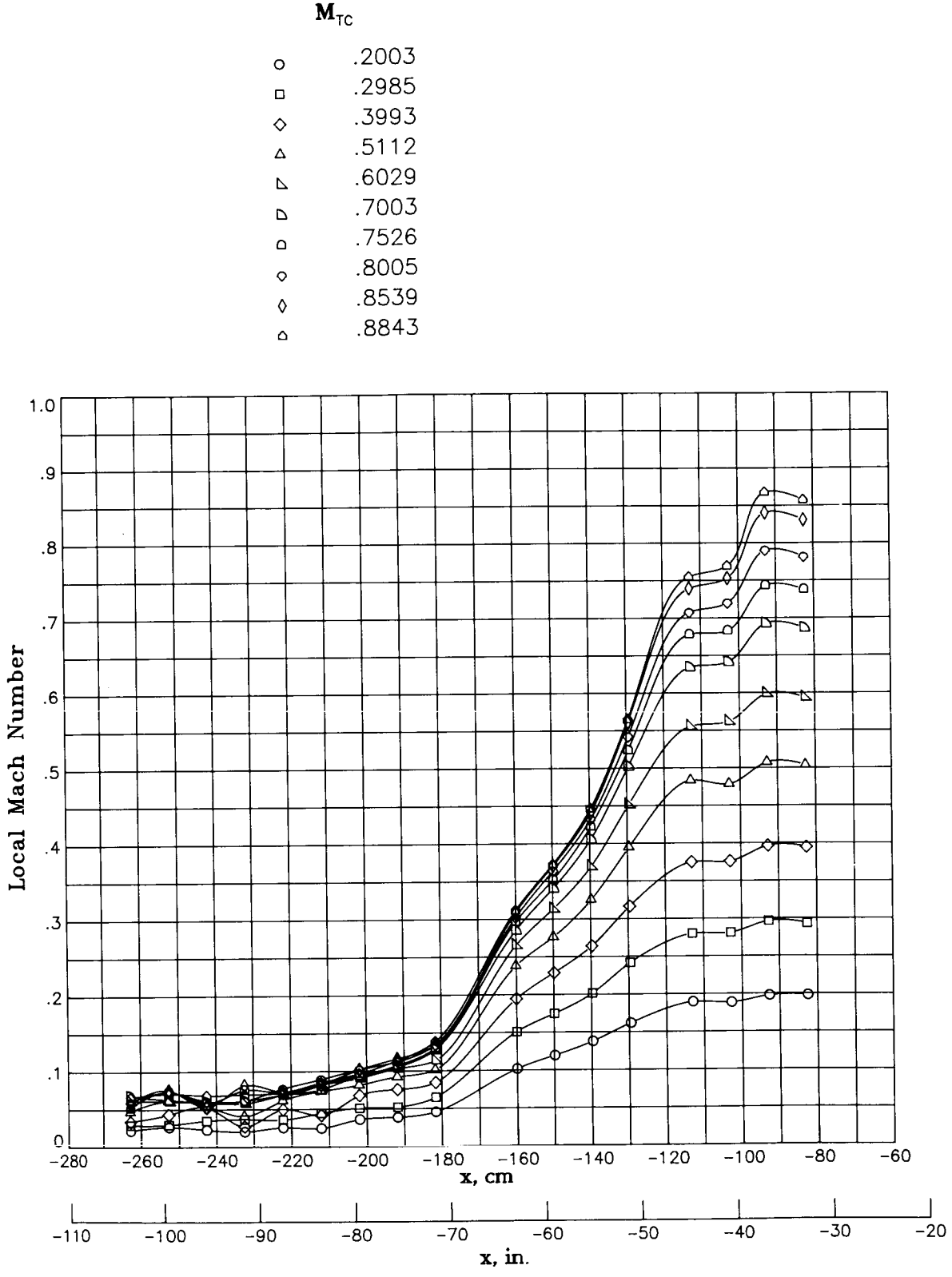

(b) T_t = 200 K.

Figure 42.- Continued.

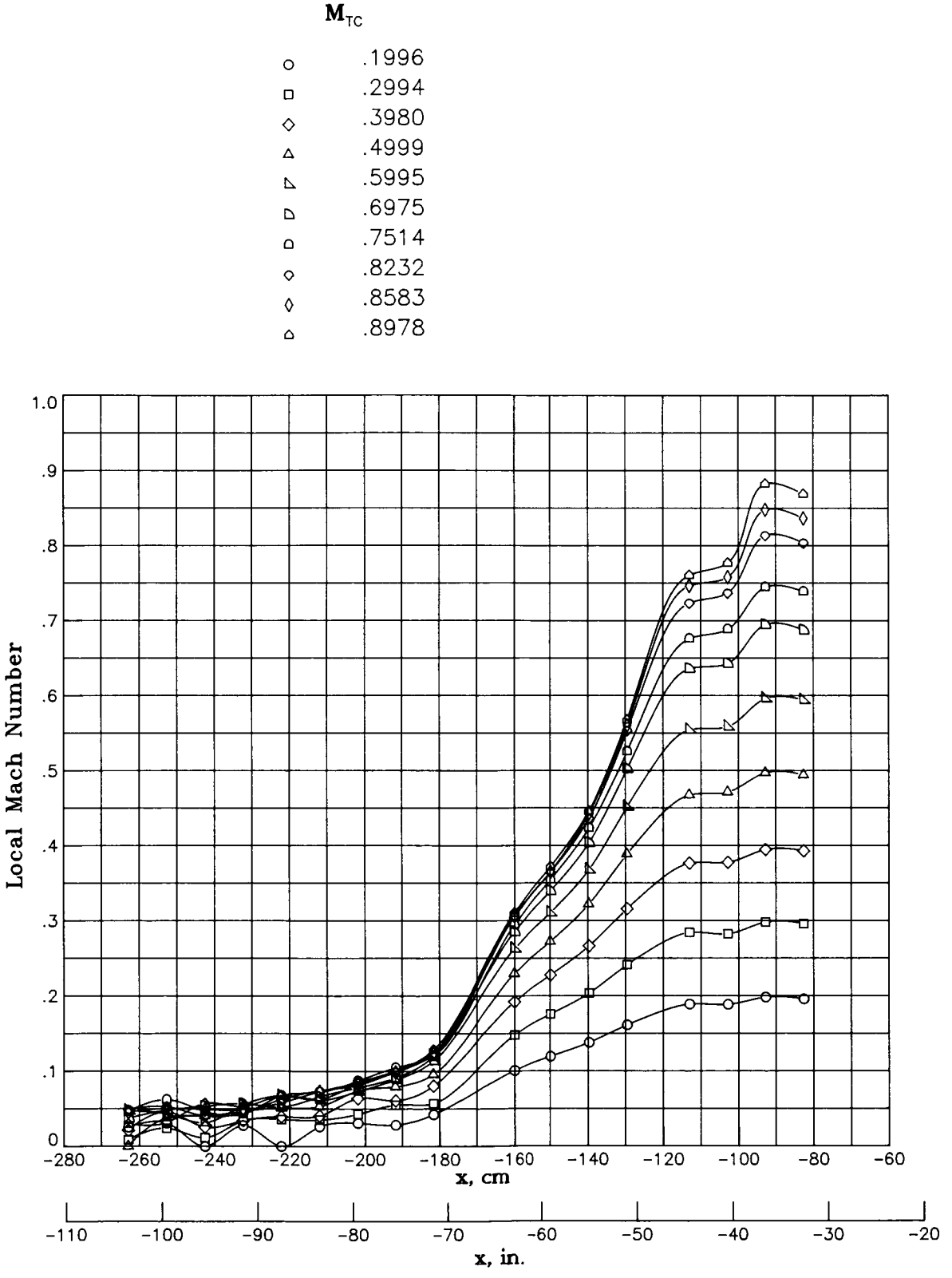

(c) T_t = 105 K.

Figure 42.- Concluded.

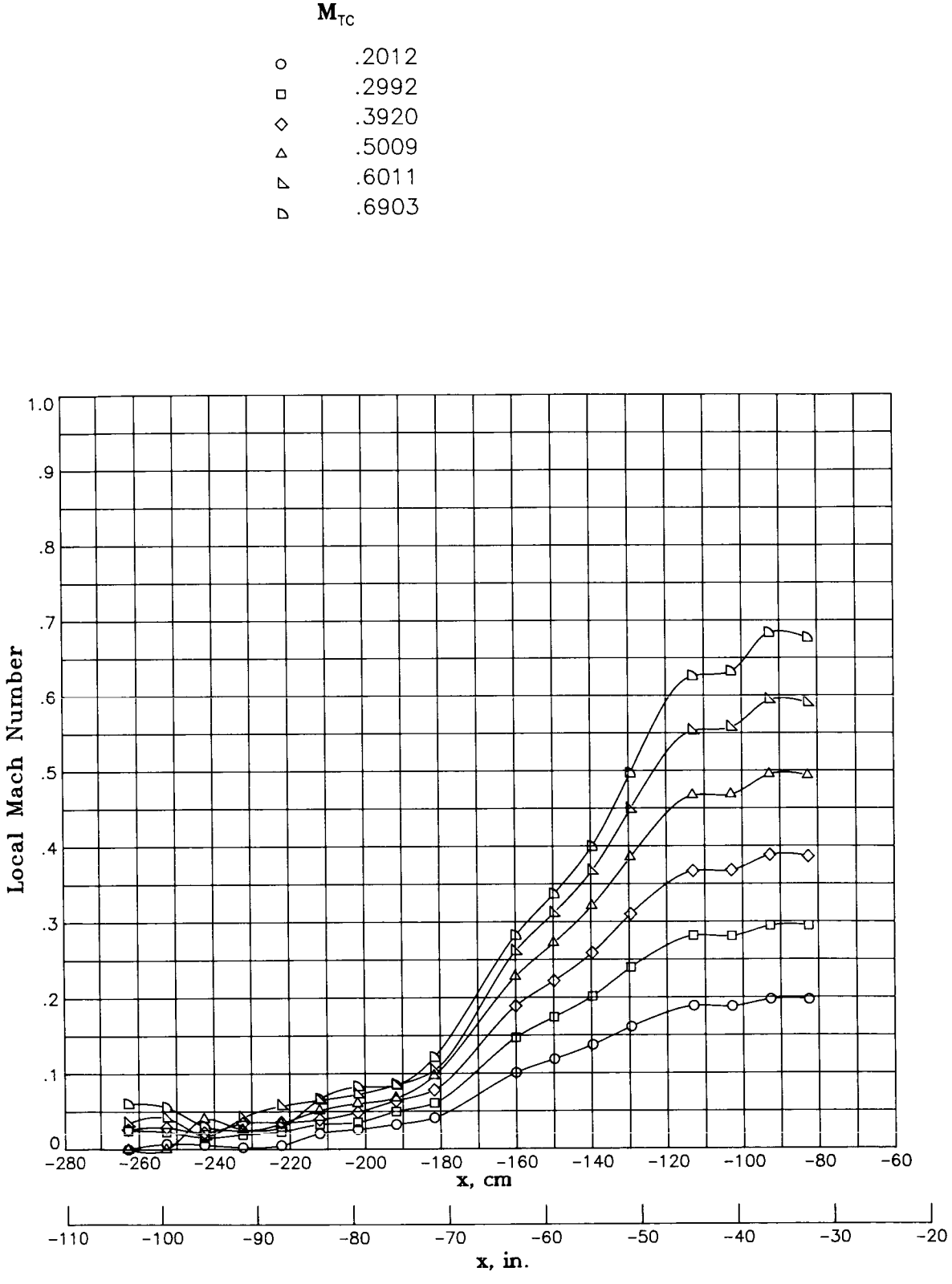

(a) T_t = 300 K.

Figure 43.- Local Mach number distribution along contraction-section sidewall at stagnation pressure of 3.1 atm.

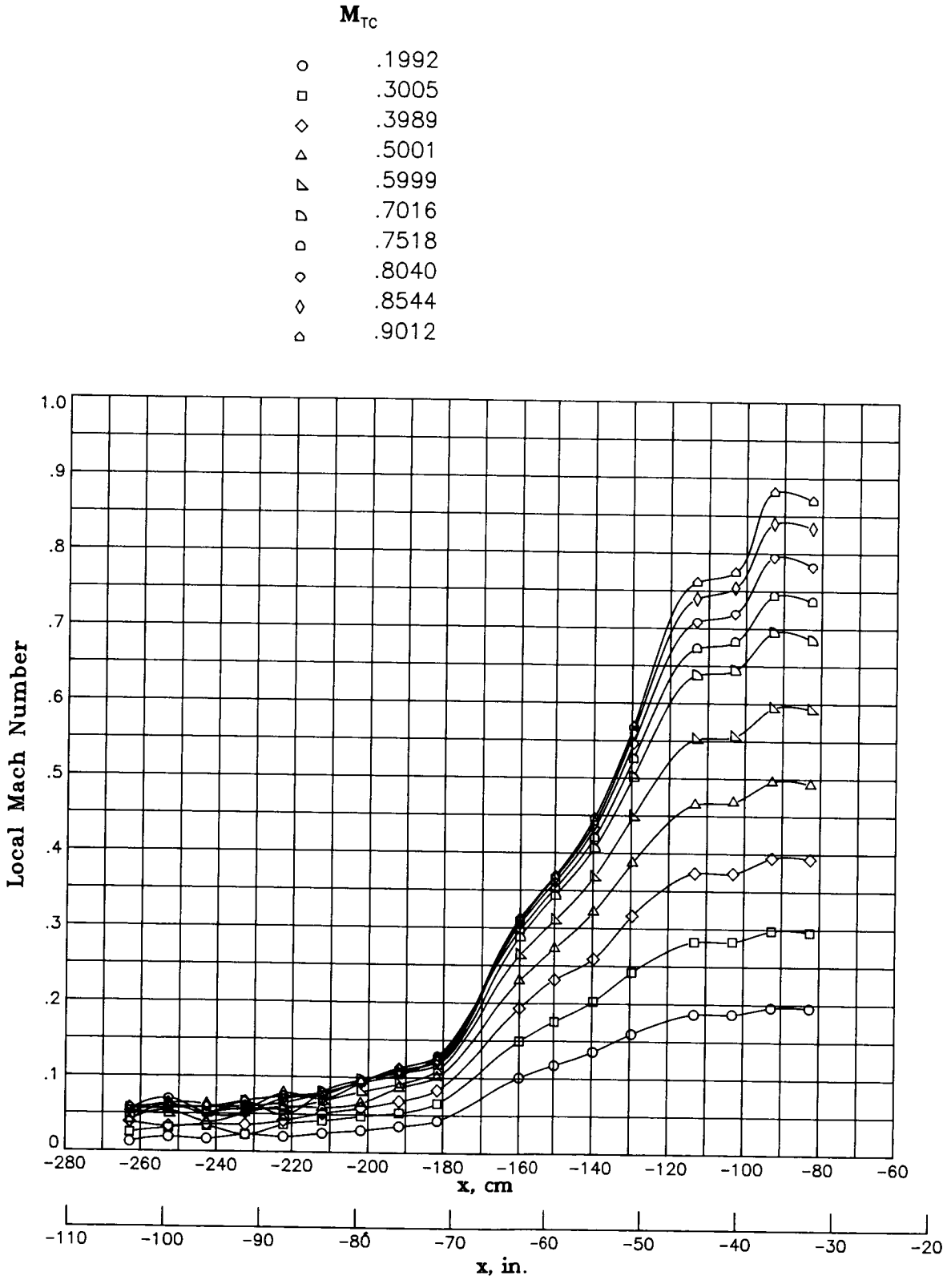

(b) T_t = 200 K.

Figure 43.- Continued.

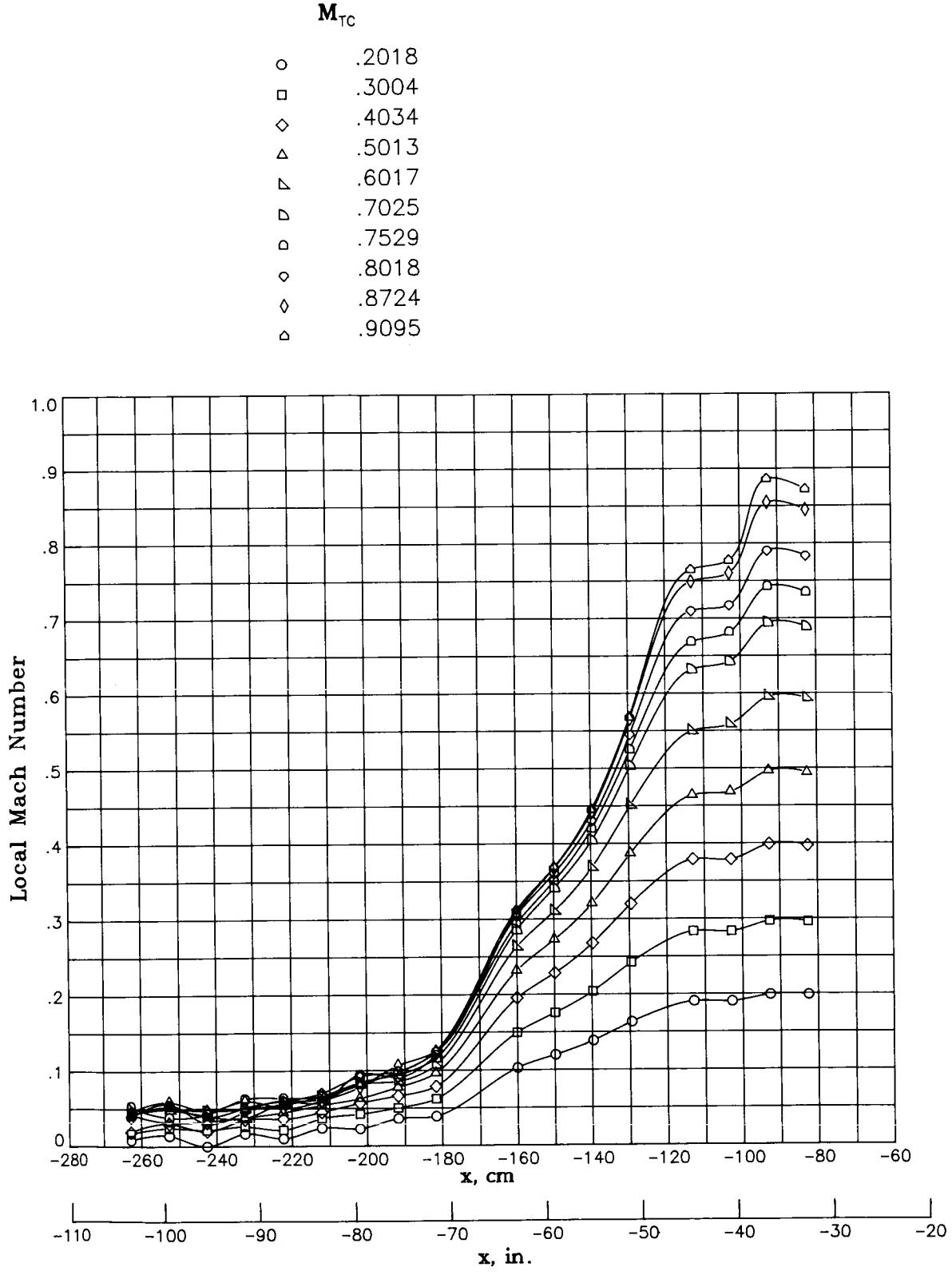

(c) T_t = 105 K.

Figure 43.- Concluded.

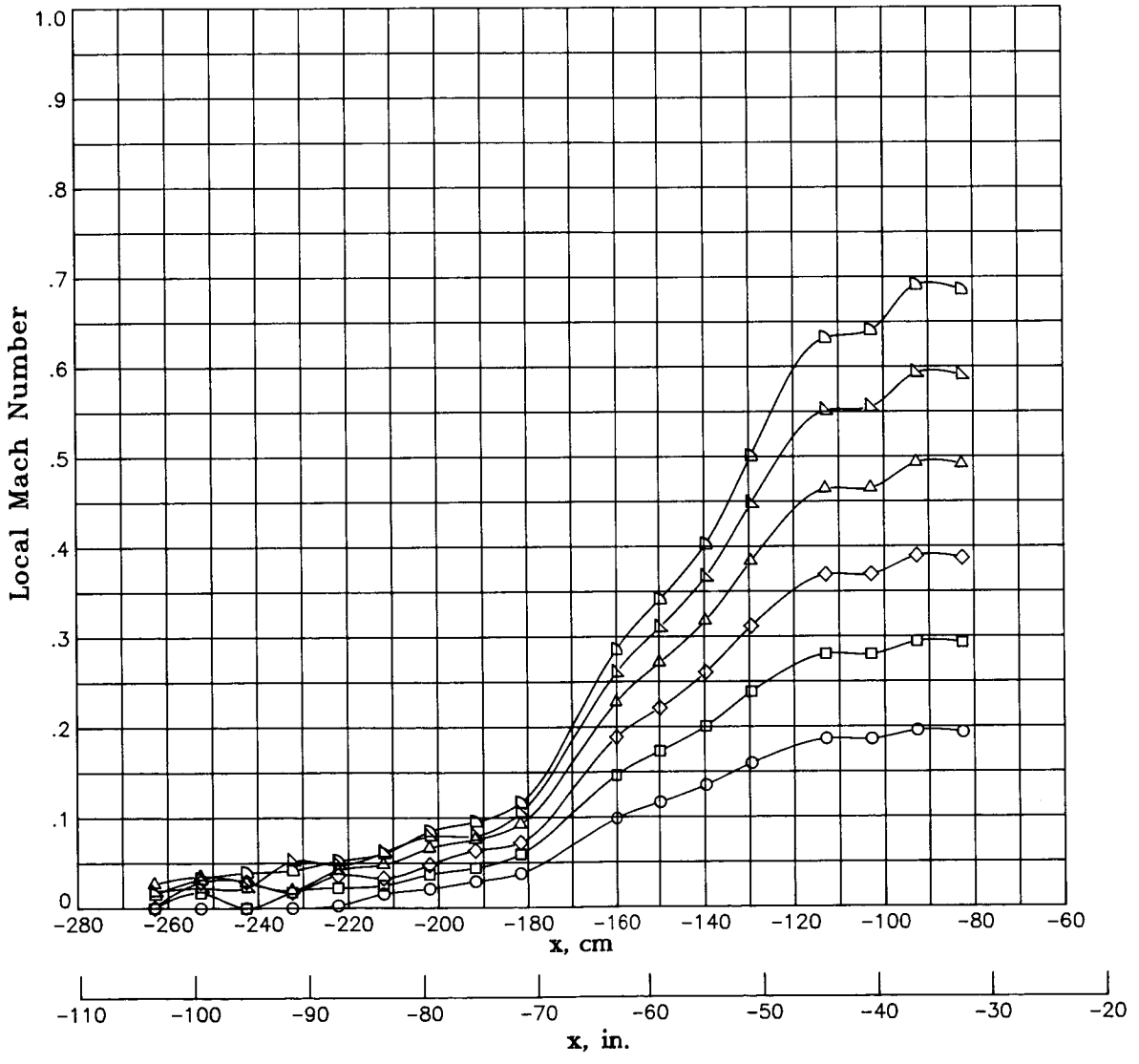

(a) T_t = 300 K.

Figure 44.- Local Mach number distribution along contraction-section sidewall at stagnation pressure of 5.1 atm.

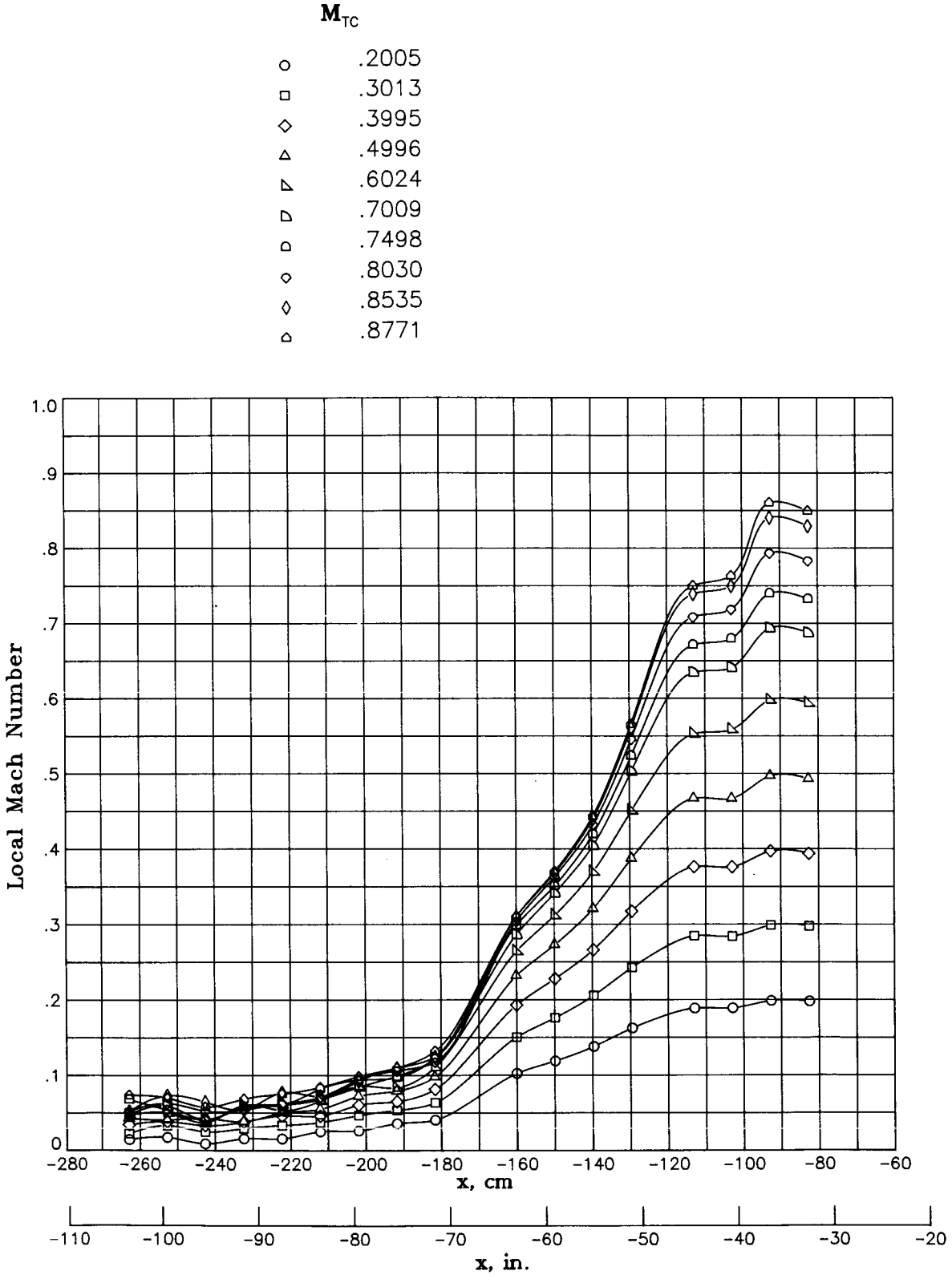

(b) T_t = 200 K.

Figure 44.- Continued.

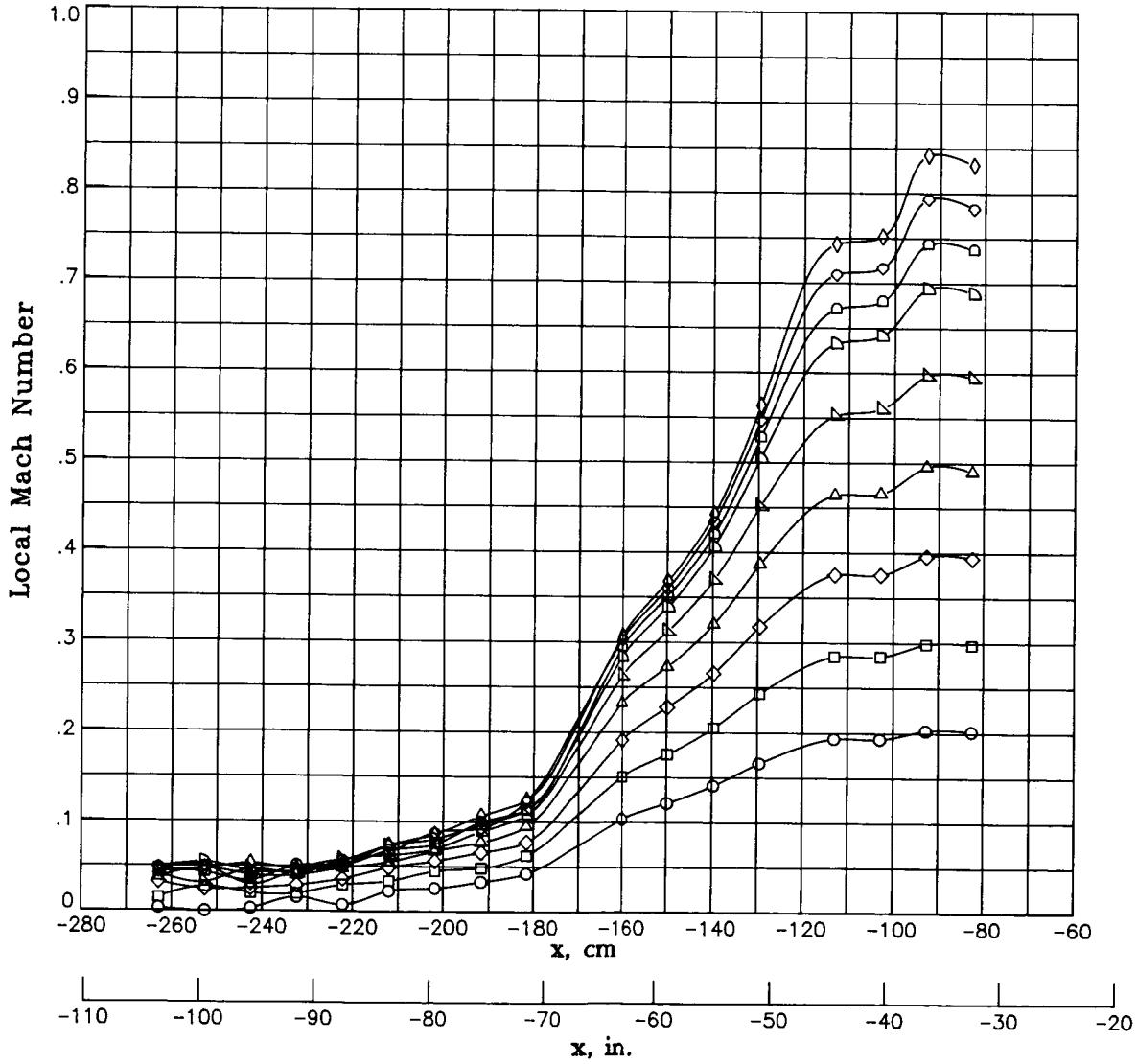

(c) T_t = 105 K.

Figure 44.- Concluded.

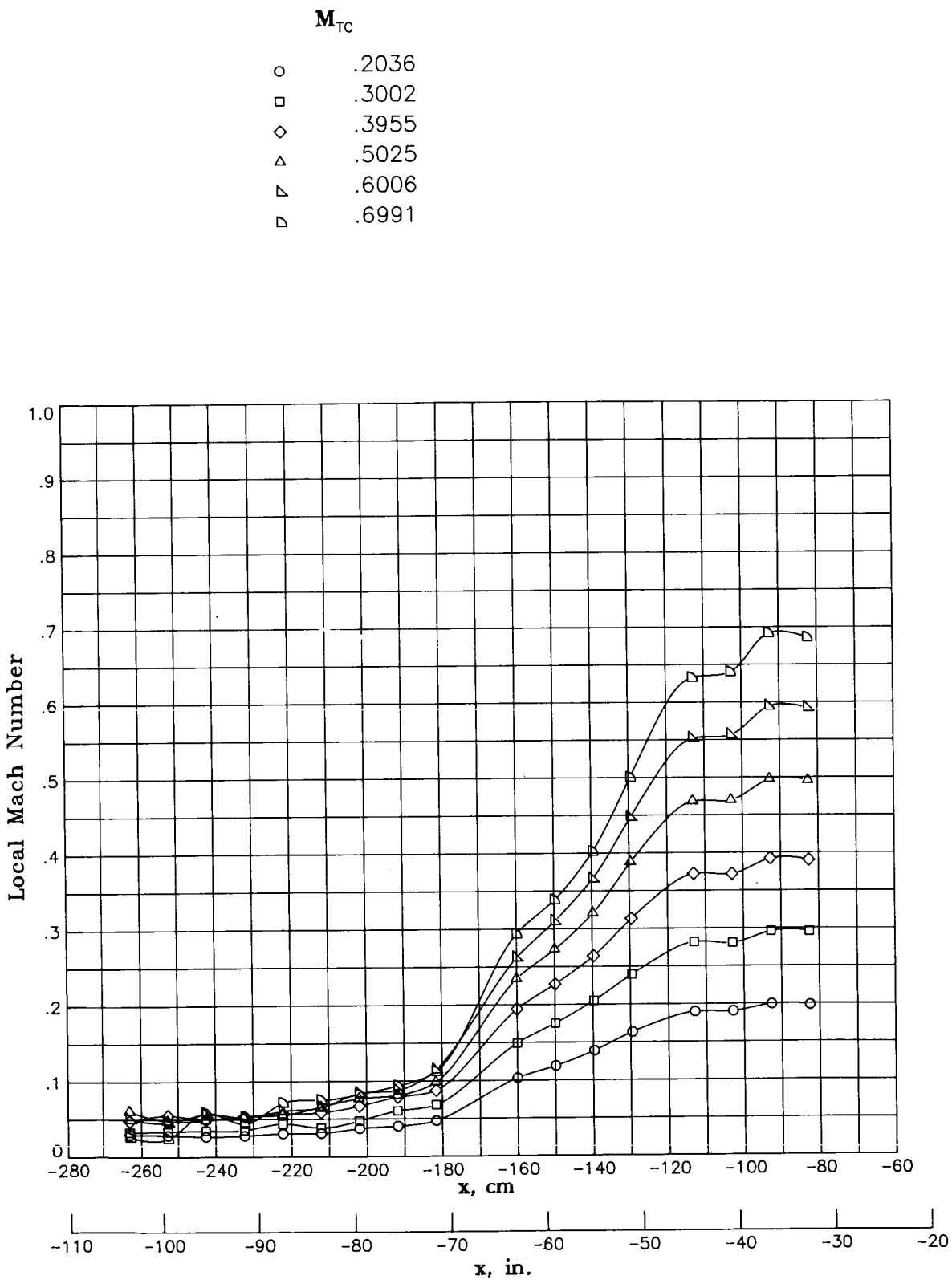

(a) T_t = 300 K.

Figure 45.- Local Mach number distribution along contraction-section sidewall at stagnation pressure of 6.0 atm.

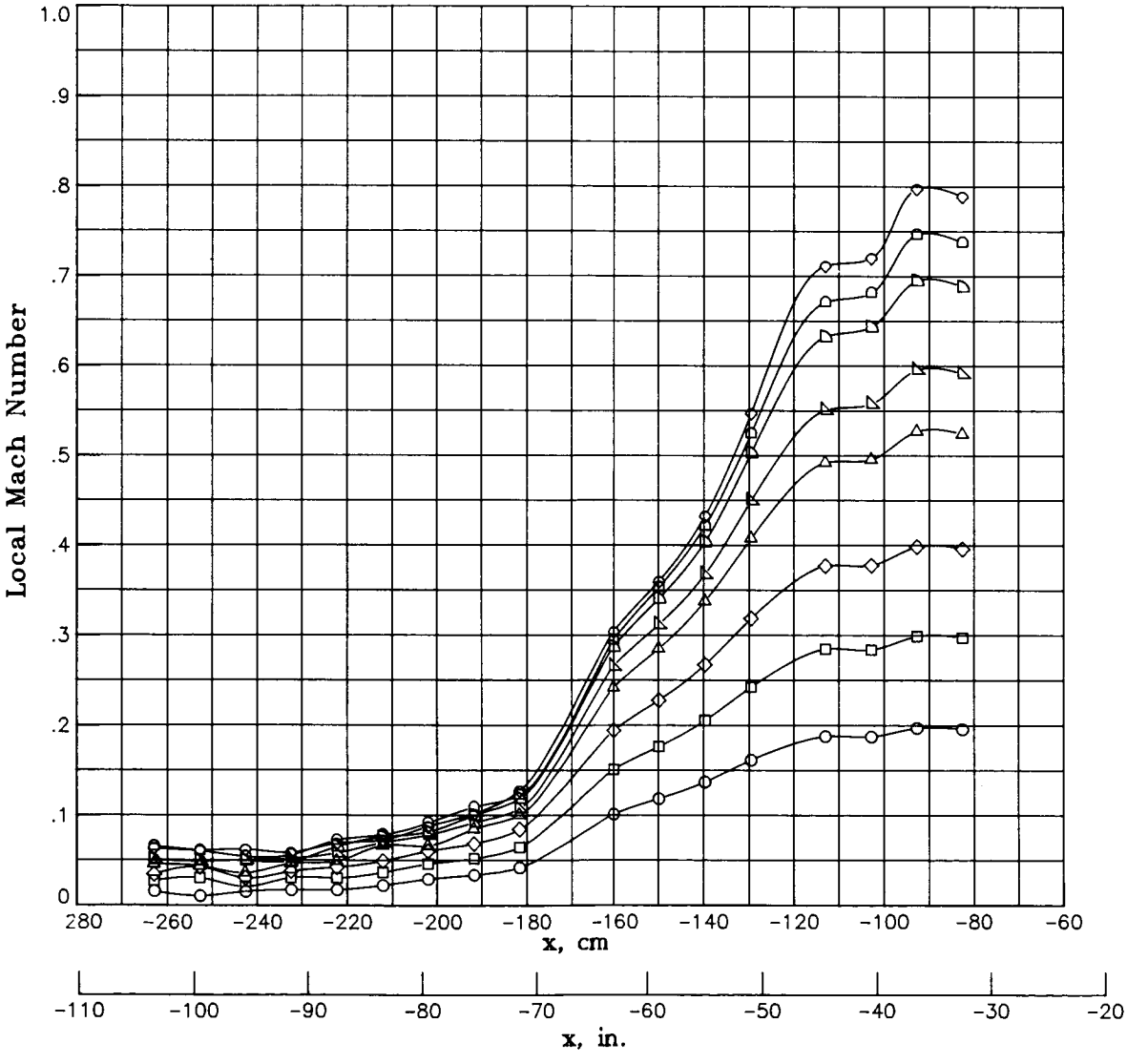

(b) T_t = 200 K.

Figure 45.- Continued.

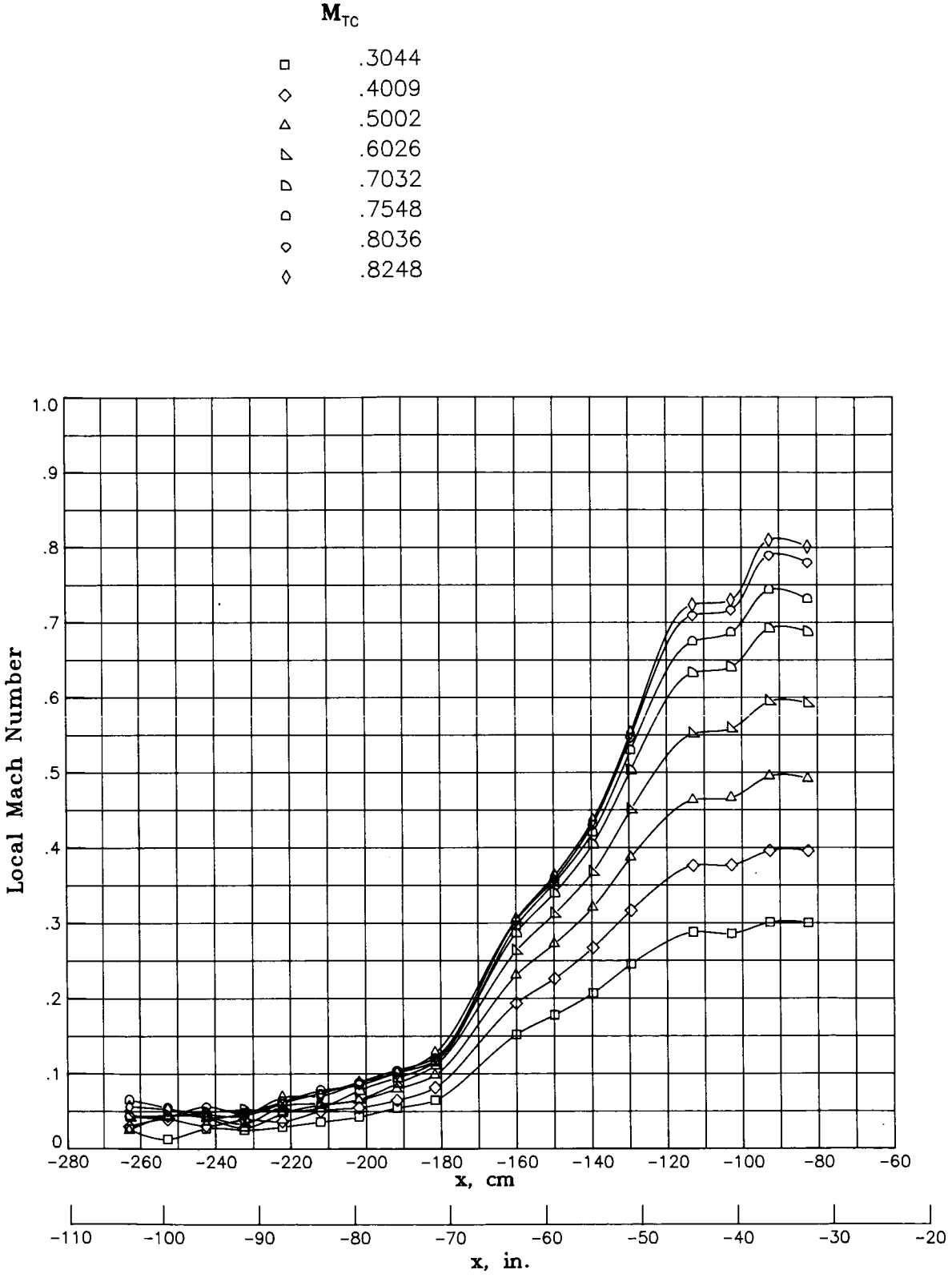

(c) T_t = 105 K.

Figure 45.- Concluded.

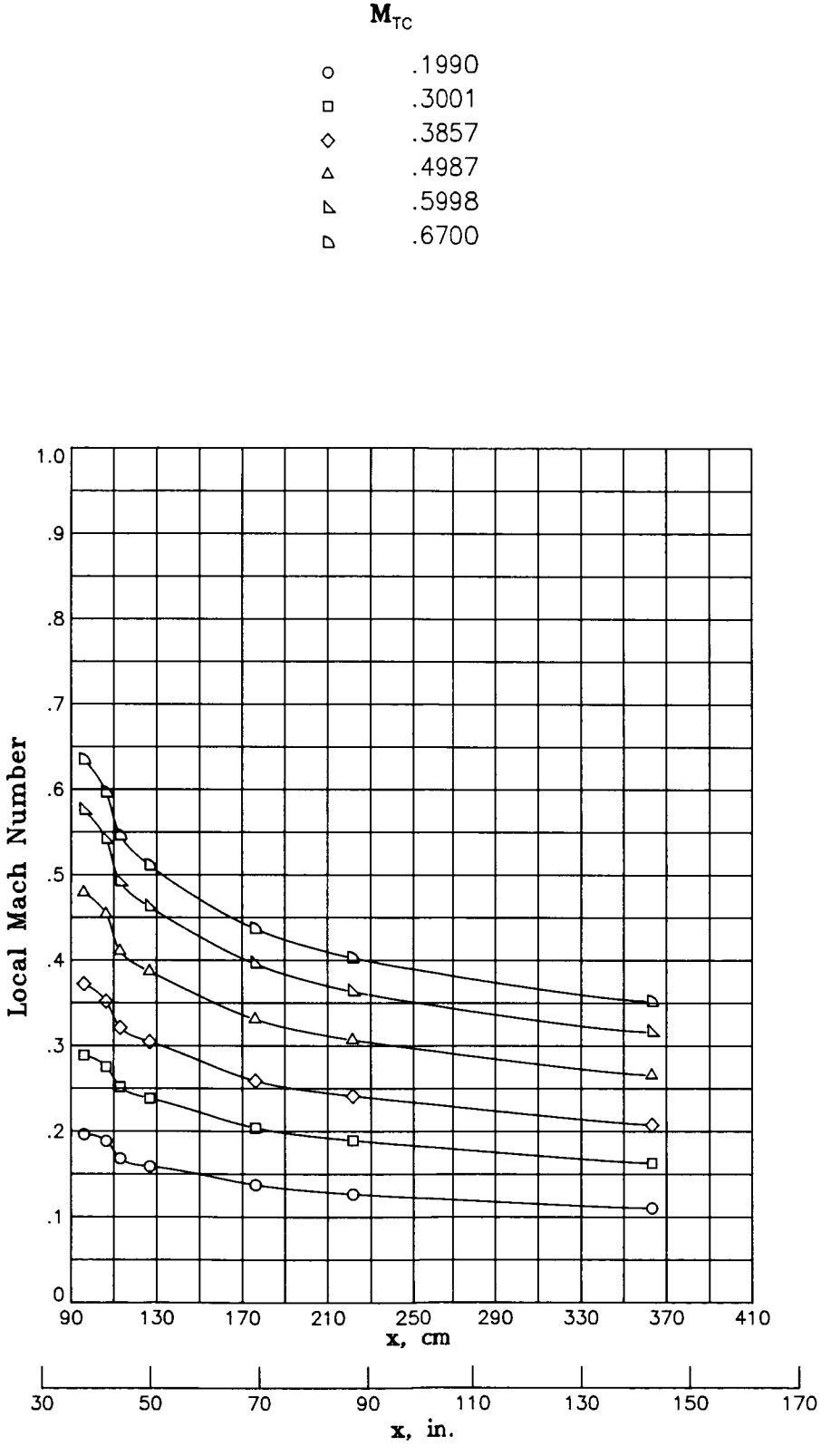

(a) T_t = 300 K.

Figure 46.- Local Mach number distribution along diffuser sidewall at stagnation pressure of 1.2 atm.

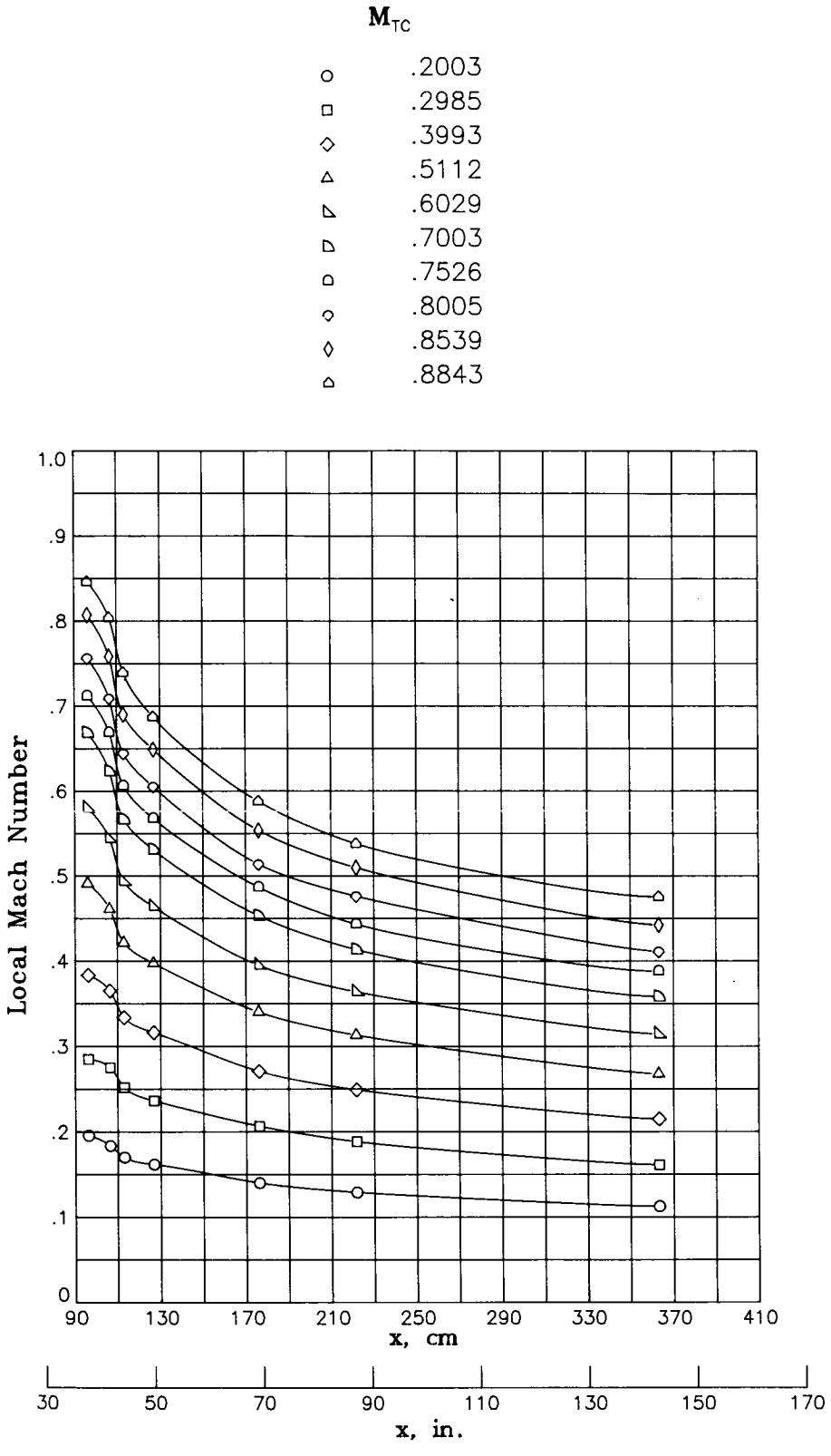

(b) T_t = 200 K.

Figure 46.- Continued.

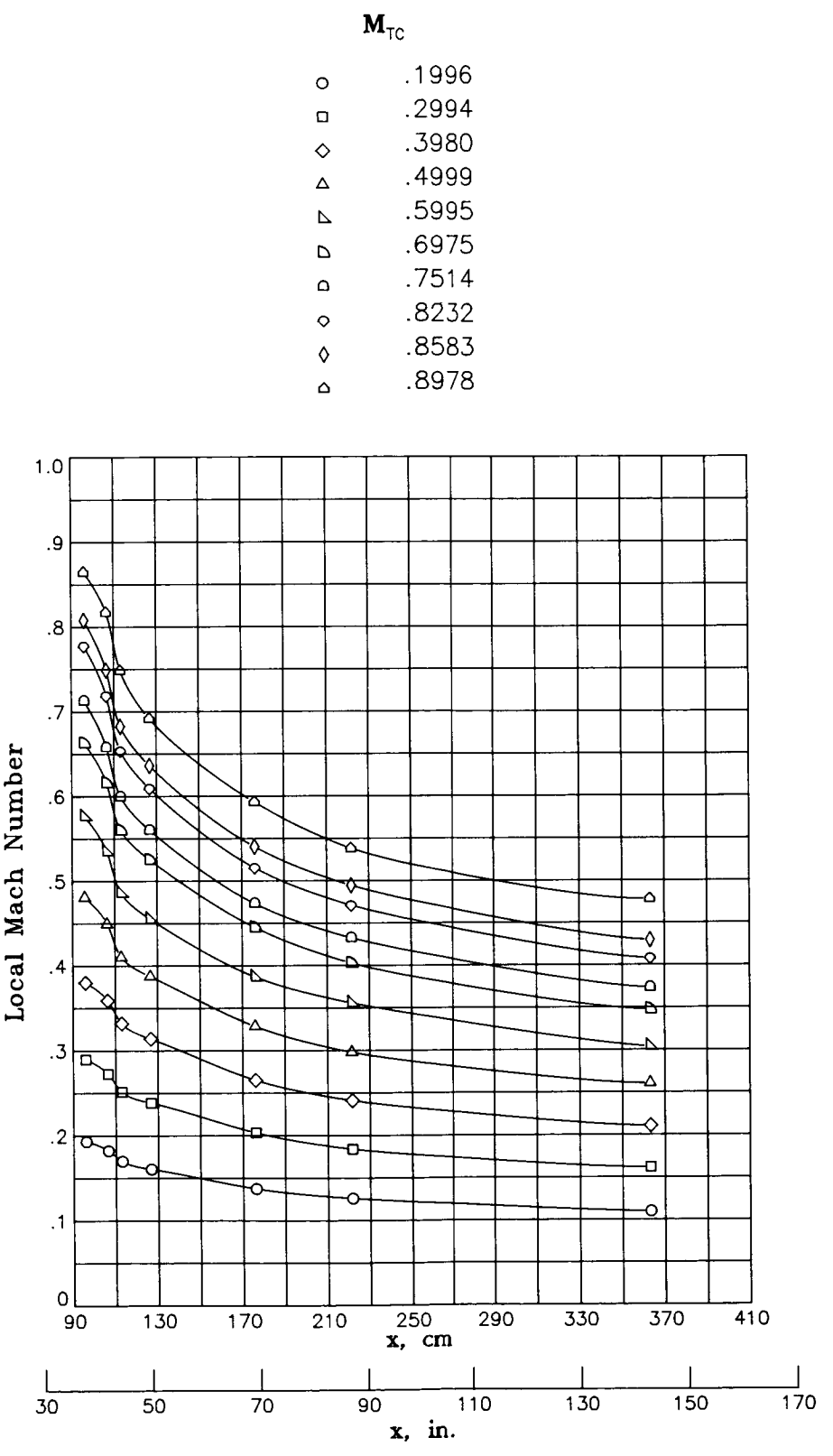

(c) T_t = 105 K.

Figure 46.- Concluded.

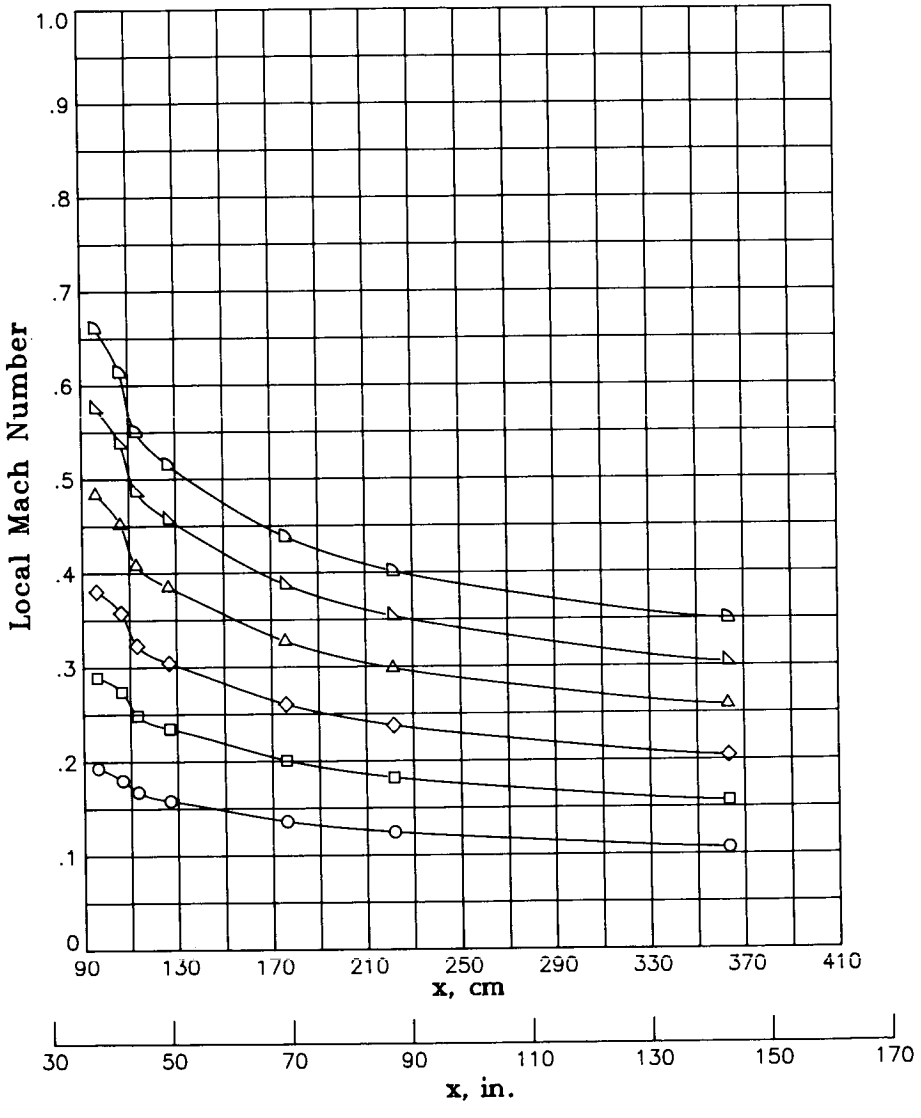

(a) T_t = 300 K.

Figure 47.- Local Mach number distribution along diffuser sidewall at stagnation pressure of 3.1 atm.

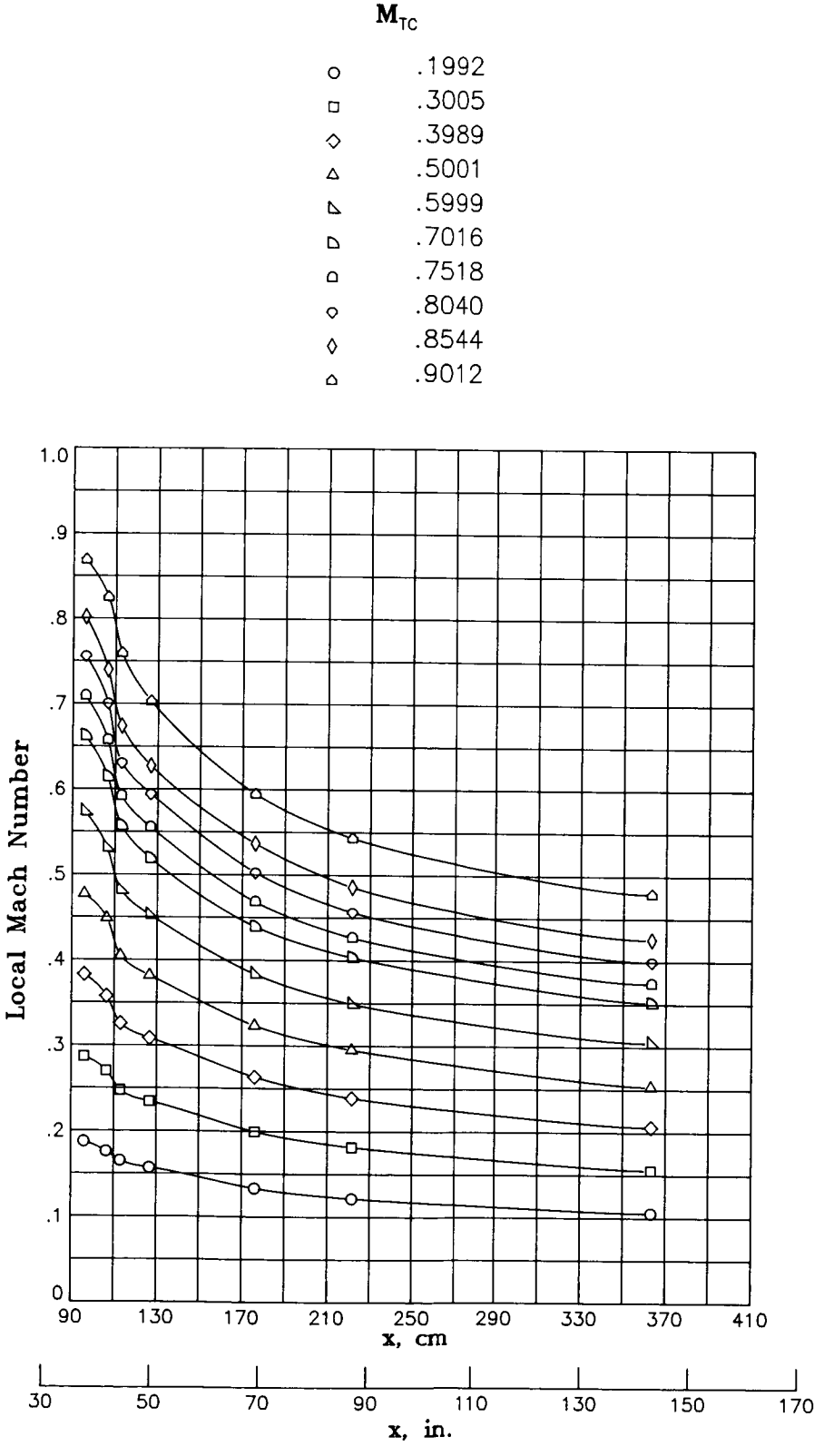

(b) T_t = 200 K.

Figure 47.- Continued.

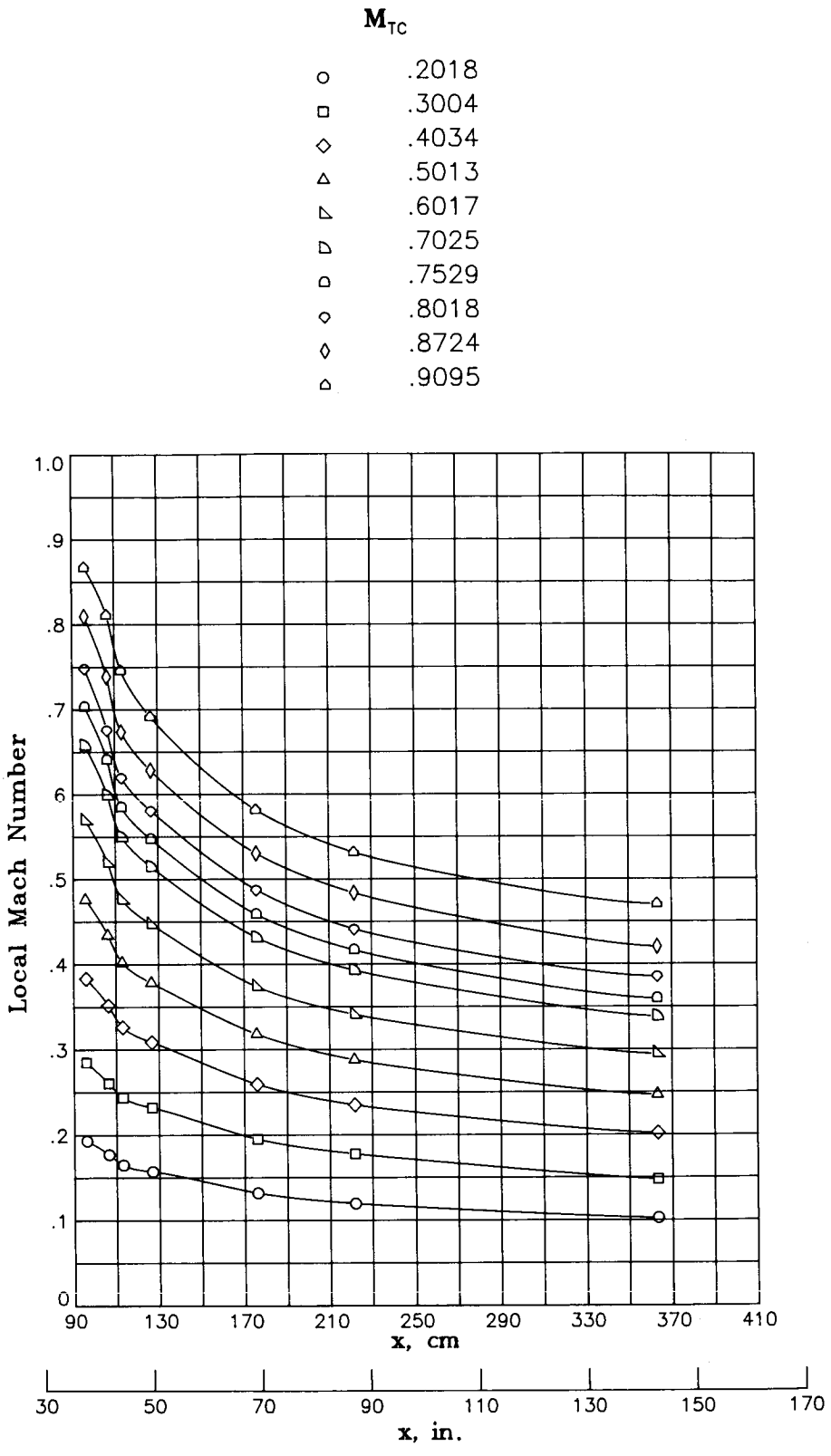

(c) T_t = 105 K.

Figure 47.- Concluded.

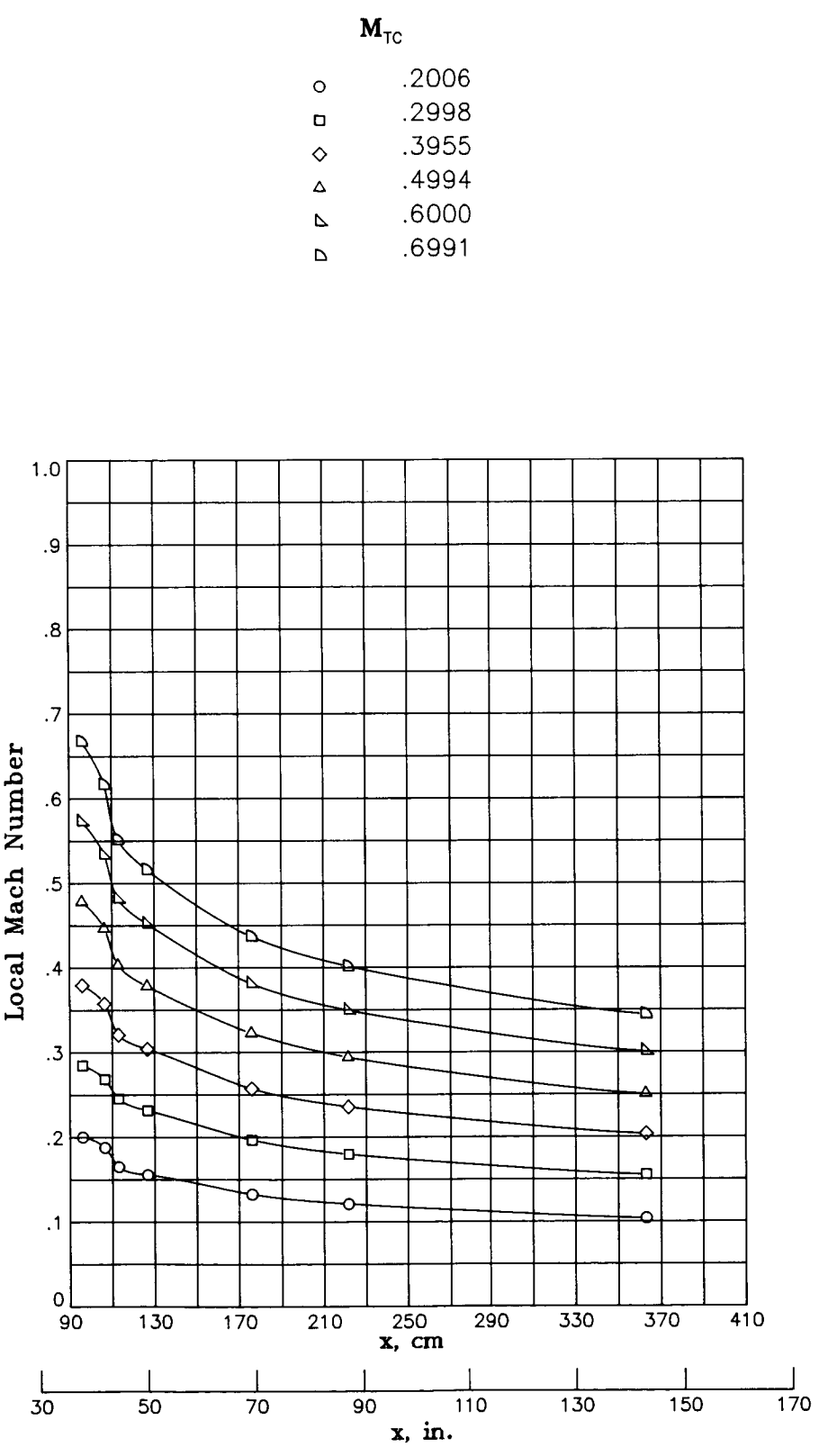

(a) T_t = 300 K.

Figure 48.- Local Mach number distribution along diffuser sidewall at stagnation pressure of 5.1 atm.

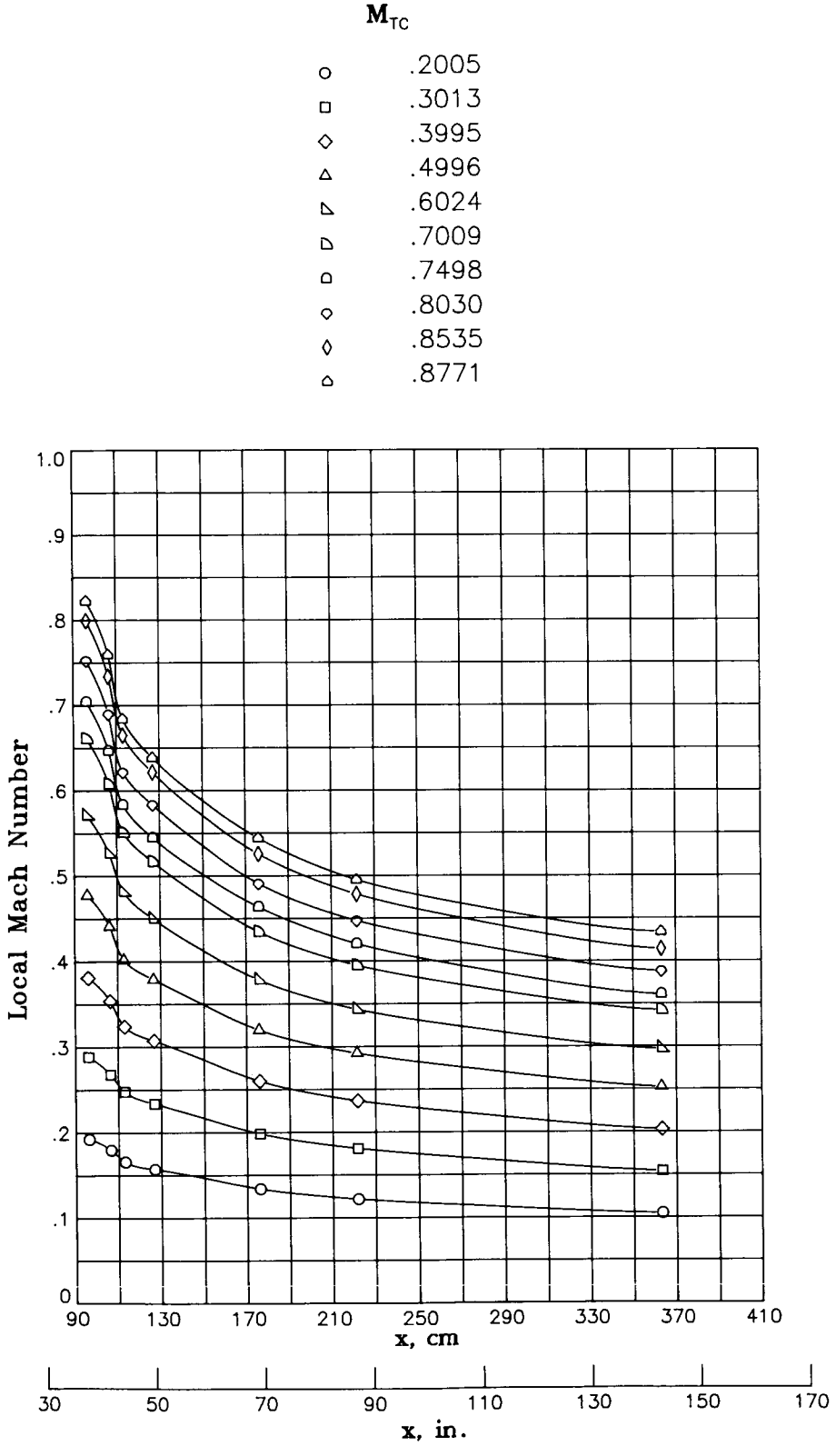

(b) T_t = 200 K.

Figure 48.- Continued.

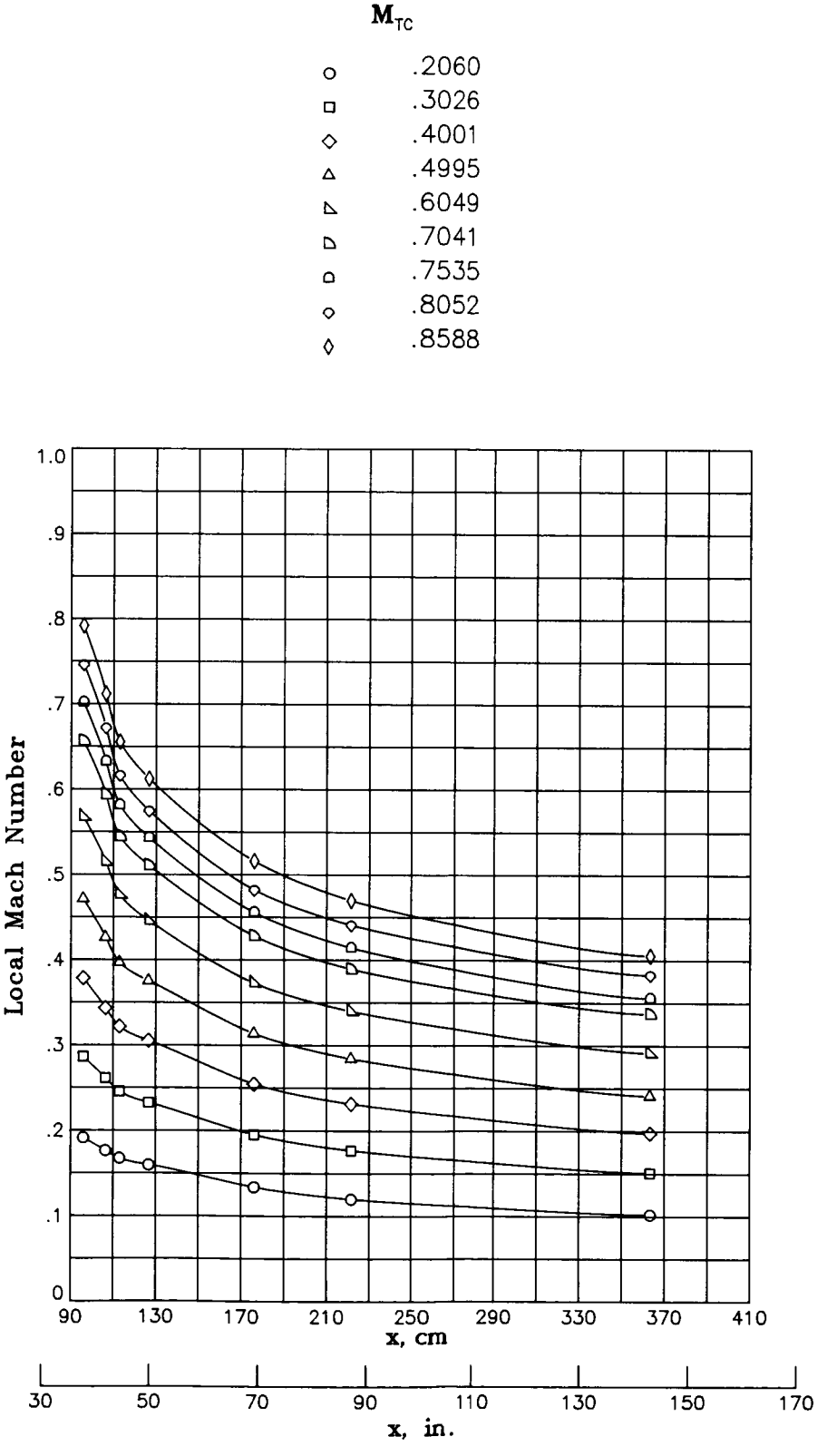

(c) T_t = 105 K.

Figure 48.- Concluded.

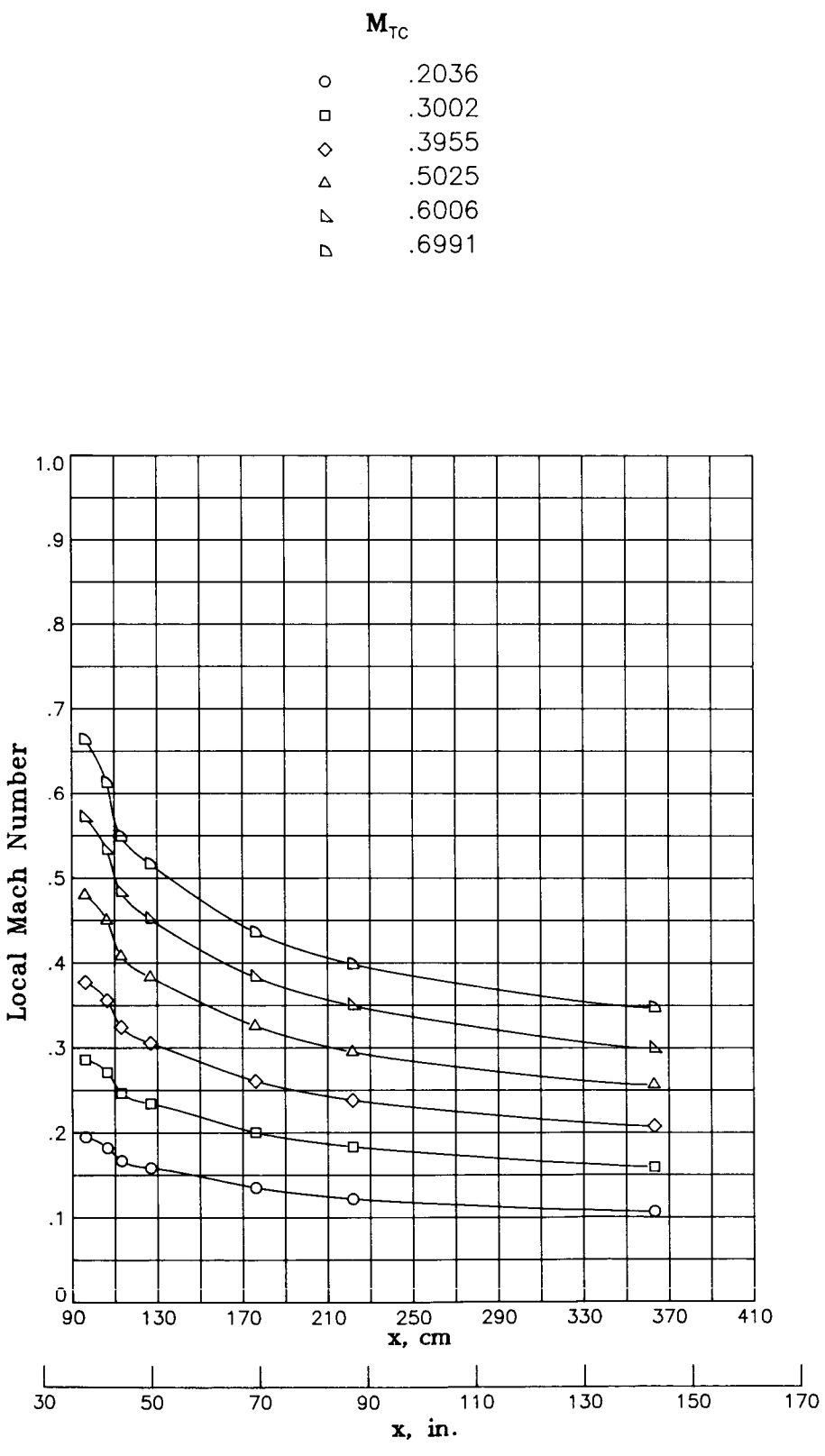

(a) T_t = 300 K.

Figure 49.- Local Mach number distribution along diffuser sidewall at stagnation pressure of 6.0 atm.

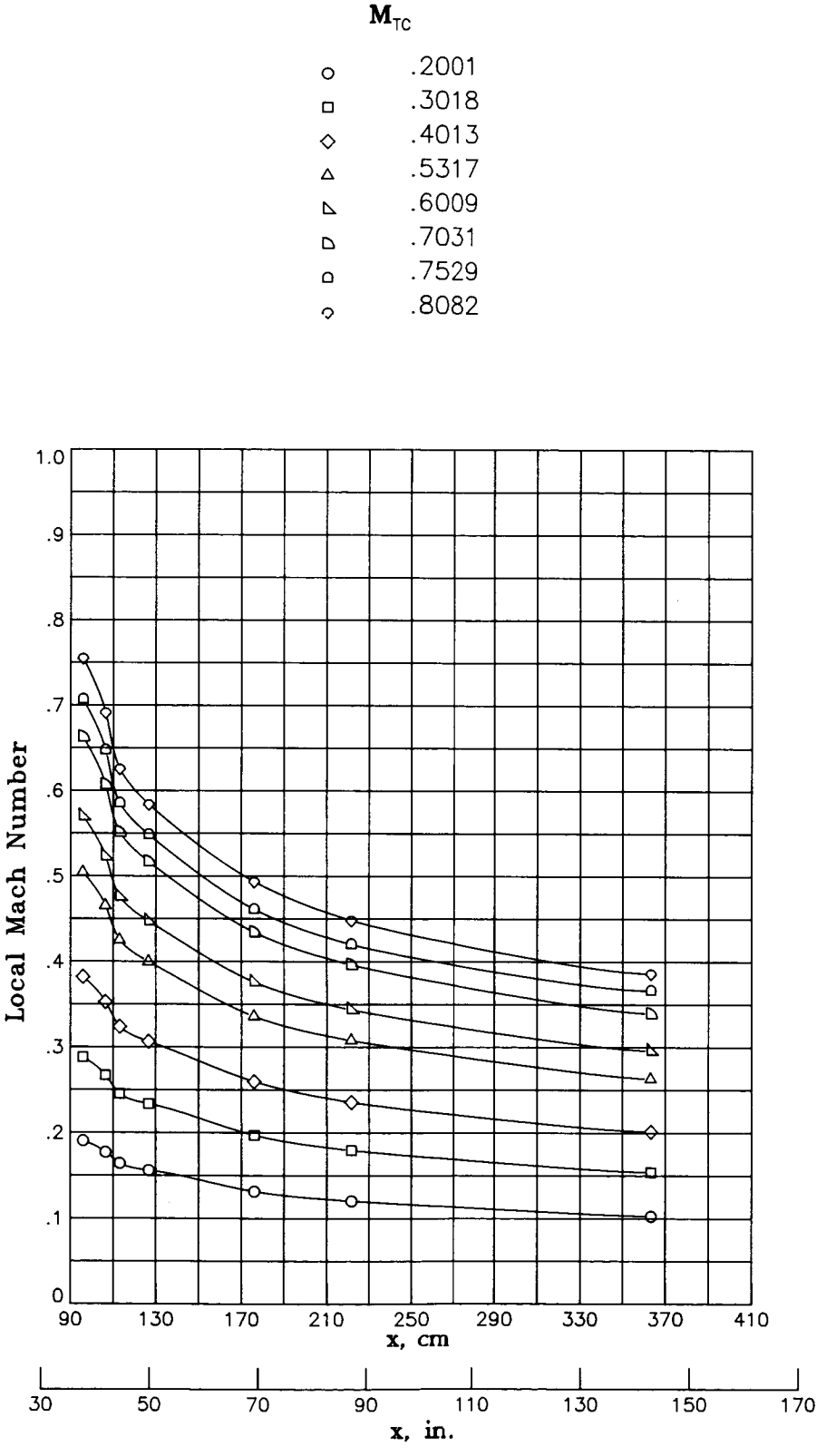

(b) T_t = 200 K.

Figure 49.- Continued.

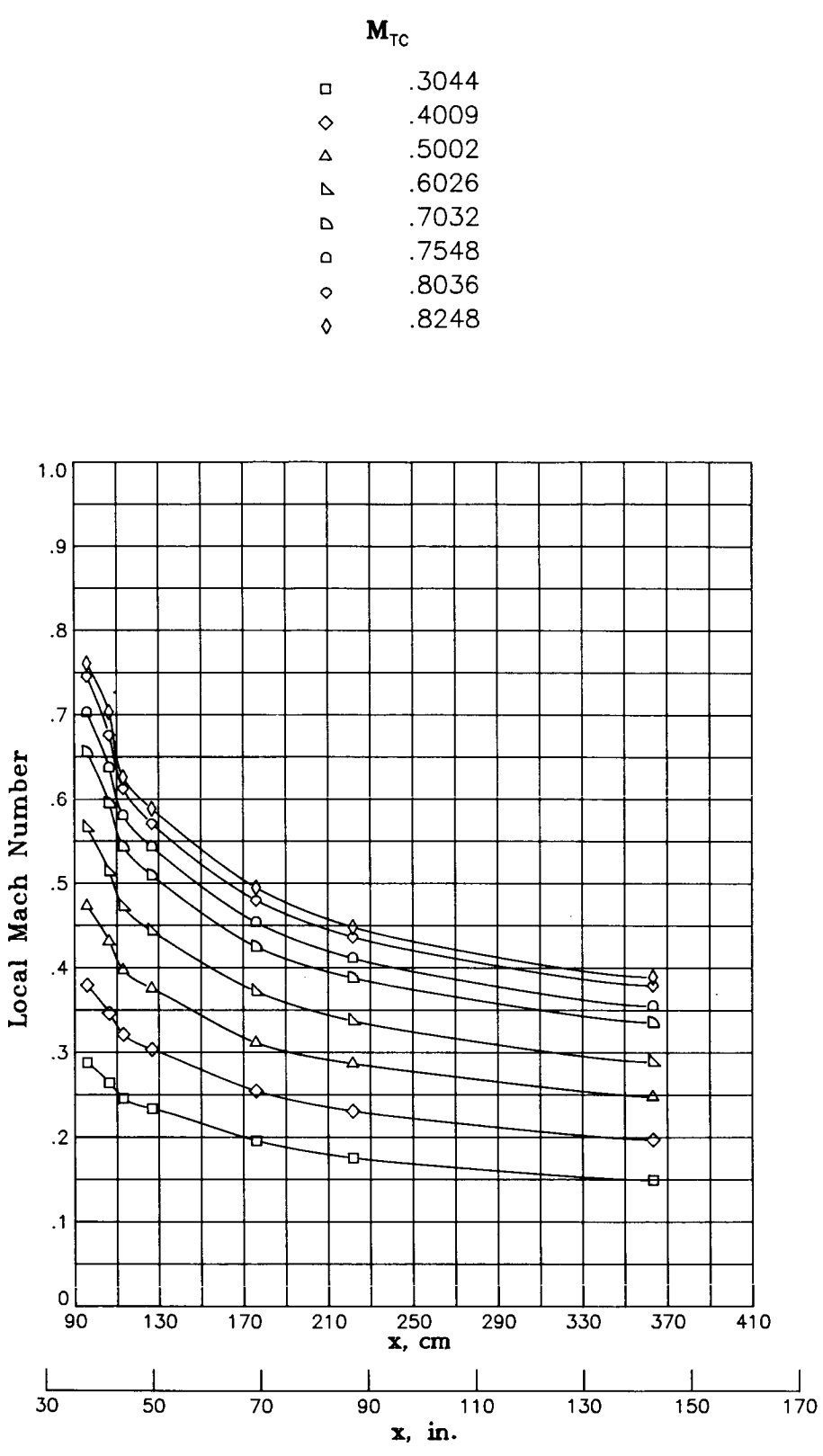

(c) T_t = 105 K.

Figure 49.- Concluded.

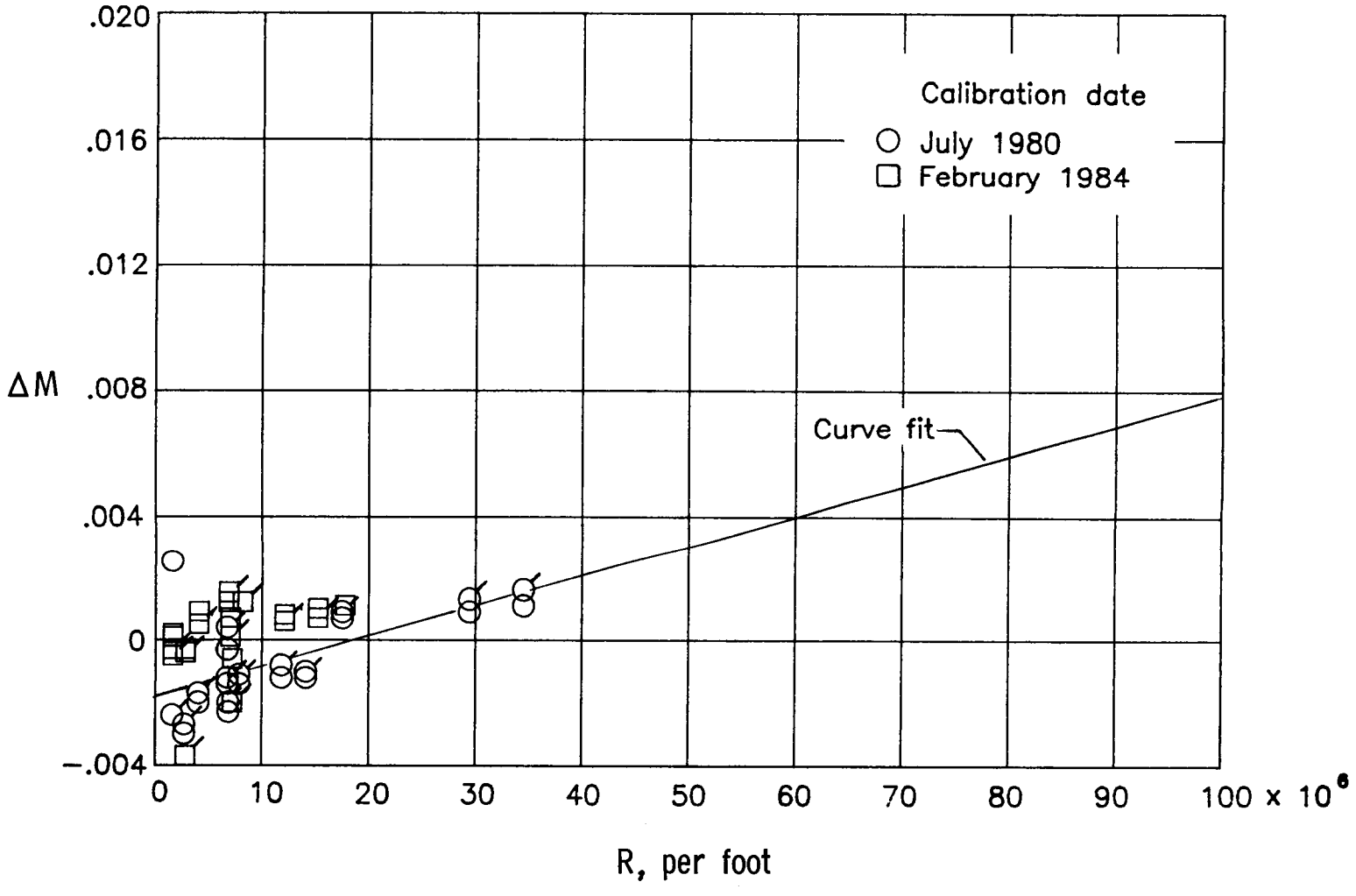

(a) $M_{TC} = 0.20$.

Figure 50.- Calibration factor as function of Reynolds number for various Mach numbers. Flagged symbols indicate left turntable.

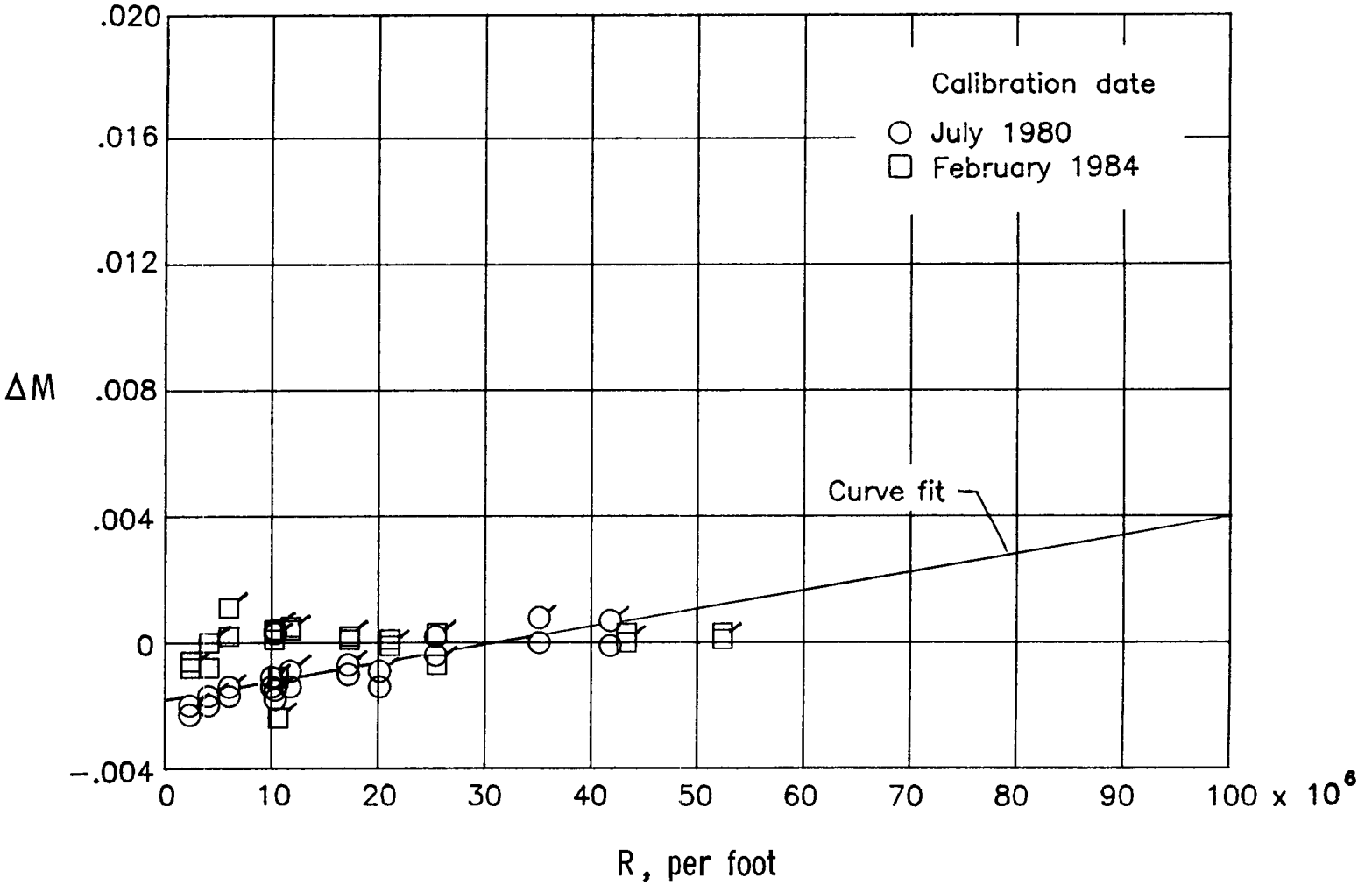

(b) $M_{TC} = 0.30$.

Figure 50.- Continued.

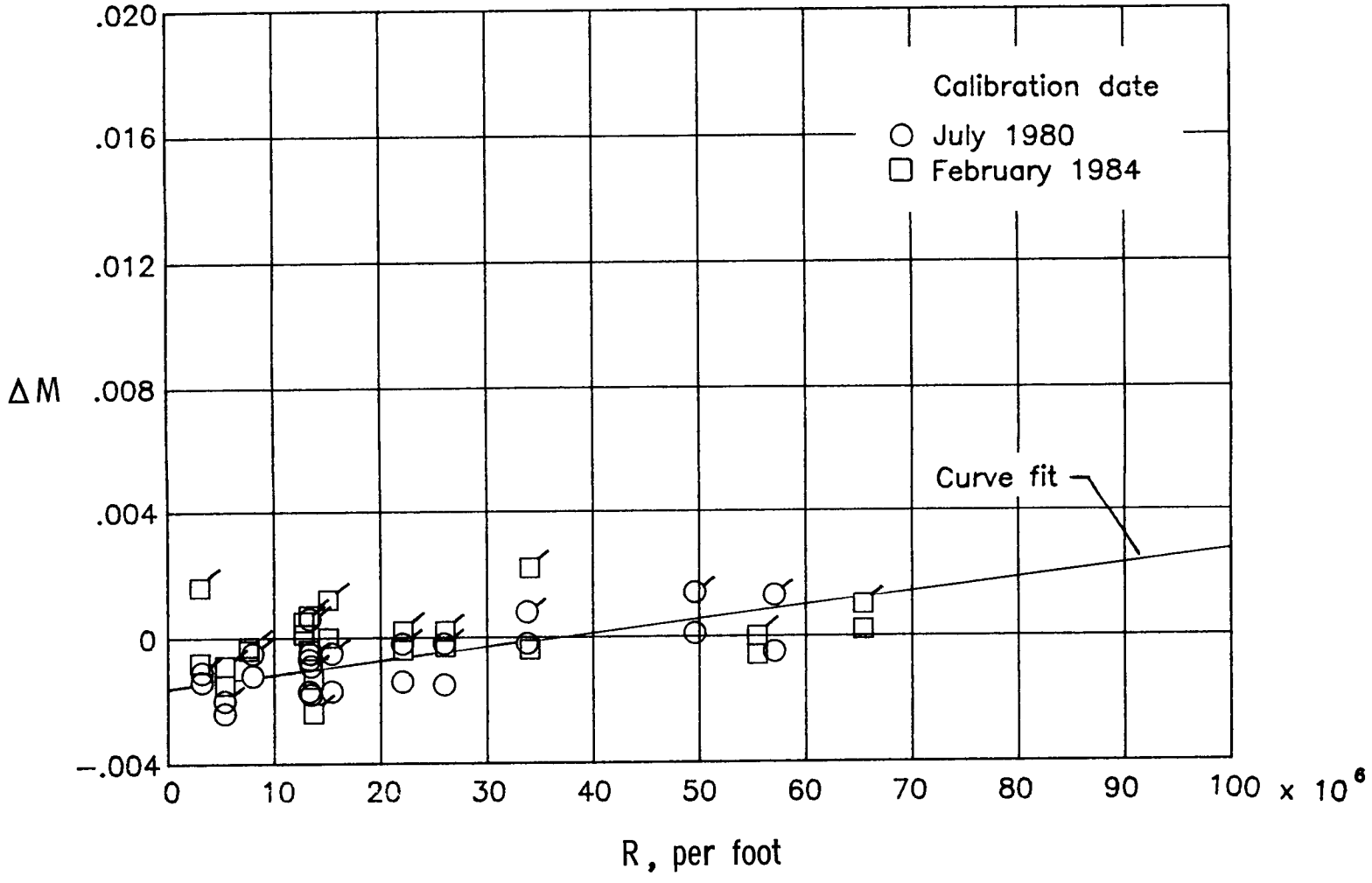

(c) M_{TC} = 0.40.

Figure 50.- Continued.

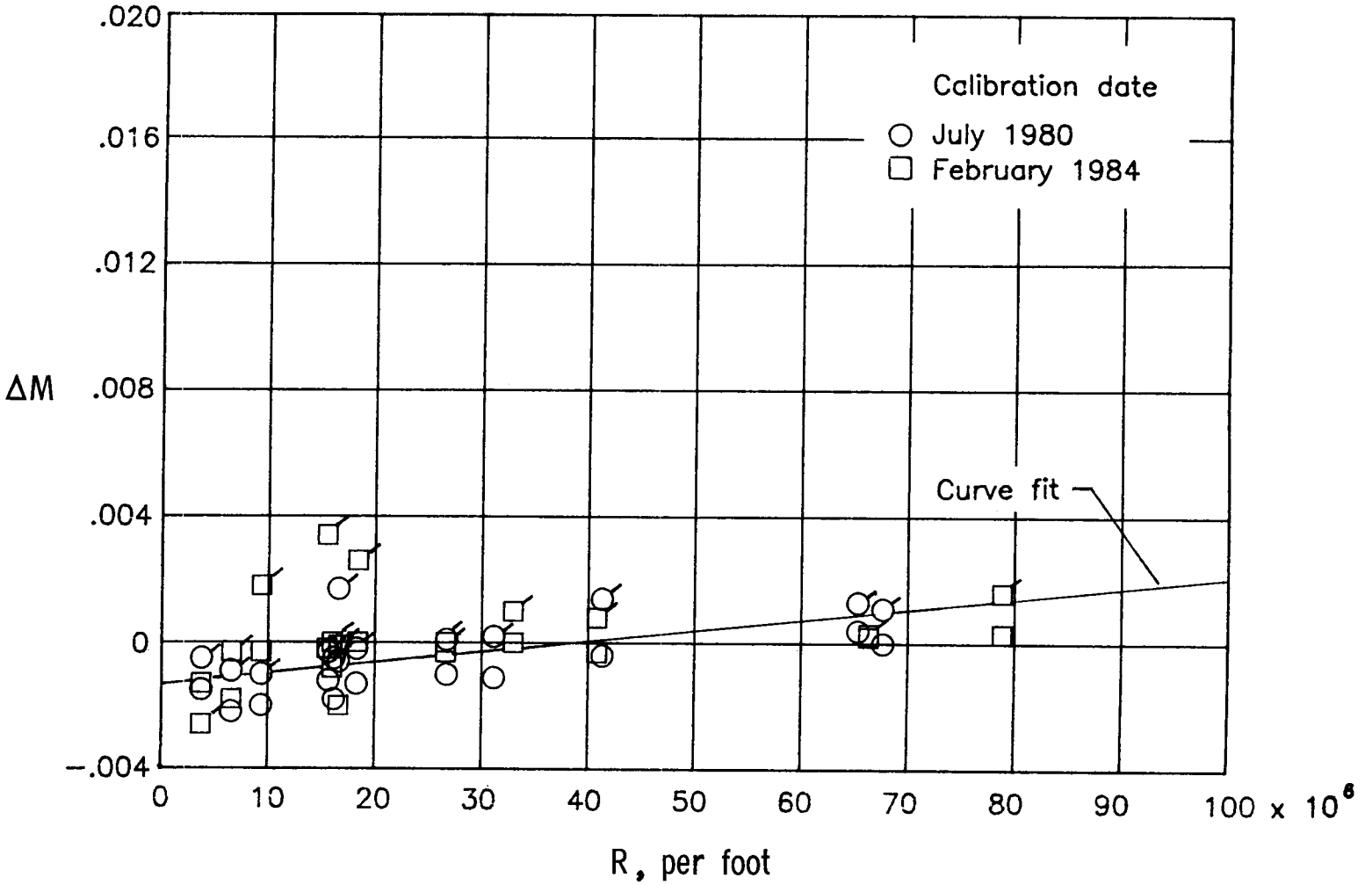

(d) $M_{TC} = 0.50$.

Figure 50.- Continued.

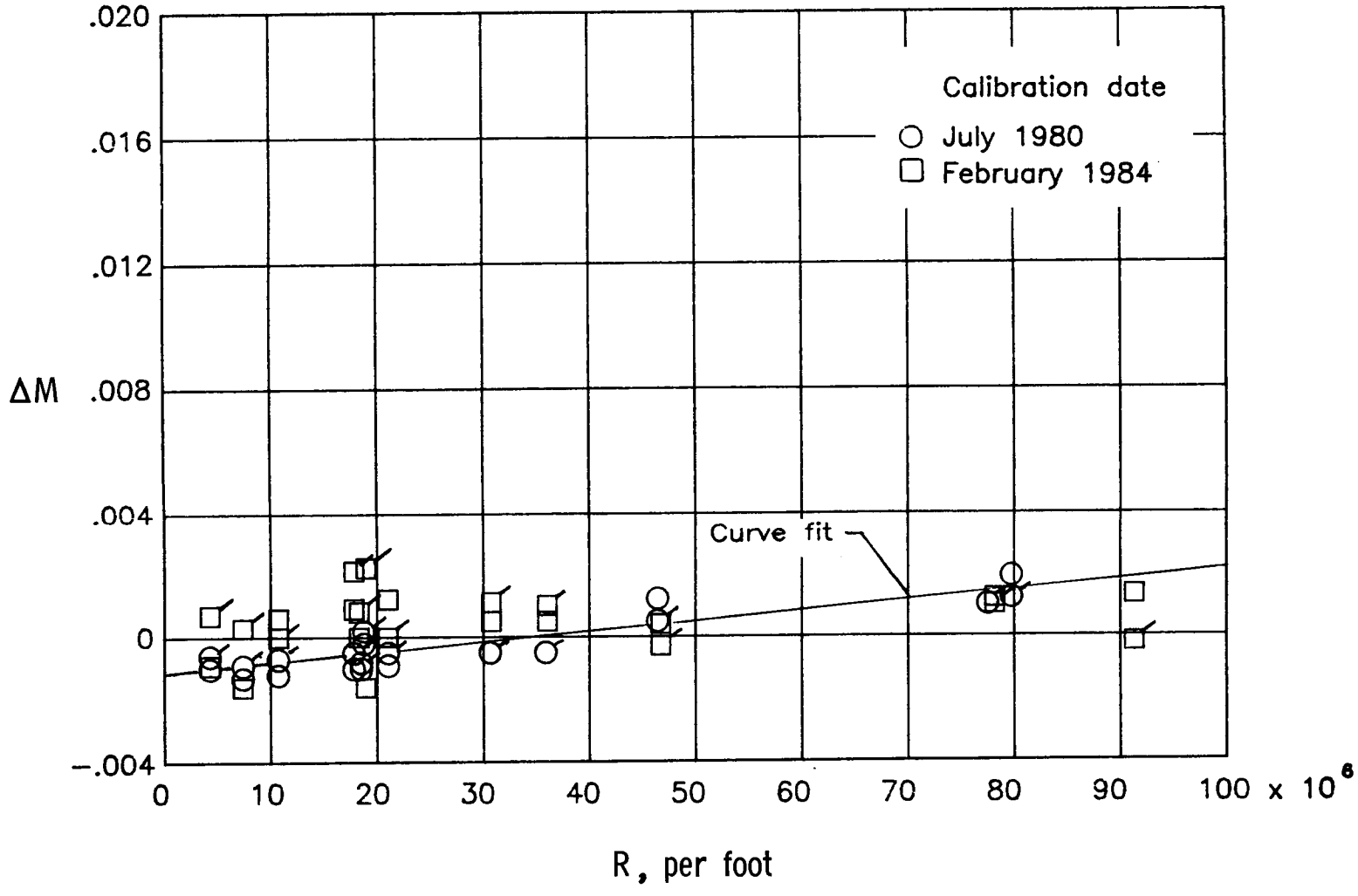

(e) $M_{TC} = 0.60$.

Figure 50.- Continued.

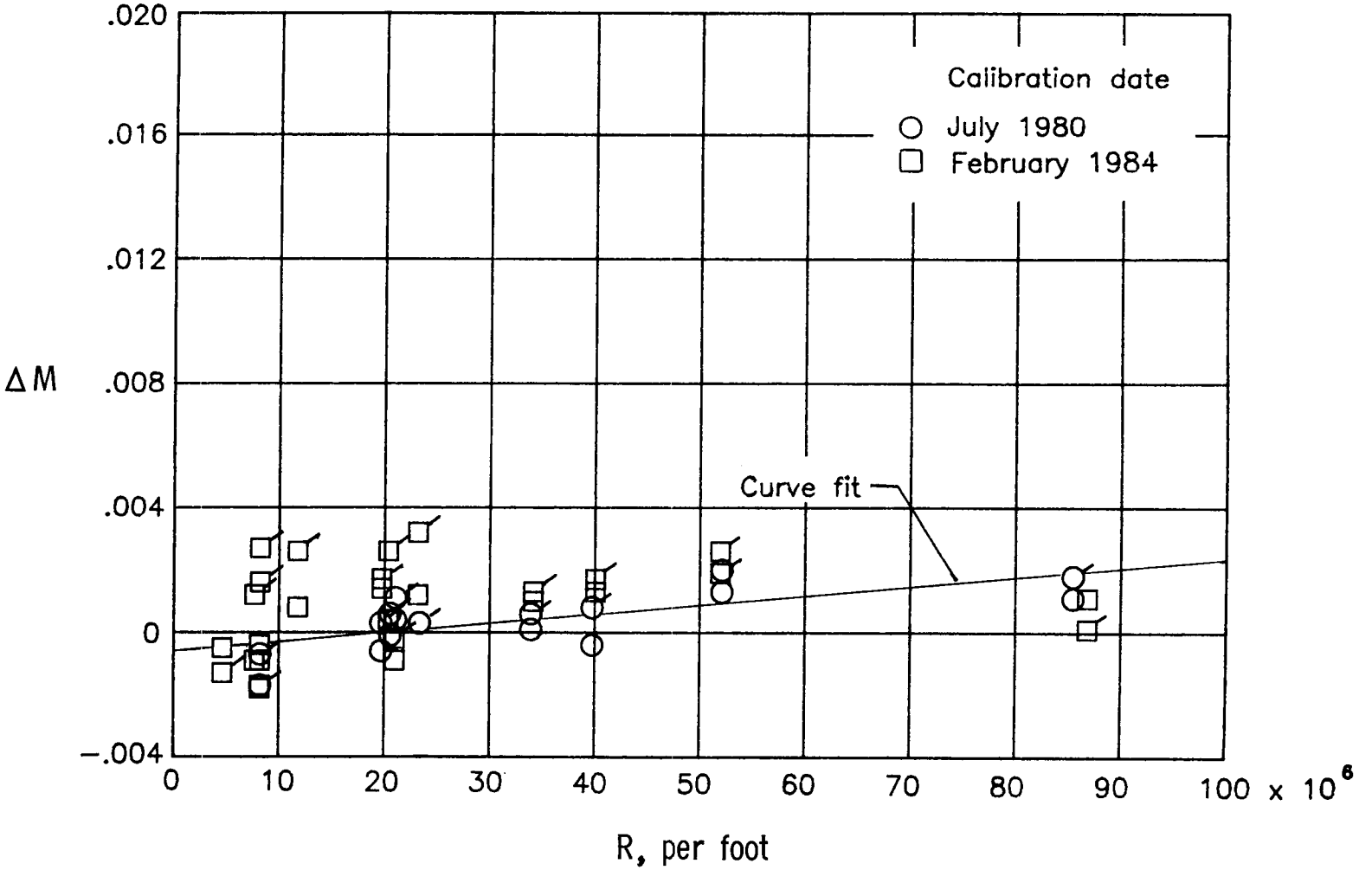

(f) $M_{TC} = 0.70$.

Figure 50.- Continued.

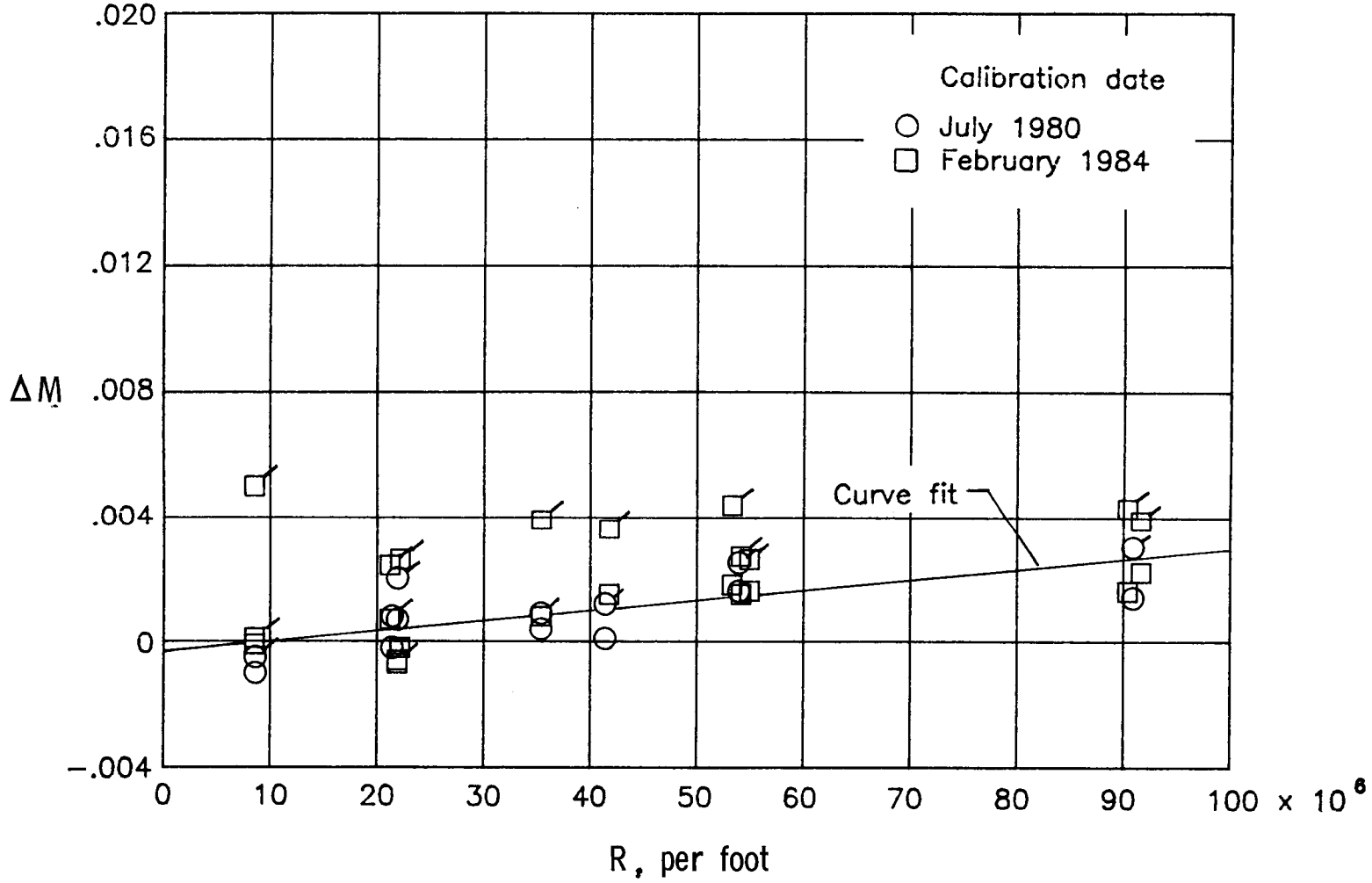

(g) $M_{TC} = 0.75$.

Figure 50.- Continued.

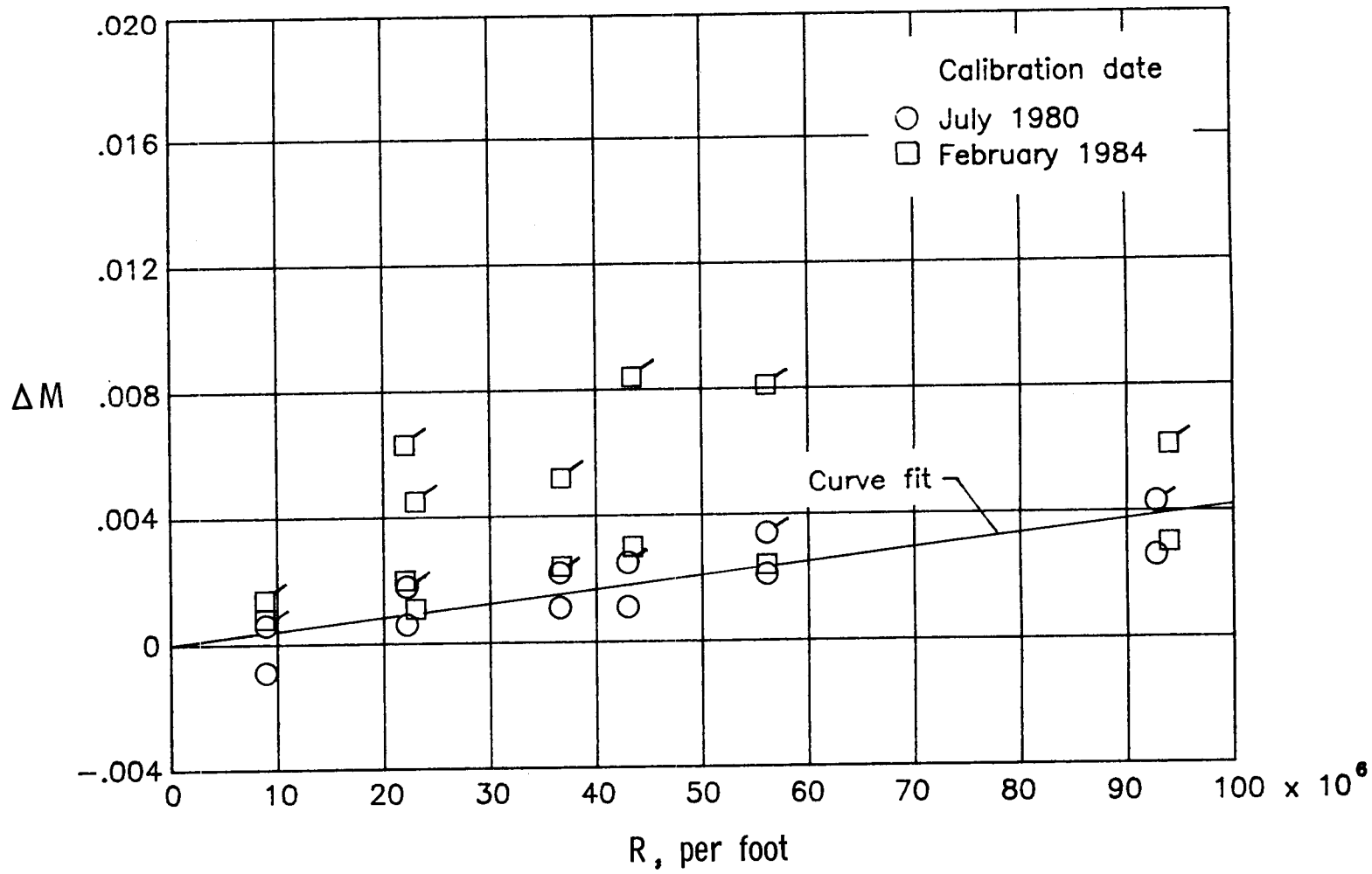

(h) $M_{TC} = 0.80$.

Figure 50.- Continued.

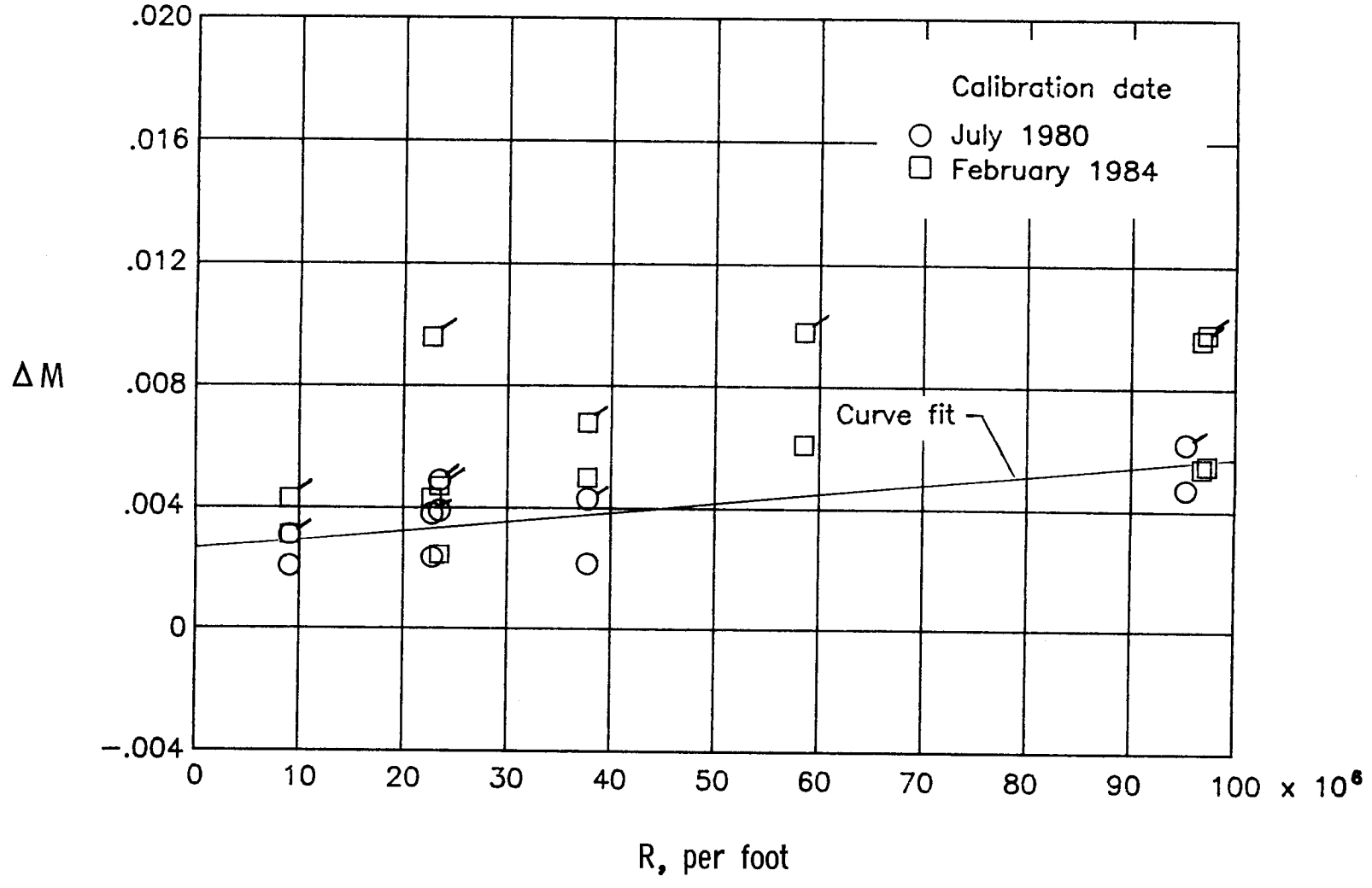

(i) $M_{TC} = 0.85$.

Figure 50.- Continued.

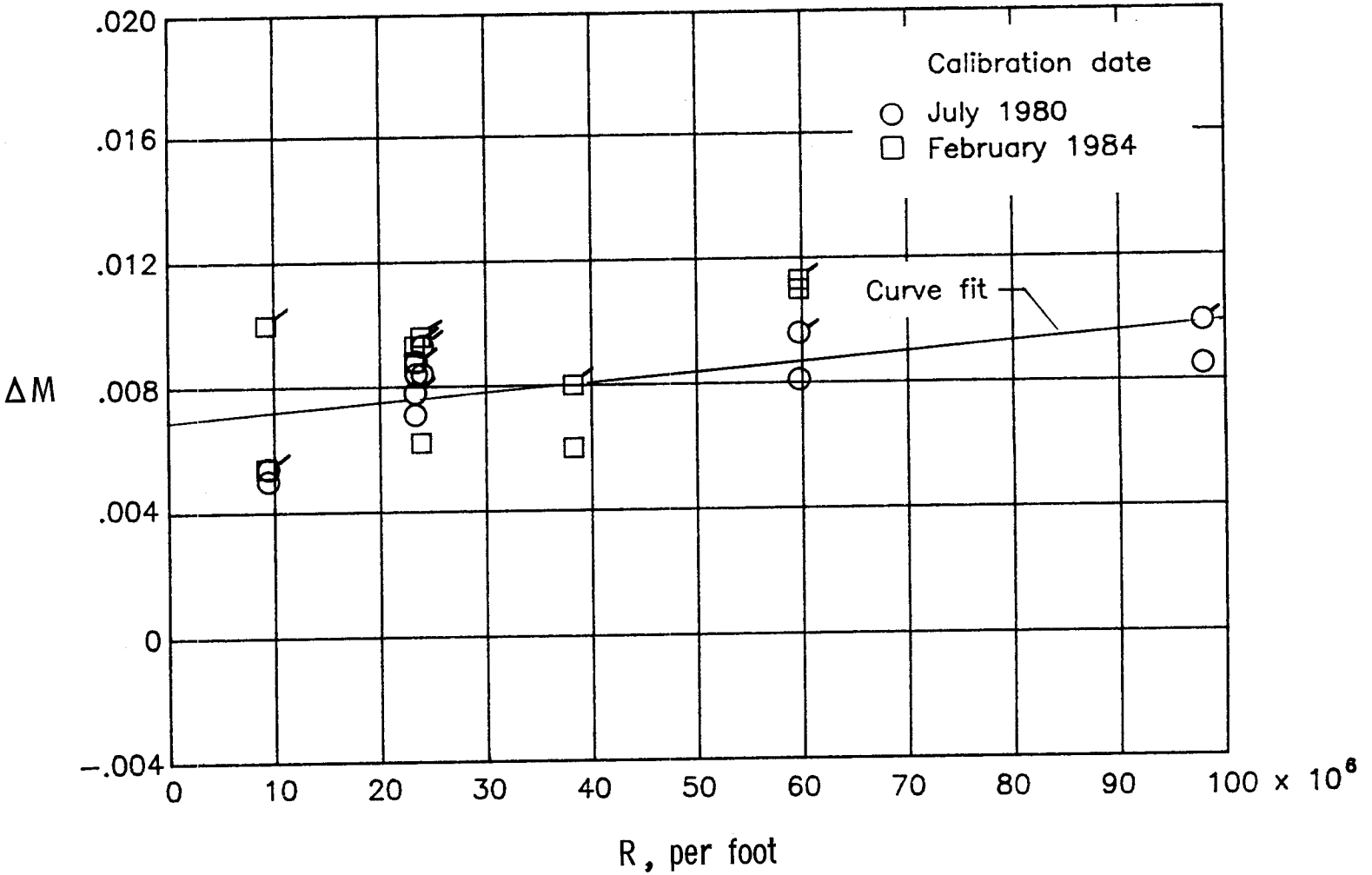

(j) $M_{TC} = 0.90$.

Figure 50.- Concluded.

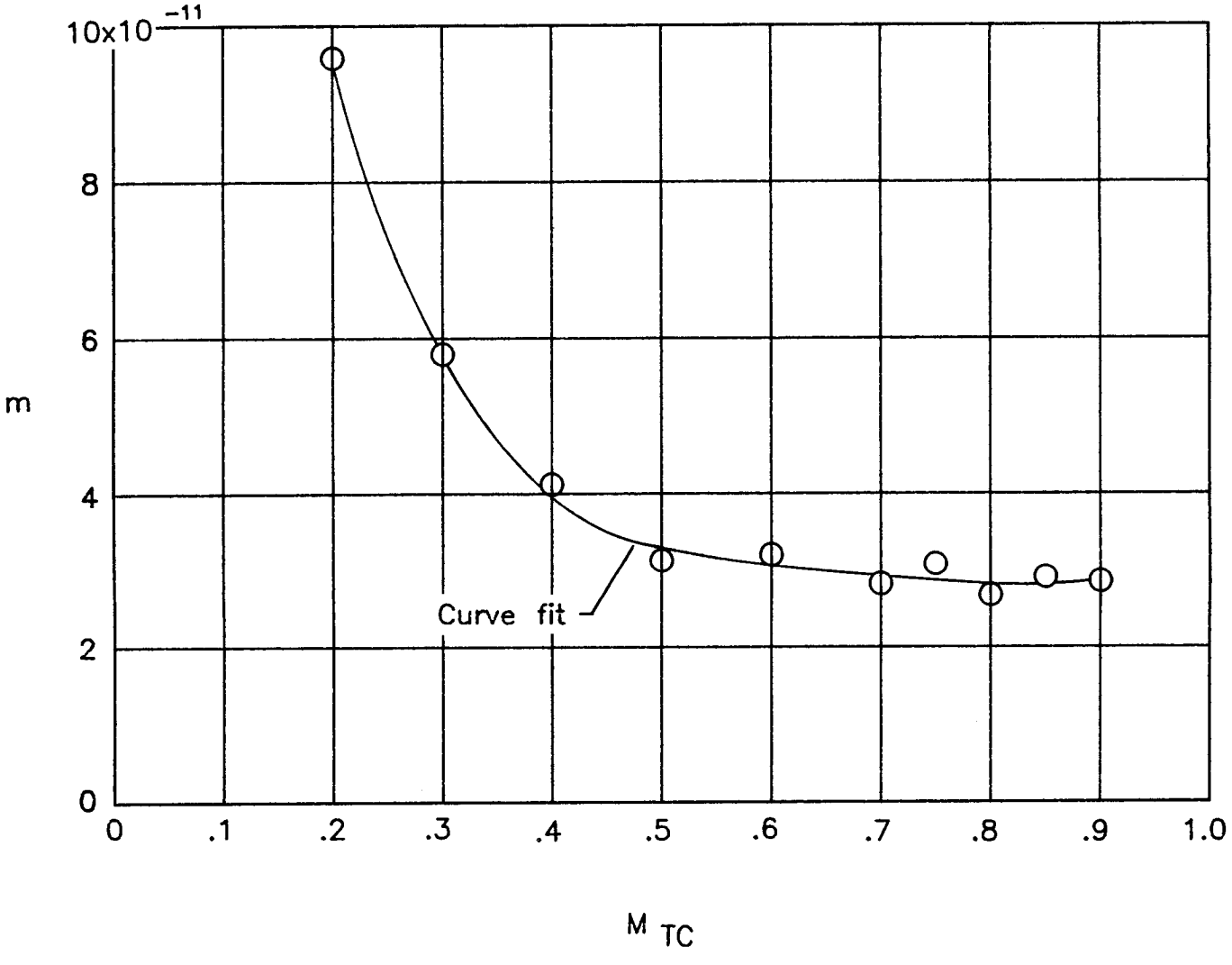

(a) Slope m.

Figure 51.- Slope and axis intercept values of curve fit to calibration factor as function of test-chamber Mach number.

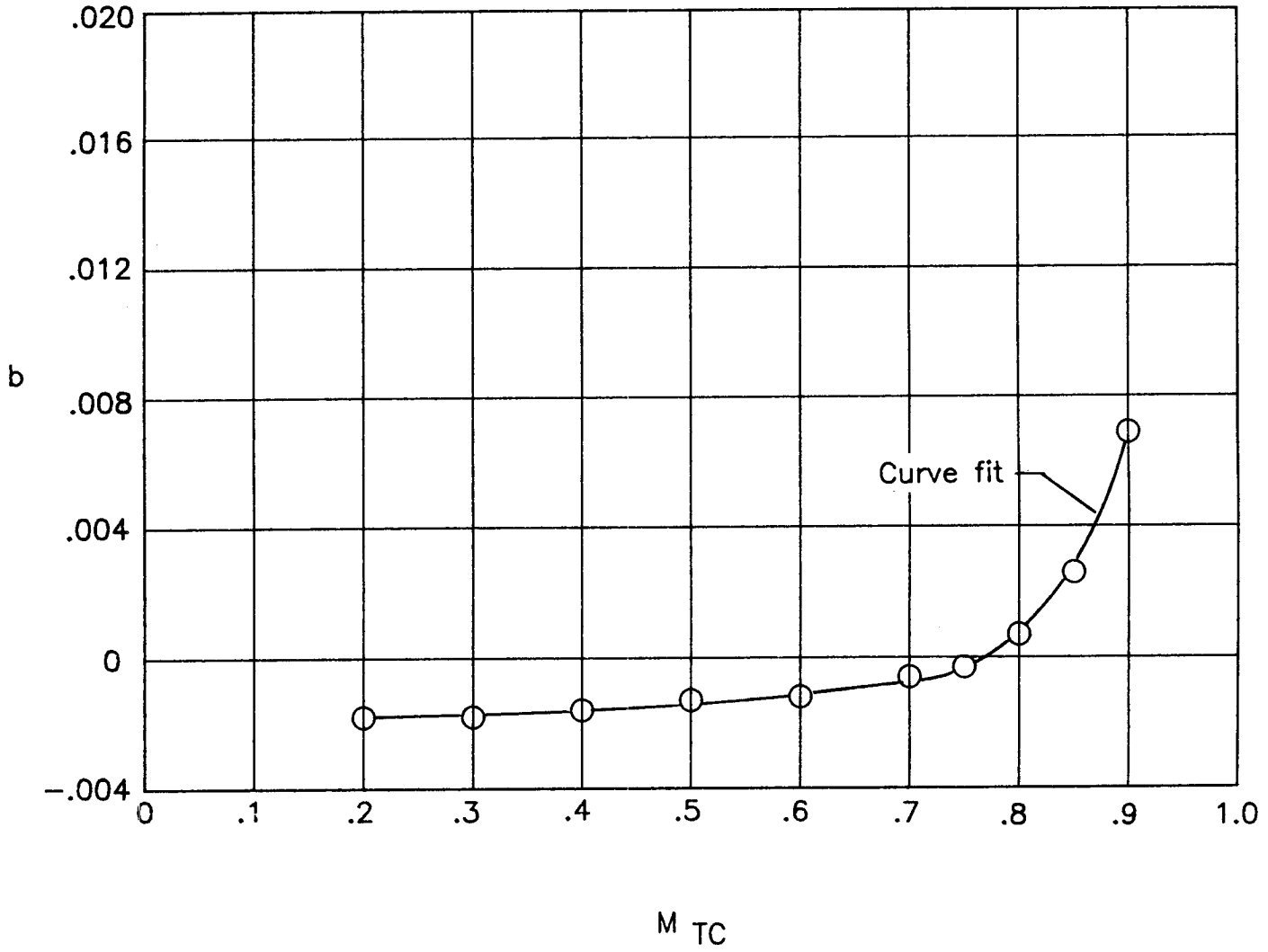

(b) Axis intercept b.

Figure 51.- Concluded.

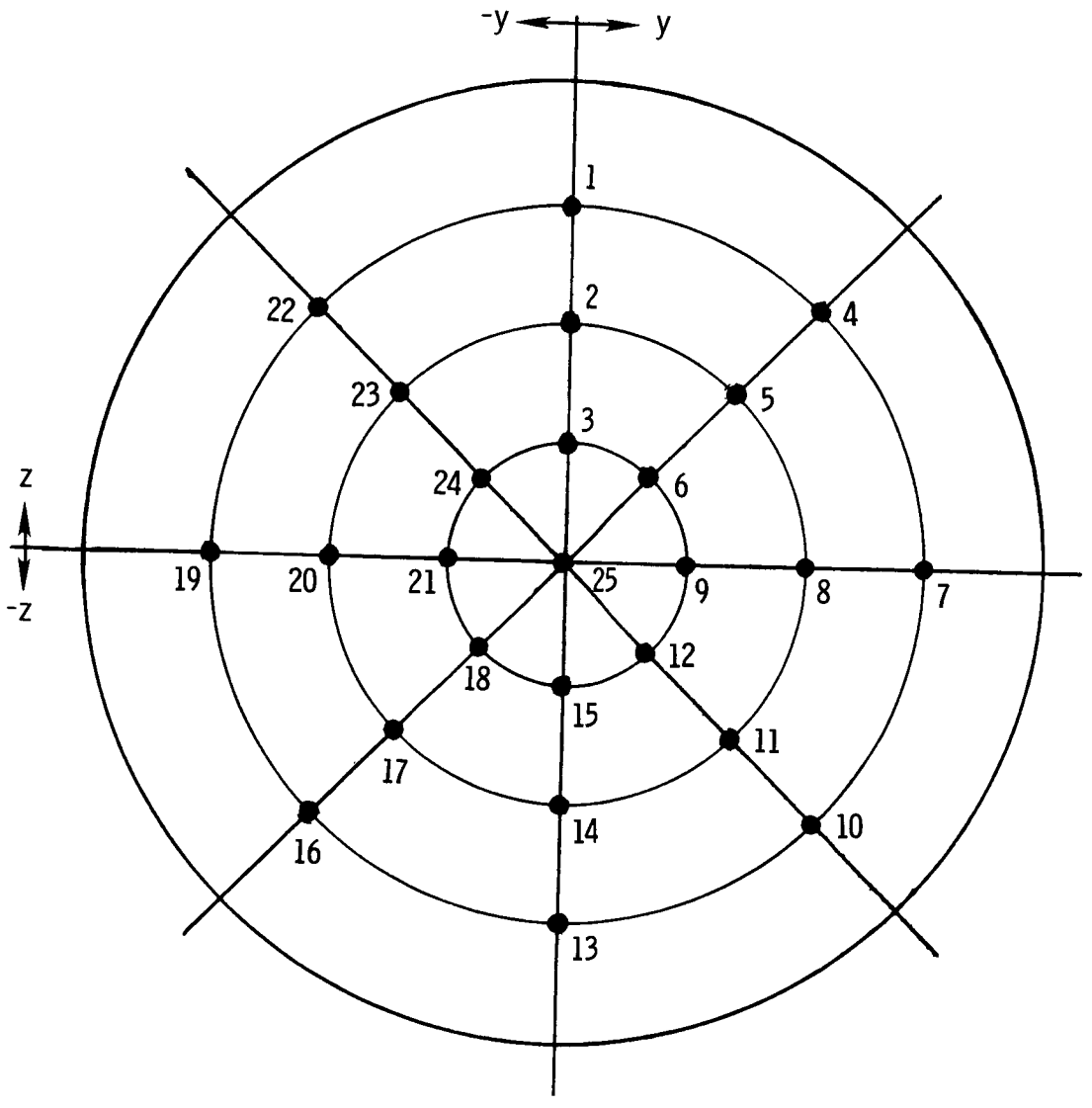

T_1 106.0 K	T_6 106.2 K	T_{11} 106.0 K	T_{16} 105.4 K	T_{21} 105.8 K
T_2 106.0	T_7 106.0	T_{12} 105.9	T_{17} 106.0	T_{22} 105.8
T_3 106.2	T_8 106.0	T_{13} 105.7	T_{18} 105.6	T_{23} 105.6
T_4 106.1	T_9 106.2	T_{14} 105.7	T_{19} 105.7	T_{24} 106.0
T_5 106.0	T_{10} 105.8	T_{15} 105.8	T_{20} 105.7	T_{25} 105.9

Figure 52.- Typical lateral temperature distribution. M = 0.70; R = 50.1 × 10^6; $\bar{T}_t$ = 105.9 K; standard deviation, 0.20 K.

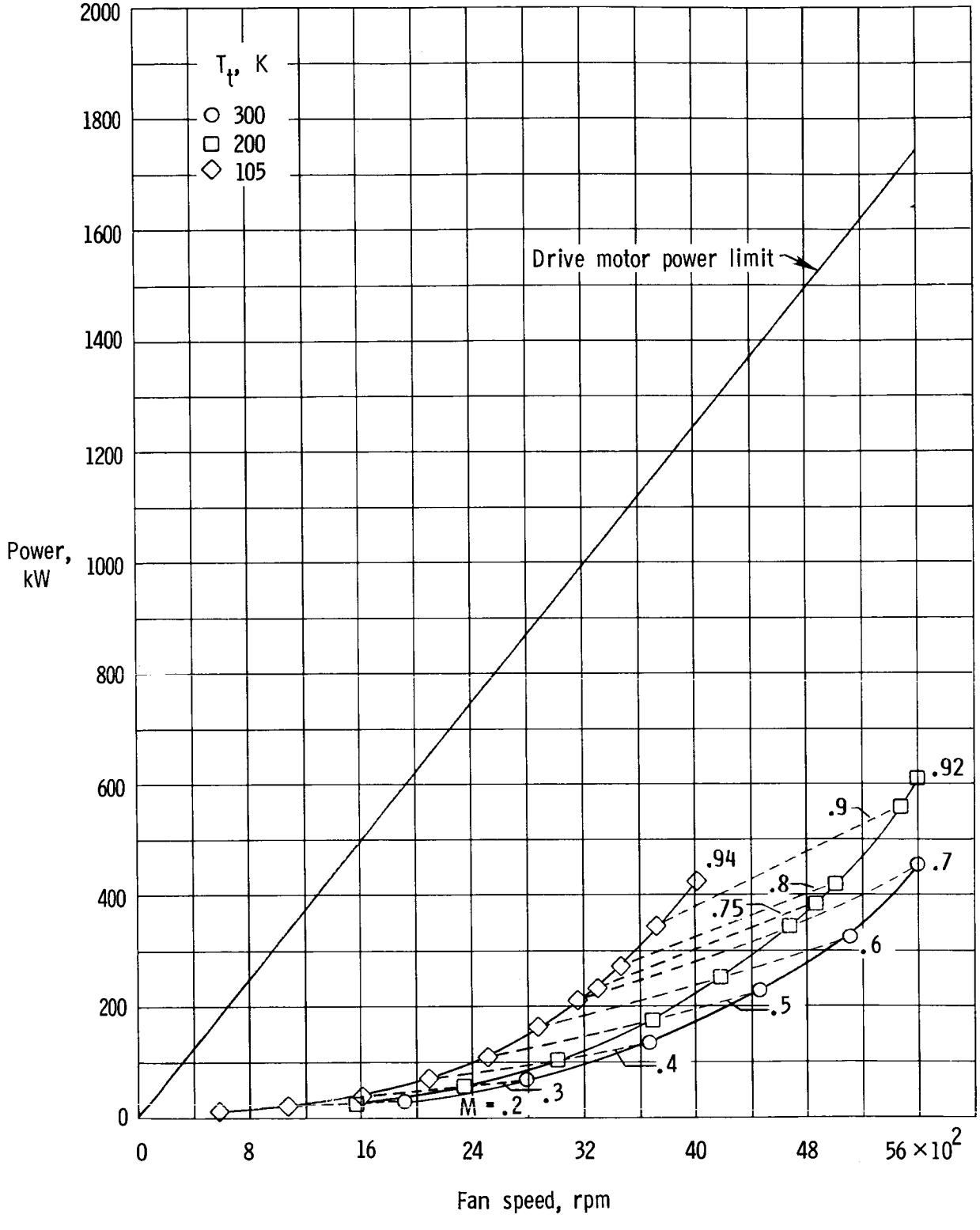

(a) p_t = 1.36 atm.

Figure 53.- Experimental drive motor power as function of fan speed and average stream Mach number.

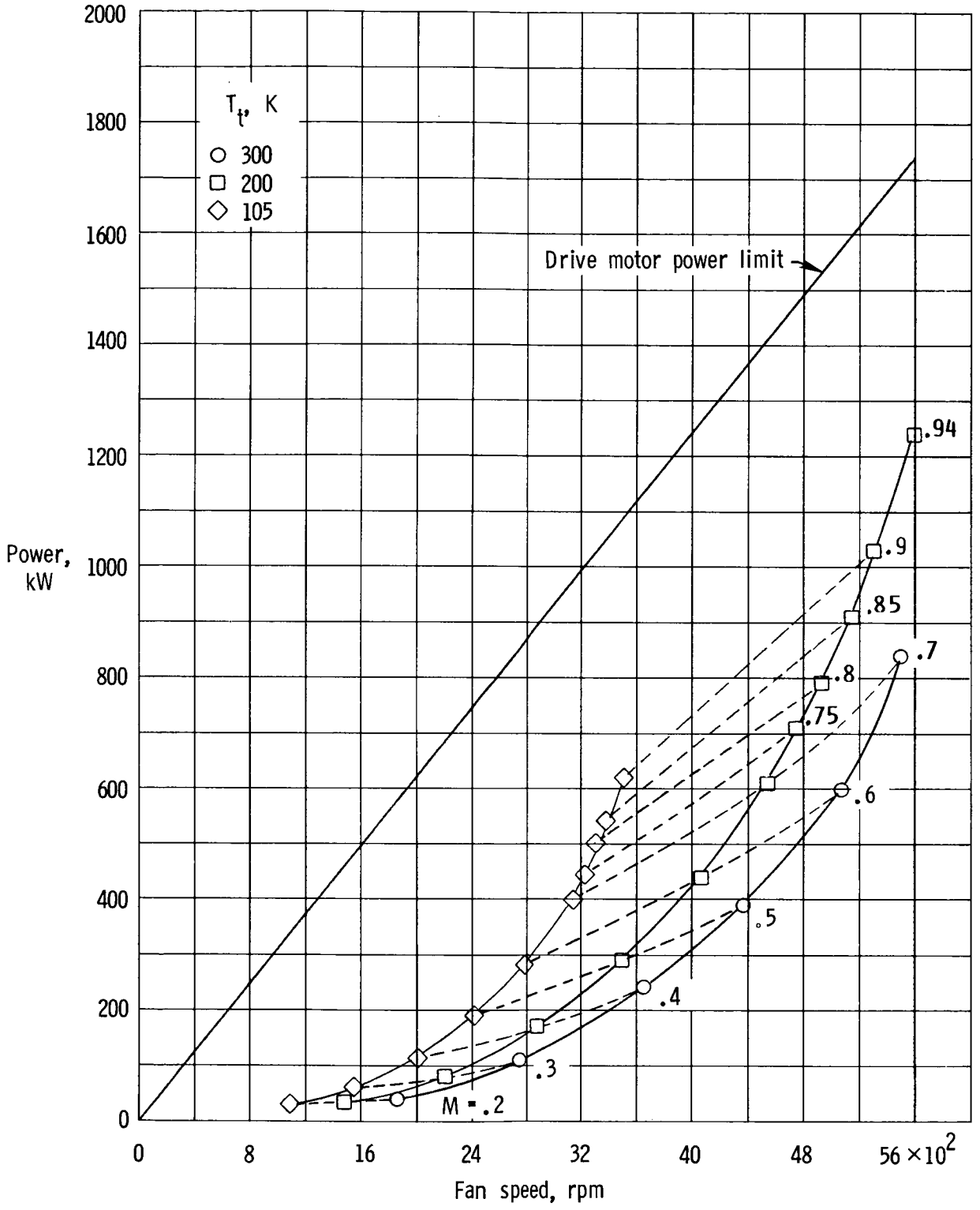

(b) p_t = 3.06 atm.

Figure 53.- Continued.

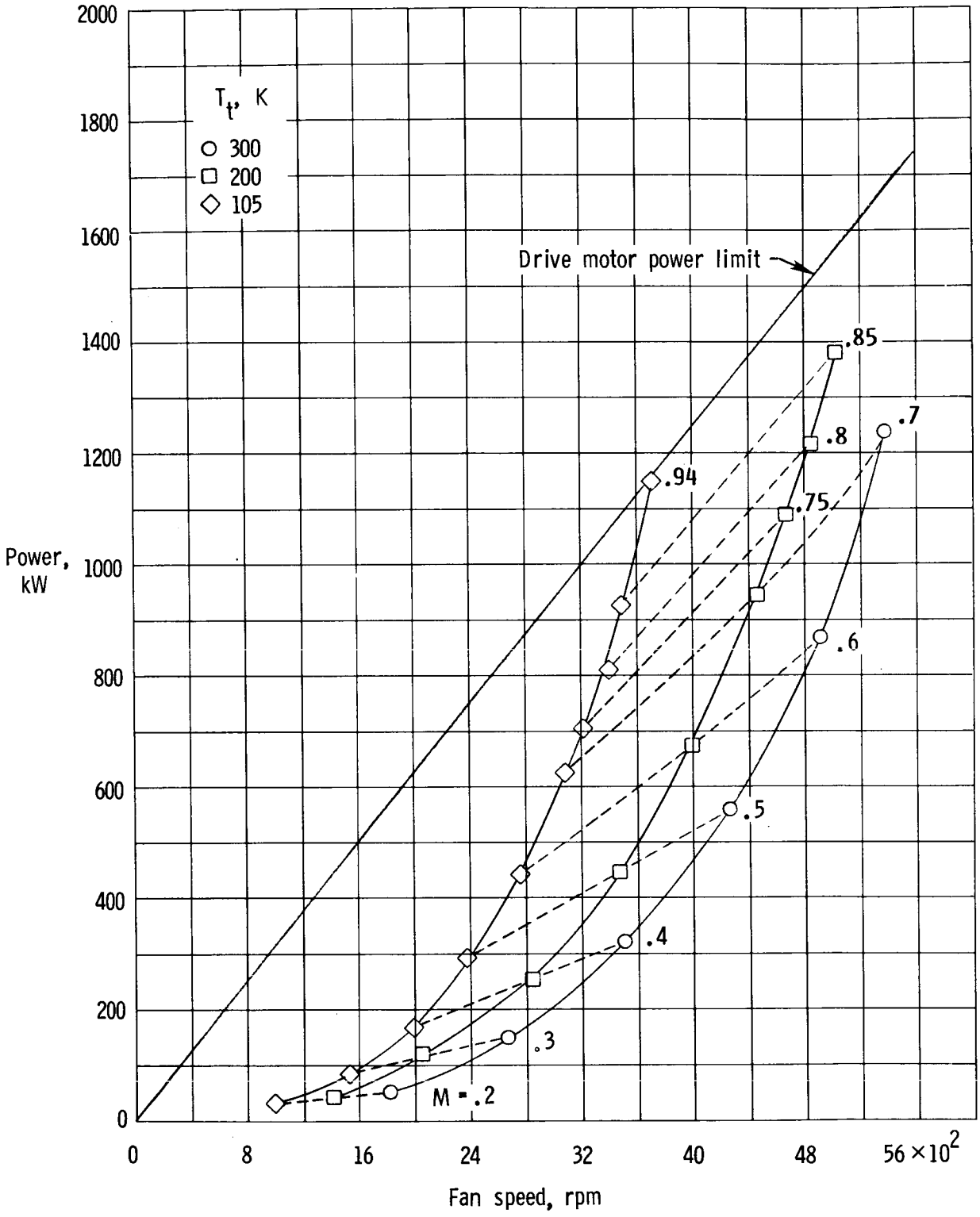

(c) p_t = 5.10 atm.

Figure 53.- Continued.

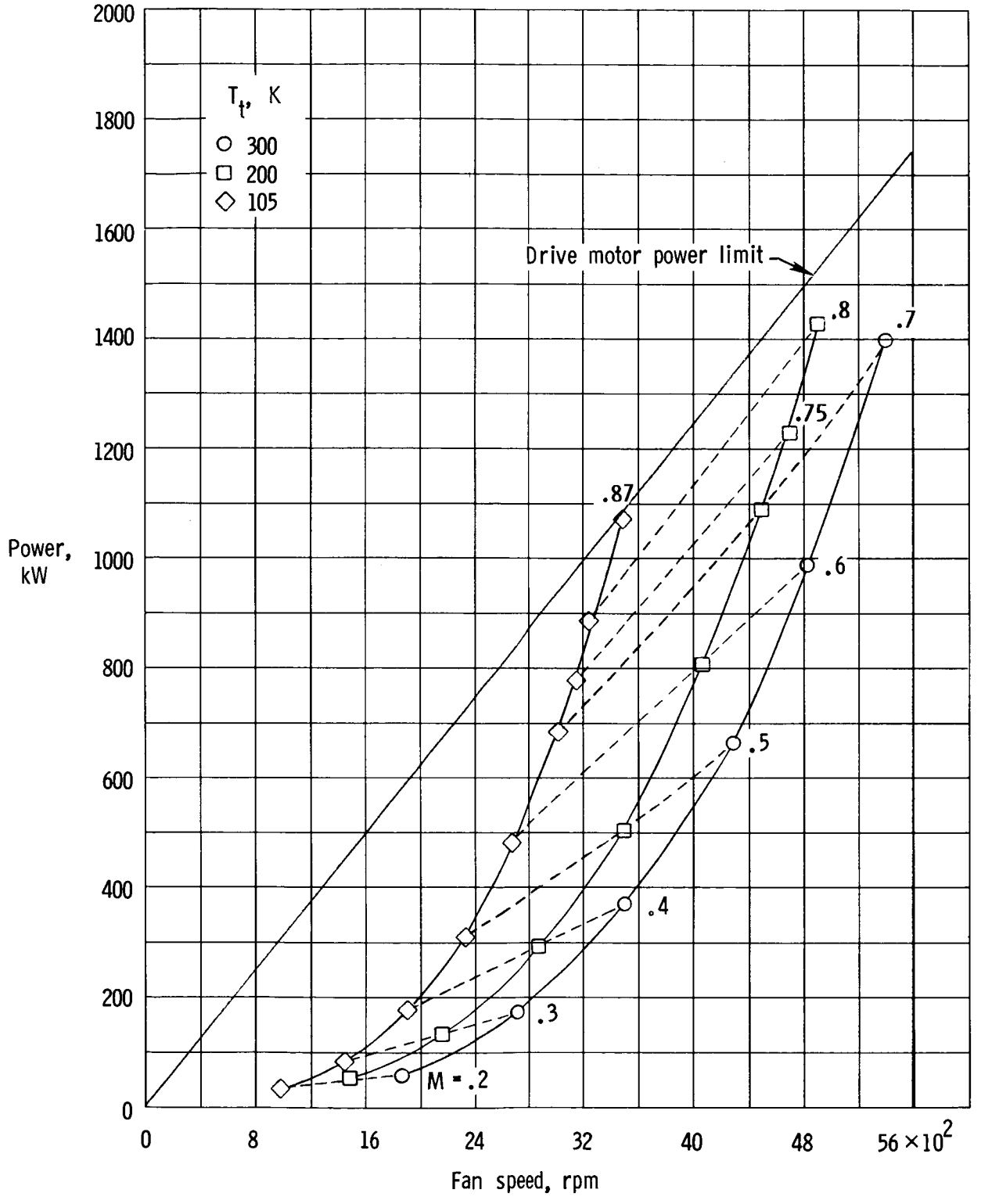

(d) p_t = 5.85 atm.

Figure 53.- Concluded.

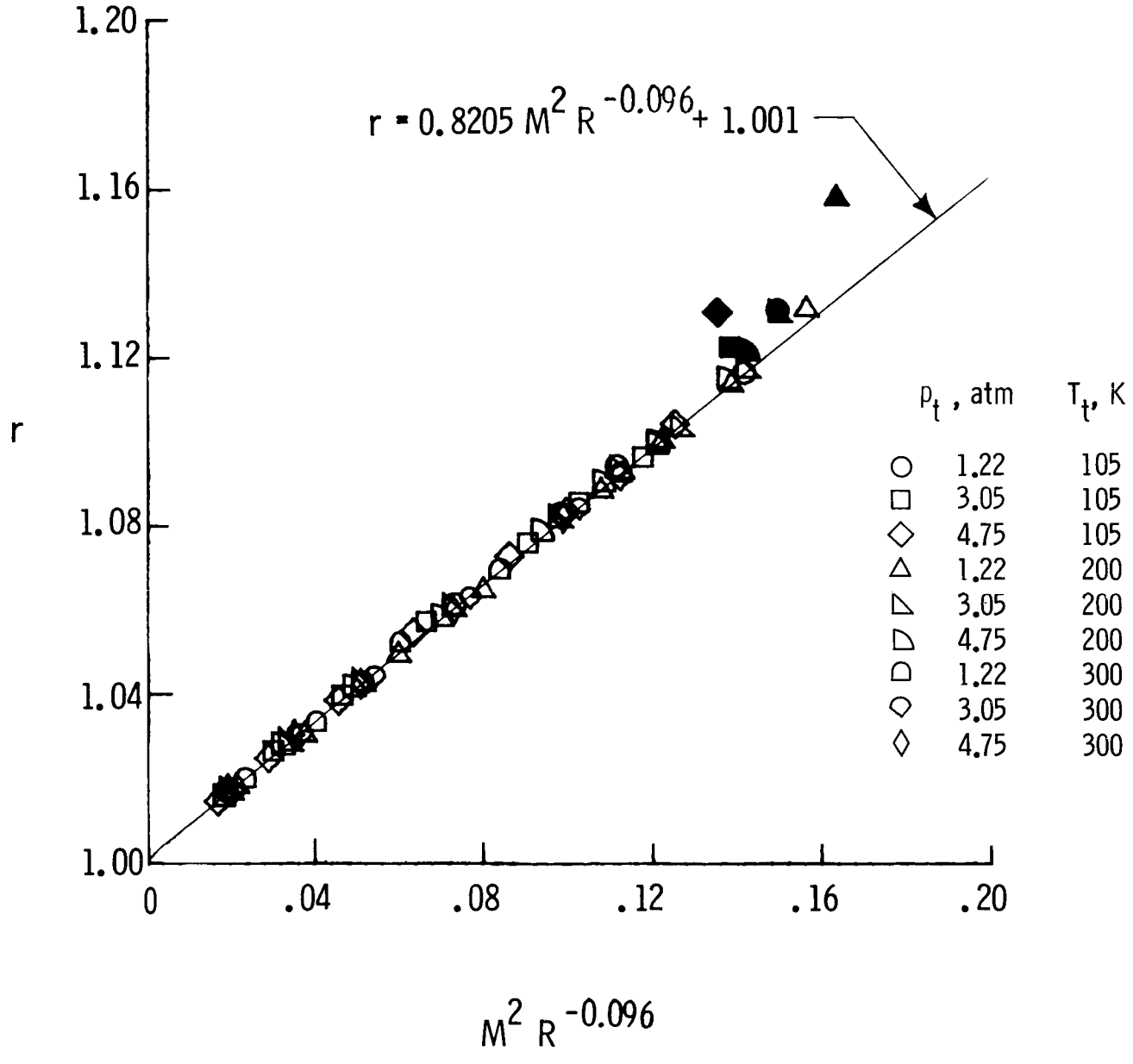

Figure 54.- Fan pressure ratio correlated in terms of Mach number and Reynolds number. Solid symbols denote choked conditions, which were not used in correlation. Data taken from reference 17.

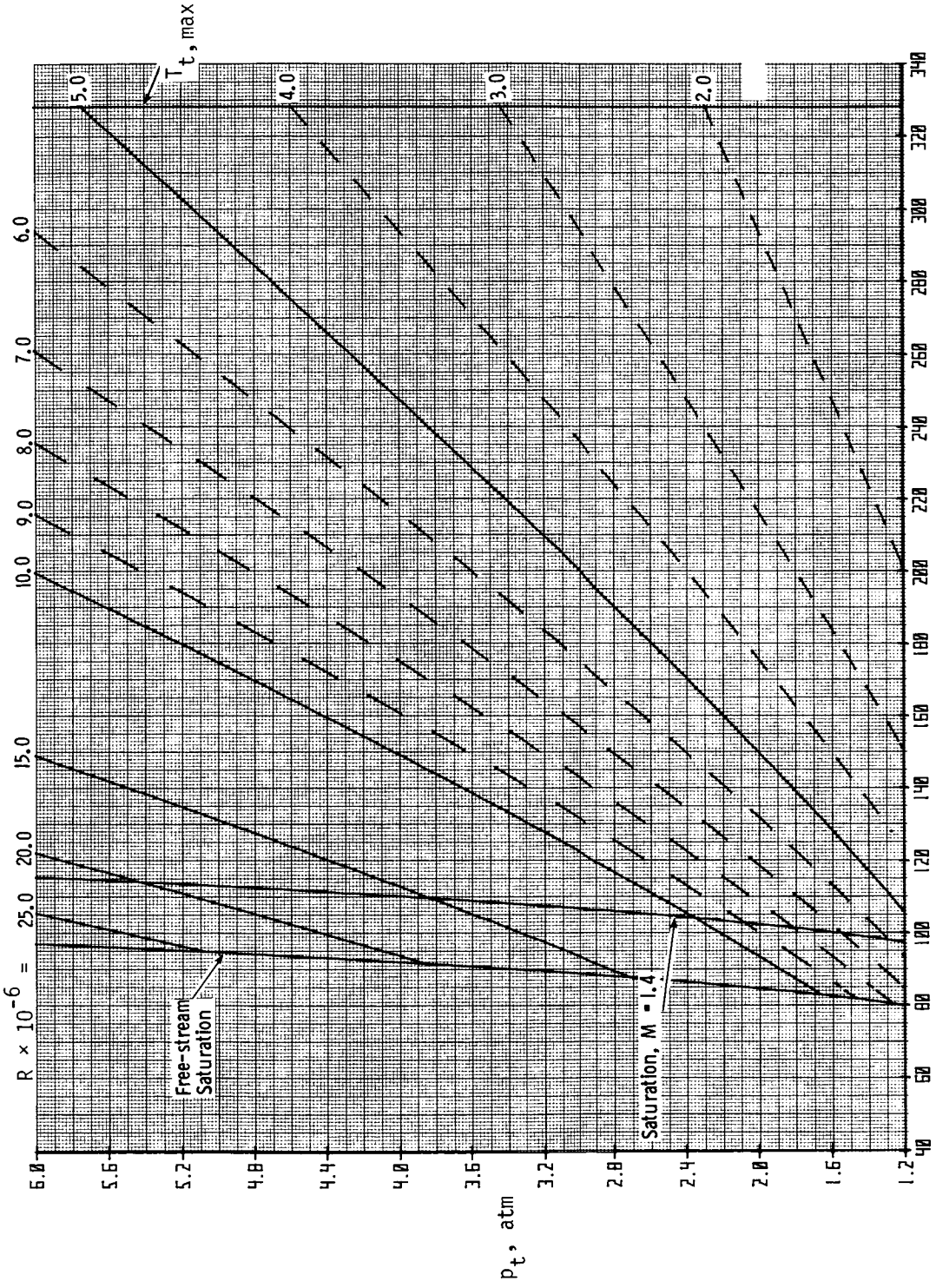

(a) M = 0.30.

Figure 55.- Envelope of tunnel operational conditions.

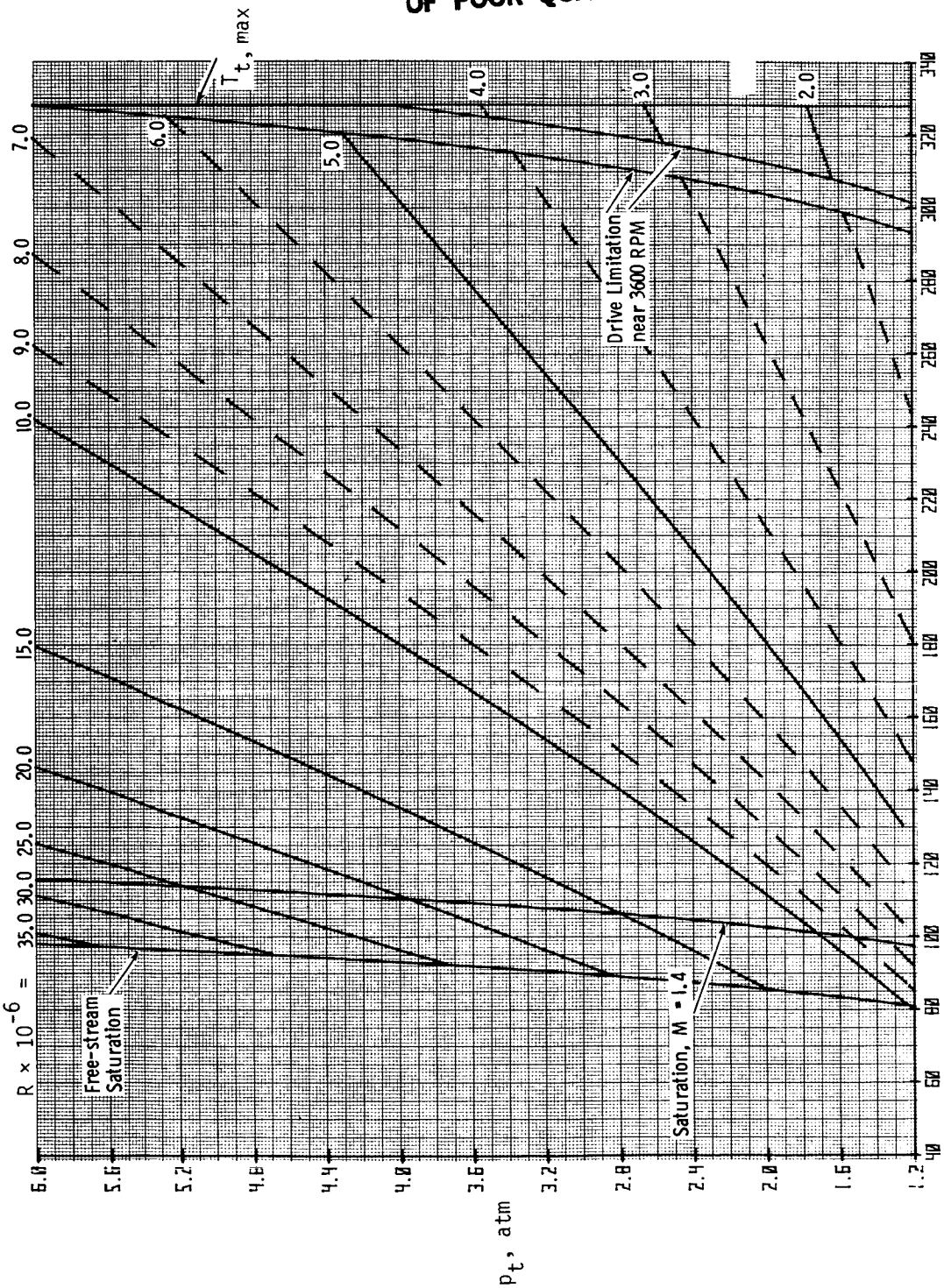

(b) M = 0.40.

Figure 55.- Continued.

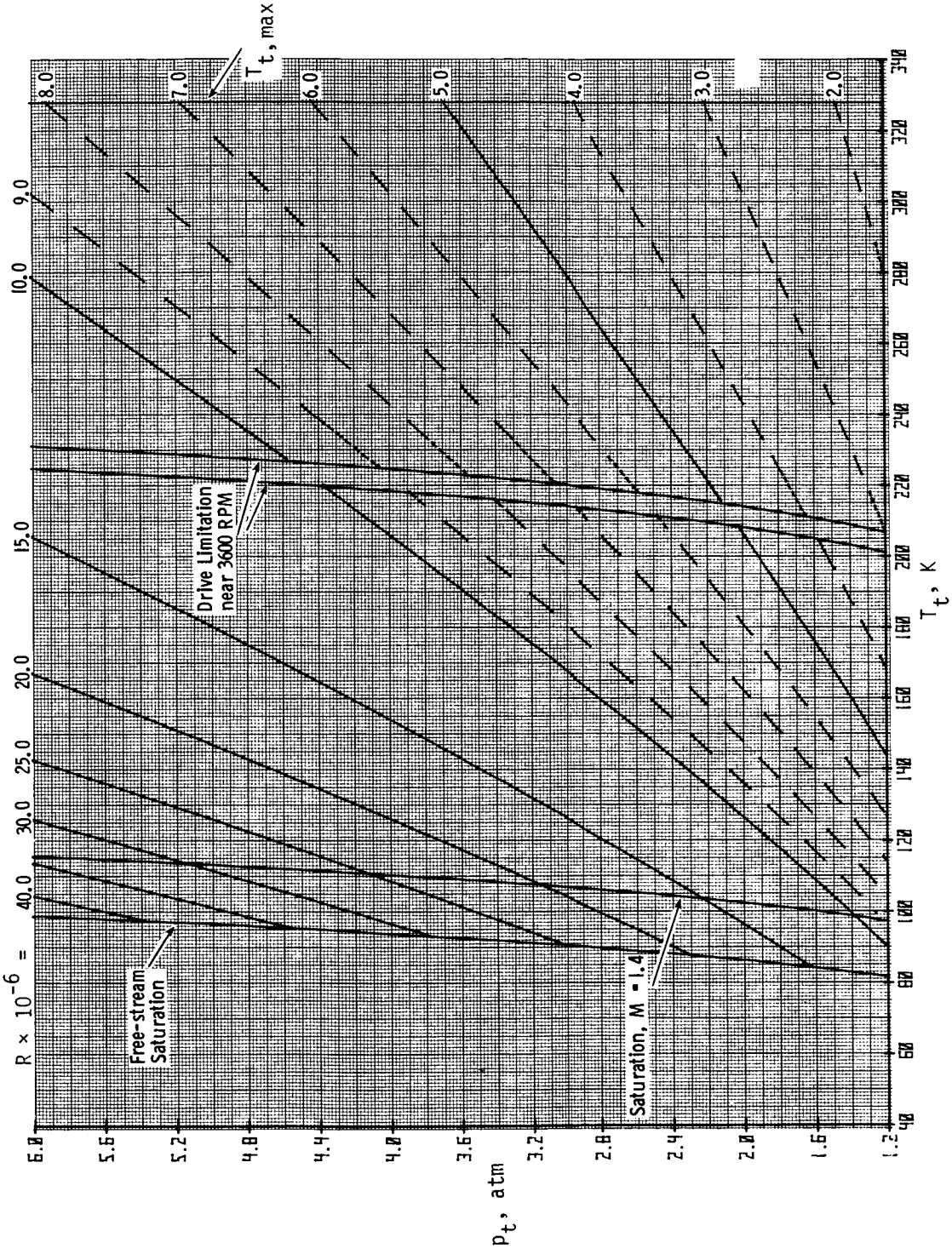

(c) M = 0.50.

Figure 55.- Continued.

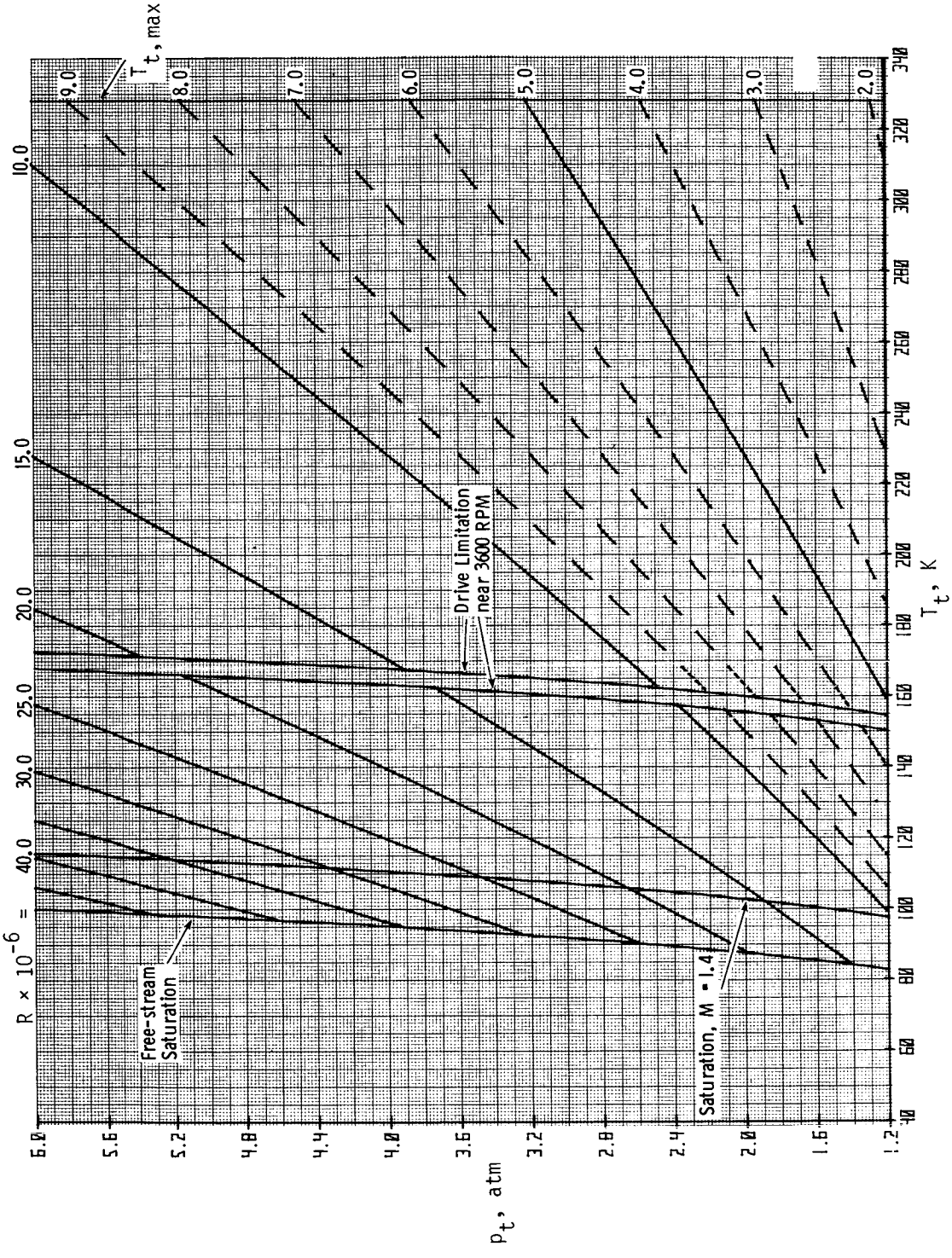

(d) M = 0.60.

Figure 55.- Continued.

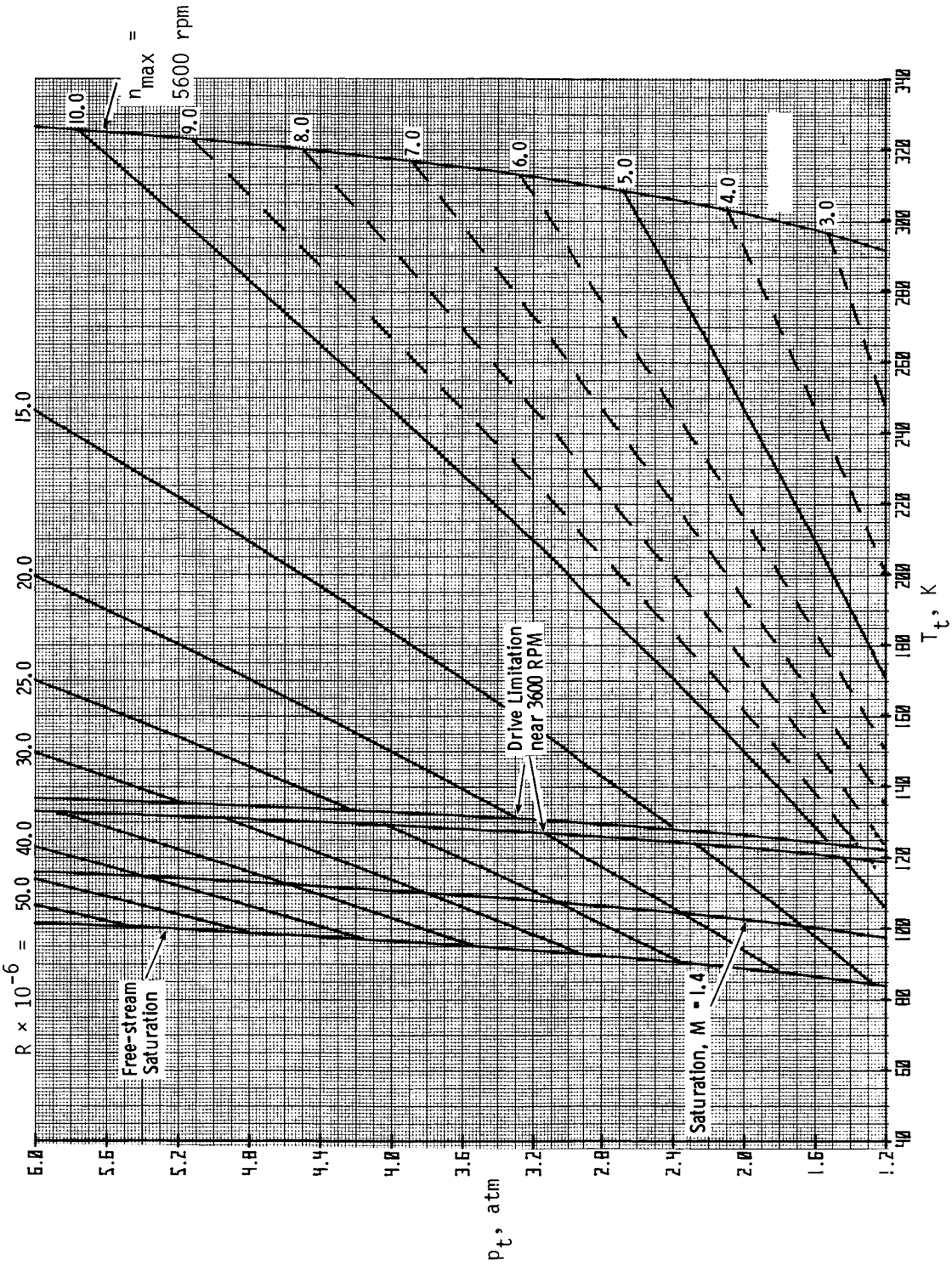

(e) M = 0.70.

Figure 55.- Continued.

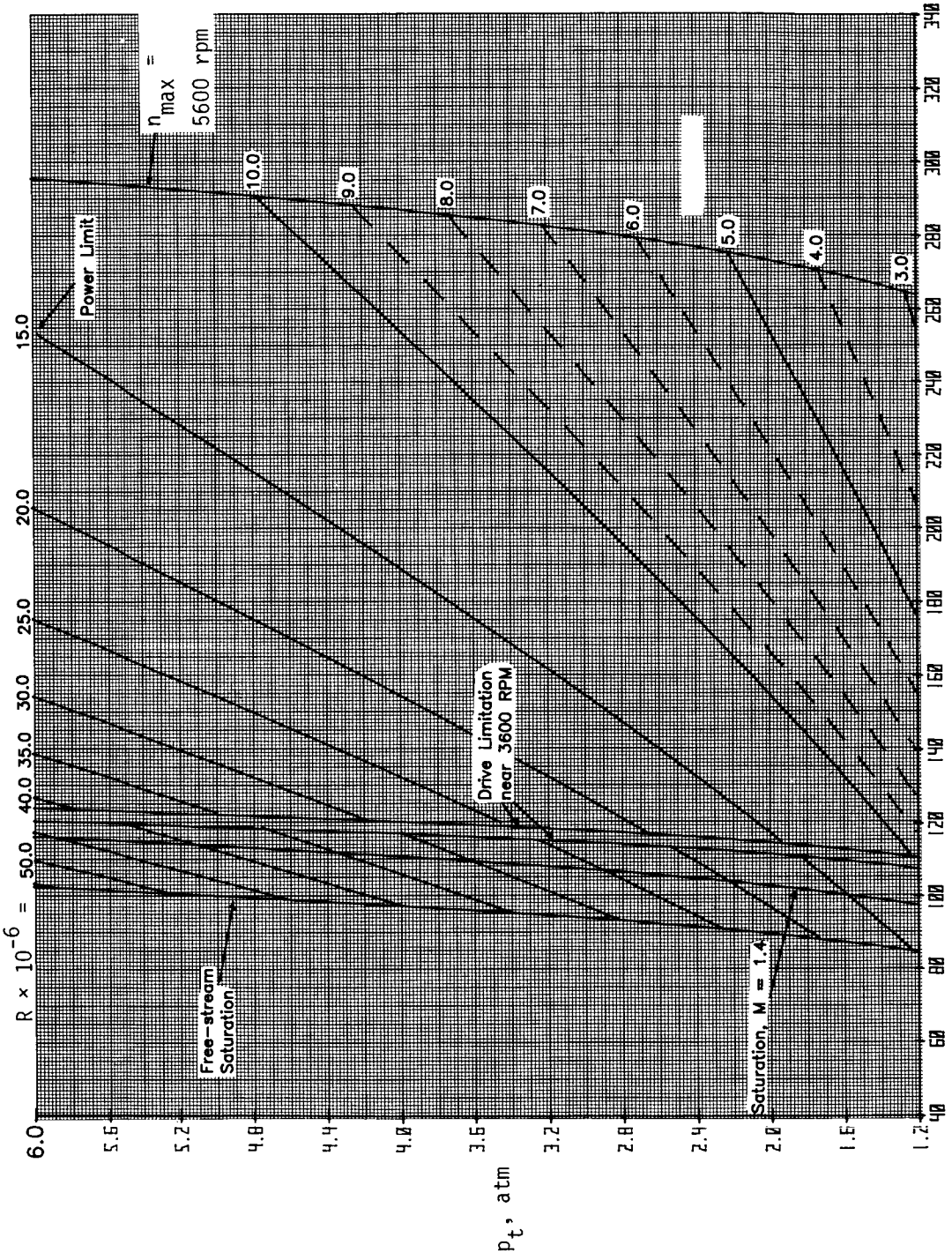

(f) M = 0.75.

Figure 55.- Continued.

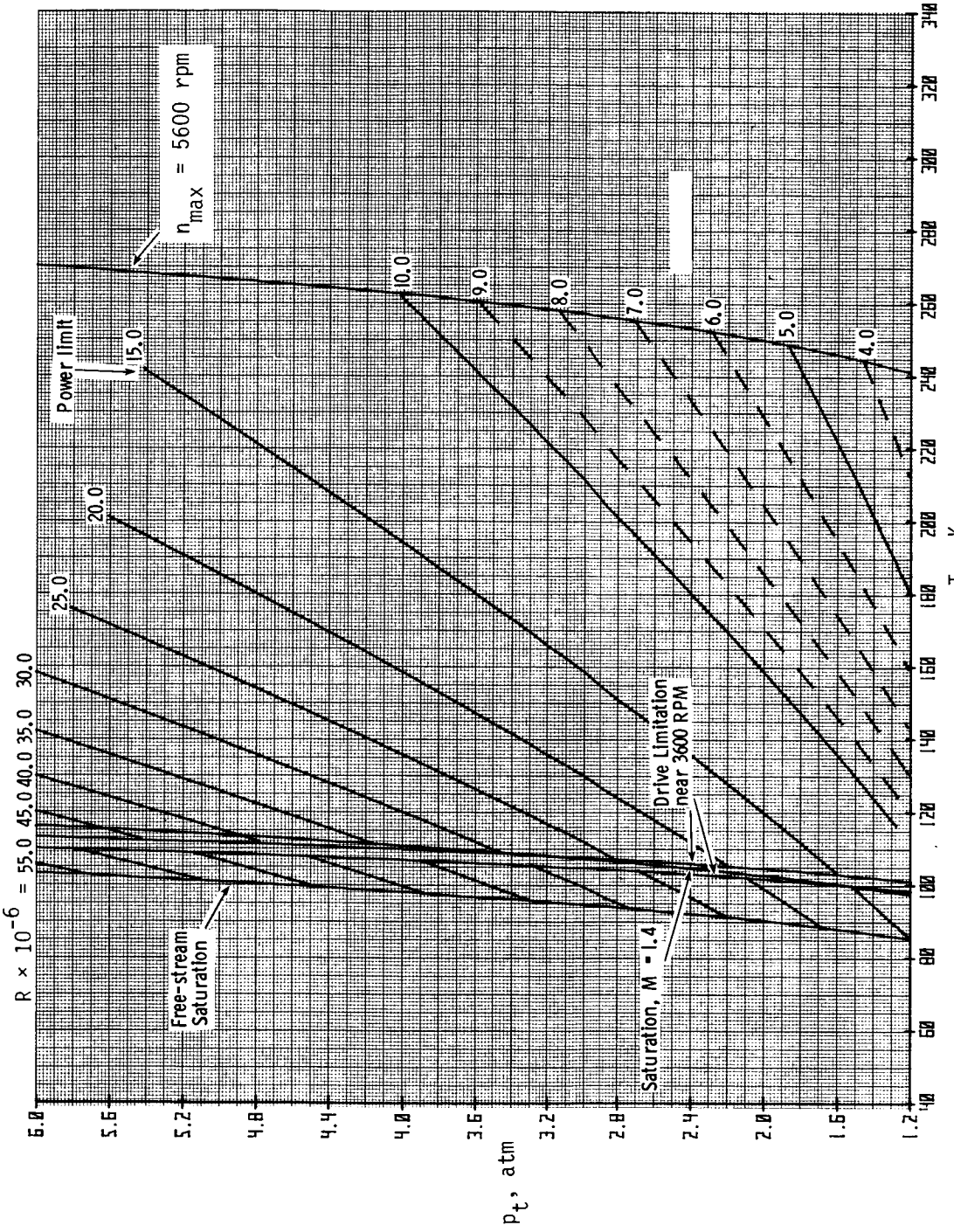

(g) M = 0.80.

Figure 55.- Continued.

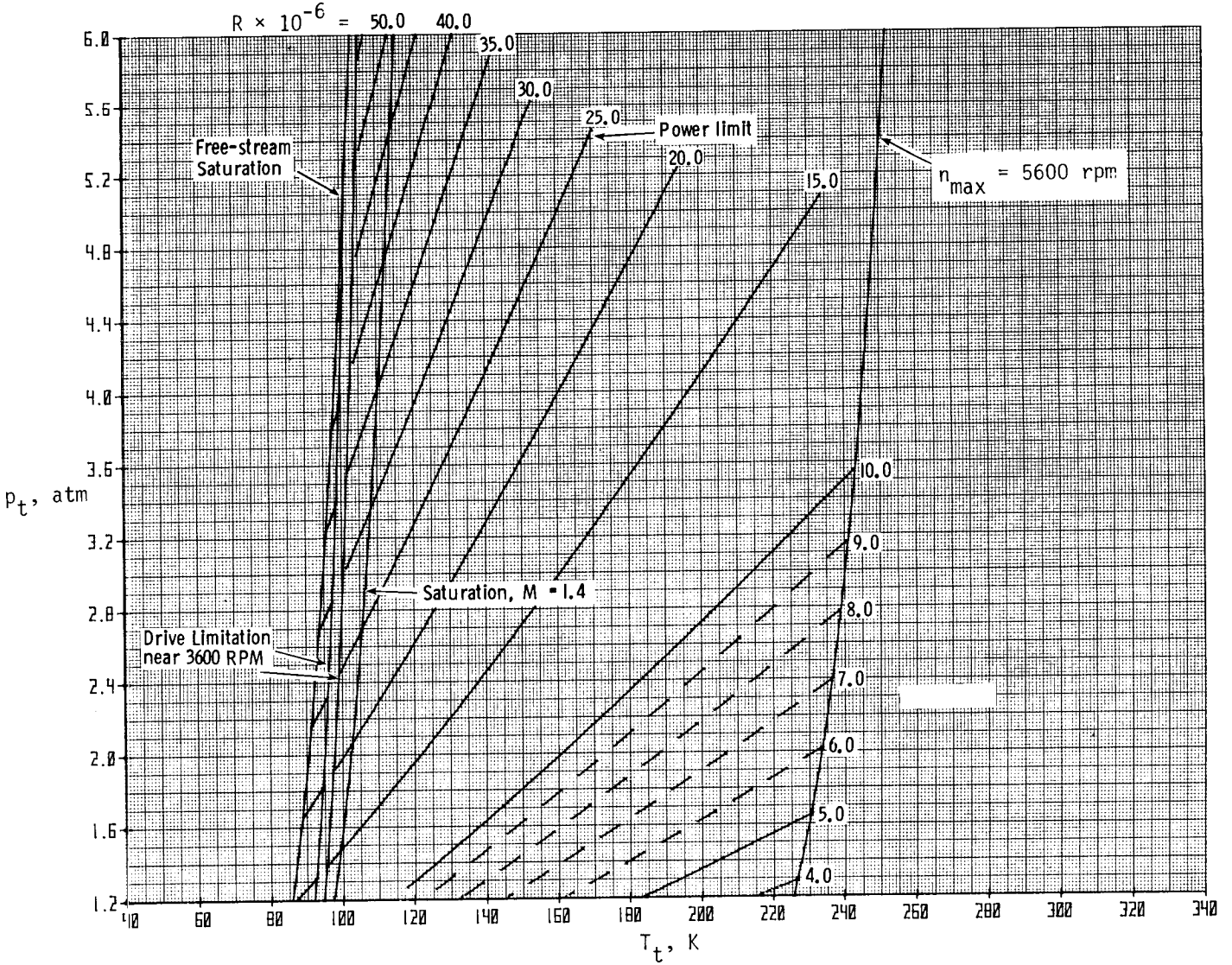

(h) M = 0.84.

Figure 55.- Continued.

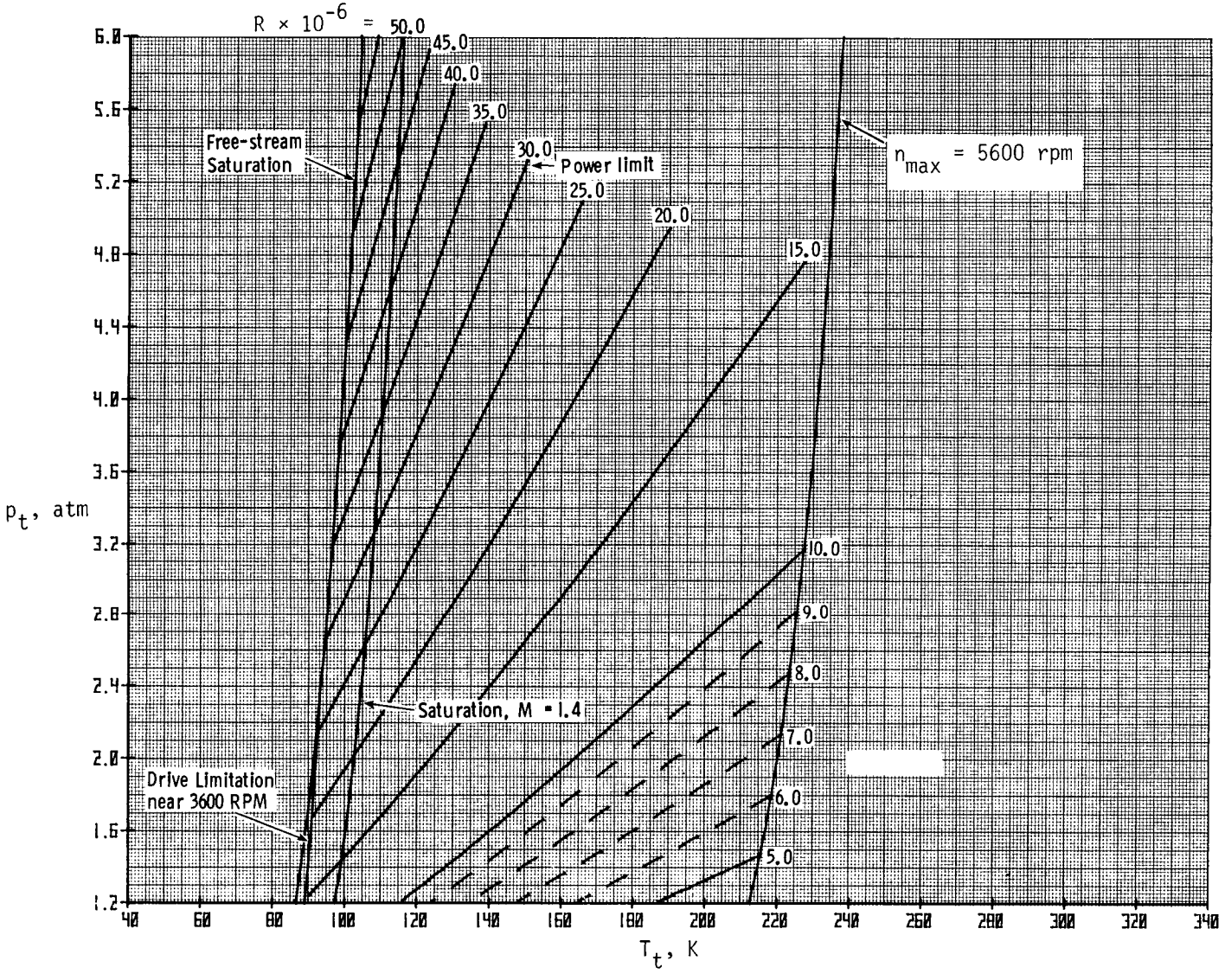

(i) M = 0.88.

Figure 55.- Concluded.

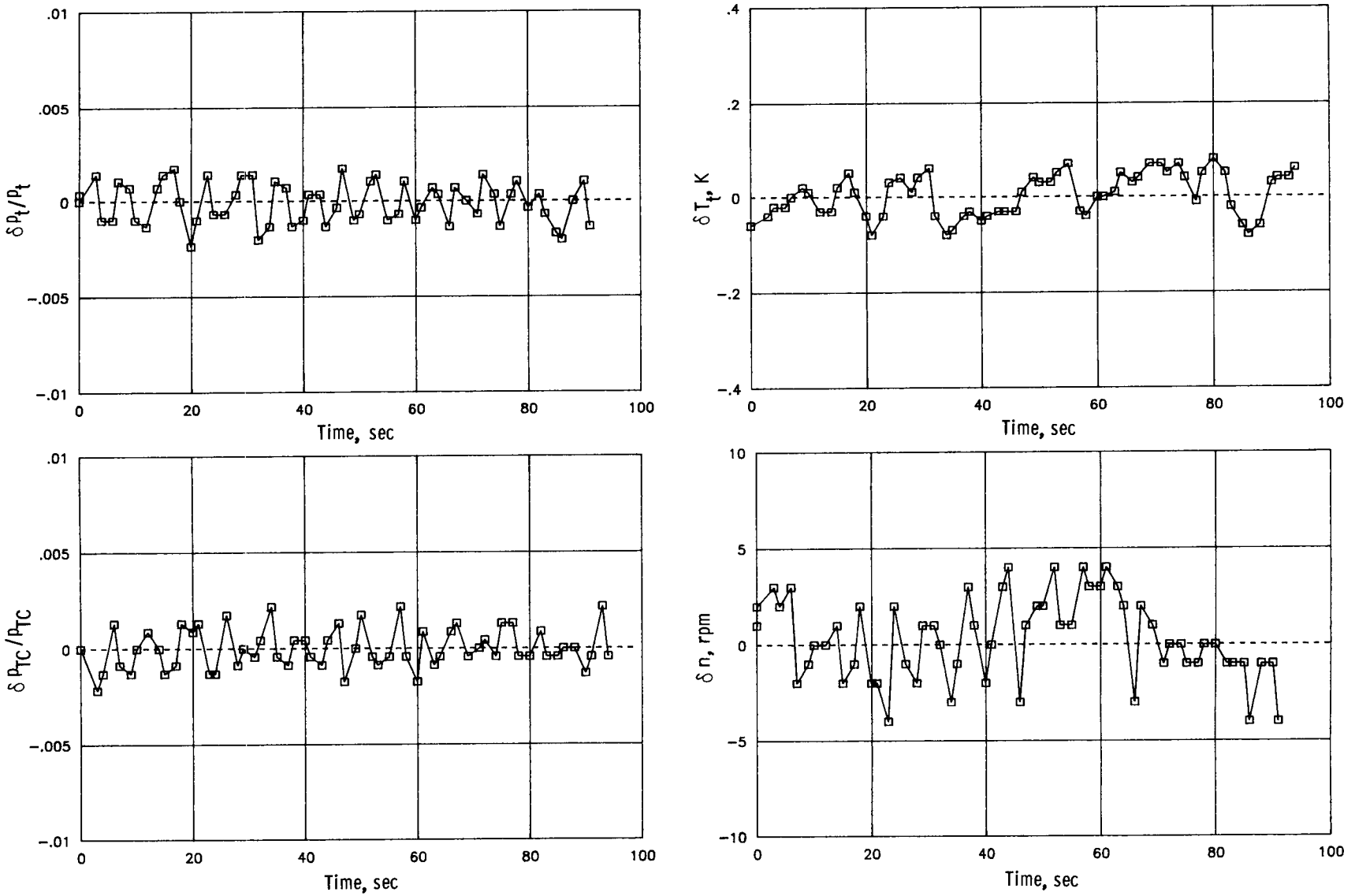

(a) $R = 6 \times 10^6$.

Figure 56.- Variation of measured and calculated tunnel parameters with time for Mach number of 0.60.

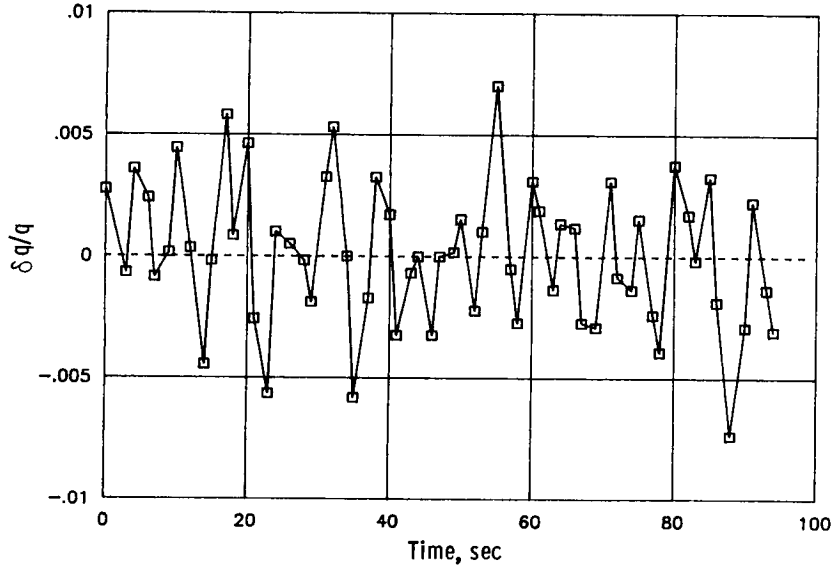

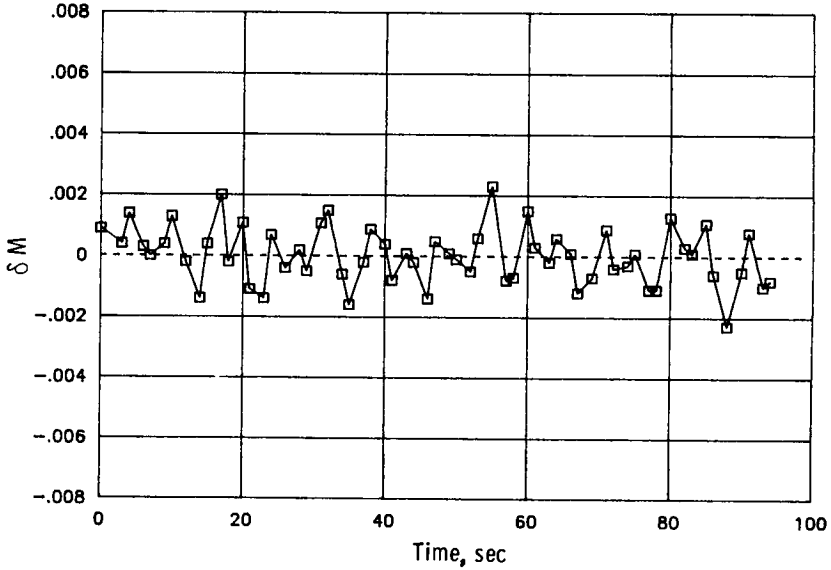

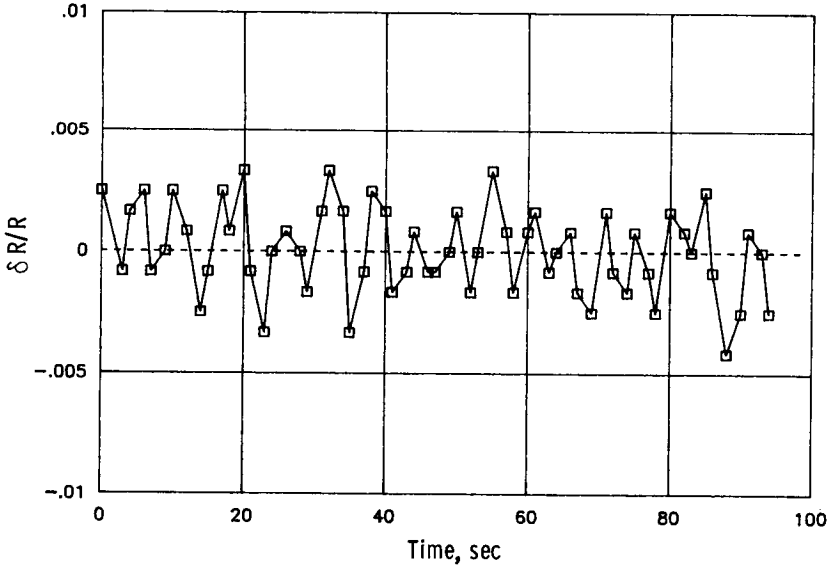

(a) Concluded.

Figure 56.- Continued.

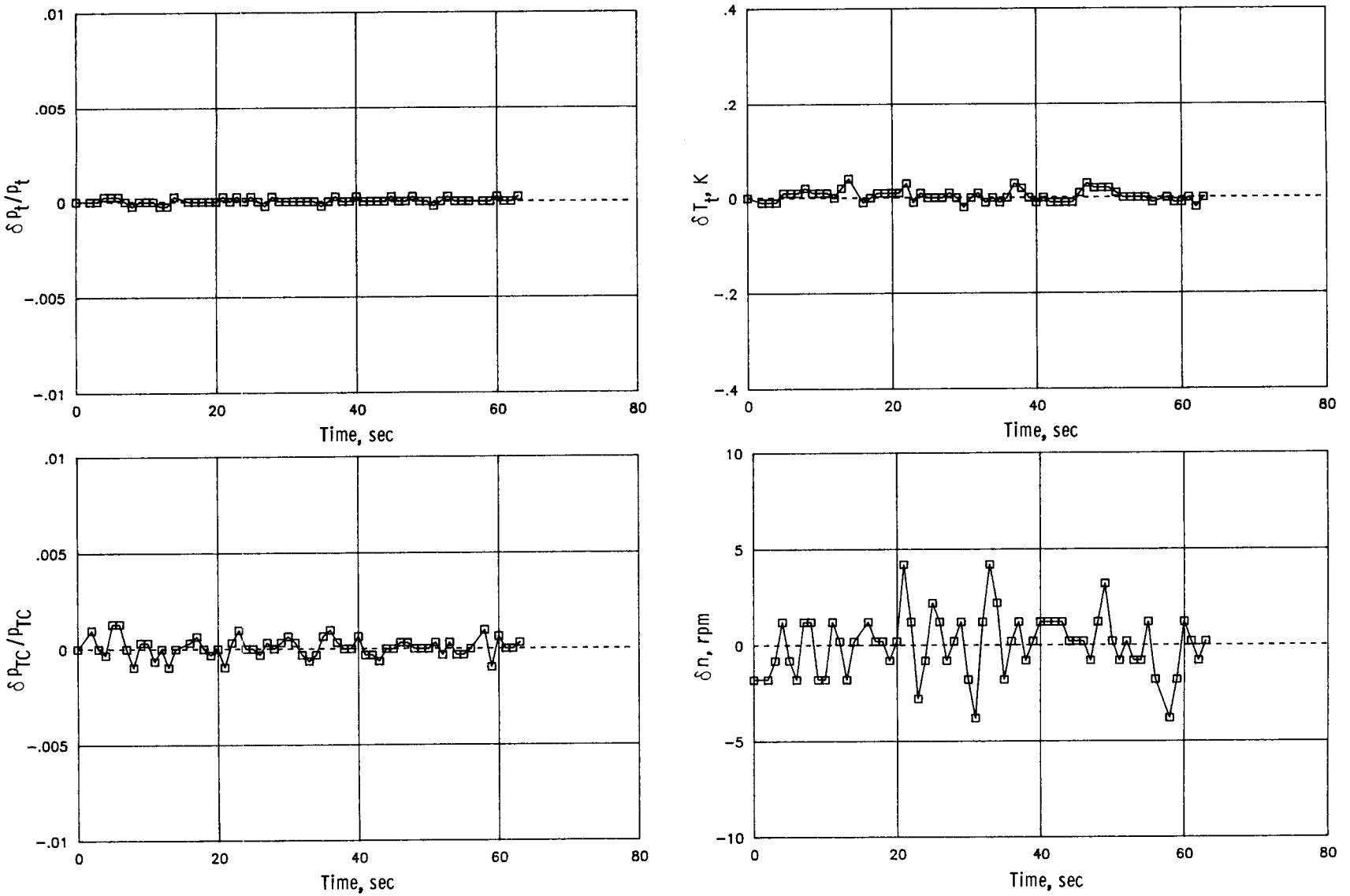

(b) $R = 15 \times 10^6$.

Figure 56.- Continued.

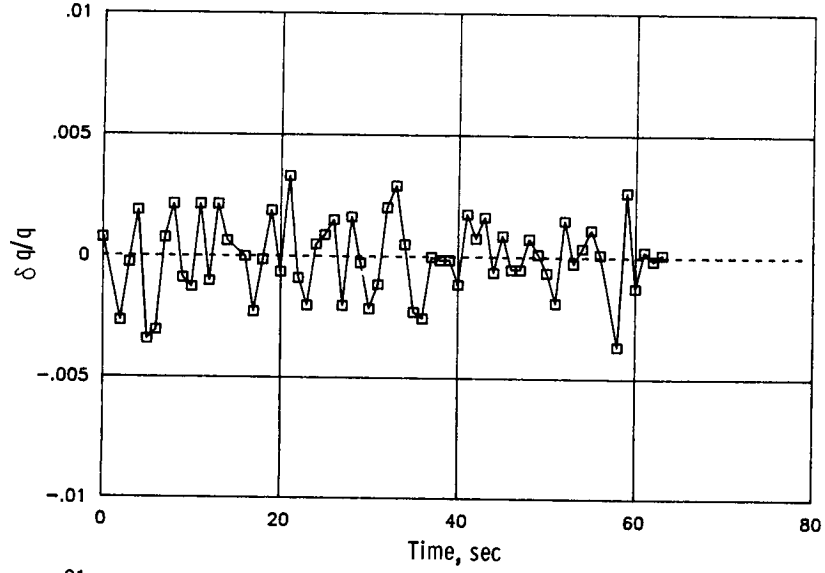

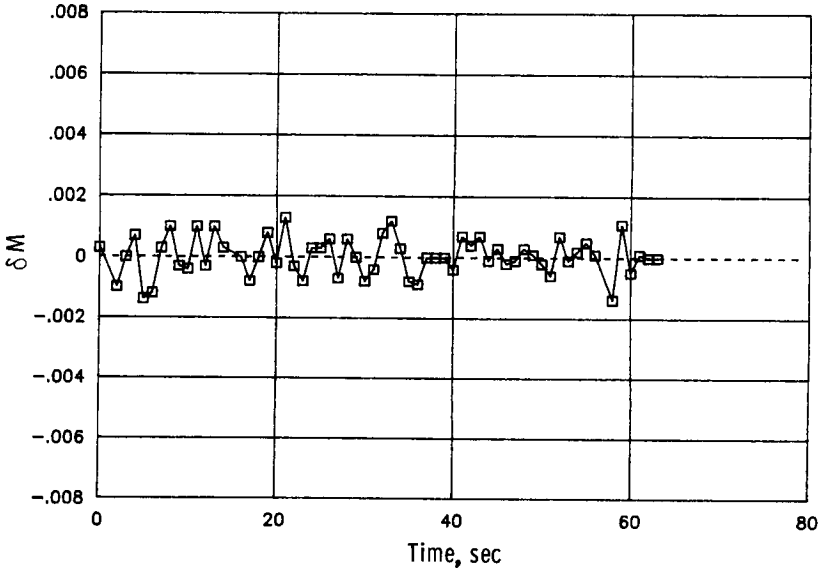

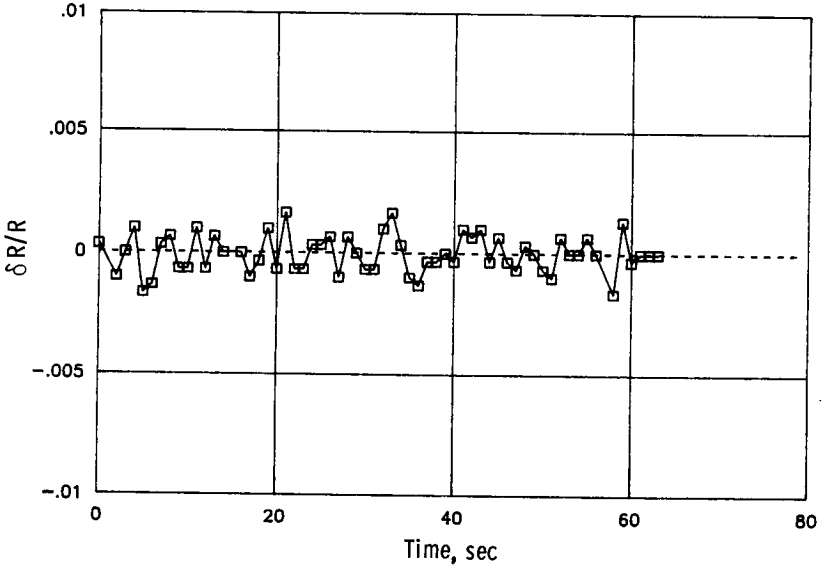

(b) Concluded.

Figure 56.- Continued.

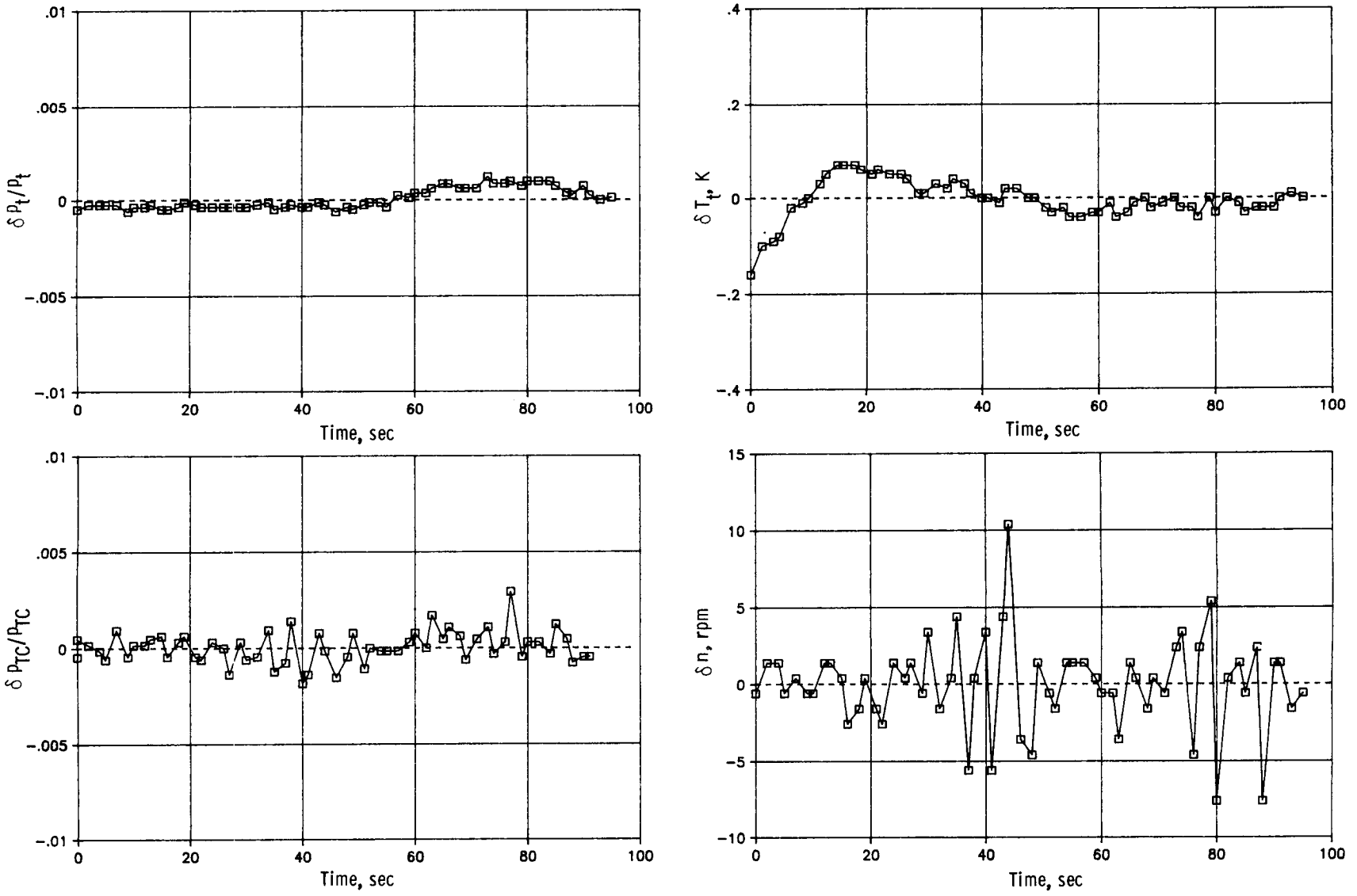

(c) $R = 40 \times 10^6$.

Figure 56.- Continued.

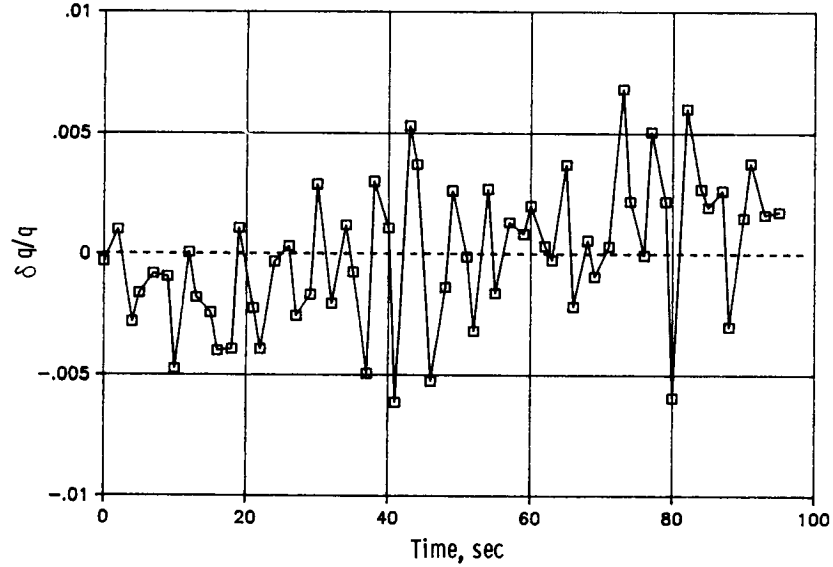

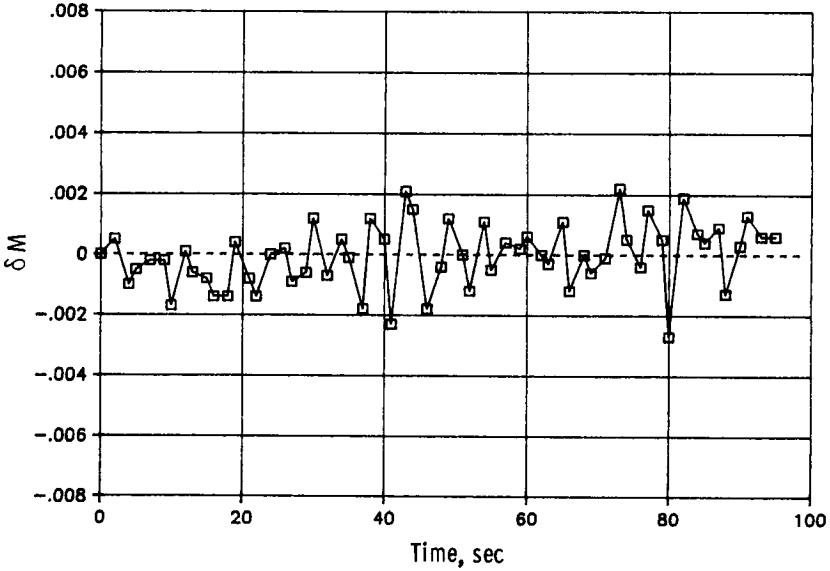

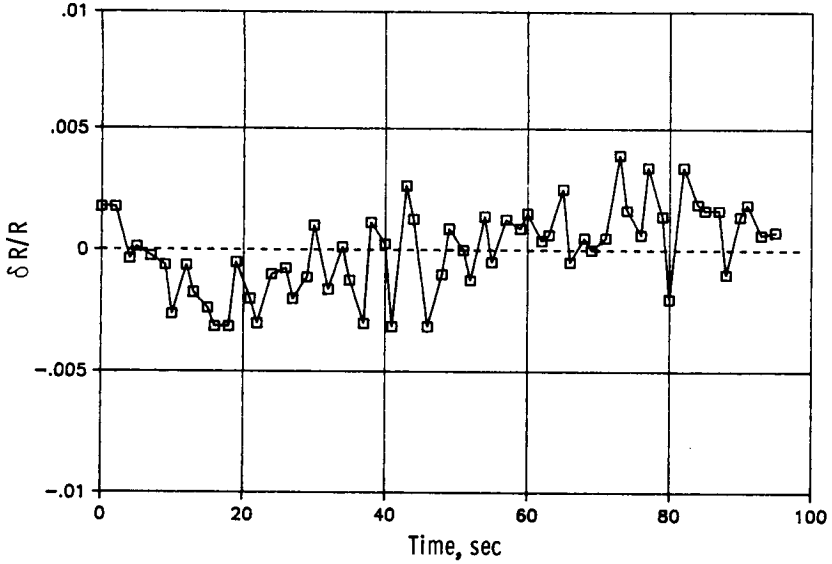

(c) Concluded.

Figure 56.- Concluded.

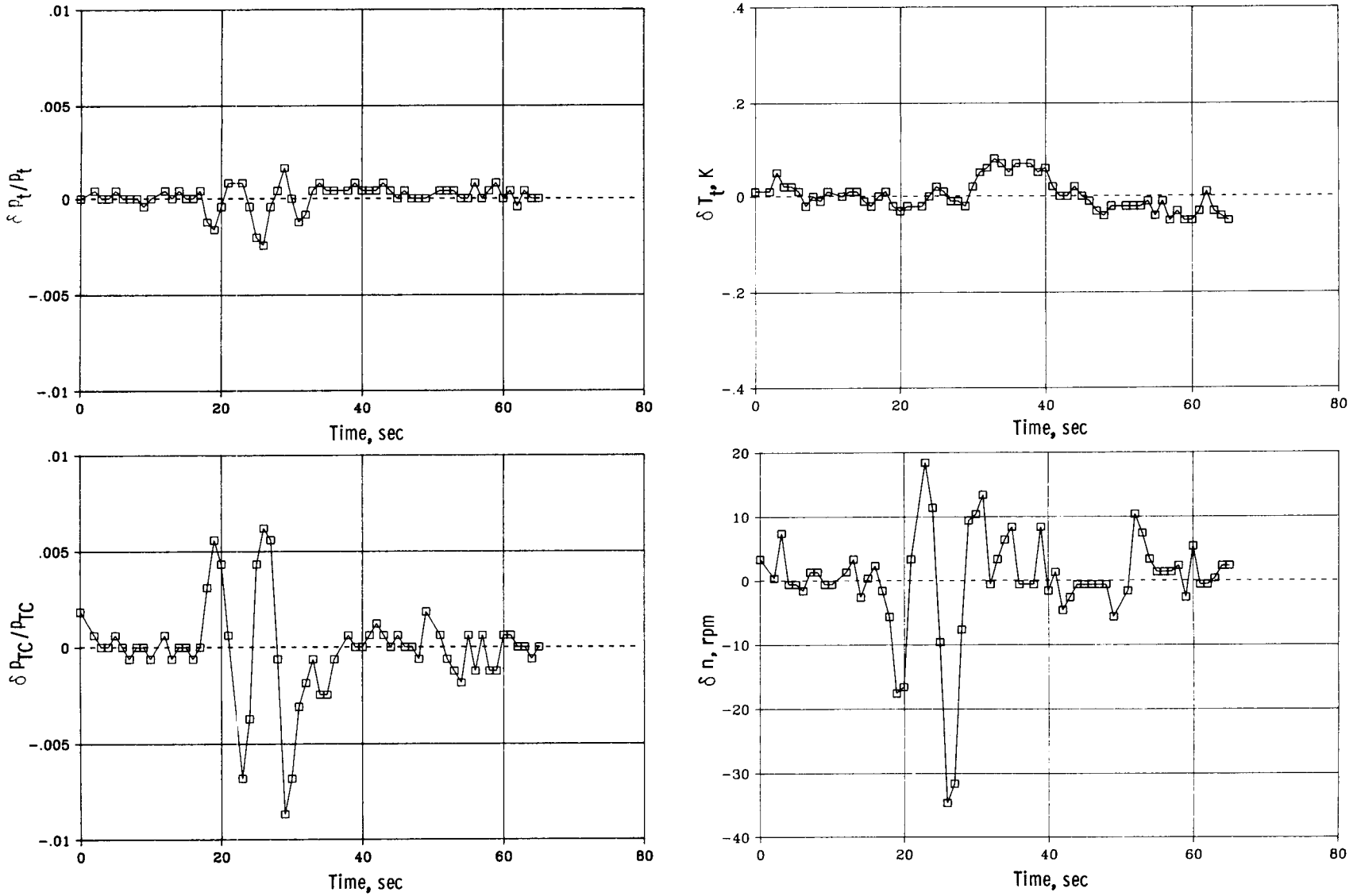

(a) $R = 6 \times 10^6$.

Figure 57.- Variation of measured and calculated tunnel parameters with time for Mach number of 0.80.

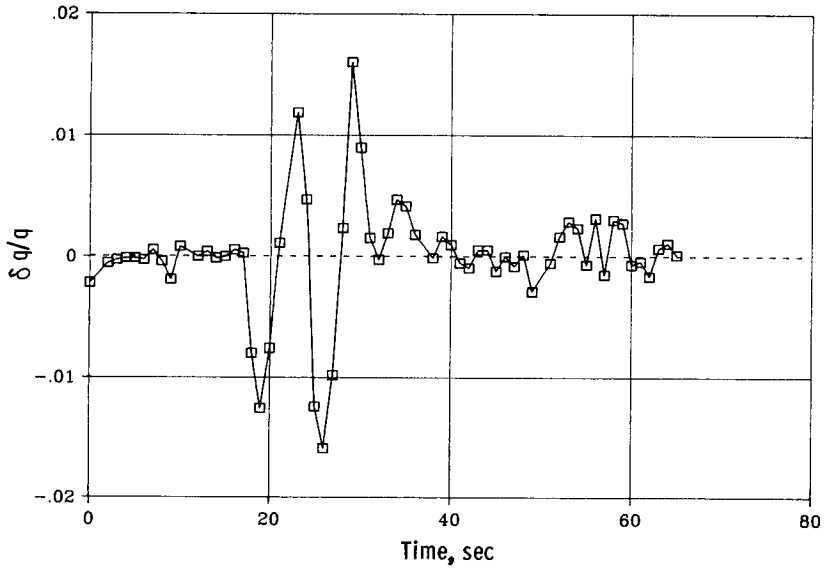

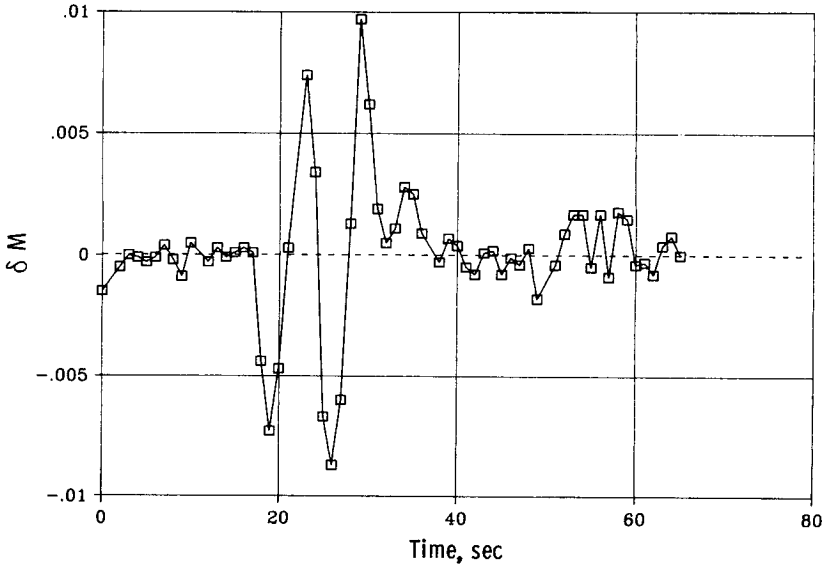

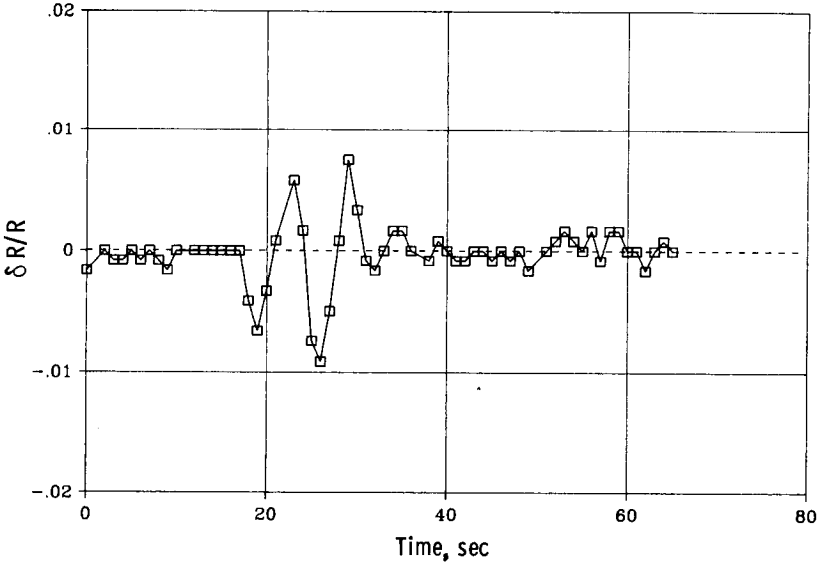

(a) Concluded.

Figure 57.- Continued.

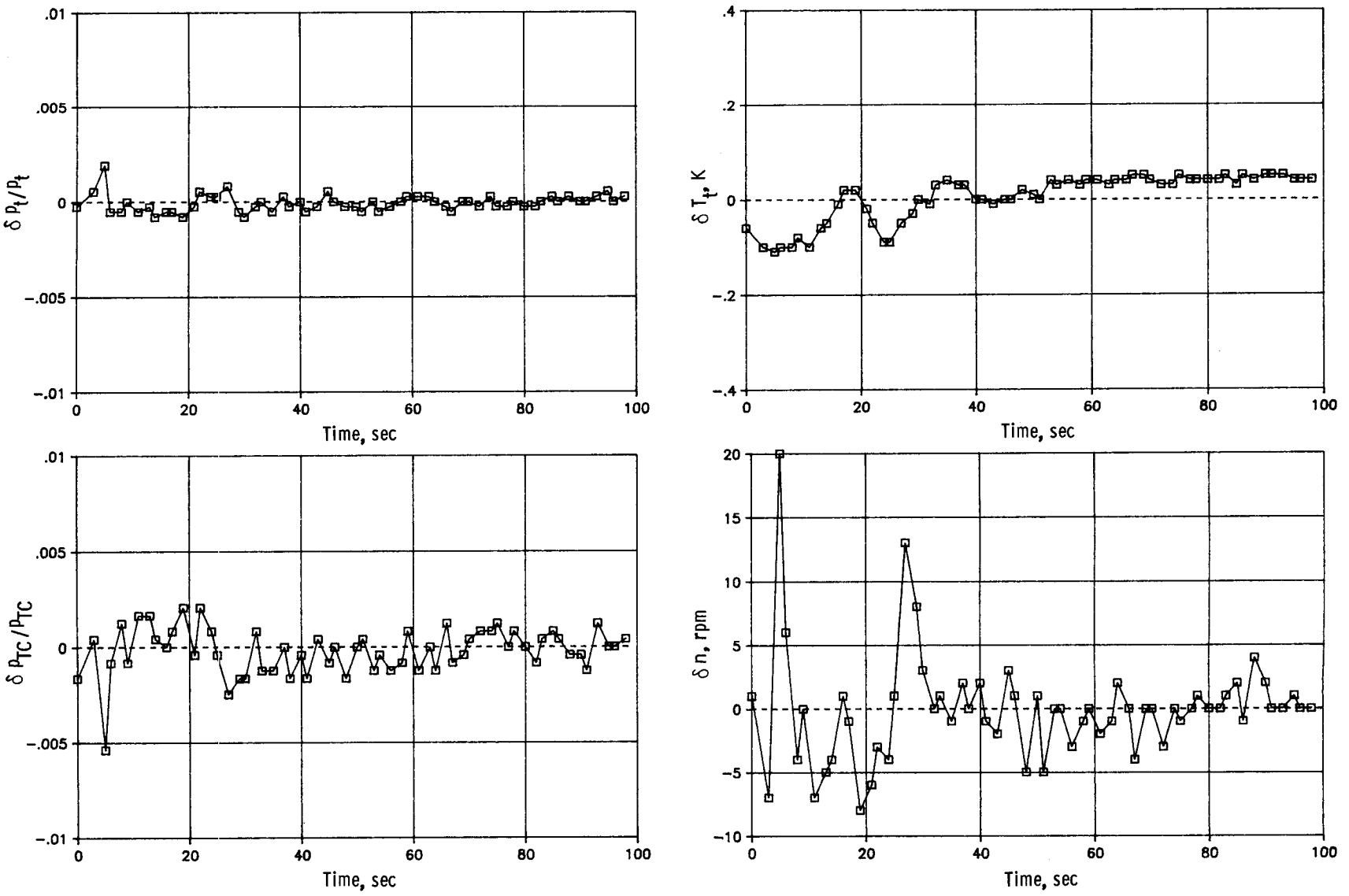

(b) $R = 15 \times 10^6$.

Figure 57.- Continued.

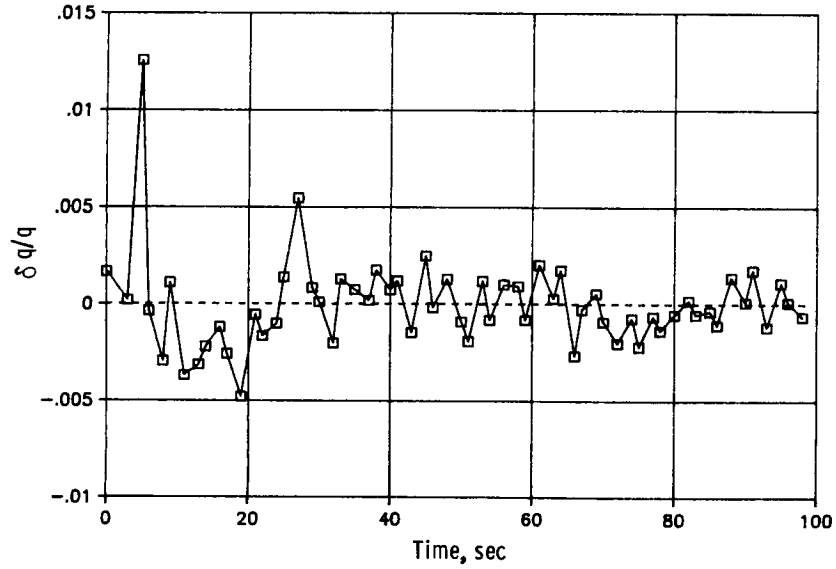

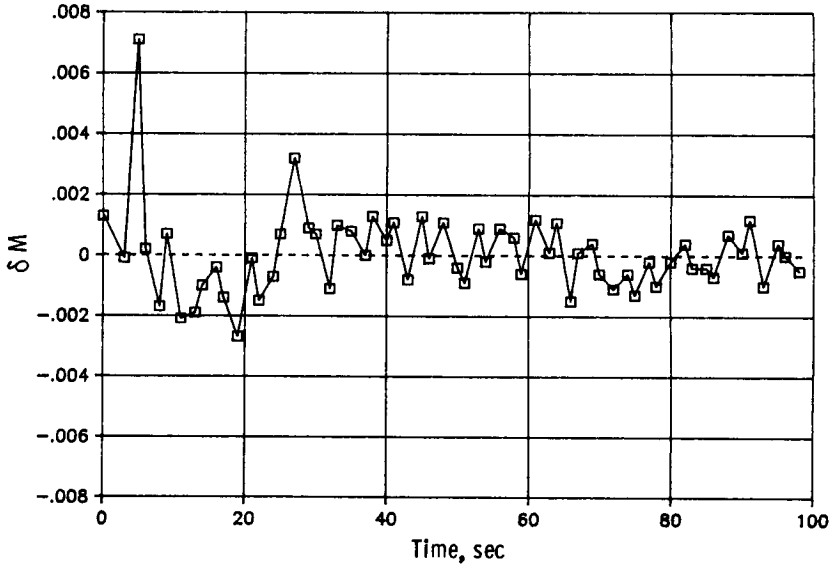

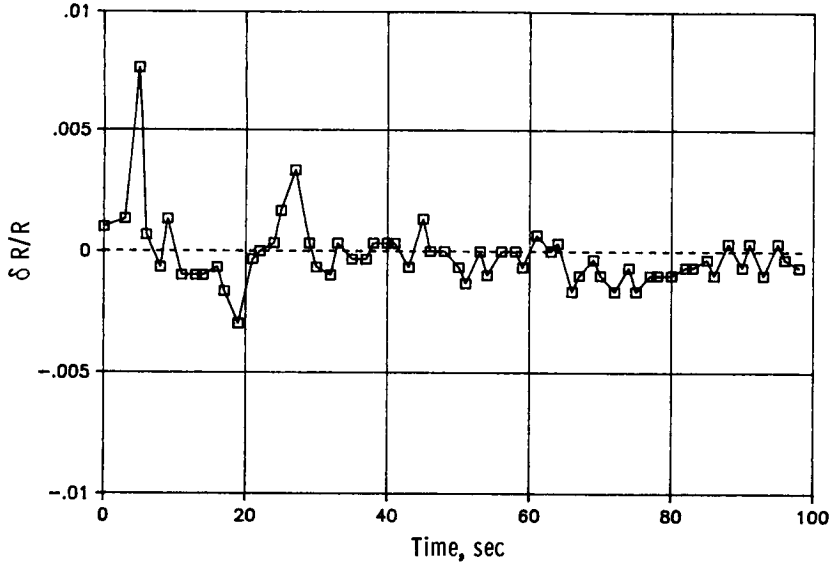

(b) Concluded.

Figure 57.- Continued.

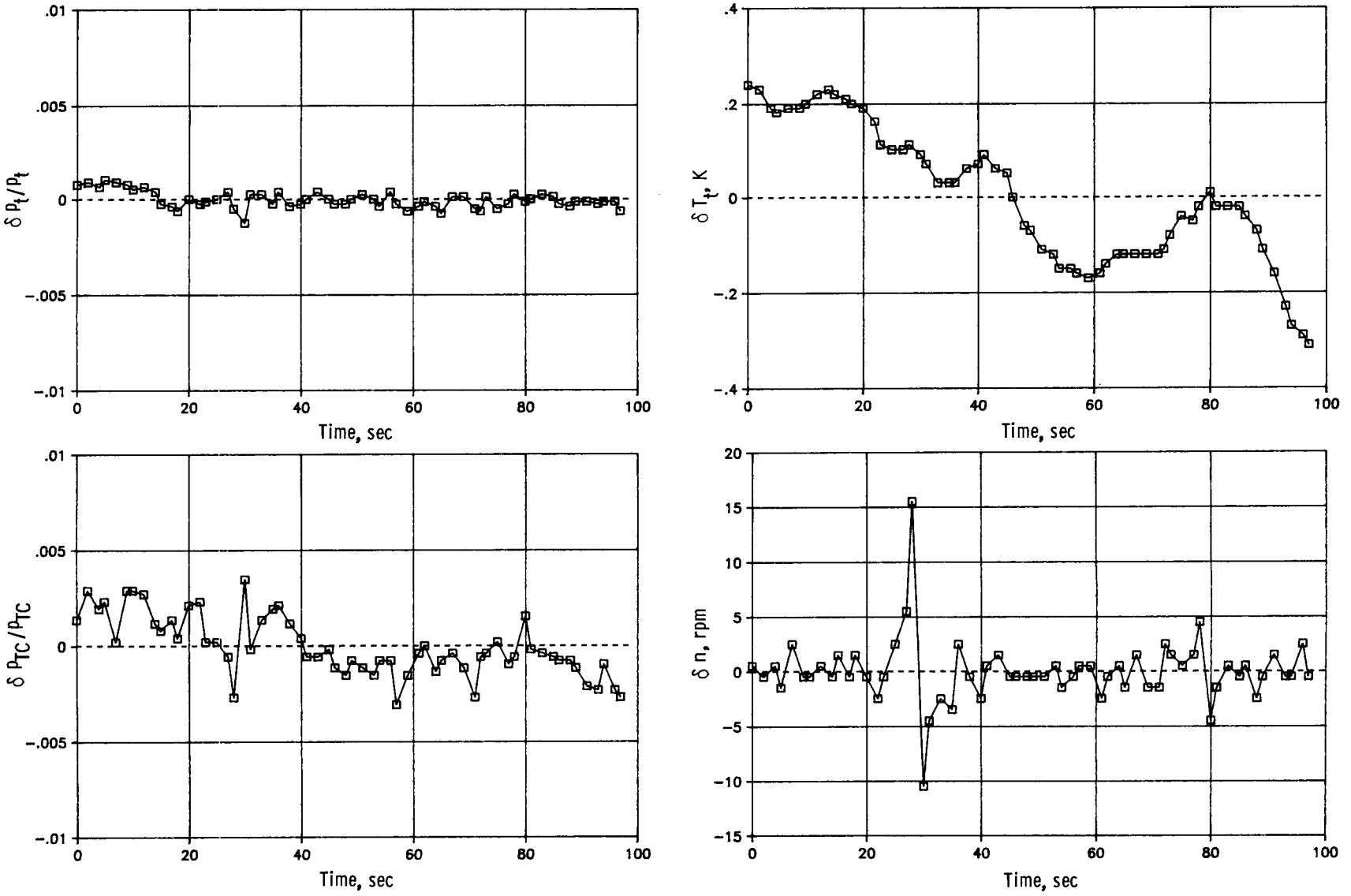

(c) R = 40 × 10^6.

Figure 57.- Continued.

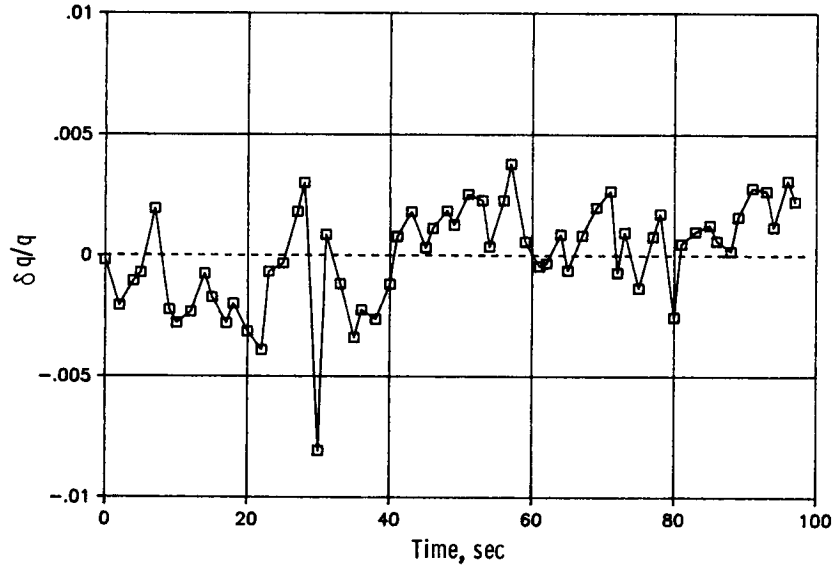

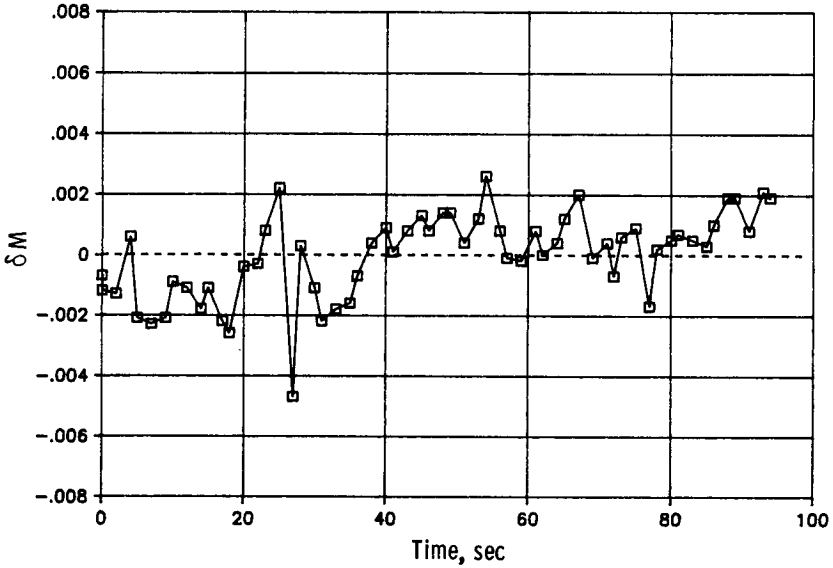

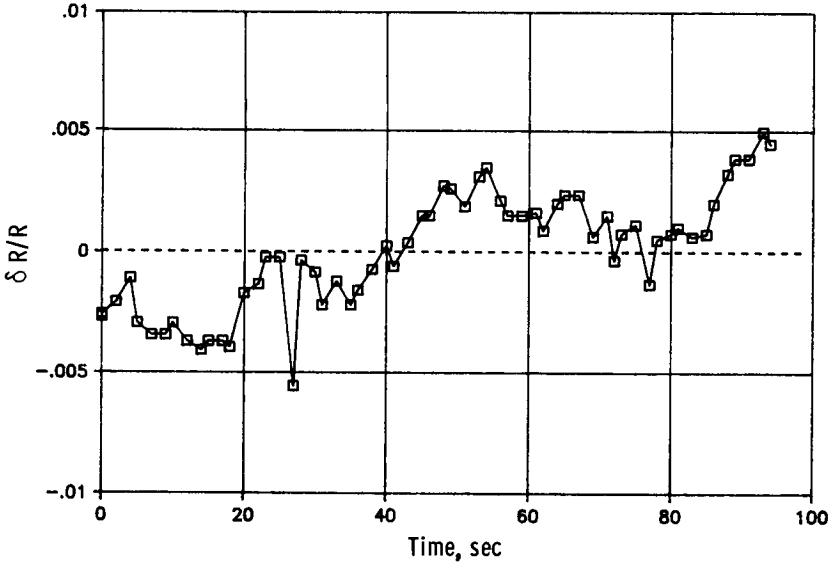

(c) Concluded.

Figure 57.- Concluded.

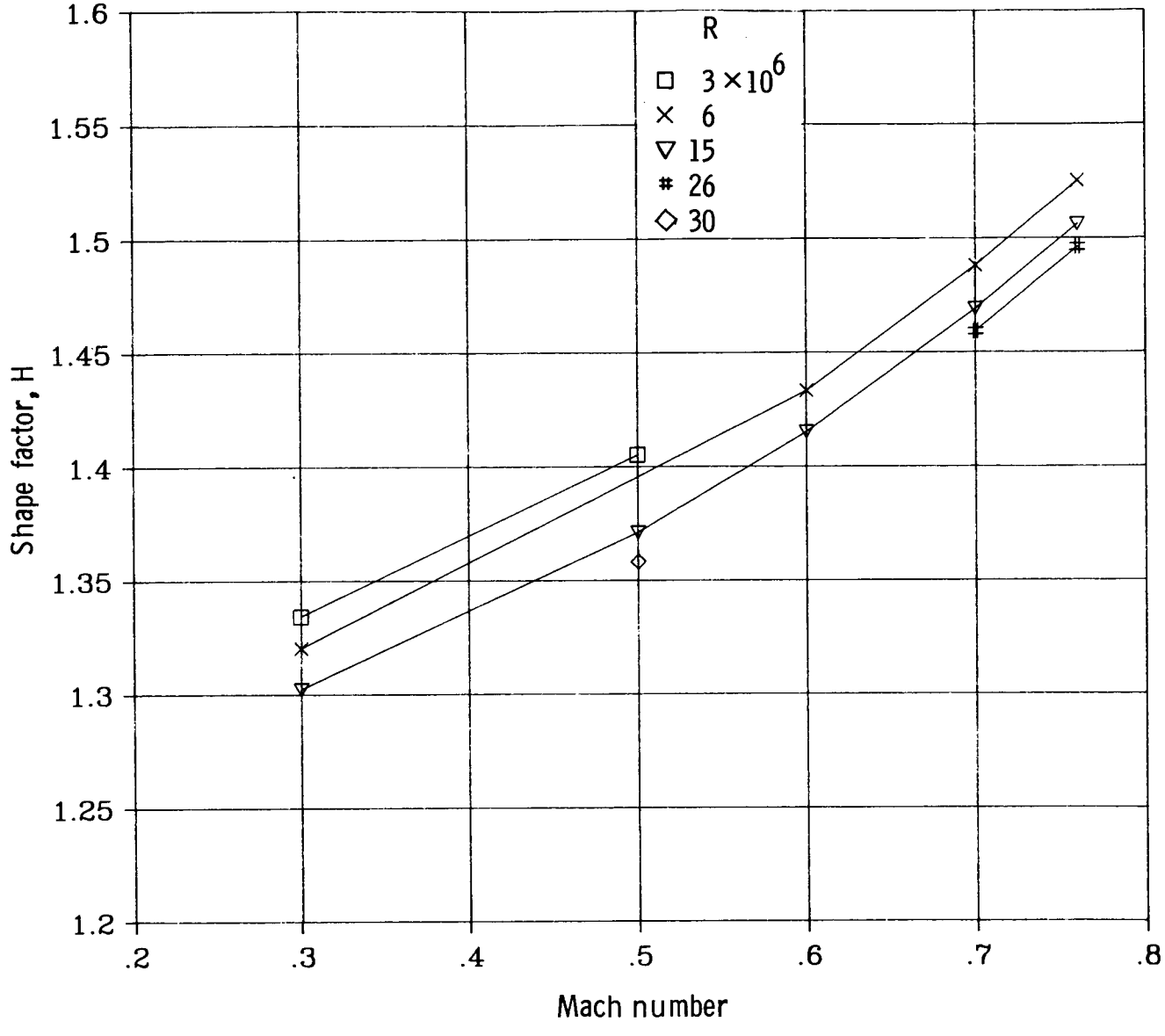

(a) Shape factor H.

Figure 58.- Test-section sidewall boundary-layer parameters as function of Mach number for several Reynolds numbers.

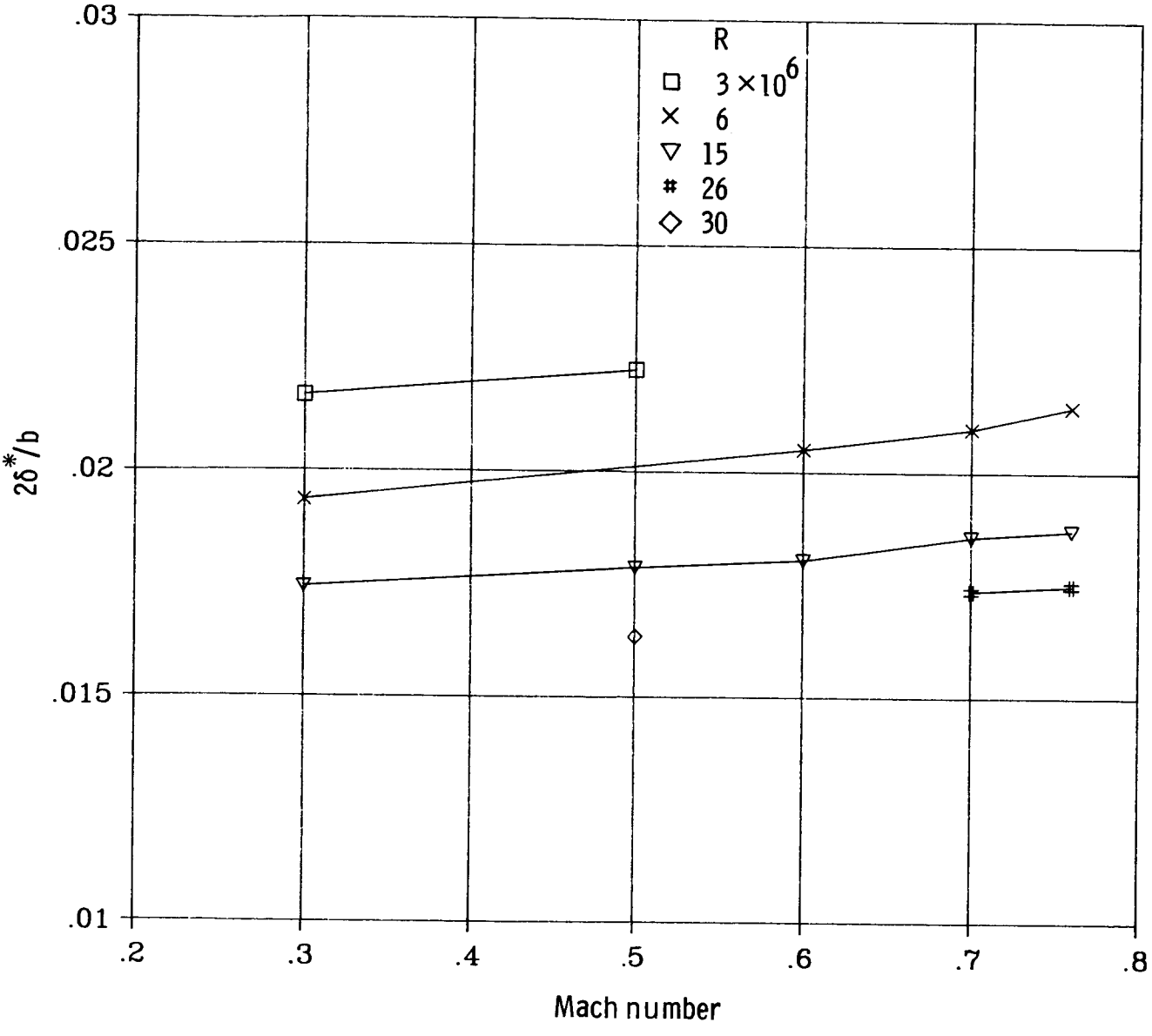

(b) Ratio of displacement thickness to tunnel semispan.

Figure 58.- Concluded.

NASA
National Aeronautics and Space Administration

Report Documentation Page

1. Report No.	2. Government Accession No.	3. Recipient's Catalog No.
NASA TP-2749		

4. Title and Subtitle	5. Report Date
Evolution, Calibration, and Operational Characteristics of the Two-Dimensional Test Section of the Langley 0.3-Meter Transonic Cryogenic Tunnel	September 1987
	6. Performing Organization Code

7. Author(s)	8. Performing Organization Report No.
Charles L. Ladson and Edward J. Ray	L-16190
	10. Work Unit No. 505-61-01-02

9. Performing Organization Name and Address	11. Contract or Grant No.
NASA Langley Research Center Hampton, VA 23665-5225	
	13. Type of Report and Period Covered: Technical Paper

12. Sponsoring Agency Name and Address	14. Sponsoring Agency Code
National Aeronautics and Space Administration Washington, DC 20546-0001	

15. Supplementary Notes

16. Abstract

This paper presents a review of the development of the world's first cryogenic pressure tunnel, the Langley 0.3-Meter Transonic Cryogenic Tunnel (0.3-m TCT). Descriptions of the instrumentation, data acquisition systems, and physical features of the two-dimensional 8- by 24-in. (20.32- by 60.96-cm) and advanced 13- by 13-in. (33.02- by 33.02-cm) adaptive-wall test-section inserts of the 0.3-m TCT are included. Basic tunnel-empty Mach number distributions, stagnation temperature distributions, and power requirements are included. The Mach number capability of the facility is from about 0.20 to 0.90. Stagnation pressure can be varied from about 1.2 to 6.1 atm, and the stagnation temperature can be varied from about 80 K to 327 K.

17. Key Words (Suggested by Author(s))	18. Distribution Statement
Cryogenic tunnels Transonic tunnels Two-dimensional tunnels	Unlimited - Unclassified Subject Category 09

19. Security Classif. (of this report)	20. Security Classif. (of this page)	21. No. of pages	22. Price
Unclassified	Unclassified	170	A08